AD-779 448

ANALYSIS OF MANEUVERABILITY EFFECTS ON ROTOR/WING DESIGN CHARACTERISTICS

N. B. Gorenberg, et al

Lockheed-California Company

Prepared for:

Army Air Mobility Research and Development Laboratory

February 1974

DISCLAIMERS

The findings in this report are not to be construed as an official Department of the Army position unless so designated by other authorized documents.

When Government drawings, specifications, or other data are used for any purpose other than in connection with a definitely related Government procurement operation, the United States Government thereby incurs no responsibility nor any obligation whatsoever; and the fact that the Government may have formulated, furnished, or in any way supplied the said drawings, specifications, or other data is not to be regarded by implication or otherwise as in any manner licensing the holder or any other person or corporation, or conveying any rights or permission, to manufacture, use, or sell any patented invention that may in any way be related thereto.

Trade names cited in this report do not constitute an official endorsement or approval of the use of such commercial hardware or software.

DISPOSITION INSTRUCTIONS

Destroy this report when no longer needed. Do not return it to the originator.

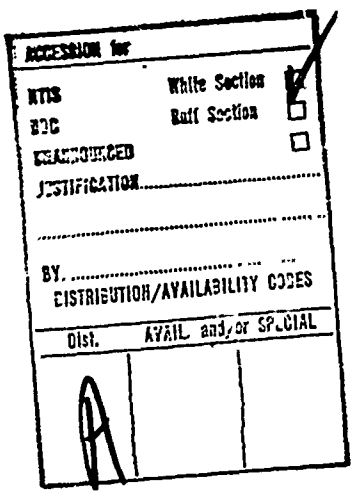

Unclassified
Security Classification

AD 779448

DOCUMENT CONTROL DATA - R & D

(Security classification of title, body of abstract and indexing annotation must be entered when the overall report is classified)

1. ORIGINATING ACTIVITY (Corporate author)	2a. REPORT SECURITY CLASSIFICATION
Lockheed-California Company Burbank, California	Unclassified 2b. GROUP

3. REPORT TITLE

ANALYSIS OF MANEUVERABILITY EFFECTS ON ROTOR/WING DESIGN CHARACTERISTICS

4. DESCRIPTIVE NOTES (Type of report and inclusive dates)

Final Report

5. AUTHOR(S) (First name, middle initial, last name)

N. B. Goremberg
W. P. Harvick

6. REPORT DATE	7a. TOTAL NO. OF PAGES	7b. NO. OF REFS
February 1974	267	15

8a. CONTRACT OR GRANT NO.	9a. ORIGINATOR'S REPORT NUMBER(S)
DAAJ02-70-C-0032 b. PROJECT NO. 1X164206D378 c. d.	USAAMRDL Technical Report 74-24 9b. OTHER REPORT NO(S) (Any other numbers that may be assigned this report)

10. DISTRIBUTION STATEMENT

Approved for public release; distribution unlimited.

11. SUPPLEMENTARY NOTES	12. SPONSORING MILITARY ACTIVITY
	Eustis Directorate U. S. Army Air Mobility R&D Laboratory Fort Eustis, Virginia

13. ABSTRACT

An analytical study was performed to contribute toward design criteria for the Utility Tactical Transport Aircraft System (UTTAS) through an analysis of maneuvers to determine effects of the maneuvers on helicopter design characteristics. Maneuverability requirements examined were combinations of maximum flight speeds and maneuvering load factors and sustained high load factors for long periods of time as might be expected in nap-of-the-earth flying. The study included analyses to examine the possibility of gaining maneuver capability at high speeds by adding wings to helicopters.

Analysis of results showed no large difference between winged and nonwinged helicopters. Those differences that did emerge, however, were in favor of adding the wing. Whether or not these differences would become more significant through additional design iterations of a particular design is not yet clear.

DD FORM 1 NOV 68 1473 REPLACES DD FORM 1473, 1 JAN 64, WHICH IS OBSOLETE FOR ARMY USE.

Unclassified
Security Classification

14. KEY WORDS	LINK A		LINK B		LINK C	
	ROLE	WT	ROLE	WT	ROLE	WT
Maneuverability effects Winged helicopters Nonwinged helicopters Helicopter design characteristics						

DEPARTMENT OF THE ARMY
U.S. ARMY AIR MOBILITY RESEARCH & DEVELOPMENT LABORATORY
EUSTIS DIRECTORATE
FORT EUSTIS, VIRGINIA 23604

This report presents the results of one study of the effects of maneuverability requirements on the design of pure and winged helicopters. The general objective was to present a rationale for a given maneuverability requirement for new Army helicopters in the utility class.

This report is published for the dissemination of information and the stimulation of new ideas.

The technical monitor for this contractual effort was Mr. Russell O. Stanton, UTTAS Project Officer, Systems Support Division.

Project 1X164206D378
Contract DAAJ02-70-C-0032
USAAMRDL Technical Report 74-24
February 1974

ANALYSIS OF MANEUVERABILITY EFFECTS ON ROTOR/WING DESIGN CHARACTERISTICS

Final Report

Lockheed Report 24051

By

N. B. Gorenberg
W. P. Harvick

Prepared by

Lockheed-California Company
Burbank, California

for

EUSTIS DIRECTORATE
U.S. ARMY AIR MOBILITY RESEARCH AND DEVELOPMENT LABORATORY
FORT EUSTIS, VIRGINIA

SUMMARY

An analytical study was performed to contribute toward design criteria for the Utility Tactical Transport Aircraft System (UTTAS) through an analysis of maneuvers to determine effects of the maneuvers on helicopter design characteristics. Maneuverability requirements examined were combinations of maximum flight speeds and maneuvering load factors and sustained high load factors for long periods of time as might be expected in nap-of-the-earth flying. The study included analyses to examine the possibility of gaining maneuver capability at high speeds by adding wings to helicopters.

Target values of maneuvering criteria were established: maneuvering load factors of 1.5, 1.75, and 2.0, in coordinated turns and symmetrical maneuvers, at flight speeds up to 150 KEAS (167 KTAS); sustaining maximum load factors for 3 seconds during coordinated turns, without excessive speed loss or altitude change.

Six analytical model aircraft were hypothesized for the study: three helicopters and three winged helicopters. Each was assigned baseline features characteristic of an earlier concept formulation design study (except that the study aircraft were not to have auxiliary propulsion systems as the Lockheed design had in the earlier study). All models were assigned a gross weight of 16,000 lb and a cruise speed of 150 KTAS. The models were assumed to have Lockheed hingeless rotors and control systems of the type used in the UTTAS concept formulation study.

Wings were added without changing the gross weight. Wing structure weight was traded for rotor weight through reducing rotor solidity; additional compensation was made by assuming some trade-off among structure, payload, and fuel.

The results of this study are numerous; some general conclusions are summarized as follows:

- The target combinations of speeds and load factors are high for helicopters (winged or unwinged).

- The need to maintain maximum load factors for several seconds during maneuvers limited attainable maximum rotor thrust to values less than could be attained in shorter-duration maneuvers.
- Analysis of results showed no large difference between winged and non-winged helicopters. Those differences that did emerge, however, were in favor of adding the wing. Whether or not these differences would become more significant through additional design iterations of a particular design is not yet clear.

FOREWORD

An analytic investigation was made to determine the effect on significant design parameters of varying requirements for nonwinged and winged helicopters having particular maneuverability capabilities. This work was done under Contract DAAJ02-70-C-0032 and is an extension of the work previously accomplished by the Lockheed-California Company under Contract DAAJ02-69-C-0014. The study reported herein was conducted at the Lockheed-California Company during 1970 by an analysis team under the direction of Project Leader N. B. Gorenberg. Major contributors of the analysis team were F. Chang, R. W. Hovey, W. J. Kaiser, D. Kawamoto, M. P. Patel, J. E. Sweers, and J. V. Werner. This report was prepared by W. P. Harvick and N. B. Gorenberg. Technical monitoring was provided by J. P. Clarke and R. O. Stanton of USAAMRDL .

TABLE OF CONTENTS

LIST OF ILLUSTRATIONS

LIST OF TABLES

LIST OF SYMBOLS

A_{ls}	rotor blade lateral cyclic pitch, deg
B_{ls}	rotor blade longitudinal cyclic pitch, deg
C_{L_A}	nonrotating airframe lift coefficient
C_T	thrust coefficient
D_A	nonrotating airframe drag, lb
D_R	rotor drag, lb
I_{xx}	aircraft minus blades moment of inertia about vehicle reference longitudinal axis
I_{yy}	aircraft minus blades moment of inertia about vehicle reference lateral axis
I_{zz}	aircraft minus blades moment of inertia about vehicle reference vertical axis
L	lift (net lift, algebraic total), lb
L_A	nonrotating airframe lift, lb
L_R	rotor lift, lb
M_A	nonrotating airframe pitching moment, ft-lb
n	normal load factor
q	dynamic pressure, lb/ft^2
x_{cs}	cyclic control stick longitudinal displacement, aft displacement positive, in.
x_p	pedal displacement, right pedal displacement positive, in.
y_{cs}	cyclic control stick lateral displacement, right displacement positive, in.
z_c	collective control stick vertical displacement, upward displacement positive, in.
α_R	rotor angle of attack, shaft normal plane reference, deg

α_{FRL} nonrotating airframe angle of attack, fuselage waterline reference, deg

γ blade Lock number

Θ_0 main rotor blade collective pitch angle, measured at the rotor centerline, deg

Θ_{TR} tail rotor blade collective pitch angle, deg

μ rotor advance ratio, flight path relative wind reference, in ft/sec, divided by main rotor tip speed

σ rotor solidity

Ω rotor blade rotational velocity, in shaft normal plane, rad/sec

ω_n blade nonrotating natural frequency, rad/sec

ω_r blade rotating structural frequency, rad/sec

INPUT COMMANDS

G_{ZC} normal load factor command, + up (body coord.), g

Z_{FC} height change command, + up (inertial), ft

Θ_C pitch attitude command, + nose up, rad

Θ_{OC} collective blade angle, + leading edge up, rad

Θ_{TR} tail rotor collective command, + nose right, rad

ϕ_C roll attitude command, + right down, rad

X_{CST} trim cyclic stick position (pitch), + aft, ft

Y_{CST} trim cyclic stick position (roll), + right, ft

Θ_T trim pitch attitude, + nose up (inertial), rad

ϕ_T trim roll attitude, + right down (inertial), rad

AUTOPILOT FILTERS

$B_{F\Theta}$ pitch forward path filter, 1/S

$B_{F\phi}$ roll forward path filter, K/S

B_{GZ} load factor command filter, $1/(\tau S + 1)$*

B_{TR} sideslip rate filter, $1/(\tau S + 1)$

B_{XF} cross-feed filter, $1/(\tau S + 1)$

B_{XFC} collective cross-feed filter, $1/(\tau S + 1)$

B_{ZF} height command filter, $1/(\tau S + 1)$

$B_{\theta C}$ pitch attitude command filter, $1/(\tau S + 1)$

$B_{\theta O}$ collective blade angle command filter, $1/(\tau S + 1)$

$B_{\phi C}$ roll attitude command filter, $1/(\tau S + 1)$

*For all filters of the form $1/(\tau S + 1)$, the specified values for each filter refer to the quantity $1/\tau$.

1.0 INTRODUCTION

In accordance with Contract DAAJ02-70-C-0032, the Lockheed-California Company conducted an analytical investigation of the maneuvering capabilities of various single-rotor helicopter configurations with and without wings.

This study is an extension of a concept formulation design study undertaken in 1968 to define the U.S. Army's Utility Tactical Transport Aircraft System (UTTAS). The objective of the study was to evaluate means of enhancing the maneuverability of helicopters, leading toward helicopters designed to perform low-level nap-of-the-earth flight.

The general approach in the study was first to establish principal design characteristics of helicopters with capabilities of performing prescribed maneuvers and then to evaluate the effects of adding wings to the helicopters.

During the study, the impact of various maneuver requirements on aircraft maneuverability was ascertained by varying certain design parameters, such as rotor solidity and wing area, and conducting maneuver simulation studies to evaluate relative maneuvering capabilities. Maneuvering capability was assessed with regard to aircraft performance, stability and control characteristics, power requirements, rotor loads, rotor system dynamic response characteristics, and overall mission requirements.

1.1 APPROACH

General baseline features were established for the hypothetical aircraft to provide a basis for comparing the results of analyses. Those features which were considered unalterable are listed in Table I. Those parameters which were subsequently fixed and those which were varied are discussed in paragraphs 2.2 and 2.3.

Based on the general baseline features, three unwinged helicopter designs were synthesized (configured to attain maximum maneuver load factors of 1.5, 1.75, and 2.0). Coordinated turns (sustained for approximately 3 sec) were the principal maneuvers used to effect the syntheses. Rotor solidity was the principal variable used to adjust maximum maneuver load factor capability. The general

TABLE I. GENERAL BASELINE DESIGN CHARACTERISTICS

Design Characteristics	Value
Aircraft Characteristics	
Design gross weight, lb	16,000
Disc loading (based on a 58-ft rotor diameter), lb/ft^2	6.06
Number of engines	2
Design Atmosphere	
Pressure altitude, ft	4,000
Ambient temperature, °F	95
Density ratio	0.808
Speed of sound, ft/sec	1,155
Aircraft Performance	
Cruise speed (≤ NRP), KTAS	150
Vertical climb rate (SHP ≤ 0.95 MRP; design atmosphere; zero forward speed; OGE), ft/min	500
Structural Requirements	
Load factor	+3.0 to -0.5
Airframe life, hr	5,000
Rotor TBO, hr	1,500
Drive train TBO, hr	1,500
Engine TBO, hr	1,500

arrangement of a representative helicopter configuration which evolved is illustrated in Figure 1.

After the unwinged helicopters were designed, analyses were performed to determine the effects of adding wings to the helicopters. Rotor solidity was exchanged for wing area in the synthesizing of these aircraft. The general arrangement of a winged helicopter is shown in Figure 2.

One important design consideration was that the aircraft be capable of maintaining an average cruise speed of 150 KTAS in nap-of-the-earth flight. In order to obtain this objective, initial efforts were directed at the more difficult problem of achieving the maximum maneuver load factors at 150 KEAS (167 KTAS at design atmosphere conditions). Ultimately, the forward speed of 150 KTAS was selected as most compatible with other performance and mission requirements. Other regions of the flight regime were explored in less depth.

The development of the six aircraft was accomplished by relatively simple preliminary design synthesis techniques. The methods used to ensure representative rotor aeroelastic behavior are discussed in Appendix I. After these aircraft were established, their respective capabilities for executing coordinated turns, pull-ups, and push-overs were studied by means of a comprehensive computer flight simulation method described in paragraph 1.3.

Certain design parameters were varied to determine their influence on performance, stability and control characteristics, power requirements, rotor loads, and rotor system dynamic response characteristics under various conditions of maneuvering flight.

The six aircraft analyzed were the product of preliminary synthesis techniques. It was not practicable to bring them to a theoretical level of perfection within the scope of this program. From the results obtained, important predictions, projections and insights emerge concerning the design concepts.

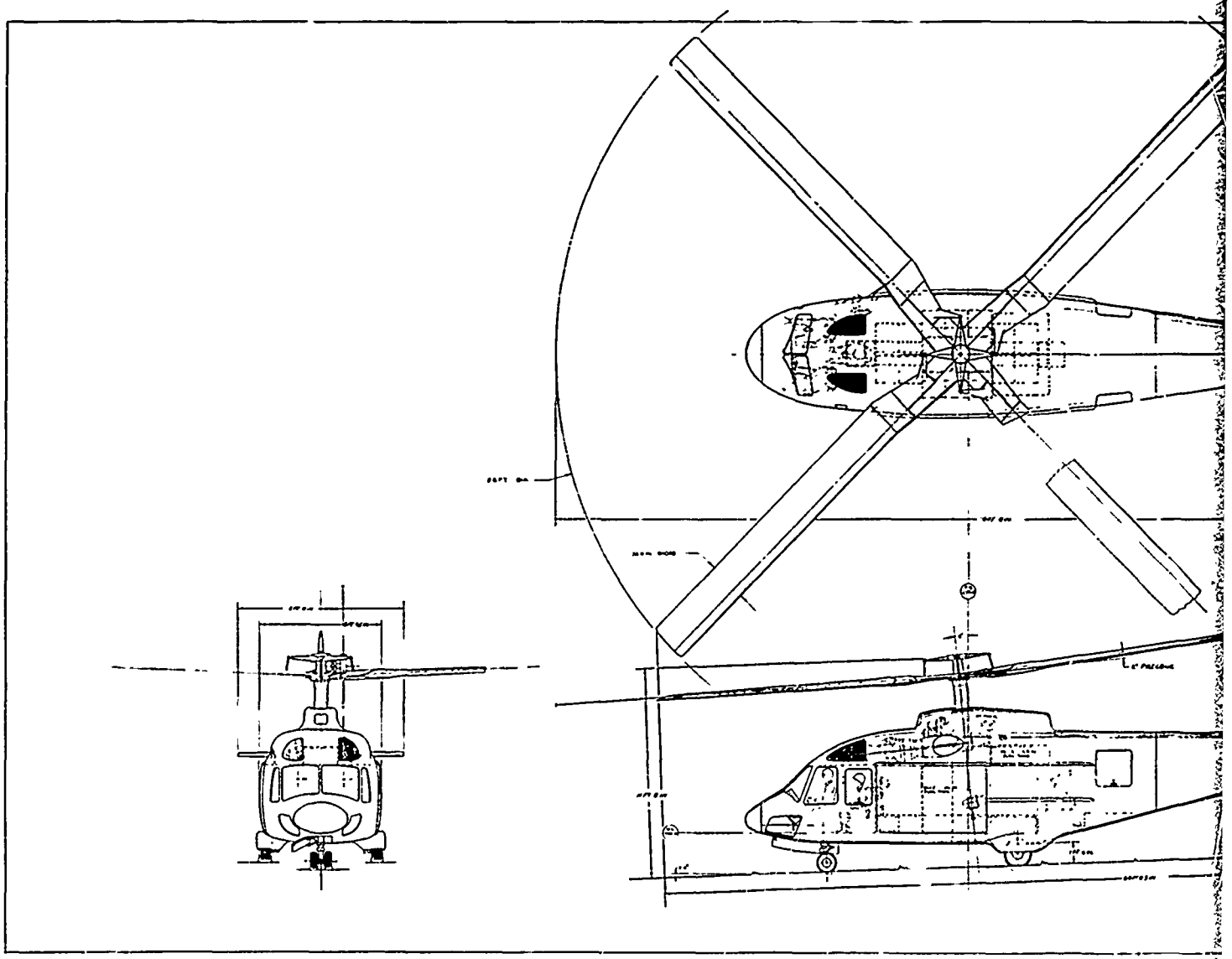

Figure 1. General Arrangement of 1.75 g Helicopter (CL 1120-2).

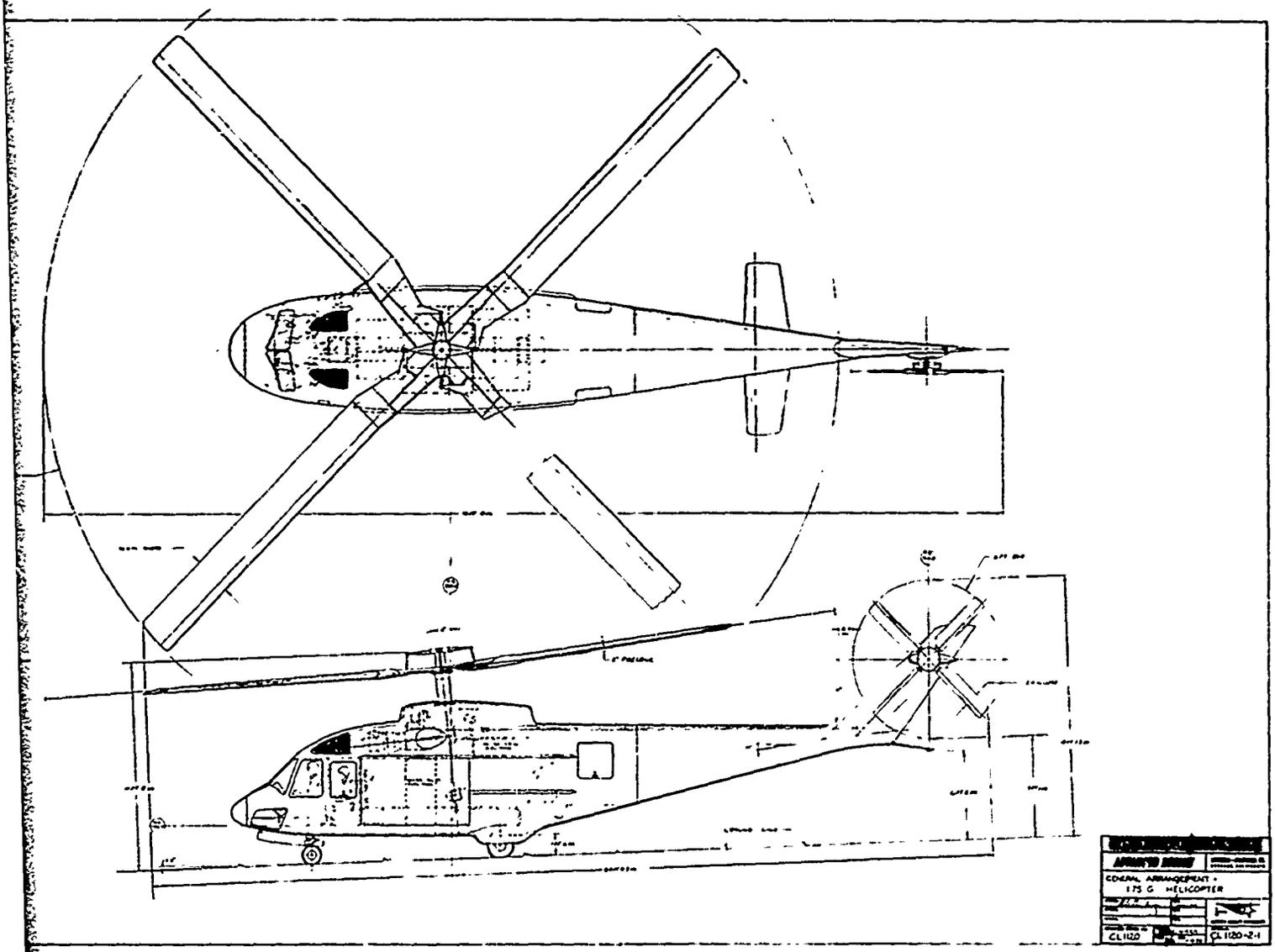

5 g Helicopter (CL 1120-2).

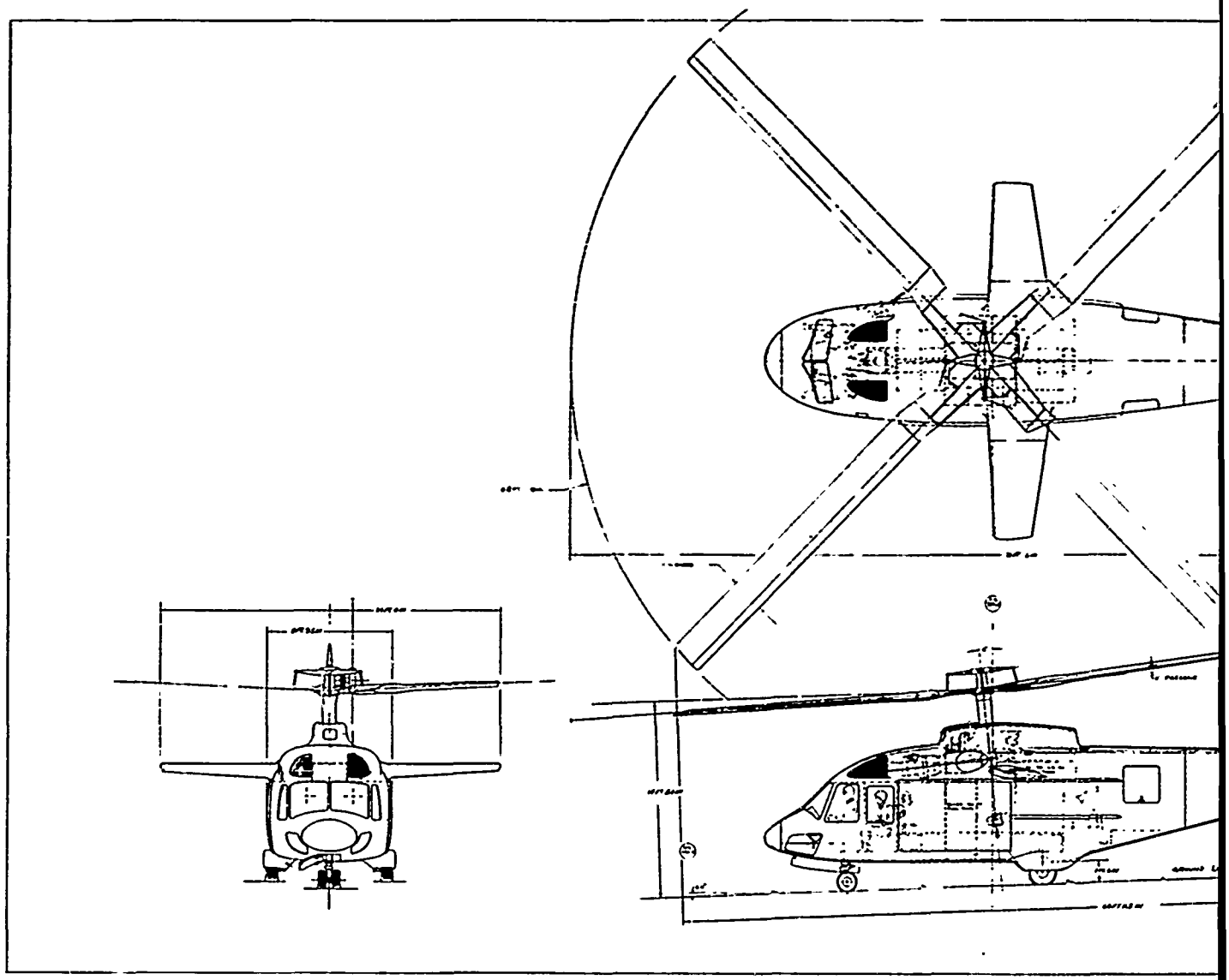

Figure 2. General Arrangement of 1.75 g Winged Helicopter (CL 1120-5).

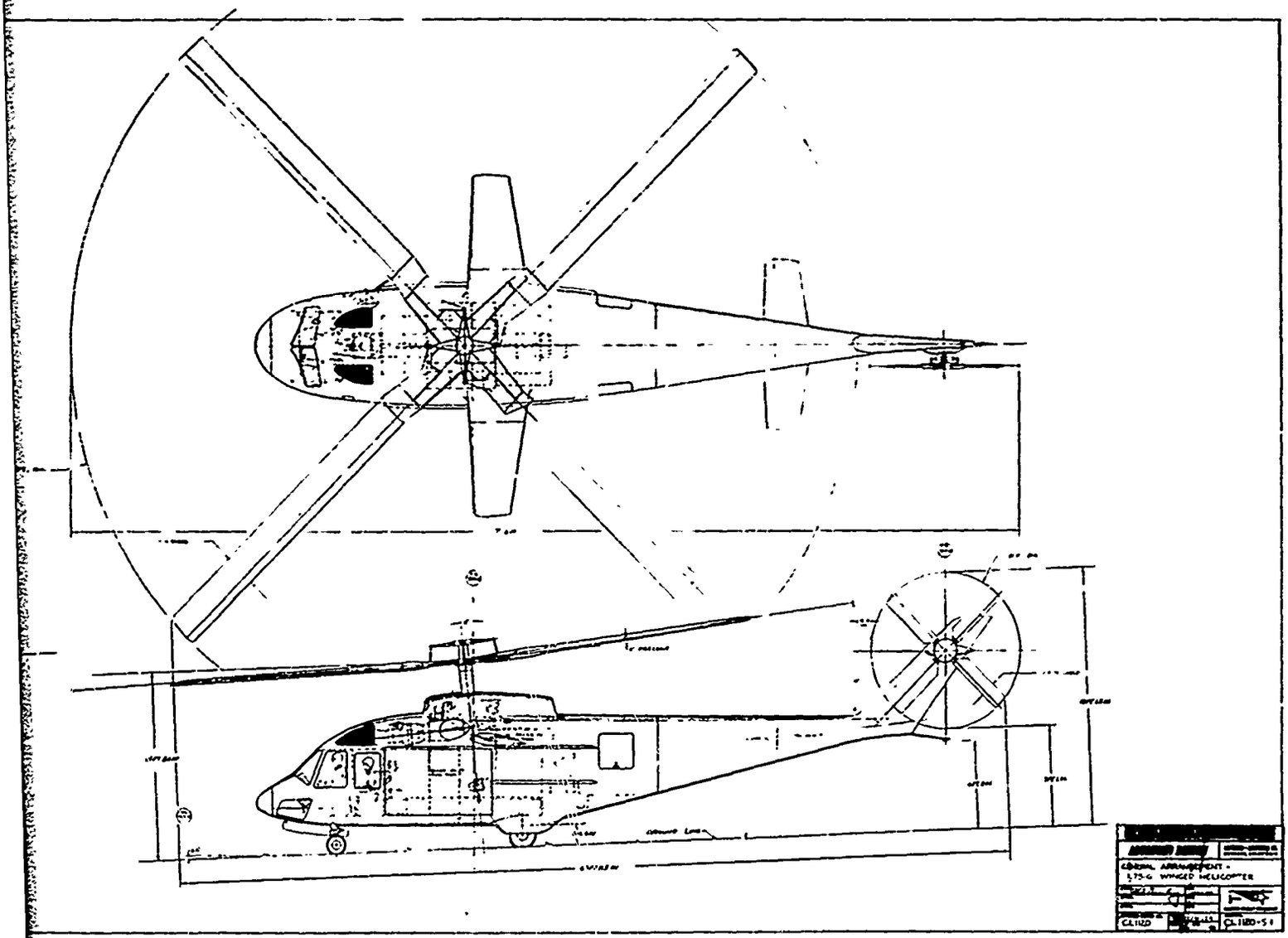

nt of 1.75 g Winged
20-5).

1.2 DESCRIPTION OF BASIC AIRCRAFT FEATURES

The hypothetical aircraft* synthesized for this study were derived from specified baseline features which are shown in Table I and the mission requirements of the UTTAS concept* described in Reference 1. This was done to ensure that the aircraft could accommodate fixed equipment and disposable load of a realistic UTTAS. The general arrangements of representative helicopter and winged helicopter configurations are shown in Figures 1 and 2, respectively. Table II summarizes the physical characteristics of all the aircraft analyzed. Brief descriptions of the main rotor and wing design concepts follow.

1.2.1 Rotor Design Concept

The main rotor is a hingeless rotor having four constant-chord blades with tapered thickness tips. The blades have an NACA 0012 airfoil section extending from 22.8 to 80 percent of the radius, and the sections then taper linearly to an NACA 0009 section at the tip. Potential improvements arising from more elaborate tip designs or trade-offs between camber and thickness variation were not investigated. The blades incorporate a negative linear twist of 5 deg measured from the rotor centerline to the tip.

Considerations influencing the amount of negative blade twist included hovering and vertical climb efficiency in the low-speed regime and alleviation of oscillatory loads, retreating blade stall and advancing-blade negative lift in the high-speed regime where the rotor is required to produce high propulsive force.

1.2.2 Wing Design Concept

Previous experience provided a guide to wing design. Each wing of the pertinent planform area has an aspect ratio of 6, a taper of 0.5 and an airfoil distribution which tapers from an NACA 23020 section at the fuselage centerline to an NACA 23015 section at the tip. The wings incorporate a negative linear twist of 3 deg measured from the fuselage centerline to the tip. The

*Lockheed model designations are used to identify these aircraft throughout the report: the analysis models of this study are designated model(s) CL 1120; the Reference 1 design was designated CL 1100.

quarter-chord is the zero sweepback chordline. A dihedral of 2 deg is used. Table II gives the geometric incidence at the mean aerodynamic chord with respect to both the rotor shaft normal plane and the fuselage waterline reference. The zero-lift chordline of the wing is 1.1 deg from the geometric chordline. Consequently, the effective incidence is 1.1 deg greater than the geometric incidence.

Longitudinal placement of the wings was selected to give desirable longitudinal stability characteristics.

1.3 METHODS OF ANALYSIS

The preliminary design technique used for synthesizing the various aircraft (the baseline helicopter configurations) includes the hover and vertical climb strip analysis and the conventional forward flight balance-of-force method of Reference 1.

The bulk of the analytical results discussed in this report were obtained from Lockheed's flight simulation computer program, REXOR (see Appendix II). It is a digital flight simulation technique, especially suited to provide time histories of various aircraft and rotor system behavioral characteristics during steady and transient maneuvers. The method embodies many degrees of freedom, 21 of which were used for the analyses:

- Six rigid-body motions (three translational and three rotational)
- First and second flapwise bending modes for each of four independently acting rotor blades
- First in-plane mode for each of the four blades
- Pitch, roll, and plunge motions of the control gyro

A graphic description of the method is shown in Figure 3.

The method involves the superposition of preestablished mode shapes. Aerodynamic loads are developed through the synthesis of two-dimensional airfoil data stored in the program for the full spectra of Mach numbers and angles of attack (the effects of compressibility, stall, and reverse flow are accounted for). The method also covers variations in airfoil thickness.

TABLE II. PHYSICAL CHARACTERISTICS

Characteristic	Configuration No. 1	2	3	4	5	6
	Value					
Main Rotor						
Diameter, ft	58.00	58.00	58.00	58.00	58.00	58.00
Number of blades	4	4	4	4	4	4
Disc loading, lb/sq ft	6.06	6.06	6.06	6.06	6.06	6.06
Solidity	0.10	0.12	0.14	0.09	0.10	0.12
Blade chord, in.	27.3	32.8	38.2	24.6	27.3	32.8
Airfoil section designation						
At root	NACA 0012	NACA 0012	NACA 0012	NACA 0012	NACA 0012	NACA 0012
At 80% of radius	NACA 0012	NACA 0012	NACA 0012	NACA 0012	NACA 0012	NACA 0012
At tip	NACA 0009	NACA 0009	NACA 0009	NACA 0009	NACA 0009	NACA 0009
Blade twist, deg	-5	-5	-5	-5	-5	-5
Blade precone, deg	2	2	2	2	2	2
Tip speed, ft/sec	700	700	700	700	700	700
Shaft incidence - forward, deg	6	6	6	6	6	6
Tail Rotor						
Diameter, ft	11	11	11	11	11	11
Number of blades	4	4	4	4	4	4
Solidity	0.20	0.24	0.28	0.20	0.24	0.28
Blade chord, in.	10.4	12.4	14.5	10.4	12.4	14.5
Airfoil designation	NACA 0009	NACA 0009	NACA 0009	NACA 0009	NACA 0009	NACA 0009
Blade twist, deg	0	0	0	0	0	0
Tip speed, ft/sec	700	700	700	700	700	700
Distance from main rotor centerline, ft	35.33	35.33	35.33	35.33	35.33	35.33
Wing						
Span, ft	-	-	-	20.78	24.00	26.83
Wing area, sq ft	-	-	-	72	96	120
Aspect ratio	-	-	-	6	6	6
Taper ratio	-	-	-	0.5	0.5	0.5
Chord						
At root (fuselage centerline), ft	-	-	-	4.62	5.33	5.96
At tip, ft	-	-	-	2.31	2.67	2.98
Mean aerodynamic, ft	-	-	-	3.59	4.15	4.64
Distance of M.A.C. c/4 behind main rotor centerline, ft	-	-	-	1.08	0.83	0.74
Airfoil designation						
At root (fuselage centerline)	-	-	-	NACA 23020	NACA 23020	NACA 23020
At tip	-	-	-	NACA 23015	NACA 23015	NACA 23015
Incidence, deg						
Mean aerodynamic chord to rotor shaft normal plane	-	-	-	11	11	11
At mean aerodynamic chord (fuselage reference)	-	-	-	5	5	5
At root (fuselage centerline)	-	-	-	6.3	6.3	6.3
At tip	-	-	-	3.3	3.3	3.3
Sweepback at 25% chord, deg	-	-	-	0	0	0
Dihedral, deg	-	-	-	2.0	2.0	2.0

TABLE II. Continued

Characteristic	Configuration No. 1	2	3	4	5	6
	Value					
Horizontal Tail						
Span, ft	12.00	12.00	12.00	12.00	12.00	12.00
Area, sq ft	36	36	36	36	36	36
Aspect ratio	4	4	4	4	4	4
Taper ratio	0.67	0.67	0.67	0.67	0.67	0.67
Chord						
At root (fuselage centerline), ft	3.60	3.60	3.60	3.60	3.60	3.60
At tip	2.40	2.40	2.40	2.40	2.40	2.40
Mean aerodynamic, ft	3.04	3.04	3.04	3.04	3.04	3.04
Airfoil section designation	NACA 0012	NACA 0012	NACA 0012	NACA 0012	NACA 0012	NACA 0012
Incidence, deg	-3.5	-3.5	-3.5	-2.5	-2.5	-2.5
Vertical Tail						
Span, ft	6.92	6.92	6.92	6.92	6.92	6.92
Area, sq ft	30	30	30	30	30	30
Aspect ratio	1.6	1.6	1.6	1.6	1.6	1.6
Effective aspect ratio	2	2	2	2	2	2
Taper ratio	0.5	0.5	0.5	0.5	0.5	0.5
Chord						
At root, ft	5.77	5.77	5.77	5.77	5.77	5.77
At tip, ft	2.88	2.88	2.88	2.88	2.88	2.88
Mean aerodynamic, ft	4.49	4.49	4.49	4.49	4.49	4.49
Distance of M.A.C. c/4 from main rotor centerline, ft	32.25	32.25	32.25	32.25	32.25	32.25
Incidence, deg	0	0	0	0	0	0
Sweepback at 25% chord, deg	51	51	51	51	51	51
General Dimensions and Clearances						
Overall width						
Rotors operating	58 ft 0 in.	58 ft 0 in.	58 ft 0 in.	58 ft 0 in.	58 ft 0 in.	58 ft 0 in.
Rotors static	41 ft 8 in.	41 ft 8 in.	41 ft 8 in.	41 ft 8 in.	41 ft 8 in.	41 ft 8 in.
Overall length						
Rotors operating	70 ft 0 in.	70 ft 0 in.	70 ft 0 in.	70 ft 0 in.	70 ft 0 in.	70 ft 0 in.
Rotors static	60 ft 11.3 in.	60 ft 11.3 in.	60 ft 11.3 in.	60 ft 11.3 in.	60 ft 11.3 in.	60 ft 11.3 in.
Height						
To main rotor	14 ft 8.0 in.	14 ft 8.0 in.	14 ft 8.0 in.	14 ft 8.0 in.	14 ft 8.0 in.	14 ft 8.0 in.
To top of tail rotor operating	18 ft 1.3 in.	18 ft 1.3 in.	18 ft 1.3 in.	18 ft 1.3 in.	18 ft 1.3 in.	18 ft 1.3 in.
Ground clearance						
Fuselage	1 ft 6.0 in.	1 ft 6.0 in.	1 ft 6.0 in.	1 ft 6.0 in.	1 ft 6.0 in.	1 ft 6.0 in.
Tail rotor	7 ft 1.0 in.	7 ft 1.0 in.	7 ft 1.0 in.	7 ft 1.0 in.	7 ft 1.0 in.	7 ft 1.0 in.
Landing gear						
Tread of main wheels	8 ft 1 in.	8 ft 1 in.	8 ft 1 in.	8 ft 1 in.	8 ft 1 in.	8 ft 1 in.
Wheel base	13 ft 8.5 in.	13 ft 8.5 in.	13 ft 8.5 in.	13 ft 8.5 in.	13 ft 8.5 in.	13 ft 8.5 in.
Troop compartment						
Height	4 ft 8.0 in.	4 ft 8.0 in.	4 ft 8.0 in.	4 ft 8.0 in.	4 ft 8.0 in.	4 ft 8.0 in.
Width	8 ft 4.5 in.	8 ft 4.5 in.	8 ft 4.5 in.	8 ft 4.5 in.	8 ft 4.5 in.	8 ft 4.5 in.
Length	20 ft 9.0 in.	20 ft 9.0 in.	20 ft 9.0 in.	20 ft 9.0 in.	20 ft 9.0 in.	20 ft 9.0 in.

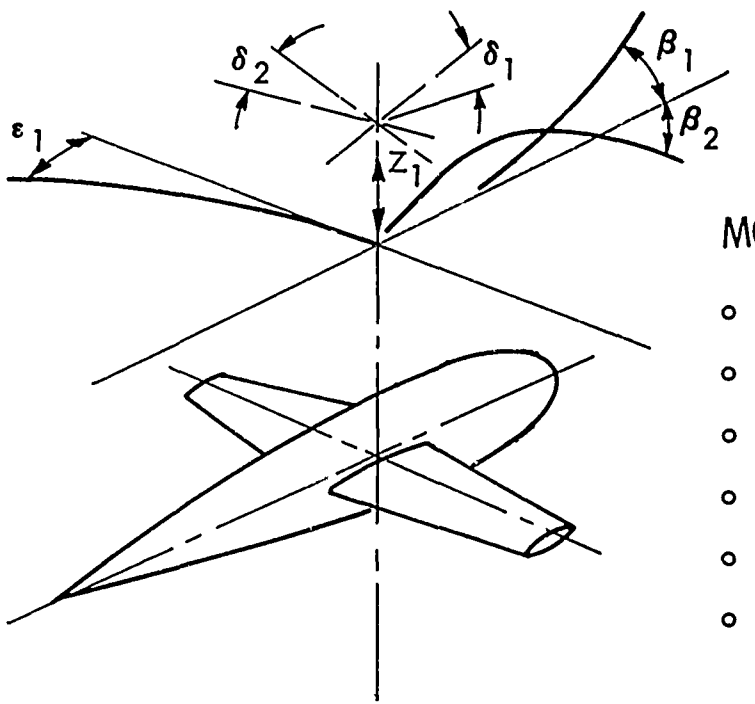

MODEL INCLUDES:

- 21 DEGREES OF FREEDOM
- NONLINEAR c_l, c_d, AND c_m
- TIME DEPENDENT AERODYNAMICS
- VARIABLE INFLOW
- VEHICLE MASS AND MOM. OF INERTIA
- VEHICLE DIMENSIONS SUCH AS CG POSITIONS AND LOCATIONS OF TAIL ROTOR
- DIGITAL LOAD TIME HISTORY SOLUTION

  USED IN SOLUTIONS OF PROBLEMS CONCERNING STABILITY, HANDLING QUALITIES AND TRANSIENT LOADS

Figure 3. Flight Simulation Mathematical Model (REXOR).

2.0 DISCUSSION

2.1 GENERAL

Aerodynamically, very high rotor thrust (at correspondingly high blade loading coefficients) involving considerable rotor stall is attainable at high advance ratios. However, as illustrated in Figure 4, test data relating blade loading coefficient to advance ratio indicate that the maximum thrust diminishes considerably with forward speed.* Excessive blade stall and compressibility significantly influence this maximum capability. Accordingly, the practical limit is a result of oscillatory rotor loads and dynamic instabilities, and is the controlling limit on rotor thrust capability at high advance ratios.

The steep rise in required power resulting from operation under conditions of excessive blade angles of attack and penetrating into blade stall is an index of the extent to which rotor load factor can be increased before operating limitations attending excessive oscillatory rotor loads and vibration are incurred. The problem of relating increasing rotor profile torque coefficient or profile power coefficient to permissible penetration into blade stall is well documented in the literature (see, for example, References 2 through 9).

The degree of blade stall and the region of the rotor disc operating in stall, factors which strongly influence rotor propulsive force, most critically affect steady-state maneuver load factor capability as distinct from the capability of attaining highly transient maneuver load factors. The coordinated turns treated in this study (enduring approximately 3 seconds) are assumed to fall between these extremes.

---

*The peak maneuver load factors shown in Figure 4 are not indicative of sustained maneuvers. The flight test points pertain to blade loading coefficients achieved in very short-duration maneuvers. The wind tunnel test points are regarded as transitory because propulsive forces provided by rotors would not have prevented deceleration or loss of altitude in free flight situations.

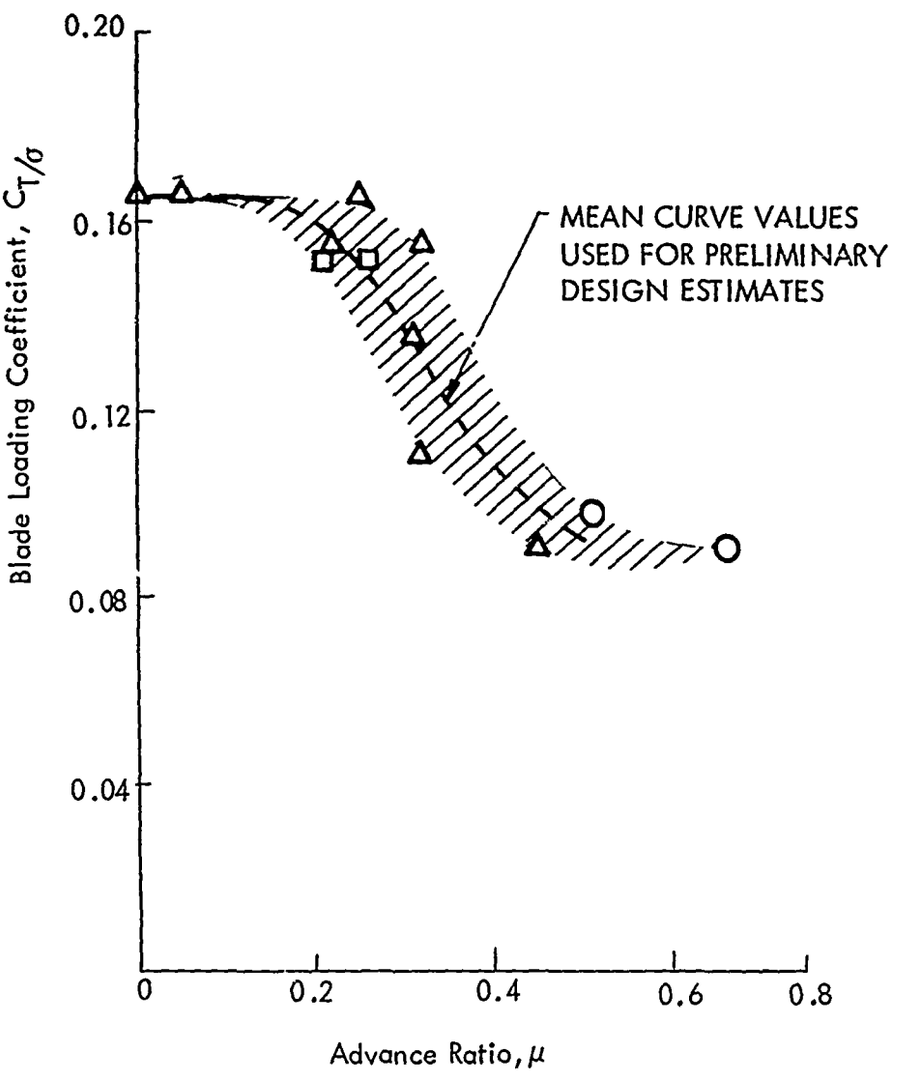

Figure 4. Blade Loading Coefficients for Short-Duration Maneuvers.

Blade angle of attack and lift coefficient were monitored at 93.6 percent of rotor blade radius in the analyses (see Figure 5). This location lies in a region of the blade where blade stall is strongly affected by the varying downwash distribution. Loads were monitored at the blade root.

Comparison of histories of the blade angles of attack and the lift coefficients which develop during coordinated turns indicates that the rotor blades of corresponding unwinged and winged configurations undergo similar variations in these parameters; and consequently, the corresponding configurations experience approximately the same limiting conditions during maneuvers. This comparison can be seen by referring to Figures 54 through 59, which show calculated time history plots of the six configurations analyzed; parts i and j of these figures show the variations of angle of attack and lift coefficient with time. For example, Figure 54i shows the angle of attack history for Configuration 1, a nonwinged helicopter, while performing a coordinated turn at 140 KTAS; Figure 57i shows the angle of attack history for Configuration 4, the comparable winged helicopter, while performing the same maneuver. The two angle of attack histories shown are almost identical. A comparison of Figures 54j and 57j shows the similarity of the histories of the lift coefficients for these same two configurations. Comparisons of these parameters for the other configurations show the same similarities. It is therefore rationalized that since angle of attack and lift coefficient histories are approximately the same for the winged and nonwinged helicopters, limiting conditions in rotor behavior expected to be encountered during maneuvers will not be influenced significantly by addition or deletion of the wing. Oscillatory rotor loads and helicopter vibrations might become unacceptable before the rotor encounters aerodynamic limitations, however. The angle of attack in the region of the retreating blade tip depends principally upon (1) the advance ratio μ, (2) the blade loading coefficient C_T/σ, and (3) the ratio of parasite drag to lift, that is,the degree to which the thrust vector must tilt to overcome the drag of the nonrotating airframe.

The maximum thrust (and therefore maneuver load factor) capability of a rotor intended for use in a particular flight speed regime is principally a function

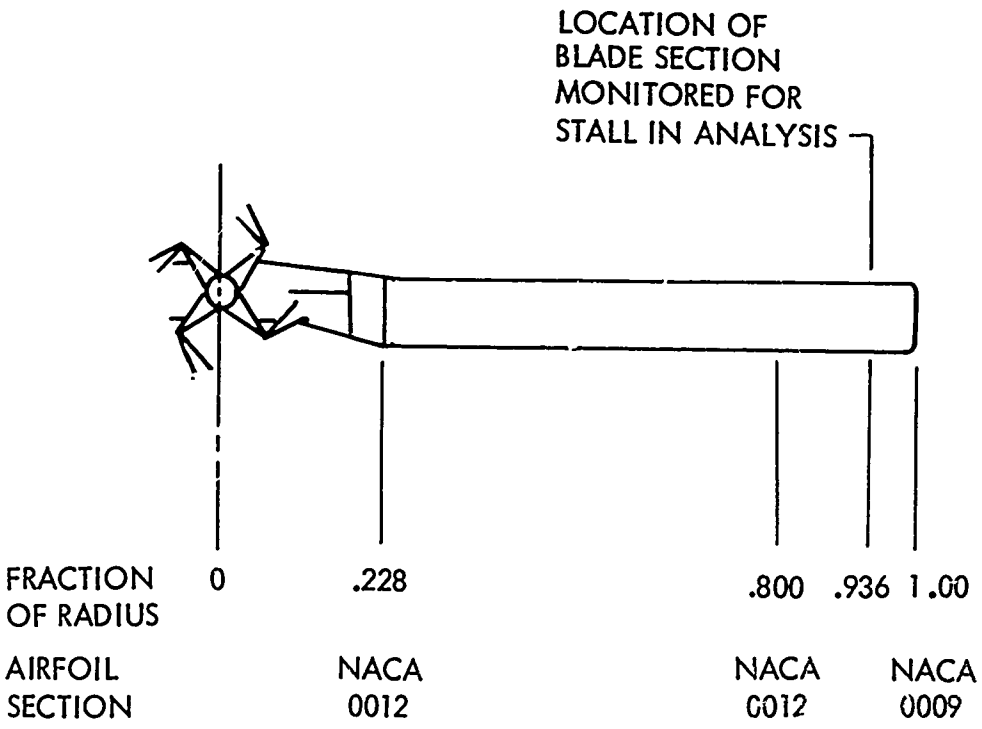

Figure 5. Rotor Blade Description.

of blade loading coefficient, C_T/σ. Reduction of the design blade loading coefficient is a powerful means of mitigating blade stall.

Another means of varying blade loading in high-speed maneuvering flight involves the use of a wing. After a rotor solidity is determined which accommodates a specified high-speed, high-load-factor maneuver, a certain amount of solidity (as limited by drag and rotor propulsive force requirements) can be exchanged for wing area.

Important considerations relating to the effects of maneuverability design considerations on performance, stability and control, rotor oscillatory loads and vibration, and maneuvering capability, as determined from results of the analytical study, are discussed in the following sections.

2.2 RESULTS OF TRANSIENT MANEUVER ANALYSES

Based on the preliminary design considerations discussed in Section 1.0 and prior experience, three unwinged helicopter point designs and three winged helicopter point designs were synthesized to satisfy three maximum maneuver load factor capabilities: 1.5, 1.75, and 2.0. Maneuver capability analyses were performed for each configuration to determine the impact of various maneuverability criteria on design parameters and operational characteristics.

Considerations of the effects of the wing on performance, stability and control, structural loads, and maneuver characteristics provided a guide to the design and placement of the wings.

2.2.1 Aircraft Weights and Sizes

Preliminary sizing of the basic CL 1120 was based on the design mission requirement which led to the UTTAS design concept, the CL 1100, described in Reference 1. This sizing was done to ensure that the study aircraft could accommodate the fixed equipment and disposable load of a realistic UTTAS. To obtain a preliminary estimate of the effect of maneuverability on fuel requirements, the fuel required to accomplish the original UTTAS design mission was determined for the boundary values initially established for solidity, 0.09 to 0.12 (see Table III). It was found that some fixed equipment specified for the UTTAS would have to be eliminated in order to retain the UTTAS

TABLE III. PRELIMINARY ESTIMATE OF MISSION FUEL REQUIRED

Segment Number*	Segment	Time (min)	CL 1100** (lb fuel)	CL 1120, σ = 0.09 (lb fuel)	CL 1120, σ = 0.12 (lb fuel)
(1)	WUTO and accel	6.0	128	99	98
(2)	Cruise	67.5	898	994	941
(3)	Loiter	16.5	185	148	150
(4)	Hover and Land	2.0	39	30	30
(5)	Takeoff	2.0	35	27	28
(6)	Dash	16.5	379	292	289
(7)	Cruise	48.0	610	569	598
(8)	Hover and Land	6.5	106	80	86
(9)	Reserve	20.0	251	232	245
	Total	185.0	2631	2471	2465

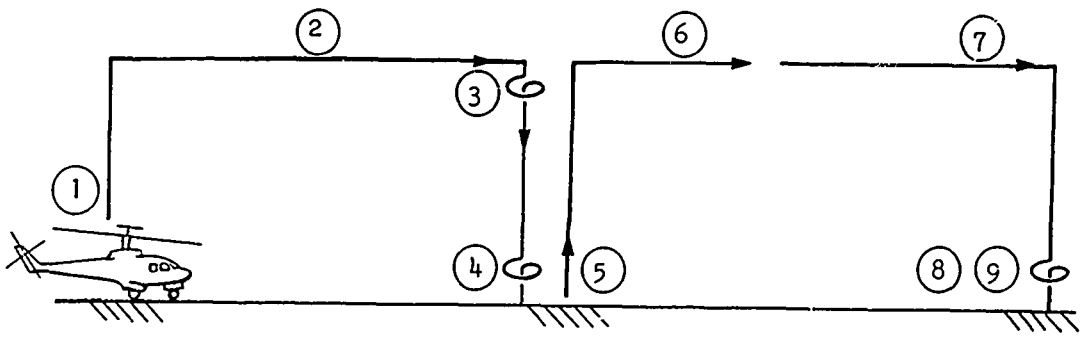

*Design mission segment numbers.

**CL 1100 fuel required included for comparison; no off-loading of basic equipment required for full fuel and payload.

disposable load and the design gross weight established for this study. Alternatively, the fixed equipment could be retained and the disposable load could be considered alterable. The latter method was adopted for this study. However, in order to arrive at a representative fuel system weight, accommodation was made for 2500 lb of fuel for all configurations.

The principal aerodynamic characteristics of the airframe (aircraft minus blades) were derived using the methods employed in the earlier UTTAS study (see Reference 1). The basis of the drag buildup for the three unwinged helicopters minus blades is given in Table IV. The calculated values of lift, drag, and pitching moments of the airframe for unit dynamic pressure are presented as functions of angles of attack in Figures 6, 7, and 8 for all six of the study aircraft models. The angles of attack shown are the reference angles of attack used in the maneuverability analysis. In addition, each figure includes an auxiliary scale showing angle of attack in terms of the fuselage waterline reference. This scale allows for the 6-degree tilt of the rotor shaft with respect to the fuselage.

Wing drag characteristics were determined on the basis of methods presented in Reference 1 and added to the minimum drag of the unwinged aircraft minus blades of Table IV to obtain the drag characteristics of the winged helicopters, Configurations 4, 5, and 6 (see Figure 7). Lift and moment characteristics were obtained in a similar manner and are shown in Figures 6 and 8. The maximum value of the lift parameter L_A/q for each of the winged configurations corresponds to C_{L_A} of 1.3. Since the wing-span to rotor-diameter ratio is relatively low (less than 0.5), the hover download due to the presence of the wings is small.

The principal physical characteristics of the various configurations are given in Table II. Table V gives a detailed weight breakdown for each configuration. Table VI gives aircraft moment of inertia characteristics.

2.2.2 Engine Size

Engine size, as represented by power and weight, was based on using two Pratt & Whitney ST 9 engines; power levels for these engines were allowed

TABLE IV. BASIS OF DRAG BUILDUP FOR BASIC HELICOPTERS*

AIRCRAFT MINUS BLADES

Component	D_A/q, ft^2	
Fuselage	3.80	
Engine Fairing	0.11	
Horizontal Tail	0.36	
Vertical Tail	0.30	
Landing Gear	0.43	
Protrusions,		
Local Interference, etc.	5.00	
		10.00
Main Rotor Hub	6.00	
Rotor-Fuselage Interference	1.00	
Tail Rotor Hub	1.00	
		8.00
TOTAL		18.00

*Drag, including the pertinent lift of the wing and of the horizontal tail at their respective incidence settings, is reflected in the minimum D_A/q values for all configurations in Figure 7.

TABLE V. CONFIGURATION COMPARATIVE WEIGHT BREAKDOWN

Component	Configuration No. 1	2	3	4	5	6
	Weight (lb)					
Rotor Group	2,029	2,270	2,495	1,901	2,029	2,270
Tail Rotor	123	124	126	122	123	124
Empennage	139	139	139	139	139	139
Wing	0	0	0	198	249	298
Body Group and Engine Section	2,140	2,140	2,140	2,140	2,140	2,140
Alighting Gear	494	494	494	494	494	494
Flight Controls	725	854	979	661	726	854
Engines (2)	605	621	641	604	609	624
Transmission and Shafting	1,244	1,255	1,265	1,243	1,246	1,257
Miscellaneous Propulsion	282	287	294	281	283	288
Fuel System	383	383	383	383	383	383
Propulsion System Total	2,514	2,546	2,583	2,511	2,521	2,552
Auxiliary Power plant	149	149	149	149	149	149
Instruments	166	166	166	166	166	166
Hydraulic and Electrical	344	344	344	344	344	344
Electronics	783	783	783	783	783	783
Armament	424	424	424	424	424	424
Furnishings and Equipment (with seats for 15 troops)	568	568	568	568	568	568
Air Conditioning and Anti-Ice	280	280	280	280	280	280
Empty Weight (dry)	10,878	11,281	11,670	10,880	11,135	11,585
Oil including unusable	10	10	11	10	10	10
Unusable Fuel	36	36	36	36	36	36
Flight Crew (2)	400	400	400	400	400	400
Minimum Operating Weight Empty	11,324	11,727	12,117	11,326	11,581	12,031
Gunner	200	200	200	200	200	200
Ammunition	100	100	100	100	100	100
Special Operating Weight Empty	11,624	12,027	12,417	11,626	11,881	12,331
Allowable Fuel and Payload	4,376	3,973	3,583	4,374	4,119	3,669
Gross Weight	16,000	16,000	16,000	16,000	16,000	16,000
Selected Loading Variation No. 1						
Special Operating Weight Empty	11,624	12,027	12,417	11,626	11,881	12,331
Payload of 11 troops	2,640	2,640	2,640	2,640	2,640	2,640
Allowed Fuel	1,736	1,333	943	1,734	1,479	1,029
Gross Weight	16,000	16,000	16,000	16,000	16,000	16,000
Selected Loading Variation No. 2						
Special Operating Weight Empty	11,624	12,027	12,417	11,626	11,881	12,331
Maximum Fuel	2,500	2,500	2,500	2,500	2,500	2,500
Allowable Payload	1,876	1,473	1,083	1,874	1,619	1,169
Gross Weight	16,000	16,000	16,000	16,000	16,000	16,000

TABLE VI. AIRCRAFT MINUS BLADES MOMENT OF INERTIA AT REFERENCE CENTER OF GRAVITY

Configuration	I_{xx}	I_{yy}	I_{zz}
1	6280	33,170	28,000
2	6600	33,500	28,000
3	6830	33,500	28,000
4	6100	33,000	28,000
5	6280	33,170	28,000
6	6600	33,500	28,000

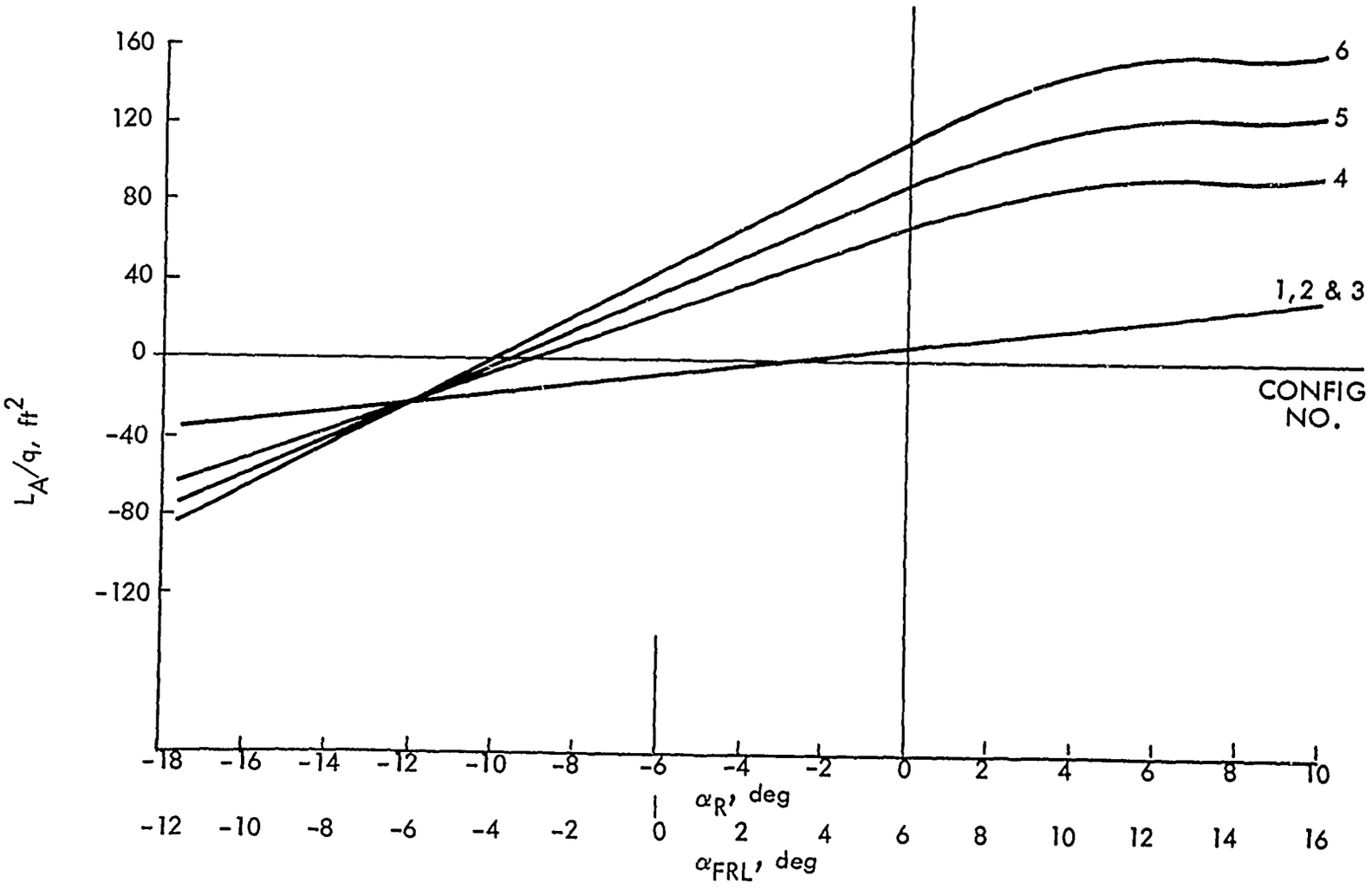

Figure 6. Lift Characteristics of Aircraft Minus Blades.

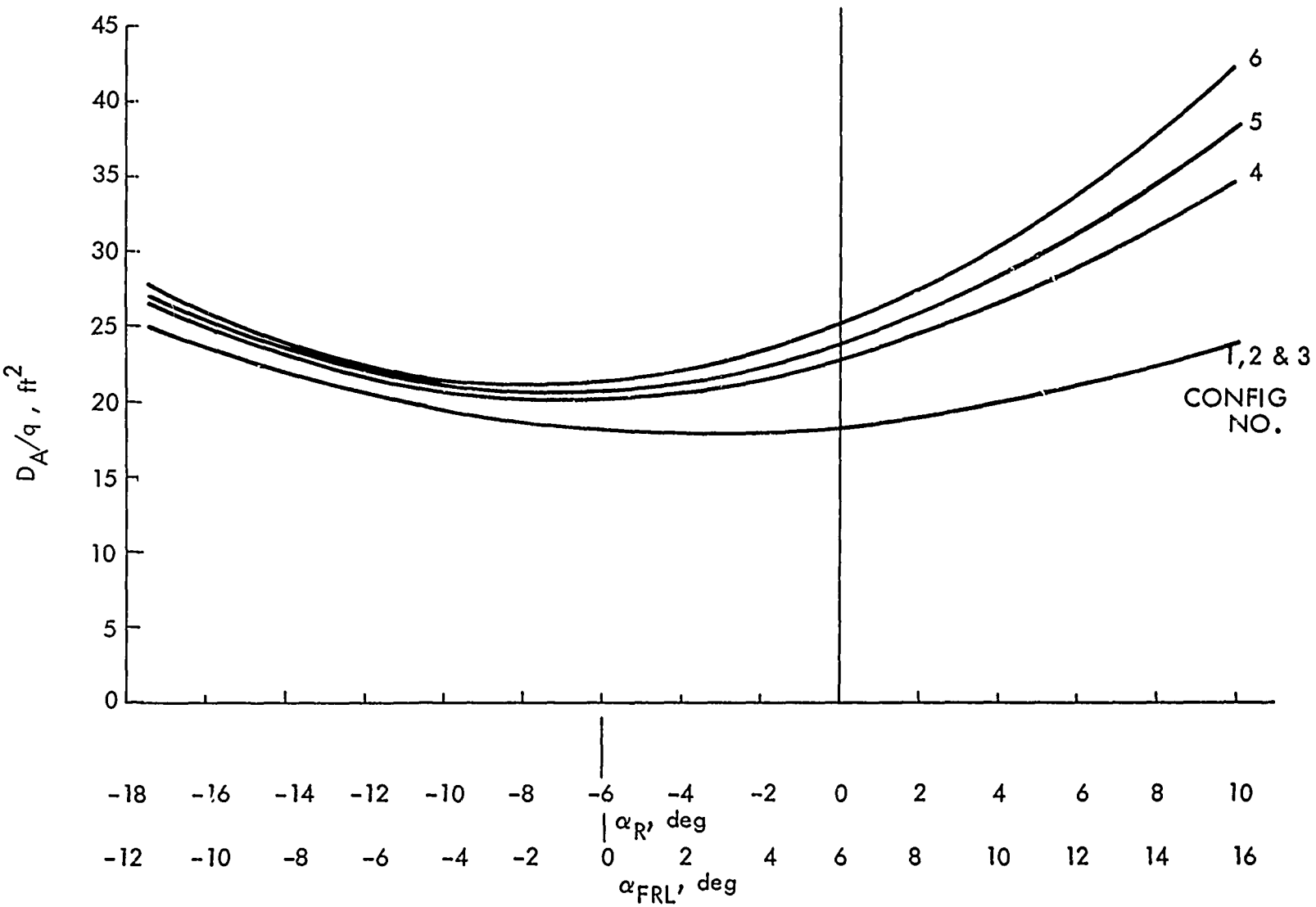

Figure 7. Drag Characteristics of Aircraft Minus Blades.

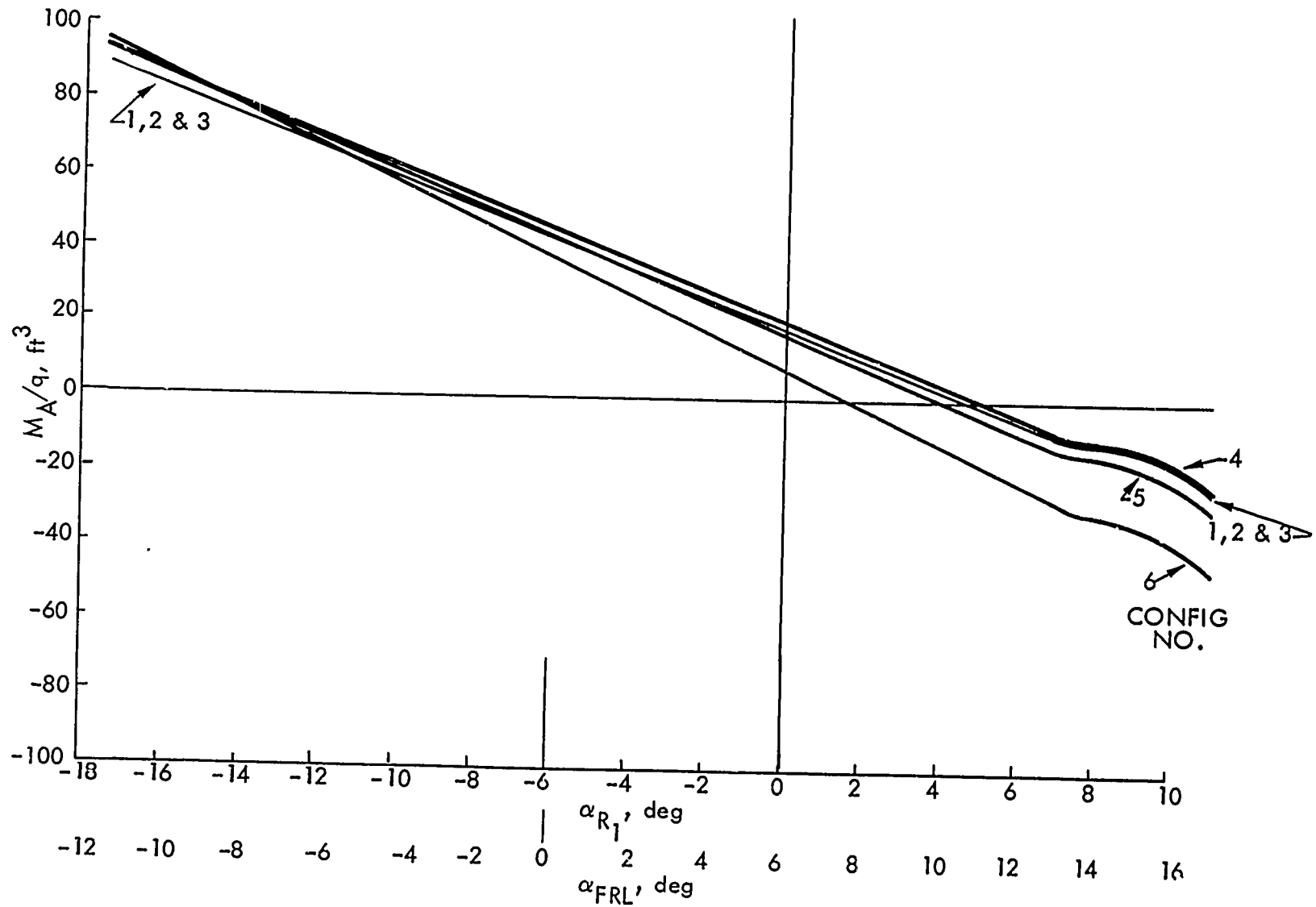

Figure 8. Moment Characteristics of Aircraft Minus Blades.

to vary as required for the analytic models, but scaling factors among relative ratings (NRP, MRP, etc.) were retained. The criterion used in establishing the installed power for each configuration was the ability to perform a 500 ft/min rate of vertical climb at a pressure altitude of 4000 feet and a temperature of 95°F. This capability was considered to exist under a no-bleed condition at 95 percent of Military Rated Power (MRP). An engine power scaling factor of 1.322 is used to derive the sea-level-static uninstalled power from that available at 4000 ft and 95°F.

Curves of total power required and Normal Rated Power (NRP) and MRP available are shown in Figures 9 through 14. All considerations of power available, other than those affecting engine size selection, take engine bleed requirements into account.

Power-required characteristics, which are reflected in engine sizing, include drive train and accessory losses. A total of 70 shp (35 shp per engine) is required to operate hydraulic pumps and electric generators. A drive efficiency of 98 percent is ascribed to the transmission and shafting system.

Tables VII and VIII summarize important power-related characteristics corresponding to the various configurations. All configurations require less than their normal rated power to attain the design cruise speed of 150 KTAS. Configuration 3 (unwinged) has the highest level-flight speed capability under both NRP and MRP conditions. However, this configuration has the highest rotor weight fraction and, consequently, the lowest combination of payload and fuel weight. Under flight conditions of hovering, vertical climb, and speed for best endurance (minimum power), the winged configurations require the least power. However, under NRP and MRP conditions, the winged configurations have somewhat inferior speed capabilities. The lower speed capabilities of the winged helicopters are not exclusively the result of their lower installed powers (climb power requirements). The gradients of the required powers with speed are highest for the winged helicopters.

As shown in Table IX, the power difference due to wing download is low (by discrete design of span/diameter ratio); in fact, the increased hover efficiency (decreased profile power) attending the reduced solidities adopted for the winged helicopters more than compensates for the download effect.

TABLE VII. PERFORMANCE SUMMARY AT DESIGN ATMOSPHERE AND RELATED POWER DATA*

Configuration No.	1	2	3	4	5	6
Condition	Value					
Design Vertical Rate of Climb (500 FPM), 95% MRP required, shp**	2240	2323	2411	2235	2260	2335
Zero Speed, MRP, shp	2195	2275	2362	2190	2214	2286
Zero Speed, NRP, shp	1746	1810	1879	1742	1761	1820
Hover Power Required, shp	2070	2155	2240	2065	2088	2175
Speed, (KTAS) for minimum power required, shp	80 1035	80 1043	80 1098	80 1029	80 1000	80 1020
Design Cruise Speed, KTAS @ power required, shp	150 1700	150 1650	150 1705	150 1745	150 1650	150 1675
Maximum Speed, KTAS @ NRP, shp	154 1815	160 1890	161 1955	152 1805	158 1840	159 1910
Maximum Speed, KTAS @ MRP, shp	168 2290	173 2390	175 2475	164 2285	169 2320	172 2400

*Conditions: design gross weight, 16,000 lb; pressure altitude, 4000 ft; ambient temperature, 95° F; density ratio, 0.808; and speed of sound, 1155 ft/sec.

**Installed with no bleed; used to determine uninstalled power, standard sea level static conditions shown in Table VIII. All other shaft power levels in Table VII allow availability and use of engine bleed.

TABLE VIII. UNINSTALLED MILITARY POWER AT STANDARD SEA-LEVEL STATIC CONDITIONS

	Configuration No.					
	1	2	3	4	5	6
Condition	Value					
Power, shp (2 engines)	3120	3232	3352	3110	3146	3250
Power per engine, shp	1560	1616	1676	1555	1573	1625

TABLE IX. COMPARISON OF SYMMETRICAL PULL-UP AND PUSH-OVER MANEUVERS

Configuration	Nominal Load Factor Capability (n)	Forward Flight Velocity (KTAS)	Height Change Command (ft)	Maneuver Time* (sec)	Horizontal Distance to Achieve Ht Change (ft)	Extremal Maneuver Load Factors (n)		Height Deviation** (ft)	Velocity Deviation (KTAS)	Power Required (hp)		Sideslip (deg)	Lateral Displ (ft)
										Trim	Deviation		
1	1.50	140	+200	9.4	2051	1.35	0.50	20	-21.0	1440	42 -63	-3.2	-24.0
1	1.50	140	-200	9.2	2231	.61	1.44	25	14.3	1430	225 -125	2.1	8.3
2	1.75	155	+200	8.5	2089	1.48	0.32	35	-20.0	1700	60 -440	5.0	27.5
2	1.75	155	-200	8.2	2159	0.50	1.60	40	12.0	1750	500 -270	3.3	-6.1
3	2.00	167	+200	7.8	2146	1.58	0.28	30	-18.0	2200	140 -650	8.0	-22.0
3	2.00	167	-200	7.8	2165	.43	1.77	27	10.3	2200	380 -440	4.8	-9.7
4	1.50	140	+200	9.4	2108	1.35	0.50	15	-20.0	1440	45 -115	-2.9	-19.8
4	1.50	140	-200	9.2	2229	.60	1.52	20	14.0	1430	75 -125	2.0	5.8
5	1.75	155	+200	8.5	2095	1.44	0.30	30	-18.8	1700	75 -360	4.7	-19.0
5	1.75	155	-200	8.3	2200	0.52	1.72	30	11.8	1750	230 -270	3.3	-8.7
6	2.00	167	+200	7.7	2071	1.58	0.21	30	-16.7	2200	220 -580	7.0	-16.5
6	2.00	167	-200	7.7	2126	0.40	1.90	30	10.4	2200	230 -470	4.8	-10.8

*Time to accomplish commanded height change.

**Maximum amount by which helicopter overshoots commanded height change.

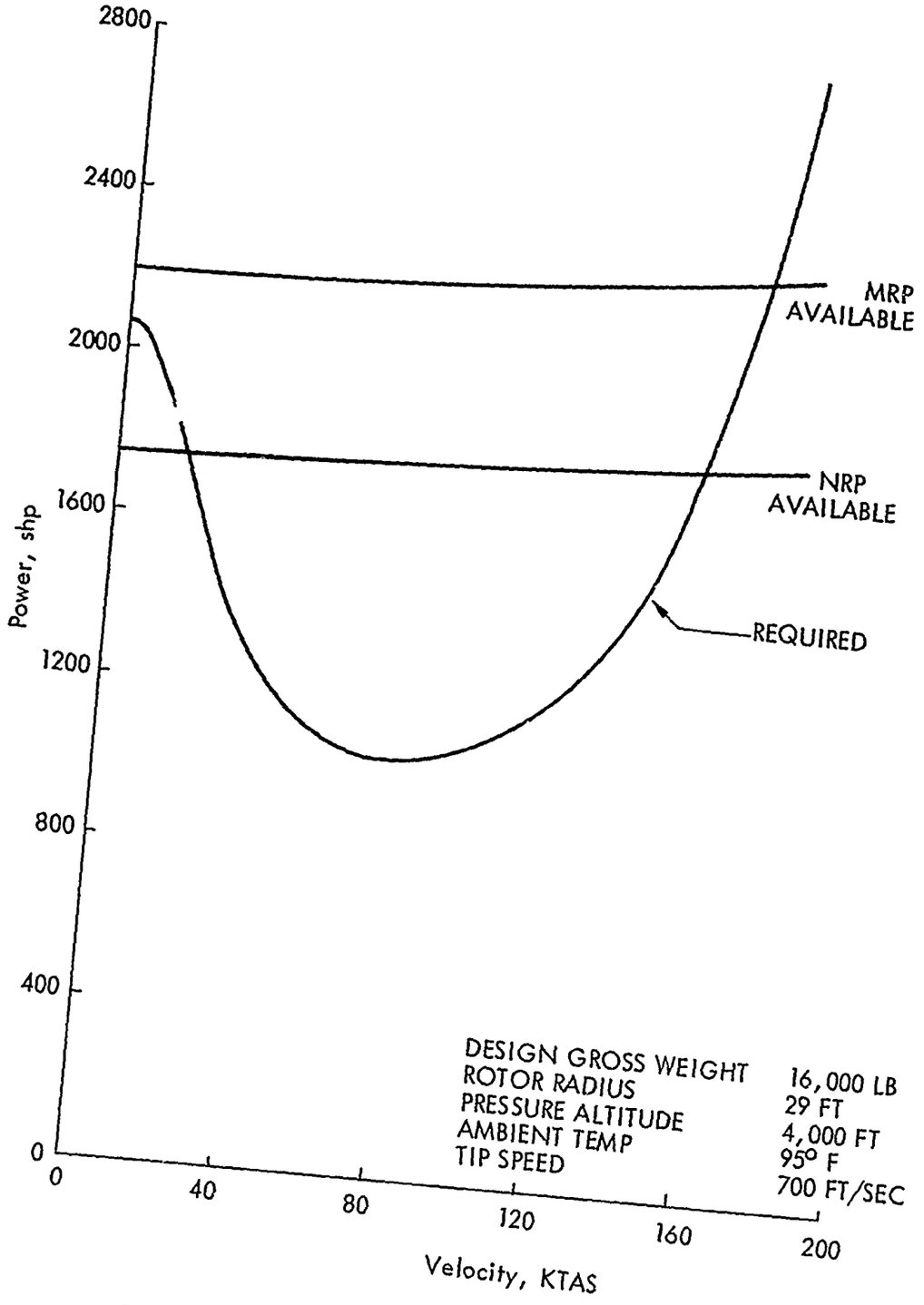

Figure 9. Power Required and Available in Level Flight for Configuration 1.

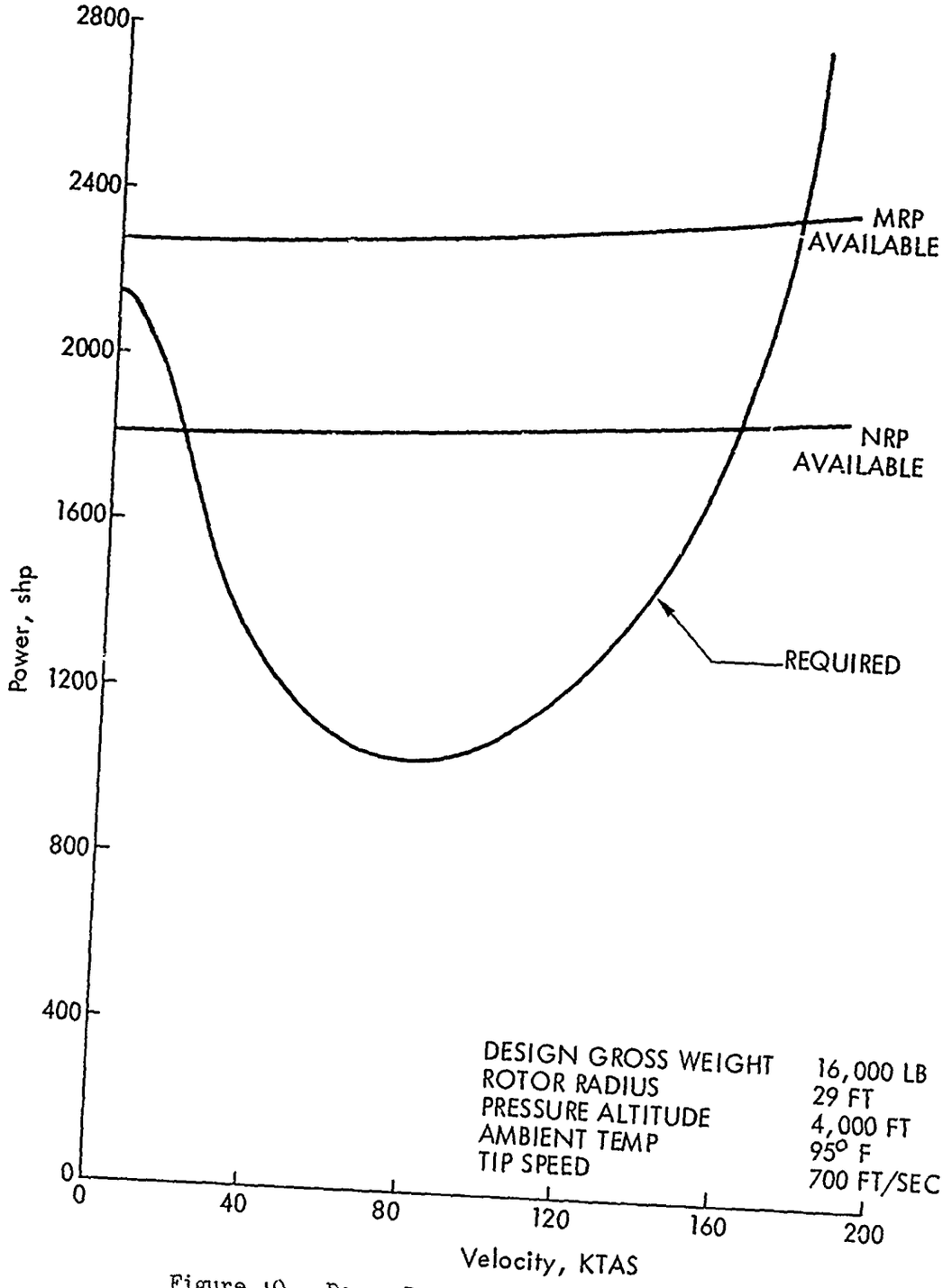

Figure 10. Power Required and Available in Level Flight for Configuration 2.

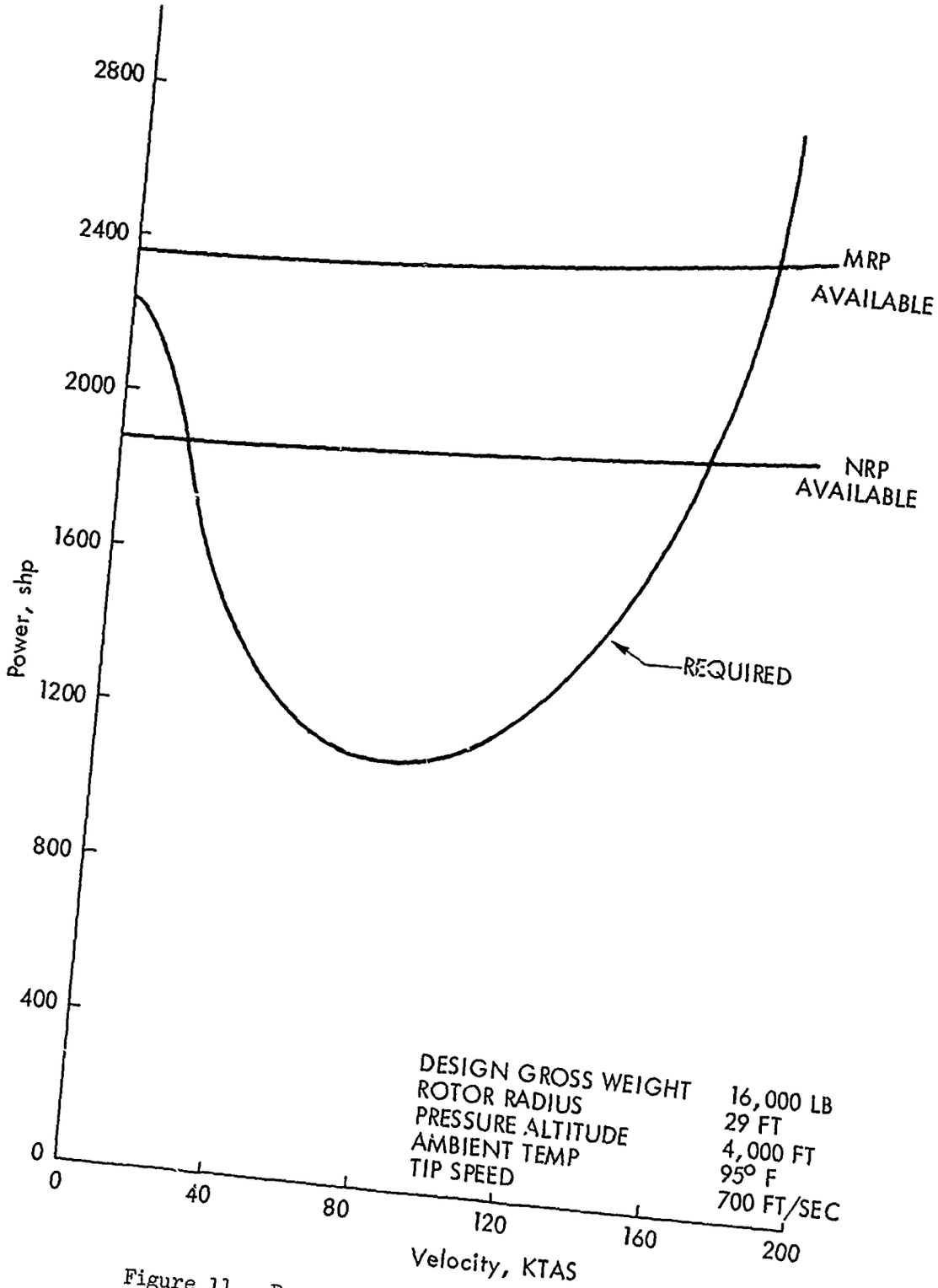

Figure 11. Power Required and Available in Level Flight for Configuration 3.

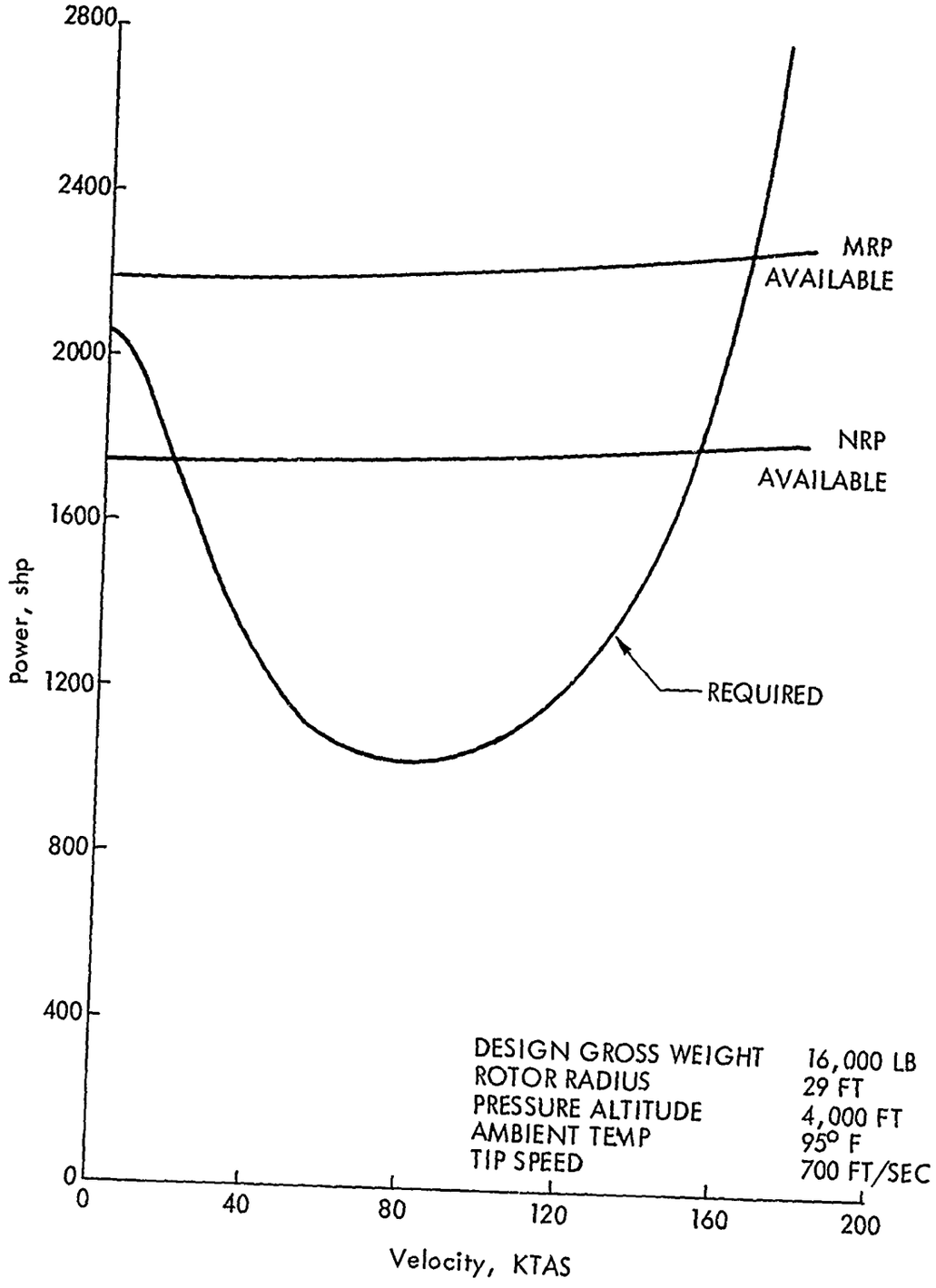

Figure 12. Power Required and Available in Level Flight for Configuration 4.

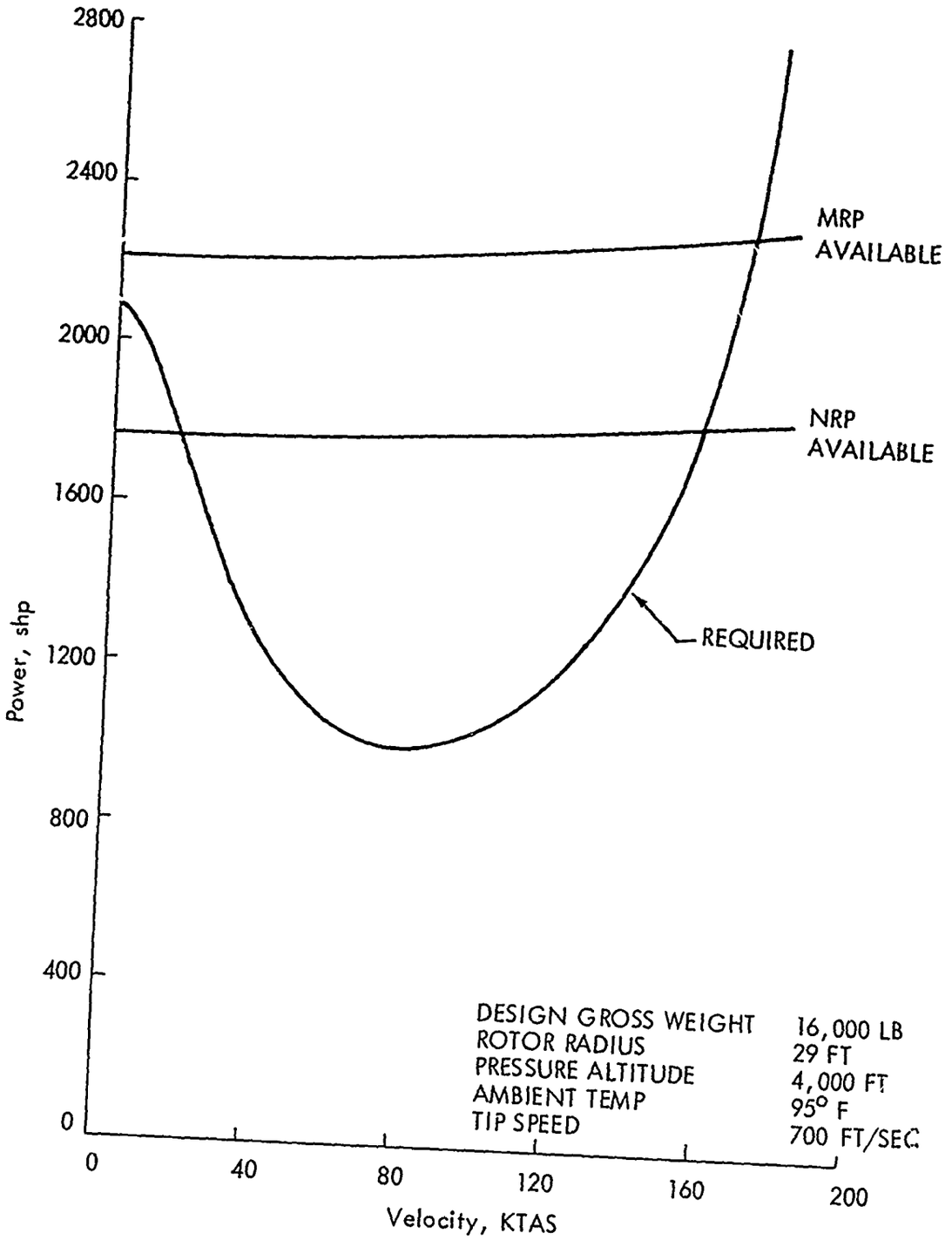

Figure 13. Power Required and Available in Level Flight for Configuration 5.

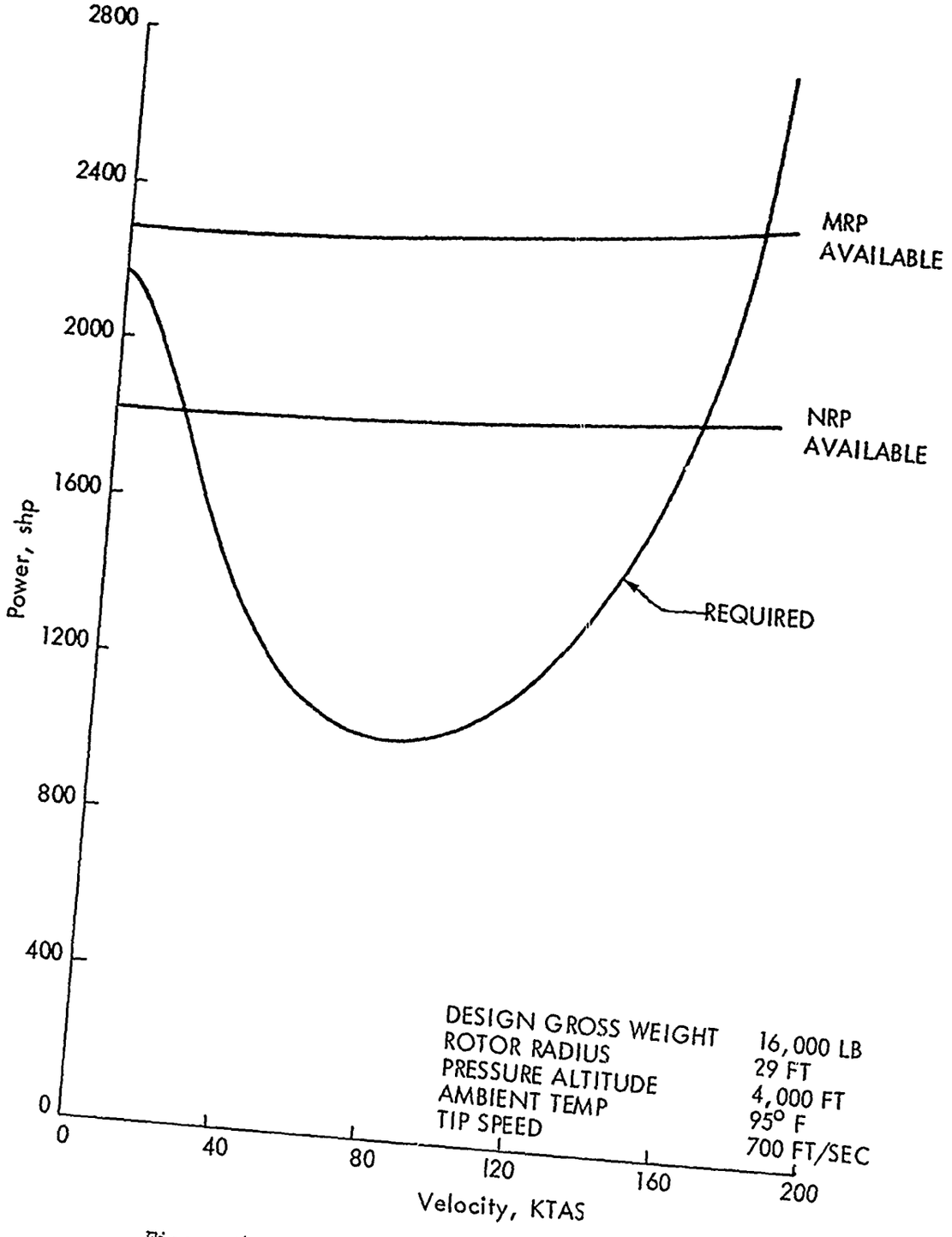

Figure 14. Power Required and Available in Level Flight for Configuration 6.

2.2.3 Center-of-Gravity Travel

Center-of-gravity envelopes corresponding to principal loading conditions were developed for each of the aircraft in a manner consistent with the UTTAS requirements reported in Reference 1. The six envelopes are shown in Figures 15 through 20. The design structural center-of-gravity limits were determined empirically in the manner described in Reference 1. These limits are primarily a function of blade and hub fatigue life design considerations and, therefore, can be altered by changing rotor geometry. A curve which summarizes the variation in design structural center-of-gravity limits as rotor solidity is varied and aircraft gross weight is held constant is shown in Figure 21.

The reference center of gravity used in the analysis of aircraft behavior during maneuvers was held at a distance of 75 in. below the hub center along the inclined rotor shaft in order to minimize the number of variables and thereby minimize the number of cases to be analyzed. As noted in Table X, this center of gravity location is at Fuselage Station 300 and Waterline 156. (Differences in control moments involved can be easily handled. This implies that flight velocity restrictions discussed in connection with rotor stresses can be further allayed by altering the center of gravity travel allowed.) The vertical position of the center of gravity was held constant for all configurations. As rotor solidity was varied, rotor group weight and, correspondingly, airframe weight were varied (gross weight was held constant), but the center of gravity at the design gross weight remained within 2 in. of the reference center of gravity. This was an important aspect of the calculations because the relative positions of centers of mass of the rotor and body would otherwise have influenced the dynamic interactions of rotor and body, particularly in the roll mode.

2.2.4 Aerodynamic Trimming Requirements

Since the aircraft studied were designed to utilize the main and tail rotors as the sole control elements throughout the flight regime, and their center-of-gravity envelopes were biased toward the forward structural limit, the trimming requirements are of minor concern. There is no need for auxiliary

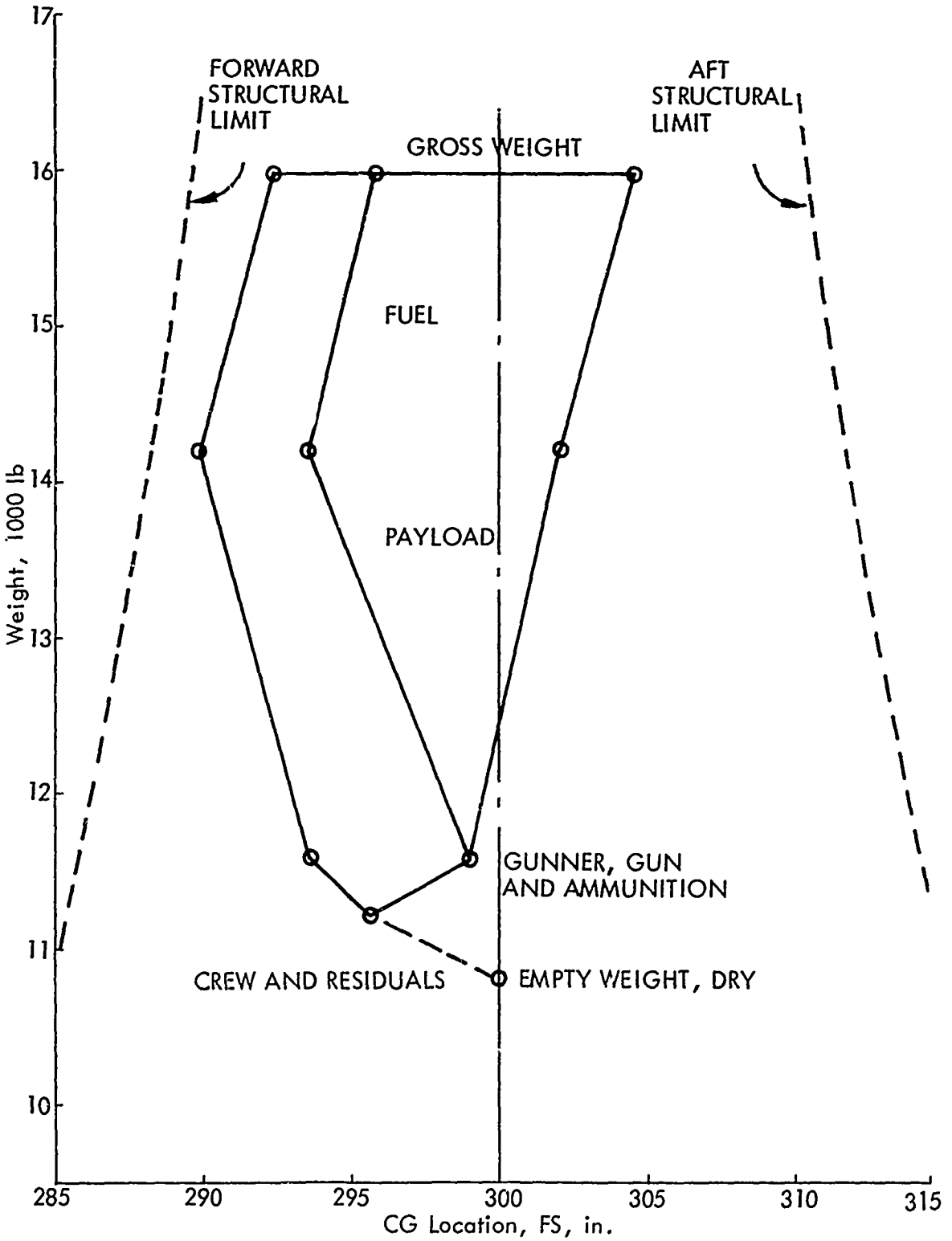

Figure 15. Center-of-Gravity Envelope for Configuration 1.

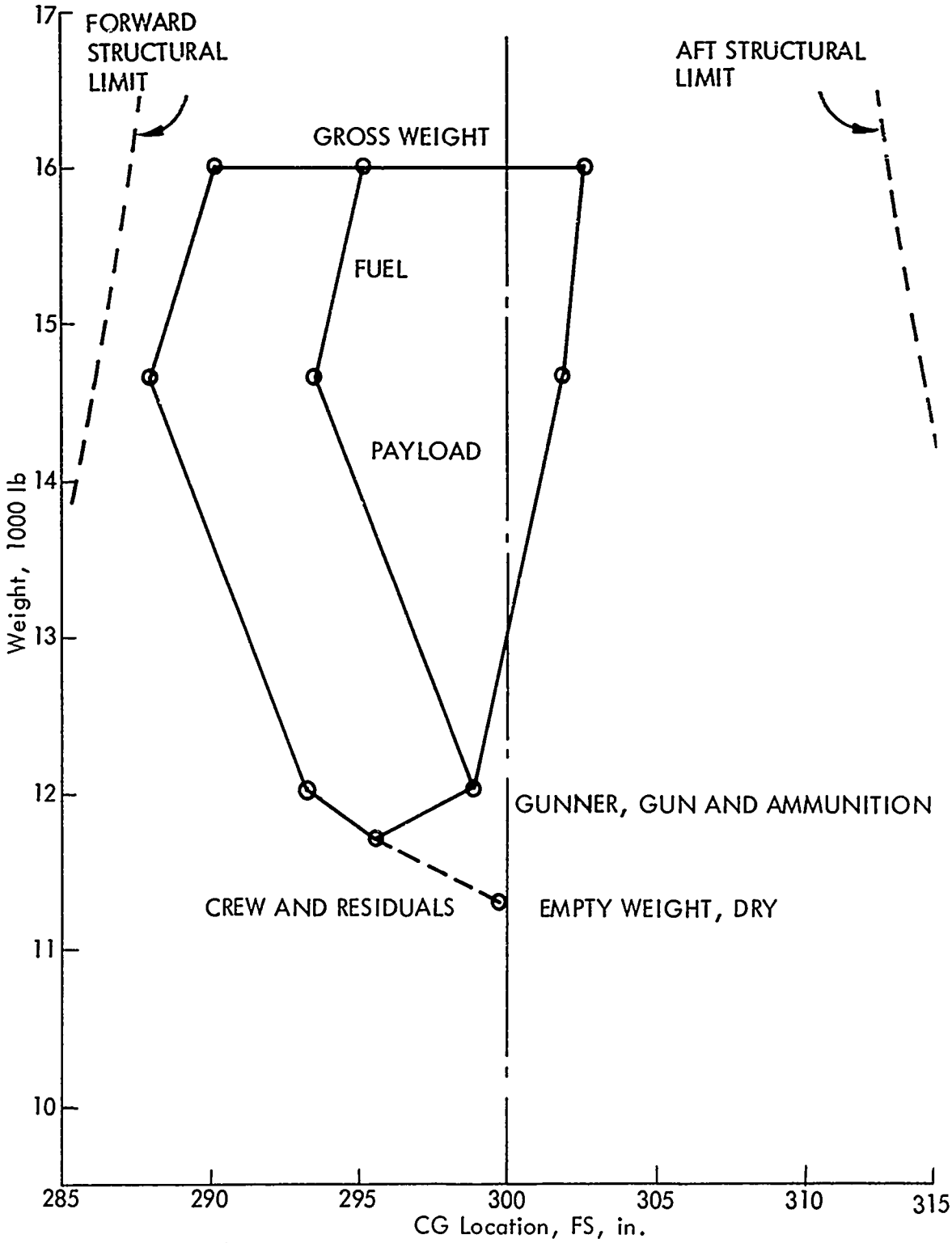

Figure 16. Center-of-Gravity Envelope for Configuration 2.

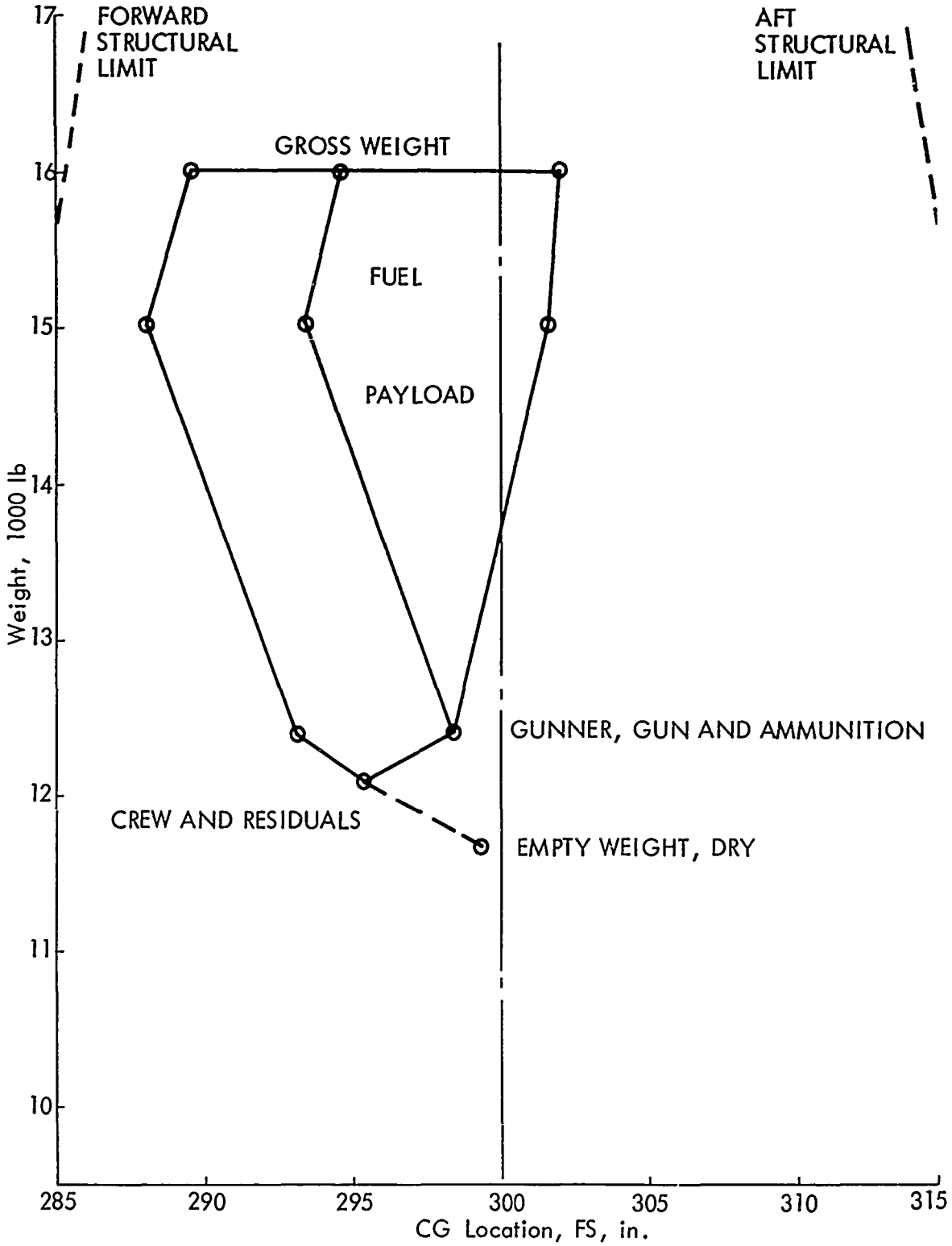

Figure 17. Center-of-Gravity Envelope for Configuration 3.

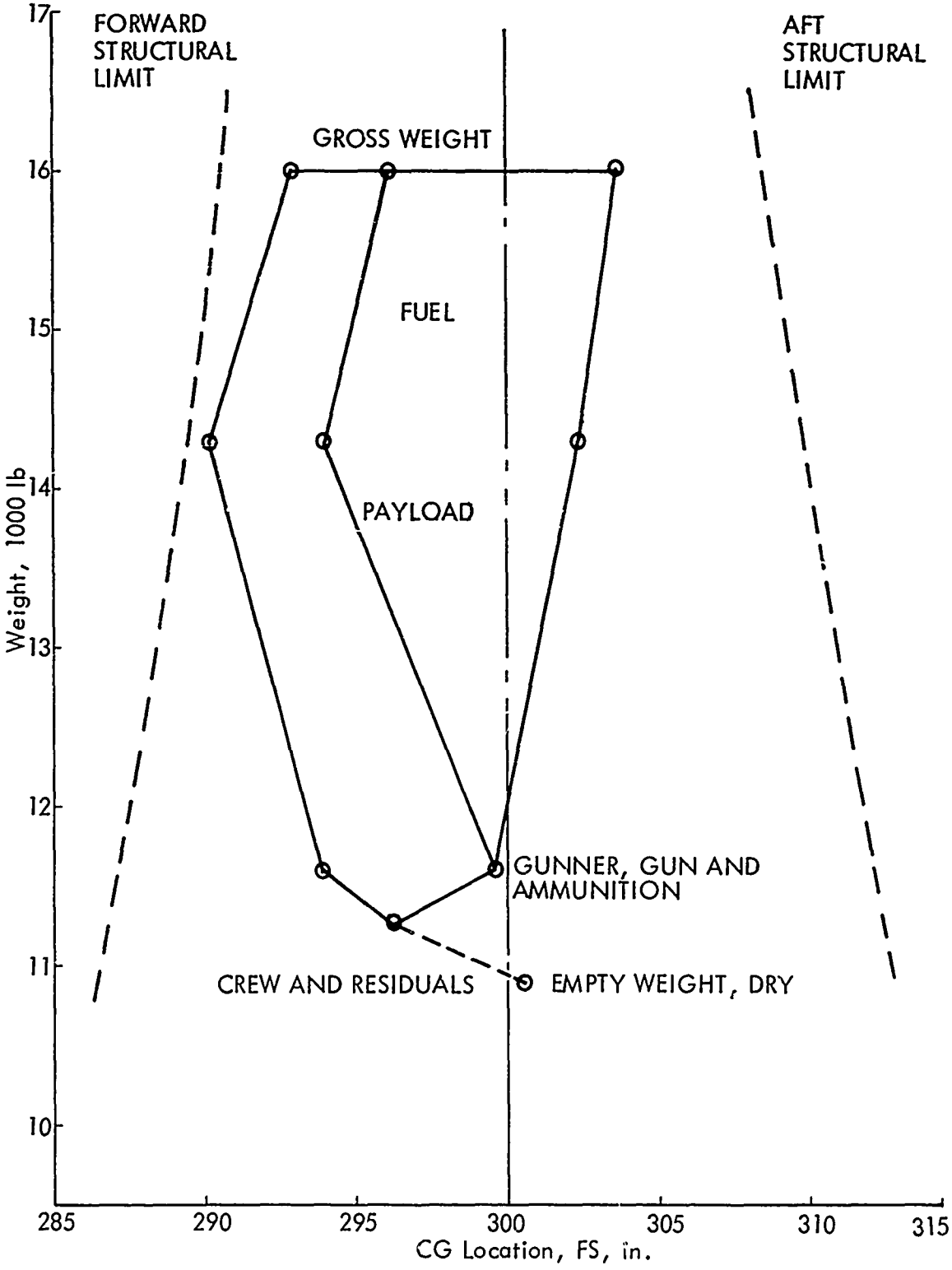

Figure 18. Center-of-Gravity Envelope for Configuration 4.

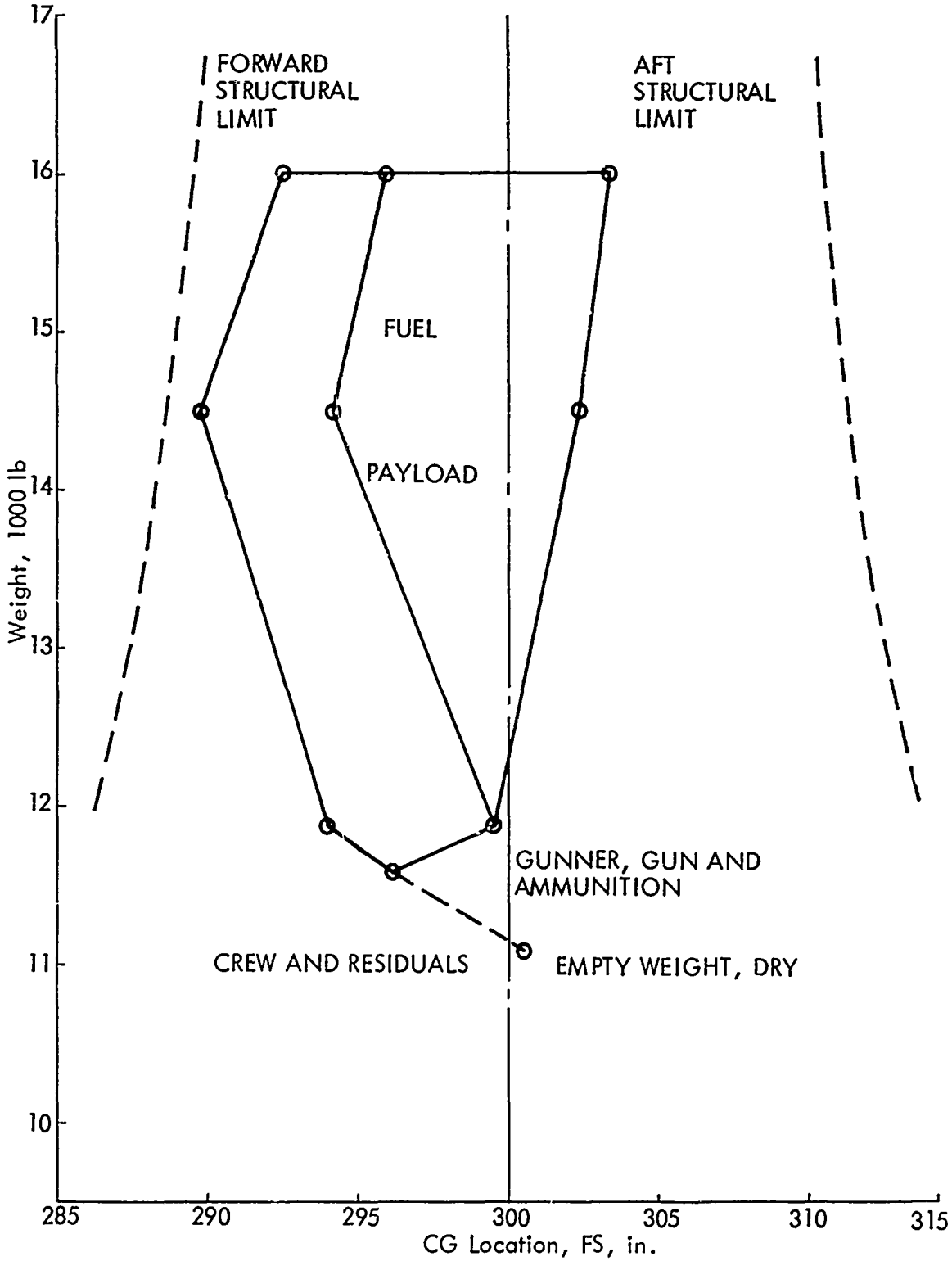

Figure 19. Center-of-Gravity Envelope for Configuration 5.

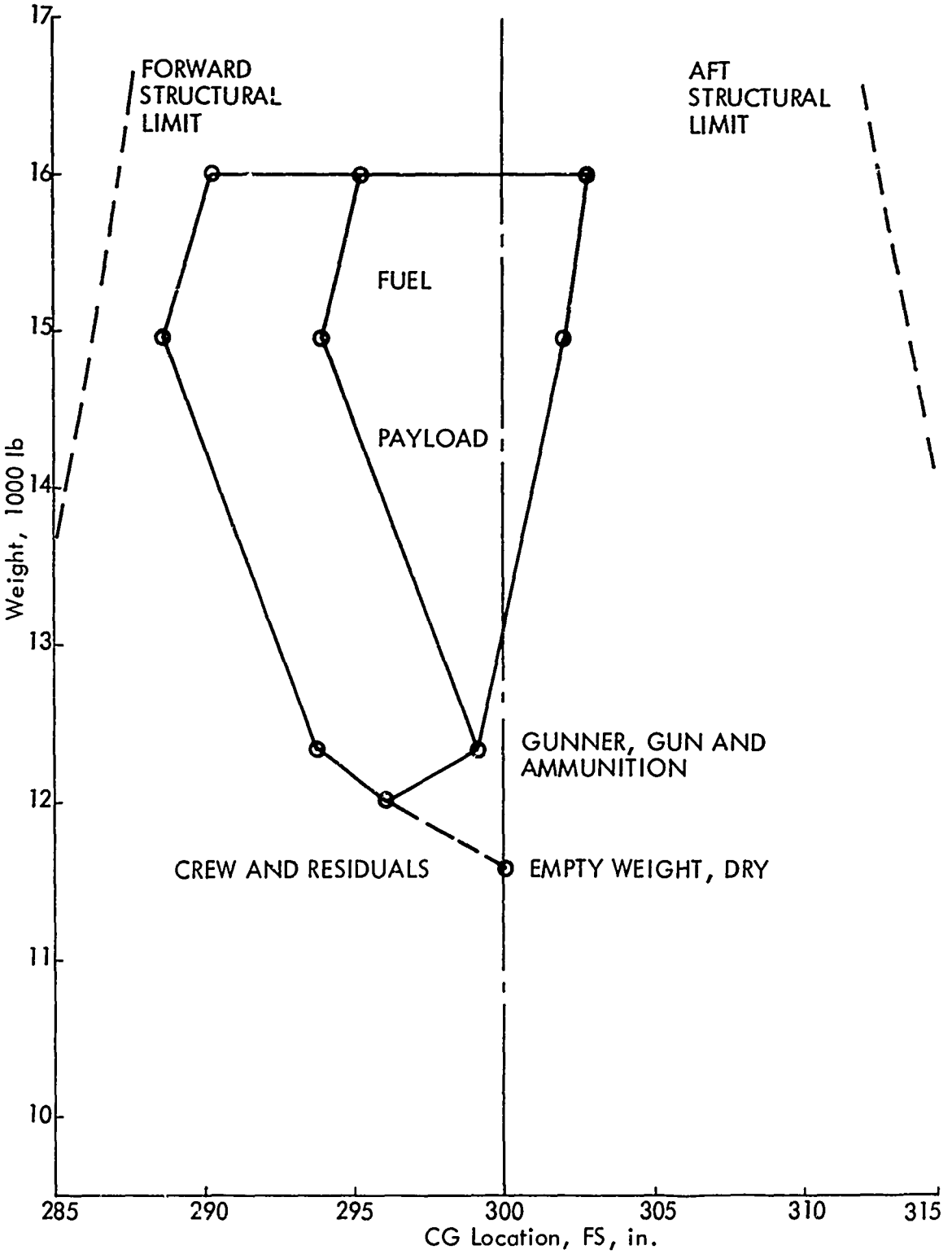

Figure 20. Center-of-Gravity Envelope for Configuration 6.

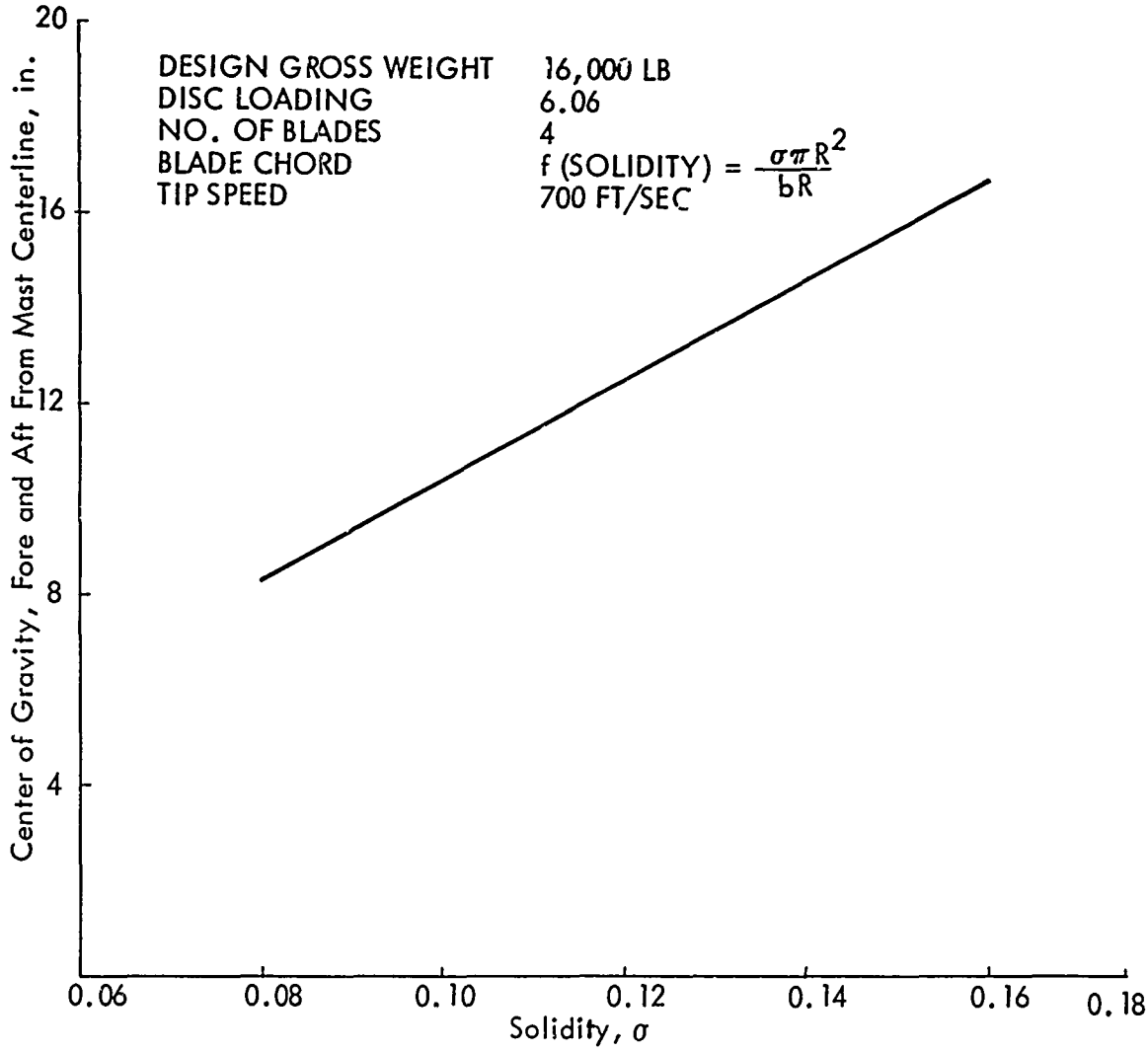

Figure 21. Structural Center-of-Gravity Limits at Design Gross Weight.

aerodynamic surface control at high forward speeds, and the aircraft can be trimmed without difficulty over the entire center-of-gravity range. Longitudinal stability is achieved through proper size and placement of the horizontal tail and, in the case of the winged configurations, the longitudinal placement of the wings.

The wing influences the design of the rotor and helicopter due to its indirect effect on the rotor angle of attack and control angle requirements. As the speed of a helicopter is increased, the rotor has to be tilted forward to provide propulsive force. The required rotor angles of attack and control angles are increased somewhat for a winged helicopter (see Tables X and XI).

2.2.5 Stability and Control Characteristics

Basic stability was provided for by the choice of nonrotating airframe aerodynamic characteristics and the placement of the center-of-gravity range. Size and incidence of the horizontal tail were selected on the basis of the longitudinal moment characteristics of the airframe less tail to provide stick-position stability with both speed and load factor. Each winged helicopter was fitted with the same horizontal tail as each unwinged helicopter except that the tail was installed at slightly different angles of incidence (-2.5 deg for the winged helicopters compared to -3.5 deg for the unwinged helicopters).

A force gradient proportional to stick displacement was achieved by assuming that artificial feel was included in the system. Because an irreversible cyclic control system is used, the neutral point and the maneuver point can be considered coincident and a simple function of the longitudinal stability characteristics of the nonrotating airframe. Neutral and maneuver points for the various aircraft are shown in Table XII.

The trade-offs in wing size (corresponding to changes in rotor solidity) influenced airframe stability. This effect was accounted for by placing the wing longitudinally to maintain a consistent level of stability for the desired maneuver response among all aircraft.

TABLE X. TRIM AND TRANSIENT CONDITIONS FOR COORDINATED TURNS

Configuration	Nominal Load Factor Capability (n)	Forward Flight Velocity (KTAS)	Rotor Characteristics*				Airframe Characteristics*					Flight Control Deflections**				Rotor Control Deflections**			
			Trim	Maneuver			Trim		Maneuver										
			T_R (lb)	L_R (lb)	α_R (deg)	D_R (lb)	L_A (lb)	C_{L_A}	L_A (lb)	C_{L_A}	D_A (lb)	z_c (in.)	x_{cs} (in.)	y_{cs} (in.)	x_p (in.)	θ_c (deg)	B_{1s} (deg)	A_{1s} (deg)	θ_{TR} (deg)
1	1.50	140	16,350	22,500	3.2	1070	-350	-	540	-	1000	6.4	1.51	-1.6	3.3	11.8	7.6	-8.1	12.0
2	1.75	155	16,550	25,000	1.6	660	-550	-	470	-	1220	6.6	1.52	-1.68	2.6	11.8	7.8	-7.8	12.7
3	2.00	167	16,850	28,000	0.6	250	-850	-	380	-	1400	6.8	1.60	-1.80	2.0	12.2	8.4	-7.7	13.4
4	1.50	140	14,400	21,000	2.5	620	1600	0.414	3750	1.04	1320	6.8	1.49	-1.68	3.2	12.3	8.0	-8.5	11.2
5	1.75	155	14,200	22,000	0.6	40	1800	0.285	5200	0.89	1640	7.2	1.51	-1.73	2.5	12.9	8.7	-8.0	11.0
6	2.00	167	14.200	27,000	-1.6	-650	1800	0.197	5900	0.68	1870	7.5	1.40	-1.80	1.8	13.5	8.8	-7.7	12.0

*Values specified coincide with maximum rotor angles of attack developed in course of maneuvers.

**Extreme deflections developed in course of maneuvers.

TABLE XI. TRIM AND TRANSIENT CONDITIONS FOR PULL-UPS AND PUSH-OVERS

Configuration	Nominal Load Factor Capability (n)	Forward Flight Velocity (KTAS)	Height Change Command (ft)	Value	Rotor Characteristics			Airframe Characteristics			Flight Control Deflections				Rotor Control Deflections			
					α_R (deg)	L_R (lb)	D_R (lb)	L_A (lb)	D_A (lb)	C_{L_A}	z_c (in.)	x_{cs} (in.)	y_{cs} (in.)	x_p (in.)	θ_o (deg)	B_{1s} (deg)	A_{1s} (deg)	θ_{TR} (deg)
1	1.50	140	+200	Trim	-3.5	16,350	-1,020	-350	1,030	-	6.4	-0.16	-0.19	-0.08	11.8	5.6	-2.4	8.6
				Max	0.2	21,000	-100	140	1,030	-	6.4	0.36	-0.07	0.35	11.8	6.1	-2.3	9.1
				Min	-9.8	8,000	-1,580	-880	820	-	6.4	-0.83	-0.28	-0.18	11.8	4.7	-2.8	6.2
1	1.50	140	-200	Trim	-3.5	16,350	-1,020	-350	1,030	-	6.4	-0.16	-0.19	-0.08	11.8	5.6	-2.4	8.6
				Max	4.1	22,000	950	910	1,340	-	6.4	0.90	-0.03	-0.08	11.8	8.0	-1.8	9.9
				Min	-6.8	10,000	-1,230	720	1,030	-	6.4	-0.64	-0.25	-0.36	11.8	5.3	-2.8	9.0
2	1.75	155	+200	Trim	-4.2	16,550	-1,270	-550	1,290	-	6.6	-0.28	-0.22	-0.31	12.0	5.8	-2.5	10.0
				Max	-1.0	23,000	-520	40	1,300	-	6.6	0.33	-0.08	-0.10	12.0	6.2	-1.5	13.8
				Min	-11.3	7,000	-1,530	-1,240	1,100	-	6.6	-1.04	-0.27	-1.00	12.0	4.6	-3.1	8.9
2	1.75	155	-200	Trim	-4.2	16,550	-1,270	-550	1,290	-	6.6	-0.28	-0.22	-0.31	12.0	5.8	-2.5	10.0
				Max	3.7	25,000	800	960	1,540	-	6.6	0.98	-0.03	0.07	12.0	8.5	-1.7	12.1
				Min	-7.8	8,000	-1,300	-1,020	1,280	-	6.6	-0.85	-0.26	-0.74	12.0	5.5	-4.0	7.8
3	2.00	167	+200	Trim	-5.5	16,000	-1,460	-800	1,500	-	6.8	-0.23	-0.28	-0.58	12.3	6.1	-2.7	11.5
				Max	-2.0	25,000	-950	-120	1,500	-	6.8	0.40	-0.19	-0.33	12.3	6.6	-1.2	17.2
				Min	-11.4	6,000	-1,630	-1,540	1,330	-	6.8	-1.04	-0.28	-1.63	12.3	5.0	-3.5	10.1
3	2.00	167	-200	Trim	-5.5	16,800	-1,460	-800	1,500	-	6.8	-0.23	-0.28	-0.58	12.3	6.1	-2.7	11.5
				Max	1.5	27,000	200	640	1,700	-	6.8	0.72	-0.14	-0.24	12.3	5.7	-1.6	14.7
				Min	-8.8	8,000	-1,460	-1,360	1,500	-	6.8	-0.87	-0.32	-1.20	12.3	8.2	-4.3	9.6
4	1.50	140	+200	Trim	-4.3	14,500	-1,200	1,500	1,200	0.38	6.7	-0.17	-0.23	-0.07	12.2	5.9	-2.4	8.4
				Max	-0.8	19,300	-440	2,600	1,230	0.72	6.7	0.35	-0.13	0.32	12.2	6.3	-2.3	8.5
				Min	-10.0	8,800	-1,670	-700	920	-0.24	6.7	-0.82	-0.28	-0.08	12.2	5.1	-2.7	6.4
4	1.50	140	-200	Trim	-4.3	14,500	-1,200	1,500	1,200	0.40	6.7	-0.17	-0.23	-0.07	12.2	5.9	-2.4	8.4
				Max	2.0	18,000	300	4,800	1,700	1.03	6.7	0.68	-0.11	-0.07	12.2	7.7	-1.9	9.8
				Min	-7.8	8,000	-1,370	250	1,200	0.10	6.7	-0.67	-0.27	-0.32	12.2	5.4	-2.8	8.4
5	1.75	155	+200	Trim	-5.9	14,250	-1,480	1,750	1,490	0.28	7.2	-0.3	-0.28	-0.26	13.0	6.5	-2.5	9.9
				Max	-2.4	19,000	-990	3,500	1,520	0.58	7.2	0.31	-0.17	-0.04	13.0	6.8	-1.6	12.8
				Min	-12.0	7,000	-1,700	-1,750	1,230	-0.34	7.2	-1.10	-0.34	-0.96	13.0	5.4	-3.1	8.5
5	1.75	155	-200	Trim	-5.9	14,250	-1,480	1,750	1,490	0.28	7.2	-0.32	-0.28	-0.26	13.0	6.5	-2.5	9.9
				Max	0.1	22,000	-100	6,700	2,000	0.93	7.2	0.63	-0.13	-0.06	13.0	8.5	-1.8	12.0
				Min	-9.0	8,000	-1,470	0	1,500	-0.01	7.2	-0.91	-0.31	-0.68	13.0	6.1	-3.5	8.8
6	2.00	167	+200	Trim	-7.2	14,300	-1,750	1,700	1,770	0.18	7.6	-0.40	-0.30	-0.59	13.8	6.8	-2.7	11.5
				Max	-4.0	21,000	-1,230	4,000	1,800	0.45	7.6	0.31	-0.20	-0.22	13.8	7.3	-1.3	16.8
				Min	-12.8	6,000	-1,940	-2,500	1,520	-0.33	7.6	-1.25	-0.29	-1.53	13.8	5.9	-3.5	9.8
6	2.00	167	-200	Trim	-7.2	14,300	-1,750	1,700	1,770	0.18	7.6	-0.40	-0.30	-0.59	13.8	6.8	-2.7	11.5
				Max	-1.5	23,000	-800	7,200	2,200	0.70	7.6	0.61	-0.32	-0.30	13.8	8.2	-1.7	14.8
				Min	-10.2	7,000	-1,750	-800	1,750	-0.08	7.6	-1.40	-0.09	-1.22	13.8	6.3	-3.8	9.8

TABLE XII. CENTER-OF-GRAVITY LOCATIONS* AND RELATED STABILITY AND CONTROL PARAMETERS

Characteristic	Configuration					
	1	2	3	4	5	6
	Distance, in.					
Forward-Most cg at Design Gross Weight	7.65	9.80	10.40	7.20	7.45	9.50
Aft-Most cg at Design Gross Weight	3.30	2.75	2.22	3.70	3.43	2.84
Neutral and Maneuver Point, Aft	12.60	12.60	12.60	12.80	13.70	15.70
Neutral and Maneuver Point, Aft of Aft-Most cg at Design Gross Weight	9.30	9.85	10.38	9.10	10.27	12.86

*Reference cg location for maneuver study: FS 300 and WL 156, all configurations

The primary effect of the wing on stability and control was reduced roll sensitivity due to the added inertia of the wing. The problem of reduced rotor control power associated with wing lift is minimized by use of the hingeless rotor.

2.2.6 Rotor Controls and Pilot Maneuver Controls

The main rotor cyclic control system is a rate response system that uses the precession response of a gyro to pilot commanded moments to provide main rotor cyclic blade pitch through irreversible power servos. System stabilization and gust load alleviation are provided by the use of a hub moment feedback sensor which detects main rotor flap bending displacements and feeds back a moment to the gyro proportional to flapwise bending.

A special feature of this system is that a small gyro is used in conjunction with power servos to feather the rotor blades. This mechanization isolates the small gyro and servo actuators from the total pitch link load. The general characteristics of the Lockheed rigid rotor control system are described in Reference 10.

A simplified functional diagram of the cyclic control subsystem of the main rotor is shown in Figure 22. The basic concept is the same as that described in Reference 1. Vehicle longitudinal and lateral control are provided by means of a conventional cyclic stick. Blade cyclic control angle limits for the main rotor are ±12 degrees. This range is available to maintain trim and to execute maneuvers.

The stick-fixed and stick-free neutral points are the same in the analytic models used. The basic control system and the normal characteristics of the nonrotating airframe provide stick position stability with speed. Similarly, stick position is stable with load factor. With this type of stick position stability and an artificial force gradient proportional only to stick displacement, the maneuver point coincides with the neutral point.

Conventional main rotor collective control is provided. The gradient of stick positions with blade angle and the pertinent operating range are shown in the upper portion of Figure 23.

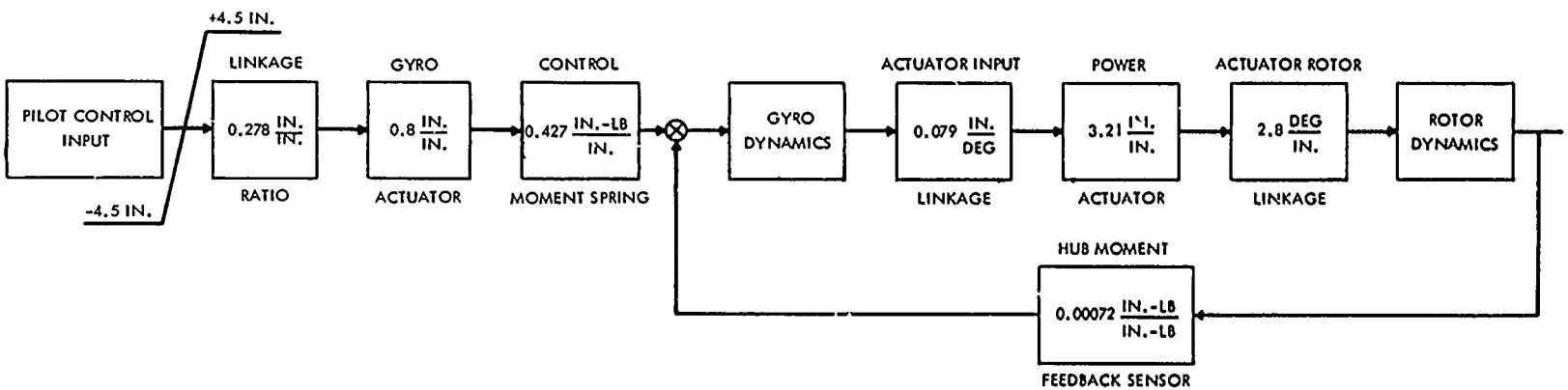

NOTE:
Values shown are for the longitudinal control system. The corresponding lateral control system values, where different, are as follows:

1. Pilot control input limit: ± 3.0 in.
2. Linkage ratio: 0.400 in./in.
3. Control moment spring: 660 in.-lb/in.
4. Actuator input linkage: 0.074 in./deg

Figure 22. Rigid Rotor Cyclic Control System Block Diagram.

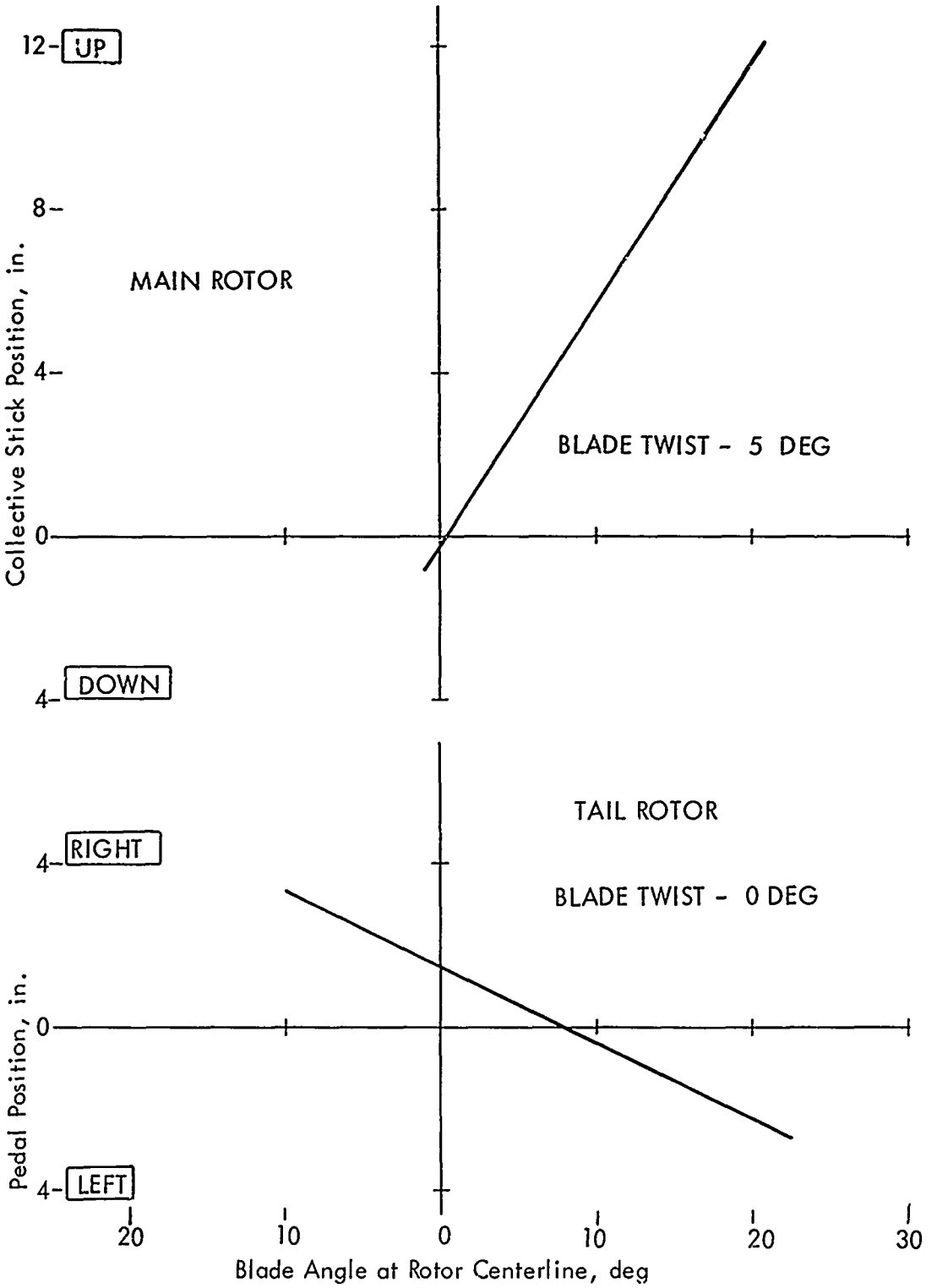

Figure 23. Control Linkage Characteristics for Main and Tail Rotor Collective Blade Angles.

The tail rotor is a two-axis, teetering rotor. Variation in blade angle with pedal position and the pertinent operating range are shown in the lower portion of Figure 17.

The overall characteristics of the control system are in compliance with the specifications of Reference 11. The gradients of main and tail rotor blade angles represent acceptable sensitivities.

No auxiliary control surfaces or trimming devices are required for an aircraft with a hingeless rotor and feedback system of this type. Aircraft control is accomplished through the main and tail rotors at all flight speeds and throughout the maneuvers.

2.2.7 Rotor Noise Characteristics

Since the rotor must provide both lift and propulsive force, it is essential that the design of the outboard section of the blade provide for an acceptable compromise between advancing blade compressibility effects and retreating blade stall effects, as well as low noise radiation.

Small changes in blade design, which might be made in the very extreme tip region to mitigate noise radiation, will not conflict with the blade design requirement to achieve a high retreating blade lift coefficient in the region of the blade between 85 and 95 percent of the radius. Therefore, potential advancements in blade design to minimize noise would be expected to have only secondary effects on the results of this study.

As tip speed is increased (at a particular forward speed), advance ratio is decreased and, concomitantly, increased blade loading coefficients are practicable (see Figure 4). However, the higher advancing blade tip Mach numbers and larger high-Mach-number region accompanying higher tip speed intensify noise. Thus the principal impact of noise considerations from the standpoint of the present study was to limit the extent to which maneuvering ability could be enhanced by increasing tip speed (see References 12 through 14). A tip speed of 700 ft/sec (M = 0.85 @ 167 KTAS) was established for all configurations.

2.2.8 Solidity

The steep increase in required power resulting from operating at high blade angle of attack and blade stall determine the extent to which rotor load factor capability can be increased before excessive oscillatory rotor loads and vibrations are incurred. Reduction of blade loading coefficient is a powerful means of mitigating these effects but, unfortunately, usually involves losses in rotor efficiency in hover and low-speed flight. Figure 24 shows the variation of blade loading coefficient with solidity at a particular tip speed for a range of normal load factors. While the larger solidities serve to enhance high-speed maneuver load factor capability, they also entail the highest rotor weight fractions, as shown in Figure 25.

In high-speed maneuvering flight, the propulsive capability of the rotor can be extended by slightly unloading the rotor in lift with a wing, thereby permitting use of reduced solidity. Since the resultant propulsive capability of the rotor must also compensate for the added drag due to the wing, the extent to which rotor solidity can be reduced before the beneficial effects are offset is limited. The combinations of wing areas and rotor solidities were ultimately determined on the basis of maneuver response in a coordinated turn. The final values were obtained in two steps. First, the solidity of each unwinged helicopter configuration was lowered and a wing was prescribed which would compensate for the corresponding reduction of thrust (lift) capability of the rotor. Then, coordinated turns were simulated and solidity and wing area were adjusted to achieve satisfactory response characteristics while retaining maneuver and speed capabilities comparable to those of the corresponding unwinged helicopters.

2.2.9 Tip Speed and Advance Ratio

The highest blade loading coefficients can be attained by operating the rotor at high tip speeds to maintain low advance ratios (see Figures 4 and 26). However, high tip speeds aggravate compressibility effects and intensify rotor noise.

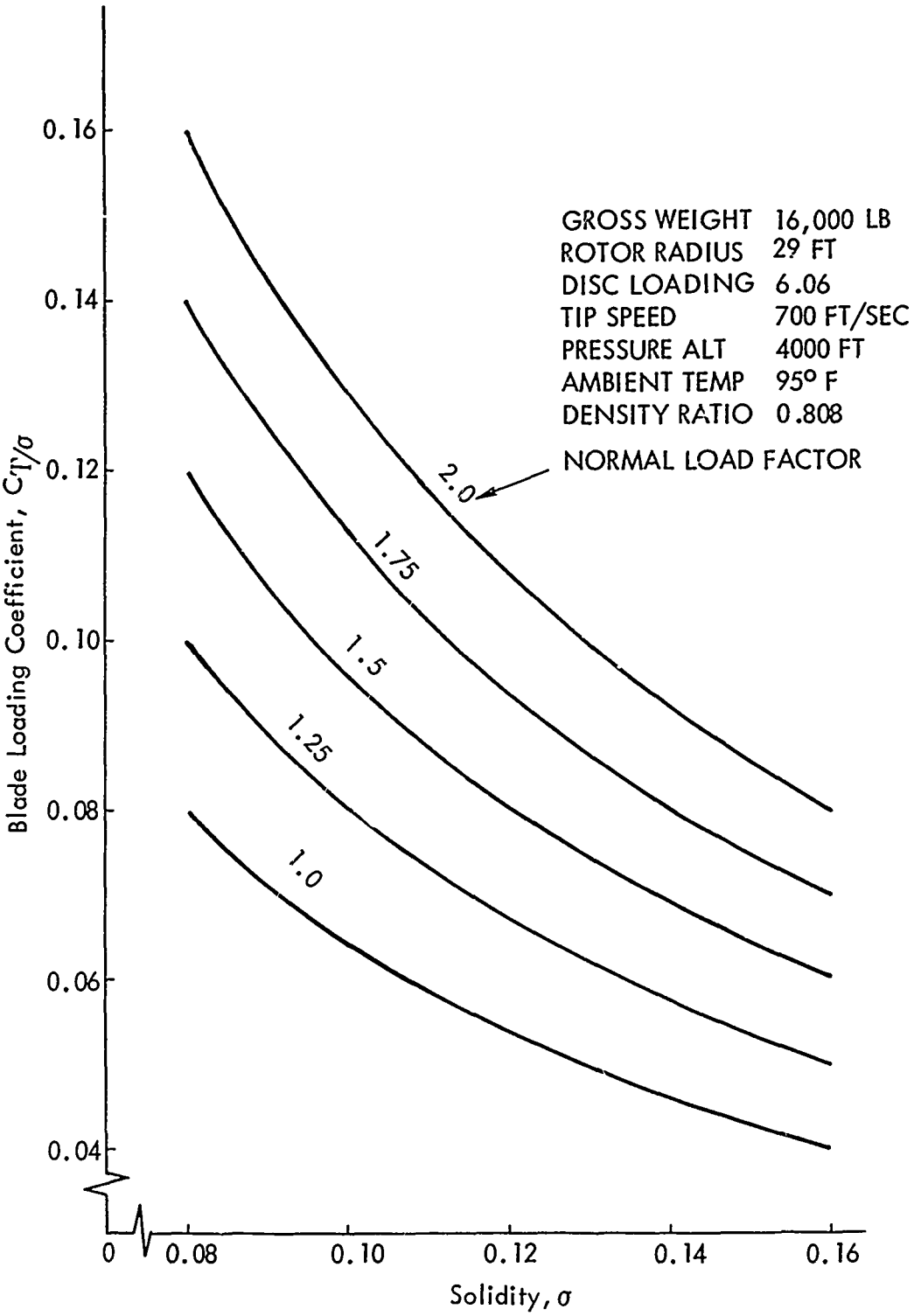

Figure 24. Blade Loading Coefficient vs Solidity for a Range of Normal Load Factors.

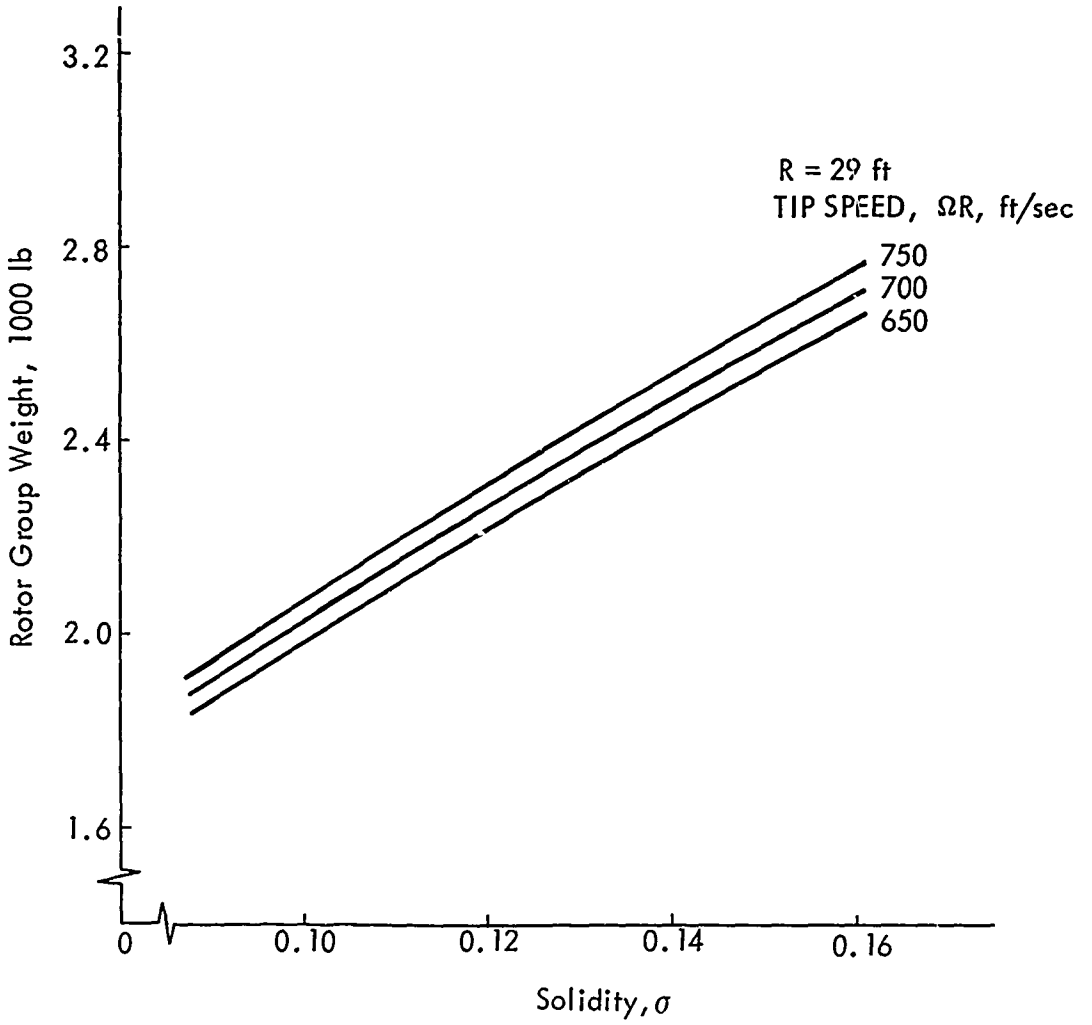

Figure 25. Rotor Group Weight vs Solidity.

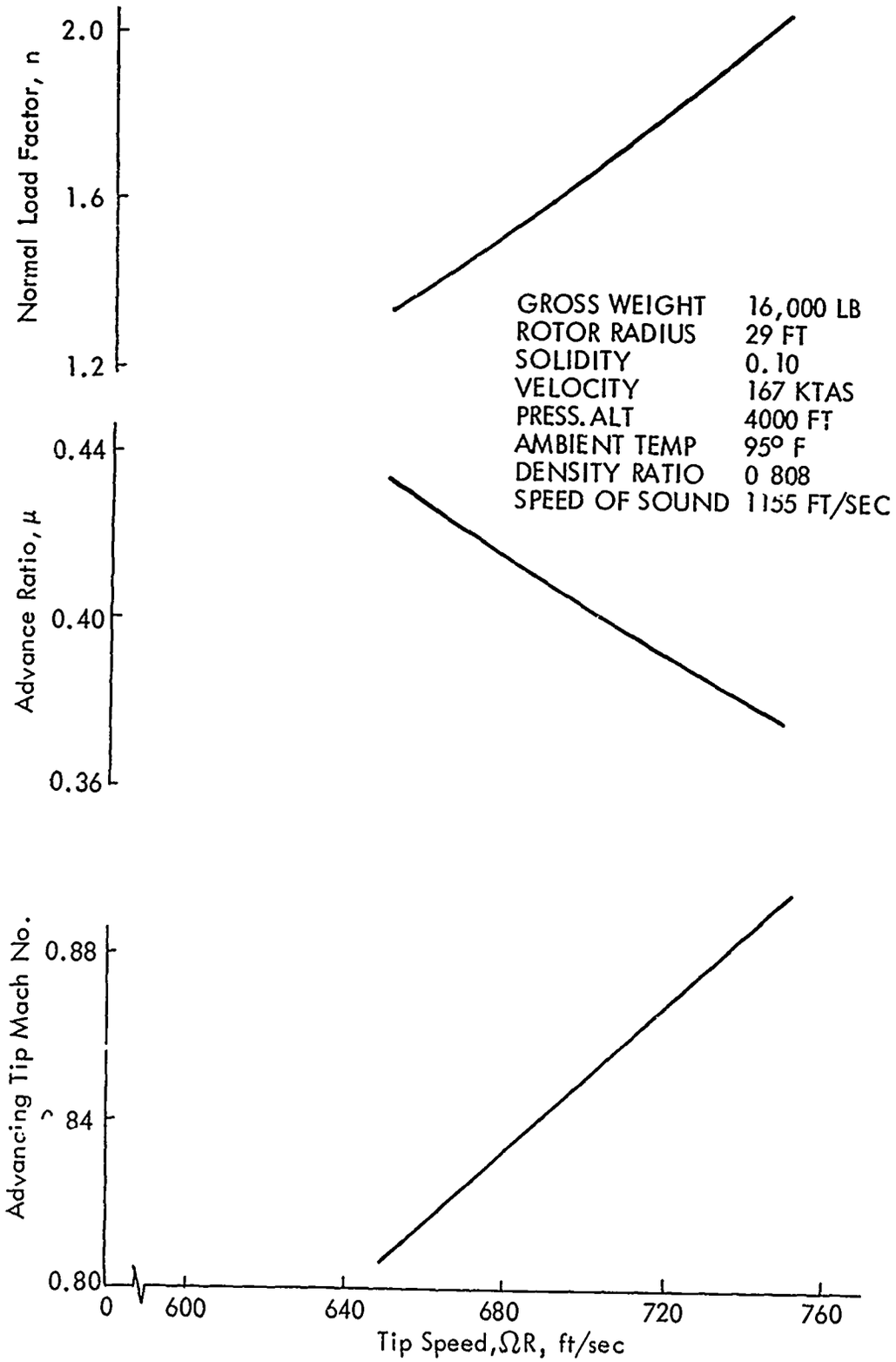

Figure 26. Effect of Tip Speed on Normal Load Factor.

Figure 26 shows the trend of the gain in load factor capability that can be accomplished by decreasing advance ratio or by increasing design tip speed. Figure 25 shows the trends of trade-offs among rotor weight solidity, and tip speed. It is emphasized that the data in these figures are trends which were determined from static analyses for the purpose of guiding the formulation of characteristics of the several study aircraft. These data were later influenced by dynamic characteristics included in the transient analyses which followed; therefore, these data are not directly comparable to those given later in the report.

2.2.10 Disc Loading

Since disc loading was regarded as a baseline design feature (6.06 psf), a special analysis of its impact on maneuverability was not undertaken. However, in the course of prior UTTAS design efforts, blade loading coefficient was found to have a more pronounced effect on maximum thrust (and therefore maneuver load factor) capability than disc loading. Variations of disc loading in the range of 6 to 8 psf are not expected to significantly alter maneuvering ability, especially at high speeds. But an increase in disc loading would be expected to decrease rotor weight and provide for a more compact aircraft.

In the case of the winged helicopter, a lower disc loading results in a lower ratio of wing span to rotor diameter and, correspondingly, less severe hovering download.

2.2.11 Mean Lift Coefficient

Reducing blade loading coefficient (a measure of mean lift coefficient) as a means of controlling blade stall has been discussed. The levels of blade loading coefficient shown in Figure 4 are not altogether indicative of maneuver load factors as might be developed for a sustained period in coordinated turns, however. Figure 27, which illustrates this point, is a reproduction of Figure 4 with the addition of two points, labeled (1) and (2). Point (1) shows the value of $C_T/\sigma = 0.107$ assumed to be attainable for a particular

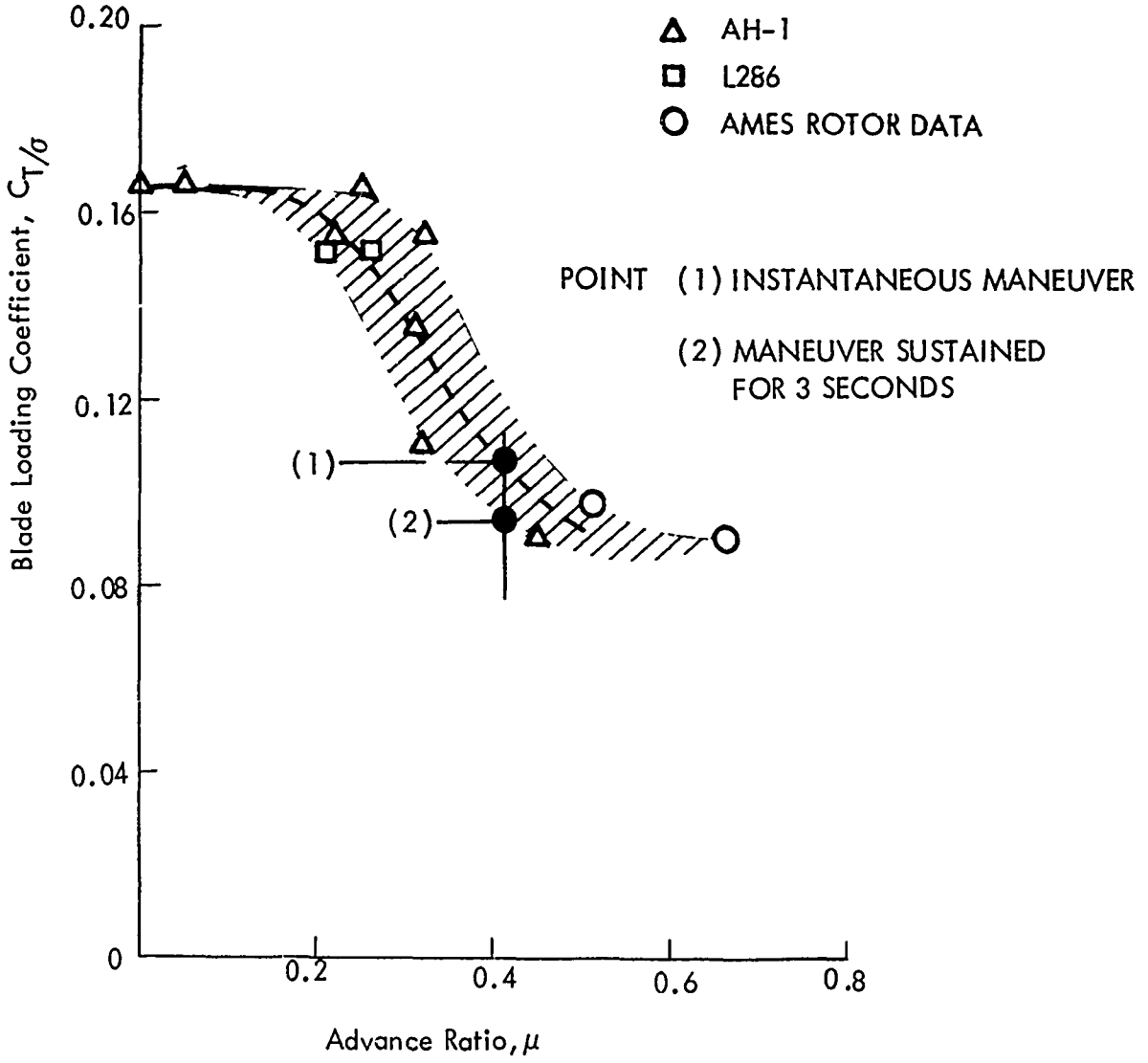

Figure 27. Illustration of Iterative Approach Used to Select Design Blade Loading Coefficients.

advance ratio in the initial stages of the analytic study. Point (2) represents a value of $C_T/\sigma = 0.094$ which is more indicative of the maximum level generally attained in simulated maneuvers when the maximum load factors were sustained for 3 seconds.

The addition of a wing provides for some reduction of blade loading (and, therefore, rotor weight) in high-speed maneuvering flight. However, as discussed above in connection with solidity, the amount of reduction possible is limited.

2.2.12 Transient Maneuver Flight Path Time Histories

After the analytic model helicopters were generally sized from trend data which had been determined by relatively simple static analyses, time history analyses were performed to examine more precisely the maneuvering capabilities of the model aircraft. Some discussion of the results of the preliminary sizing analyses is given in Section 2.2.9; more is given in a subsequent paragraph in this section. The decision logic which stemmed from results of the more comprehensive analyses and resulted in adjusting pertinent configuration parameters from those which were established by the preliminary analyses is discussed here.

Coordinated turn maneuvers and pull-up/push-over maneuvers which have predefined characteristics were prescribed as criteria for the analytic maneuvers. Figure 28 generally describes the prescribed maneuvers and shows the time segments which were selected for guiding the analyses. The characteristics which were established to guide the maneuver analyses are as follows:

(1) Maximum load factors of 1.5, 1.75, and 2.0, and a minimum load factor between 0 and 1.0, are to be investigated.

(2) The maximum load factor during any maneuver shall be sustained for approximately 3 seconds.

(3) The maximum speed of interest at which any maneuver is to be initiated is 167 KTAS (150 KEAS).

(4) The rotor blade collective pitch angle shall be determined for level unaccelerated flight prior to a maneuver, and shall remain invariant during the maneuver. (Note: It was also considered desirable to

MANEUVER SEGMENTS

1	PILOT RESPONSE LAG TIME	=	0.7 SEC
2	AIRCRAFT RESPONSE LAG TIME	=	INTERVAL BETWEEN CONTROL INPUT AND AIRCRAFT RESPONSE
3	LOAD FACTOR BUILDUP TIME	=	TIME BETWEEN INITIAL AIRCRAFT RESPONSE AND ATTAINMENT OF LOAD FACTOR
4	MANEUVER EXECUTION TIME	=	INTERVAL DURING WHICH LOAD FACTOR EQUALS OR EXCEEDS SPECIFIED LEVEL APPROXIMATELY 3 SEC
5	RETURN TO LEVEL FLIGHT	=	TIME TO RETURN TO LOAD FACTOR OF 1.0

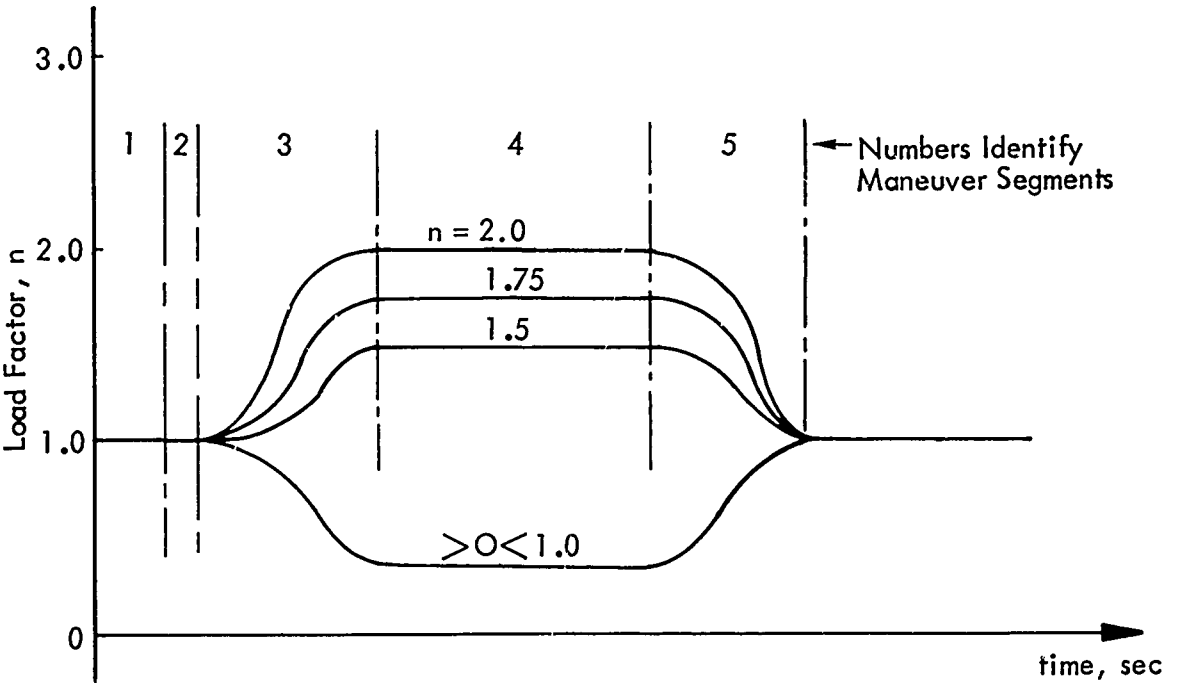

Figure 28. Definition of Maneuver Segments.

determine the lower boundary of speeds at which maneuvers could be executed with a constant collective, in other words, the speed below which it would be necessary to change collective in order to attain a reasonably high load factor.)

(5) During a coordinated turn, the aircraft height (flight altitude) shall not vary more than ±300 feet at constant speed, nor more than ±15 knots at constant height. (Note: In the analyses, these tolerances were applied simultaneously; that is, some combination of speed change and height change, within the prescribed limits, was accepted as practical.)

(6) During a pull-up/push-over maneuver, the aircraft speed shall not vary more than ±15 knots and the height change during the maneuver, including recovery, shall approximate a preselected value. (Note: Initially, investigation of the effects of prescribing various height changes was considered, but within the scope of the study, it was established that only one height change could be investigated: 200 feet was selected as the height change to be approximated in all symmetrical maneuvers.)

(7) The coordinated turn maneuvers shall be used to size the aircraft. (The load factor capabilities in pull-up/push-over maneuvers will not be used to influence sizing, and will therefore, be fall-outs of the analyses.)

A review of the entire procedure for sizing the analytic model aircraft is presented here to explain the decisions made during the various analysis iterations, from static preliminary design analyses through time history analyses of transient maneuvers. Initially, the test data of Figure 4 and the baseline design parameters of Table I were used to construct the trend curves of Figure 26. A 700 fps tip speed (corresponds to an advance ratio of 0.403 at 167 KTAS) and a blade loading coefficient of 0.107 were used to initiate the design of a basic nonwinged helicopter. Then, preliminary performance calculations were made, using the analysis methods of Reference 1, to estimate power required. Power required was estimated for unaccelerated flight and for climb at 500 ft/min; the climb criterion was more critical. This was followed by calculations to determine the additional power required to perform maneuvers. Quasi-transient maneuvers at various levels of load factor were examined over a range of solidities selected from the trend curves. Indications were that the greatest power demands occur during maneuvers involving a load factor of 2.0 in the speed range of 150 and 167 KTAS. A

general conclusion was that approximately 30 percent more power was needed to perform the maneuvers than for unaccelerated flight at 167 KTAS. At this point it was decided not to limit the aerodynamic potential of the rotor during the transient maneuver analyses by imposing power limitations; therefore, available power was allowed to vary as required to carry out the maneuverability analyses.

The preliminary work had indicated that load factors between 1.5 and 2.0 were attainable at 167 KTAS with rotor solidity values between 0.09 and 0.12. However, when the more comprehensive transient maneuver analyses were made, inadequacies of the simpler static analyses were revealed. For example, the added demand on rotor thrust to provide the propulsive force component needed to maintain the high flight speed became evident. At this point a choice had to be made: either blade solidity must be increased or the design requirement, to attain the specified load factors at 167 KTAS, must be modified. Since an increase in solidity is accompanied by an increase in rotor weight, it was decided that a compromise, leaning toward modifying the design criterion,was a practical choice. (Allowing the rotor group weight to grow could seriously affect the payload, for example.) Therefore, the range of solidities was increased slightly. A study of the analyses at this point resulted in establishing combinations of solidities and design speeds for the nonwinged helicopter models as follows:

Configuration Designation	Rotor Solidity	Maneuver Design Speed
1	0.10	140 KTAS
2	0.12	155
3	0.14	167

Later it is shown that Configurations 1, 2, and 3 are capable of attaining load factors of 1.5, 1.75, and 2.0, respectively, all at approximately 150 KTAS.

Complete descriptions of these analytic models are given earlier in the report, in Table II. Time histories of various parameters which were studied

in making these decisions, the results of analyses of coordinated turn maneuvers, are shown in Figures 54, 55, and 56. Pertinent aspects of these maneuvers are summarized in Figure 29 and Table XIII.

After the iterations to generally size the models, the earlier assumption of not restricting power was eliminated by selecting practical engines for the helicopters and calculating their effects on maneuver capabilities. Selection of the engines is discussed in Section 2.2.2. The general results were as follows:

- Configuration 1 can attain a load factor of 1.5 in a coordinated turn at 140 KTAS, dropping off to around 1.25 at 167 KTAS.
- Configuration 2 can attain a load factor of 1.75 at 150 KTAS, dropping off to around 1.5 at 167 KTAS.
- Configuration 3 can attain a load factor of 2.0 at 150 KTAS, drc off to around 1.8 at 167 KTAS.

These results are again summarized in Figure 45,which appears later in the report.

Configurations 4, 5, and 6, which are winged counterparts of Configurations 1, 2, and 3, were sized in the following manner. Each combination of wing area and rotor solidity was determined on the basis of comparable maneuver response (between winged and nonwinged counterparts) in a coordinated turn. Results of the time history analyses used in this part of the study are shown in Figures 57, 58, and 59; summary data are included in Table XIII. Results of the configuration sizing are as follows:

Configuration Designation	Rotor Solidity	Wing Area
4	0.09	72 sq ft
5	0.10	96
6	0.12	120

It is of interest to note that within the restrictions of general aircraft size, rotor and engine sizes specifically, it was not possible to significantly increase the maneuver capability by adding a wing. (Figure 45,which appears later in the report,shows very little difference between each of the

TABLE XIII. COMPARISON OF COORDINATED TURN MANEUVERS

Configuration	Nominal Load Factor Capability (n)	Forward Flight Velocity (KTAS)	Duration of Maneuver Segments (sec)					Mean Load Factor During Maneuver Execution (n)	Max Load Factor During Maneuver Execution (n)	Horizontal Distance Along Original Heading** (ft)	[illegible] Along Original Heading*** (ft)	Lateral Distance**	Height Deviation** (ft)	Velocity Deviation** (KTAS)	Power Required (hp)	
			Segment 1	Segment 2	Segment 3	Segment 4	Segment 5								Trim	Deviation
1	1.50	140	0.70	0.25	1.70	3.00	1.20	1.50	1.60	1488	1282	300	65	-14.4	1470	650 -100
2	1.75	155	0.70	0.15	1.85	3.00	1.10	1.65	1.75	1639	1342	350	74	-13.3	1750	740 -200
3	2.00	167	0.70	0.10	1.55	3.00	1.40	1.75	1.98	1718	1366	420	92	-12.0	2150	850 -150
4	1.50	140	0.70	0.20	1.50	3.00	1.40	1.52	1.60	1462	1290	330	68	-13.5	1500	660 -120
5	1.75	155	0.70	0.15	1.65	3.00	1.25	1.70	1.80	1604	1332	375	80	-12.3	1770	750 -100
6	2.00	167	0.70	0.10	1.70	3.00	1.10	1.80	1.95	1703	1370	400	100	-10.5	2150	800 -70

*Segment 1 represents pilot response time; Segment 2, aircraft response lag; Segment 3, load factor build-up; Segment 4, maneuver execution; Segment 5, return to load factor of 1.0. (See Figure 22)

**Upon return to 1g flight.

***When lateral displacement is 200 feet.

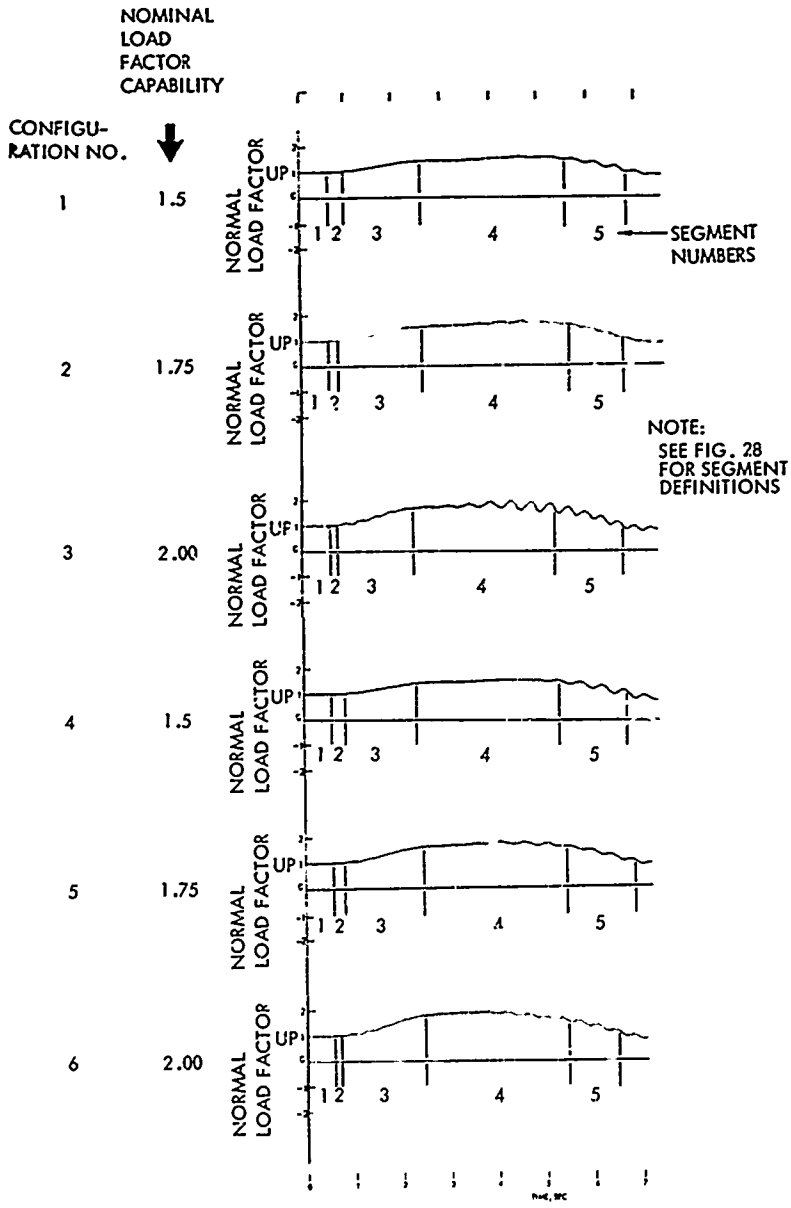

Figure 29. Duration of Maneuver Segments.

pairs of winged and nonwinged helicopters.) The reason that adding a wing does not provide an increased maneuver capability for a winged helicopter (no auxiliary propulsion) at high flight speed is quite simple. Since the propulsion force is provided by the rotor, whose solidity is reduced in trading for wing area, and since the addition of a wing adds to vehicle drag at high speed, it is not possible to define a practical configuration to accomplish a higher maneuver capability at high speed by adding a wing; in other words, the requirement to reduce effective rotor size and the requirement to produce more rotor thrust (more propulsive component to overcome wing drag) are opposing requirements.

Finally, the various configurations were studied for their capabilities to perform height change maneuvers (pull-ups/push-overs). The maneuvers were designed to approximate height changes of 200 feet. This decision stemmed from a compromise between performing nap-of-the-earth flying maneuvers and not becoming readily exposed to enemy fire by allowing larger height changes. Time histories, the results of height change maneuver analyses, are shown in Figures 60 through 71 of Appendix V. In all cases, peak load factors occurred during recovery. Results of these analyses are summarized in Table IX. Results show lower load factors in the height change maneuvers than in turns. The lower load factors are a result of the total height excursion limitation imposed on the maneuvers. This result occurred only because of the limited number of analysis iterations that were possible within the scope of the program. The control input rates used in formulating the analytic autopilot (see Appendix III) were selected, from knowledge of human response characteristics, as first approximations that would be compatible with 200 feet total height changes. It is probable that additional analysis iterations, wherein control input rates would be adjusted, would result in more severe maneuvers within the pre-established height change.

2.2.13 Rotor Loads, Stresses and Weights

Time histories of blade bending moments at the root are presented in Appendix V along with the time histories of many other parameters of interest. In order to obtain blade loads in a meaningful form for evaluation as to their

impact on fatigue life (based on a mission profile for the aircraft), the maximum and minimum values of the root bending moments time history traces were read, from which the mean and cyclic bending loads were determined. As illustrated in Figure 30 the time histories were read at points (a) and (b), where point (a) represents the trim condition immediately preceding the maneuver and point (b) represents the maximum transient load experienced in reaching the maneuver.

Mean and cyclic flapwise and in-plane bending moments at the root and at three discrete blade locations are presented in Tables XIV and XV; the selected locations are illustrated in Figure 31. Table XIV summarizes the bending loads developed during coordinated turn maneuvers and Table XV presents the bending loads obtained in pull-up and push-over maneuvers.

The bending moments at the three blade stations were obtained by applying normalized spanwise bending moment distribution curves to the blade root bending moments determined from the time histories. The distribution curves used are based on experience gained on the Lockheed AH-56A aircraft; inasmuch as the blade stiffnesses and weight distributions used in the analyses were scaled to be similar to those of the main rotor blades on the Lockheed AH-56A, this procedure produced meaningful results.

Blade stresses were computed at the three blade locations identified in Figure 31. The neutral axis was assumed to be located at the maximum blade thickness, which is at 30% chord. For the purpose of the analyses, it was assumed that the weight centroid location coincides with the neutral axis location. Figure 32 illustrates the blade section characteristics used for computing stresses. The maximum mean and cyclic flapwise stresses (at the maximum thickness) and the maximum mean and cyclic in-plane stresses (at the trailing edge) are reported. The contribution of centrifugal forces to stresses is added to all mean stresses.

The stiffness and weight distributions used for the blades are shown in Figures 33, 34, and 35. The points used in the stress analyses are shown on the stiffness curves of Figures 33 and 34.

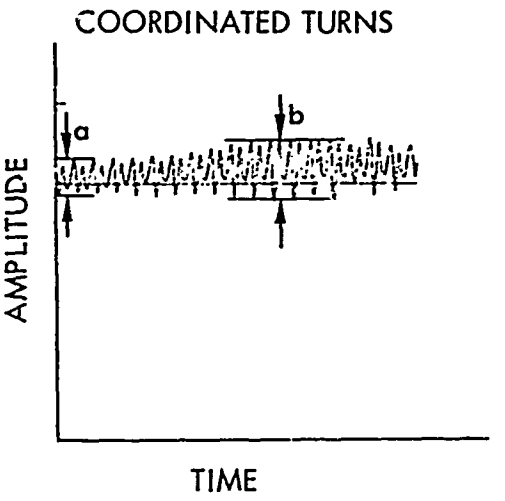

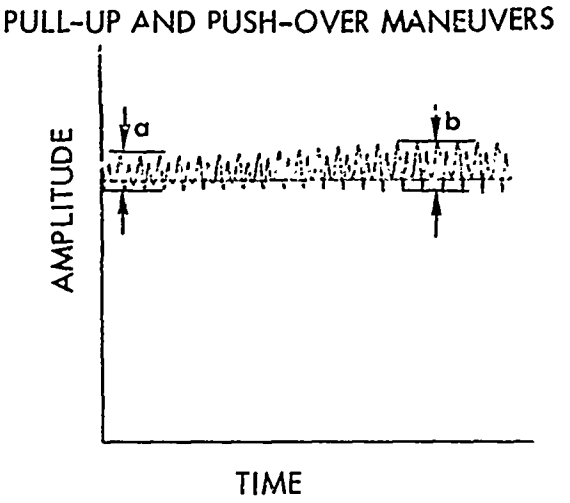

Figure 30. Definition of Quantities Characterizing Oscillatory Load Amplitudes.

TABLE XIV. BLADE LOADS FOR COORDINATED TURN MANEUVERS

Config.	Nominal Load Factor	Conditions	blade root flap mean	blade root flap cyclic	blade root inplane mean	blade root inplane cyclic	sta. 3.6.6 ft flap mean	sta. 3.6.6 ft flap cyclic	sta. 3.6.6 ft inplane mean	sta. 3.6.6 ft inplane cyclic	sta. J 10 ft flap mean	sta. J 10 ft flap cyclic	sta. J 10 ft inplane mean	sta. J 10 ft inplane cyclic	sta. 3 17 ft flap mean	sta. 3 17 ft flap cyclic	sta. 3 17 ft inplane mean	sta. 3 17 ft inplane cyclic
1	1.5	a	82.5	87.5	70.0	108.0	21.4	22.7	42.7	65.9	16.5	17.5	34.3	52.9	9.9	10.5	16.8	25.9
		b	140.0	210.0	75.0	245.0	36.4	54.6	45.7	149.4	28.0	42.0	36.7	120.1	16.8	25.2	18.0	58.8
2	1.75	a	60.0	110.0	96.0	126.0	15.6	28.6	58.6	76.9	12.0	22.0	47.0	61.7	7.2	13.2	23.0	30.2
		b	127.5	252.5	110.0	270.0	33.2	65.7	67.1	164.7	25.5	50.5	53.9	132.3	15.3	30.3	26.4	64.8
3	2.0	a	60.0	150.0	135.0	135.0	15.6	39.0	82.3	82.3	12.0	30.0	66.2	66.2	7.2	18.0	32.4	32.4
		b	175.0	325.0	165.0	315.0	45.5	84.5	100.6	192.1	35.0	65.0	80.8	154.4	21.0	39.0	39.6	75.6
4	1.50	a	67.5	87.5	75.0	100.0	17.5	22.7	45.7	61.0	13.5	17.5	36.7	49.0	8.1	10.5	18.0	24.0
		b	122.5	207.5	80.0	230.0	31.8	54.0	48.8	140.3	24.5	41.5	39.2	112.7	14.7	24.9	19.2	55.2
5	1.75	a	60.0	100.0	92.5	117.5	15.6	26.0	56.4	71.7	12.0	20.0	45.3	57.6	7.2	12.0	22.2	28.2
		b	125.0	250.0	95.0	245.0	32.5	65.0	57.3	149.4	25.0	50.0	46.5	120.1	15.0	30.0	22.8	58.8
6	2.0	a	40.0	120.0	130.0	140.0	10.4	31.2	79.3	85.4	8.0	24.0	63.7	68.6	4.8	14.4	31.2	33.6
		b	135.0	265.0	135.0	215.0	35.1	68.9	82.3	131.1	27.0	53.0	66.2	105.3	16.2	31.8	32.4	51.6

NOTES:

(1) All loads are bending moments in 1000 in.-lb.

(2) Conditions a and b are defined in Figure 30.

(3) Blade stations are shown in Figure 31.

TABLE XV. BLADE LOADS FOR PULL-UP AND WASH-OVER MANEUVERS

1	1.5	a	82.5	87.5	70.0	108.0	21.4	22.7	42.7	65.9	16.5	17.5	34.3	52.9	9.9	10.5	16.8	25.9
		b	115.0	115.0	60.0	170.0	29.9	29.9	36.6	103.7	23.0	23.0	29.4	83.3	13.8	13.8	14.4	40.8
1	1.5	a	82.5	87.5	65.0	113.0	21.4	22.7	39.6	68.9	16.5	17.5	31.8	55.4	9.9	10.5	15.6	27.1
		b	25.0	75.0	80.0	70.0	6.5	19.5	48.8	42.7	5.0	15.0	39.2	34.3	3.0	9.0	19.2	16.8
2	1.75	a	60.0	110.0	96.0	126.0	15.6	28.6	58.6	76.9	12.0	22.0	47.0	61.7	7.2	13.2	23.0	30.2
		b	117.5	147.5	75.0	200.0	30.5	38.4	45.7	122.0	23.5	29.5	36.7	98.0	14.1	17.7	18.0	48.0
2	1.75	a	60.0	110.0	96.0	126.0	15.6	28.6	58.6	76.9	12.0	22.0	47.0	61.7	7.2	13.2	23.0	30.2
		b	10.0	90.0	100.0	70.0	2.6	23.4	61.0	42.7	2.0	18.0	49.0	34.3	1.2	10.8	24.0	16.8
3	2.0	a	60.0	150.0	135.0	135.0	15.6	39.0	82.3	82.3	12.0	30.0	66.2	66.2	7.2	18.0	32.4	32.4
		b	145.0	185.0	120.0	220.0	37.7	48.1	73.2	134.2	29.0	37.0	58.8	107.8	17.4	22.2	28.8	52.8
3	2.0	a	60.0	150.0	135.0	135.0	15.6	39.0	82.3	82.3	12.0	30.0	66.2	66.2	7.2	18.0	32.4	32.4
		b	35.0	115.0	125.0	95.0	9.1	29.9	76.2	57.9	7.0	23.0	61.3	46.5	4.2	13.8	30.0	22.8
4	1.5	a	67.5	87.5	75.0	100.0	17.5	22.7	45.7	61.0	13.5	17.5	36.7	49.0	8.1	10.5	18.0	24.0
		b	90.0	100.0	65.0	145.0	23.4	26.0	39.6	88.4	18.0	20.0	31.0	71.0	10.8	12.0	15.6	34.8
4	1.5	a	67.5	87.5	75.0	100.0	17.5	22.7	45.7	61.0	13.5	17.5	36.7	49.0	8.1	10.5	18.0	24.0
		b	10.0	70.0	70.0	70.0	2.6	18.2	42.7	42.7	2.0	14.0	34.3	34.3	1.2	8.4	16.8	16.8
5	1.75	a	60.0	100.0	92.5	117.5	15.6	26.0	56.4	71.7	12.0	20.0	45.3	57.6	7.2	12.0	22.2	28.2
		b	110.0	140.0	80.0	170.0	28.6	36.4	48.8	103.7	22.0	28.0	39.2	83.3	13.2	16.8	19.2	40.8
5	1.75	a	60.0	100.0	92.5	117.5	15.6	26.0	56.4	71.7	12.0	20.0	45.3	57.6	7.2	12.0	22.2	28.2
		b	5.0	85.0	97.5	77.5	1.3	22.1	59.5	47.3	1.0	17.0	47.8	38.0	.6	10.2	23.4	18.6
6	2.0	a	40.0	120.0	130.0	140.0	10.4	31.2	79.3	85.4	8.0	24.0	63.7	68.6	4.8	14.4	31.2	33.6
		b	102.5	167.5	117.5	207.5	26.6	43.6	71.7	126.6	20.5	33.5	57.6	101.7	12.3	20.1	28.2	49.8
6	2.0	a	40.0	120.0	130.0	140.0	10.4	31.2	79.3	85.4	8.0	24.0	63.7	68.6	4.8	14.4	31.2	33.6
		b	25.0	105.0	105.0	95.0	6.5	27.3	64.0	57.9	5.0	21.0	51.5	46.5	3.0	12.6	25.2	22.8

NOTES:

(1) All loads are bending moments in 1000 in.-lb.

(2) Conditions a and b are defined in Figure 30.

(3) Blade stations are shown in Figure 31.

(4) Sequence in which maneuvers are listed is identical to sequence given in Table IX; refer to Table IX to determine which maneuvers represent height increases and which represent height decreases.

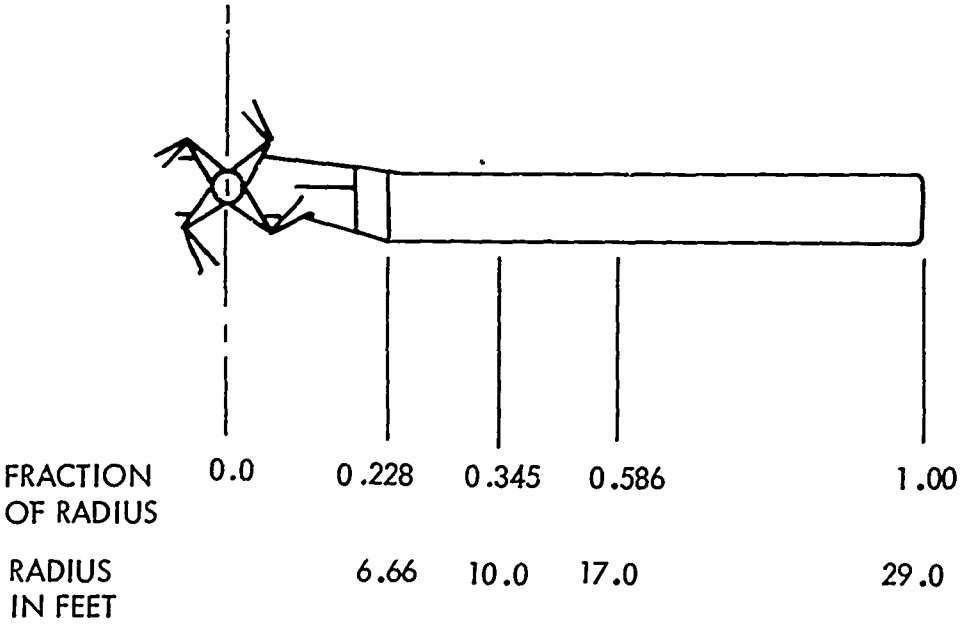

Figure 31. Locations of Blade Stations Cited in Connection with Loads and Stresses.

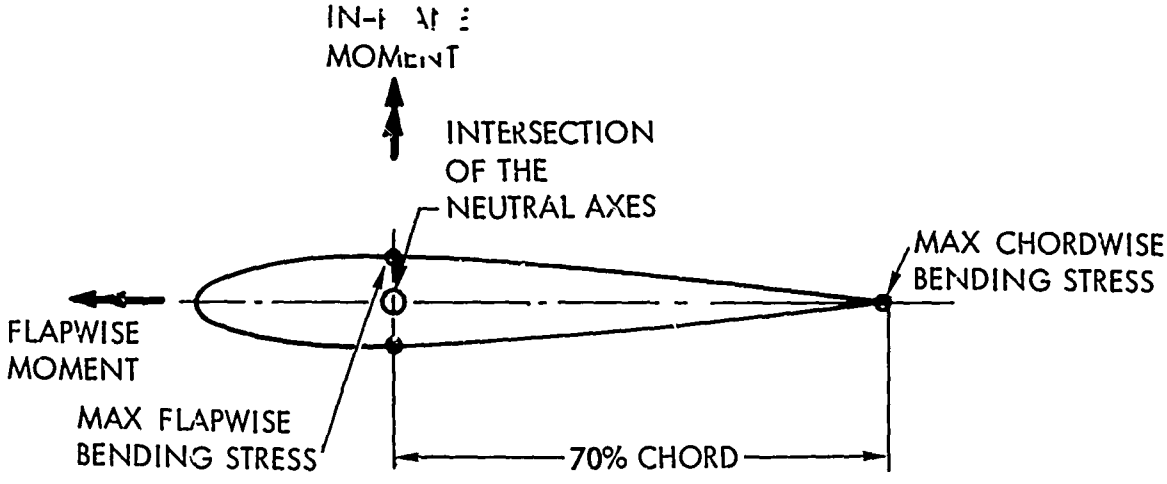

Figure 32. Parameters Used in Computation of Maximum Bending Stresses.

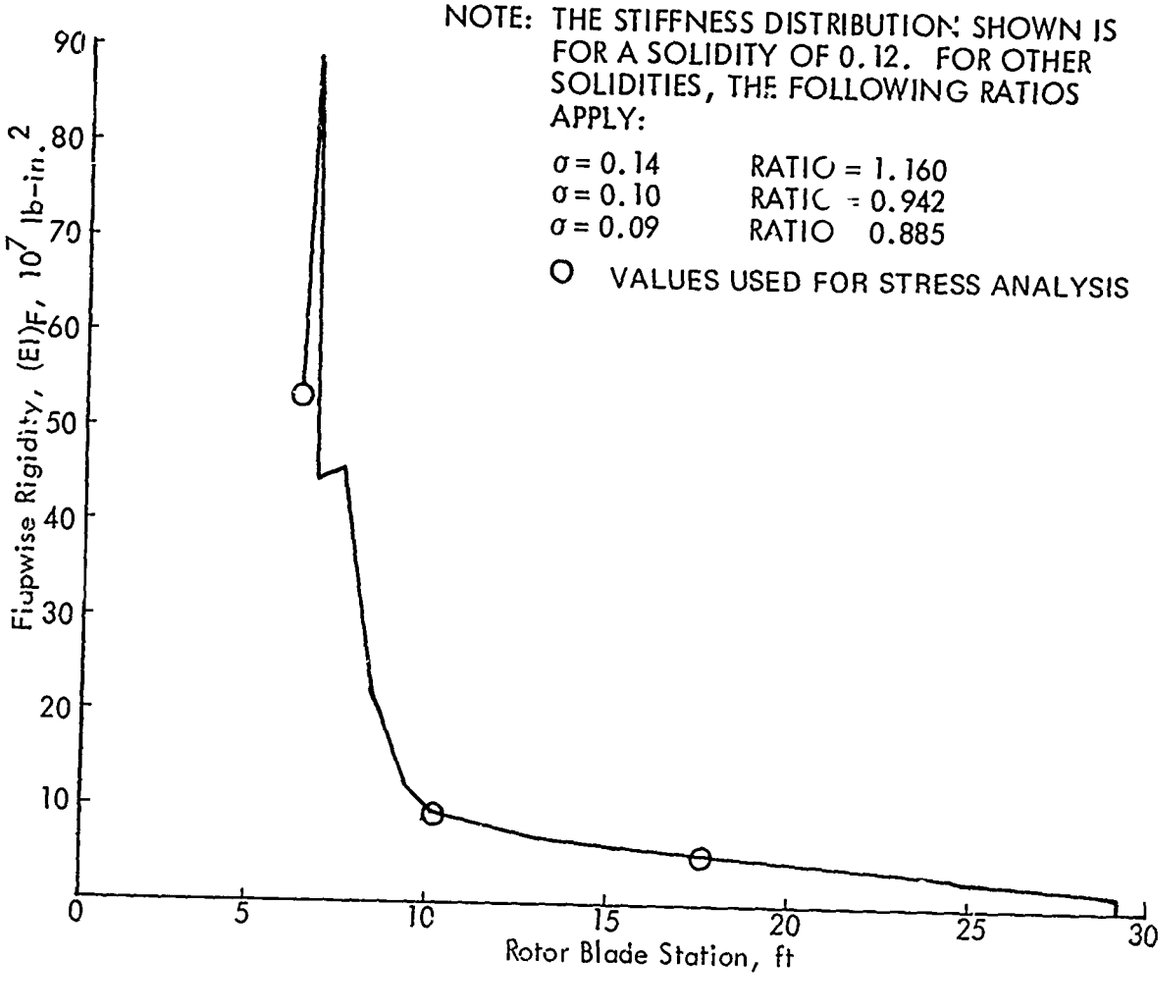

Figure 33. Rotor Blade Flapwise Bending Stiffness.

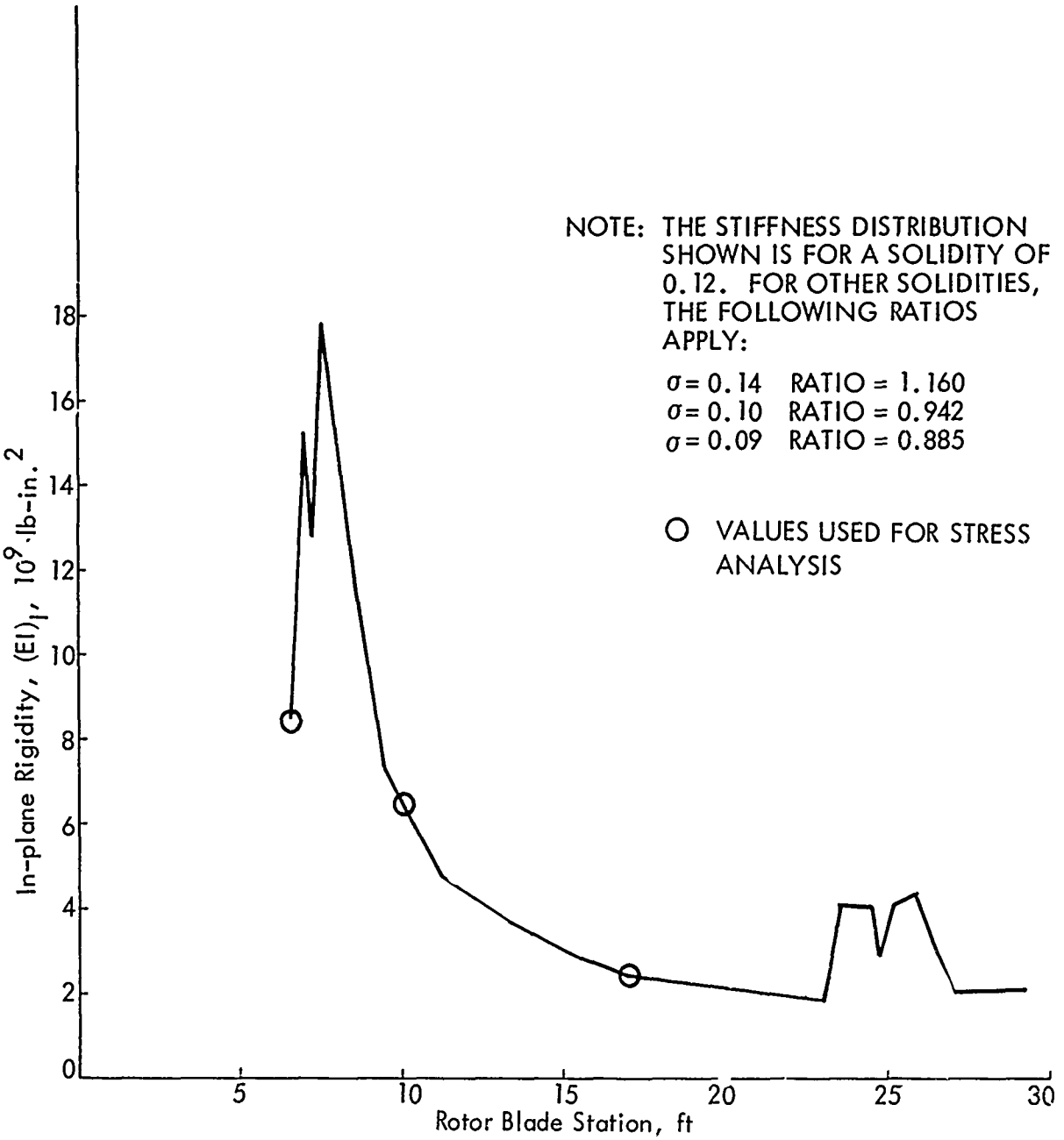

Figure 34. Rotor Blade In-Plane Bending Stiffness.

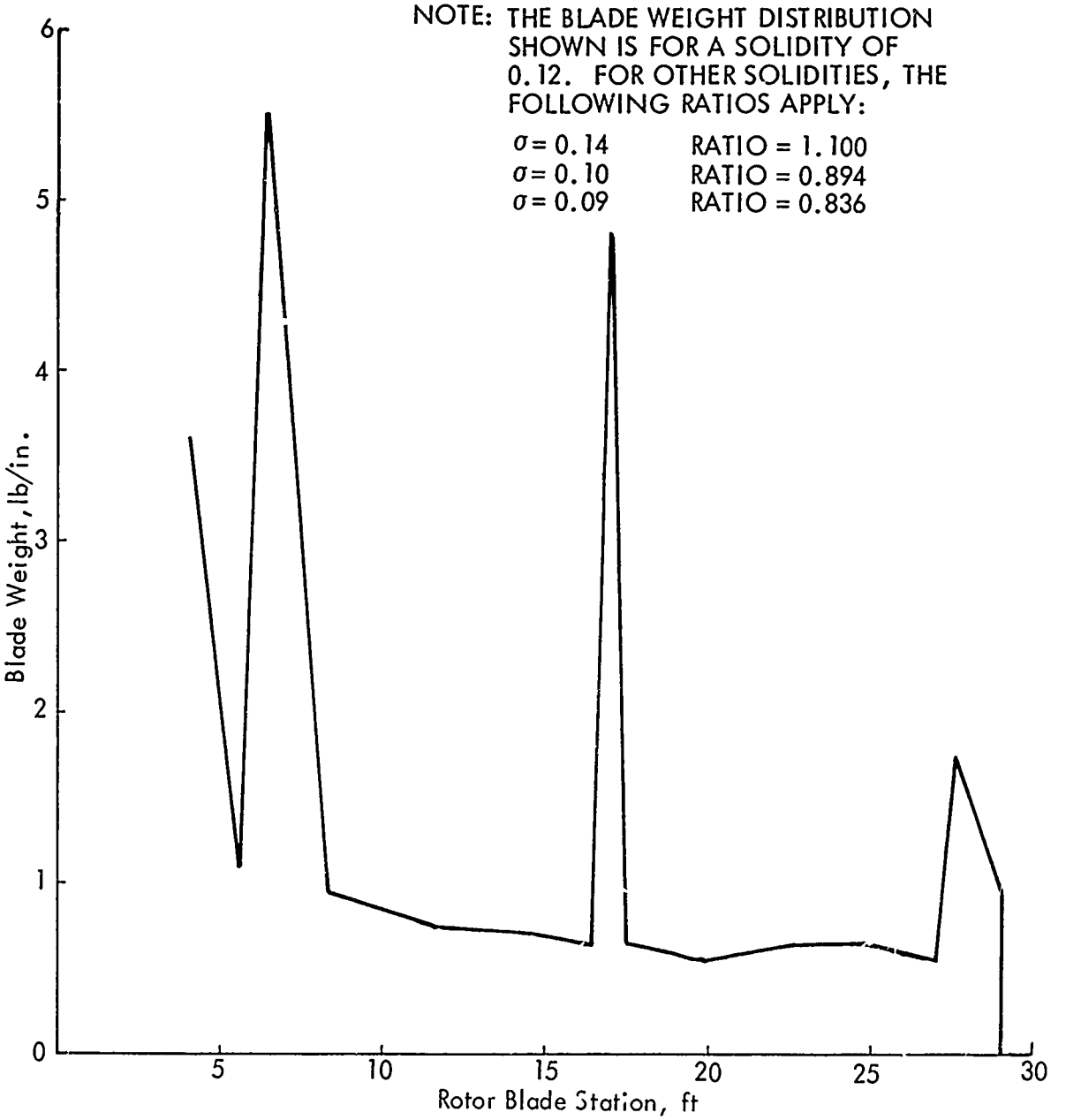

Figure 35. Rotor Blade Weight Distribution.

The blade stiffness and weight distributions were modeled after those of the AH-56A rotor blades which have a variable thickness along the span from a 12-percent-thick section at the root to a 6-percent-thick section at the tip. This influence was appropriately considered in evaluating the theoretical stress levels of the analysis model blades. The resulting mean and cyclic stresses are presented in Tables XVI and XVII.

In evaluating the practicality of the stress levels, it must be borne in mind that (1) stress allowables would be for steel blades, and (2) additional iterations on rotor design would likely result in some structural optimization. Stress allowables recommended for preliminary evaluation are: transient stresses should not exceed ±50,000 psi; endurance stresses (cyclics) should not exceed ±20,000 psi.

Variations in rotor weights among the analytic models were first indicated by Figure 25, which showed variations of rotor-group weights with changes in solidity and tip speeds. These were determined per the parametric trend equations described in Reference 1. Of particular interest at this point in the discussion is the comparison of the rotor-group weights among the configurations, as the gross weight is held constant. The rotor-group changes among the configurations reflect the changes assigned to rotor solidity in the helicopters (Configurations 1, 2, and 3) and the reductions in solidity as wings of various sizes were added (Configurations 4, 5, and 6).

2.2.14 Vibrations

The vibratory loads impressed on the rotor hub by the vibrating blades are a primary source of body vibrations.

The helicopter vibrations arising during the execution of coordinated turns are exhibited by the time histories in Figure 36. The predominant frequency of vibration is either 4 cyc/rev (characteristic of a 4-blade rotor) or 0.7 cyc/rev, depending upon maneuvering conditions. Since the latter frequency is not a multiple of the fundamental harmonic (integral multiple of the number of blades) frequency of the rotor, it must represent either a self-excited vibration of the helicopter system (requiring no external alternating

TABLE XVI. BLADE STRESSES FOR COORDINATED TURN MANEUVERS

Config	Nominal Load Factor	Conditions	sta. @ 6.6 ft flap mean	flap cyclic	in-plane mean	in-plane cyclic	sta. @ 10 ft flap mean	flap cyclic	in-plane mean	in-plane cyclic	sta. @ 17 ft flap mean	flap cyclic	in-plane mean	in-plane cyclic
1	1.5	a	6.52	1.88	7.79	4.70	28.74	6.65	25.67	4.93	32.87	6.24	31.06	6.28
		b	7.76	4.52	8.01	10.65	33.11	15.95	25.90	11.19	36.97	14.98	31.35	14.25
2	1.75	a	6.20	2.67	9.46	6.19	27.62	9.44	27.43	6.50	31.82	8.87	33.30	8.28
		b	7.84	6.14	10.15	13.27	33.42	21.68	28.15	13.94	37.27	20.36	34.22	17.75
3	2.0	a	6.21	3.67	11.42	6.67	27.65	12.95	29.48	7.01	31.85	12.17	35.91	8.93
		b	9.02	7.95	12.90	15.57	37.58	28.07	31.04	16.36	41.18	26.36	37.90	20.83
4	1.50	a	6.14	1.80	7.87	4.16	27.38	6.37	25.75	4.38	31.60	5.98	31.16	5.57
		b	7.27	4.28	8.08	9.58	31.39	15.10	25.97	10.06	35.36	14.18	31.44	12.81
5	1.75	a	6.04	2.15	8.77	5.11	27.03	7.60	26.70	5.37	31.27	7.13	32.37	6.83
		b	7.43	5.38	8.87	10.65	31.97	18.99	26.81	11.19	35.90	17.83	32.51	14.25
6	2.0	a	5.72	2.92	11.13	6.88	25.91	10.30	29.18	7.23	30.21	9.68	35.53	9.20
		b	8.03	6.44	11.38	10.57	34.06	22.75	29.44	11.10	37.87	21.37	35.86	14.13

NOTE:

(1) All values in tables are for 1000 psi.

(2) Conditions a and b are defined in Figure 30.

(3) Blade stations are shown in Figure 31.

(4) See discussion in Section 2.2.13 for allowable stress.

TABLE XVII. BLADE STRESSES FOR PULL-UP AND PUSH-OVER MANEUVERS

1	1.5	a	6.52	1.88	7.79	4.70	28.74	6.65	25.67	4.93	32.87	6.24	31.06	6.28
		b	7.22	2.47	7.35	7.39	31.21	8.74	25.21	7.76	35.19	8.20	30.47	9.39
1	1.5	a	6.52	1.38	7.57	4.91	28.74	6.65	25.44	5.16	32.87	6.24	30.77	6.57
		b	5.28	1.61	8.22	3.04	24.37	5.70	26.13	3.20	28.77	5.35	31.64	4.07
2	1.75	a	6.20	2.67	9.46	6.19	27.62	9.44	27.43	6.50	31.82	8.87	33.30	8.28
		b	7.60	3.59	8.43	9.83	32.56	12.66	26.34	10.33	36.46	11.89	31.92	13.15
2	1.75	a	6.20	2.67	9.46	6.19	27.62	9.44	27.43	6.50	31.82	8.87	33.30	8.28
		b	4.99	2.19	9.66	3.44	23.33	7.73	27.63	3.61	27.79	7.26	33.56	4.60
3	2.0	a	6.21	3.67	11.42	6.67	27.65	12.95	29.48	7.01	31.85	12.17	35.91	8.93
		b	8.29	4.52	10.68	10.87	34.99	15.98	28.70	11.42	38.75	15.00	34.92	14.55
3	2.0	a	6.21	3.67	11.42	6.67	27.65	12.95	29.48	7.01	31.85	12.17	35.91	8.93
		b	5.60	2.81	10.92	4.70	25.49	9.93	28.96	4.93	29.82	9.33	35.25	6.28
4	1.5	a	6.14	1.80	7.87	4.16	27.38	6.37	25.75	4.38	31.60	5.98	31.16	5.57
		b	6.60	2.06	7.45	6.04	29.02	7.28	25.32	6.34	33.14	6.83	30.61	8.08
4	1.5	a	6.14	1.80	7.87	4.16	27.38	6.37	25.75	4.38	31.60	5.98	31.16	5.57
		b	4.95	1.44	7.66	2.92	23.20	5.09	25.53	3.06	27.67	4.78	30.89	3.30
5	1.75	a	6.04	2.15	8.77	5.11	27.03	7.60	26.70	5.37	31.27	7.13	32.37	6.83
		b	7.11	3.01	8.22	7.39	30.83	10.63	26.13	7.76	34.83	9.99	31.64	9.89
5	1.75	a	6.04	2.15	8.77	5.11	27.03	7.60	26.70	5.37	31.27	7.13	32.37	6.83
		b	4.85	1.83	8.98	3.37	22.85	6.46	26.92	3.54	27.34	6.06	32.66	4.51
6	2.0	a	5.72	2.92	11.13	6.88	25.91	10.30	29.18	7.23	30.21	9.68	35.53	9.20
		b	7.24	4.07	10.52	10.20	31.27	14.38	28.54	10.71	35.25	13.51	34.71	13.64
6	2.0	a	5.72	2.92	11.13	6.88	25.91	10.30	29.18	7.23	30.21	9.68	35.53	9.20
		b	5.35	2.55	9.90	4.67	24.62	9.02	27.89	4.90	29.00	8.47	33.89	6.25

NOTE:

(1) All values in tables are for 1000 psi.

(2) Conditions a and b are defined in Figure 30.

(3) Blade stations are shown in Figure 31.

(4) See discussion in Section 2.2.13 for allowable stress.

(5) Sequence in which maneuvers are listed is identical to sequence given in Table IX; refer to Table IX to determine which maneuvers represent height increases and which represent height decreases.

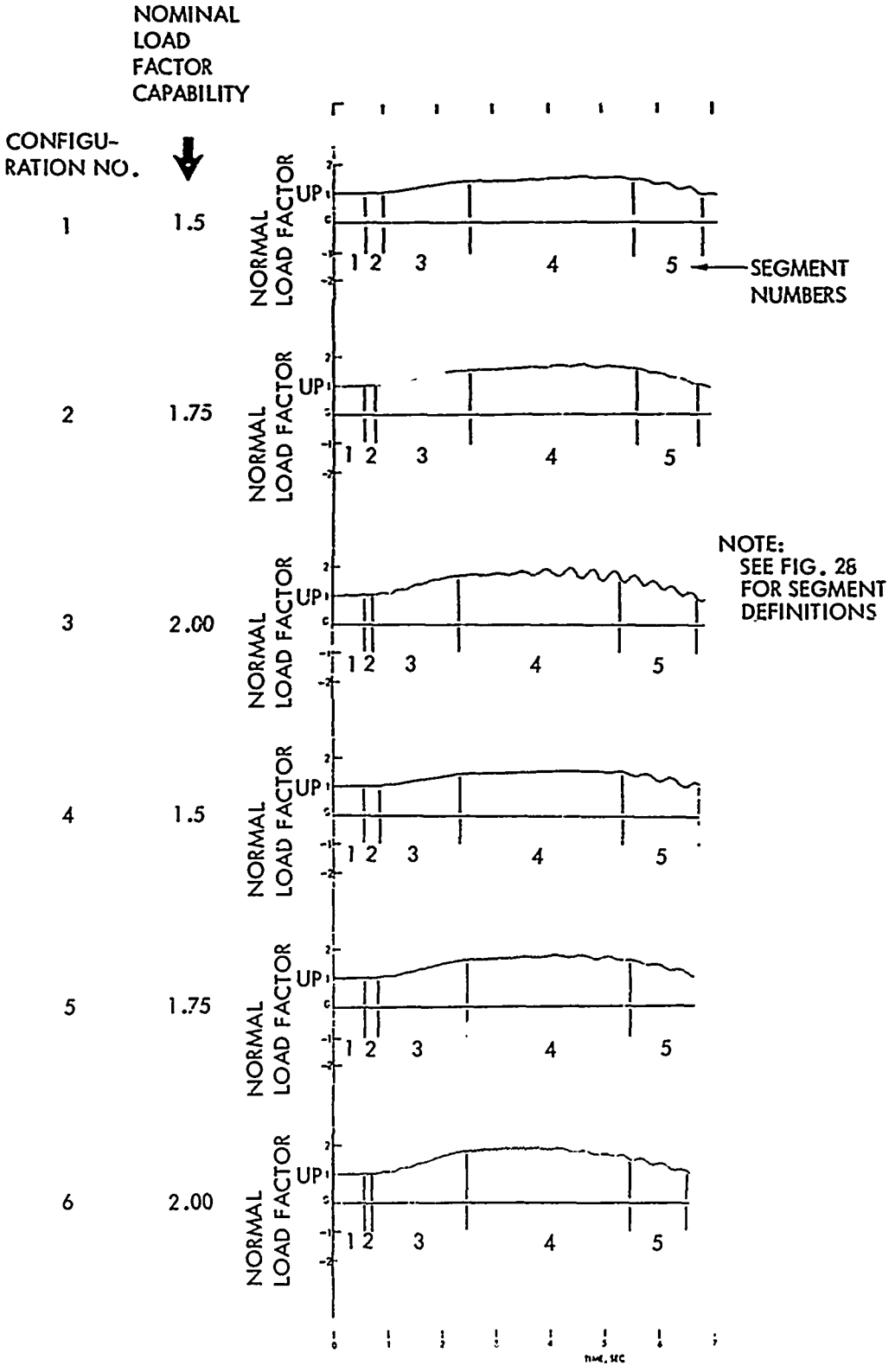

Figure 36. Vibrations Arising During the Execution of Coordinated Turns.

force for sustention) or an ordinary vibration induced by commands to the analytic autopilot. That the latter is not the case can be established by comparing the time histories of the commands (see Figure 47) and the oscillation in load factor (see Figure 37).

Figure 37 shows two of the curves from Figure 36, superimposed on each other to demonstrate differences that occurred in the vibration characteristics of the unwinged and winged helicopters. It is readily apparent from Figure 37 that the winged helicopter provides a smoother ride during the maneuver. This fact, and concern over what phenomenon might underlie the large vibrations, is the subject of the following qualitative explanation.

The principal difference between the two concepts (unwinged and winged) is that the winged helicopter has a rotor of lower solidity than the helicopter. Therefore, except for whatever small contribution the wing makes in the form of damping in plunge, the fact that the wing is relieving the rotor of lift during the maneuver is the effective difference, and this suggests that the vibratory phenomenon is associated with normal rotor blade loads.

Examination of the load factor time history for the unwinged helicopter reveals that the severe vibratory behavior is manifested only after it has been at high load factor for some time. It is rationalized that an adverse airloads coupling arises due to excessive coning caused by the high blade loads. Note that the unwinged as well as the winged helicopters evidence this behavior, but the effect is less severe for the more lightly loaded and, consequently, less coned rotor of the winged helicopter.

The vibration subsides as the aircraft is returned to level unaccelerated flight. It is hypothesized, then, that the incitement of the vibration is a function of load factor level, and that possibly during maneuvers at lower load factors and/or speeds, the phenomenon would not appear. This rationale certainly is consistent with the effect of periodic loading amplification due to excessive coning.

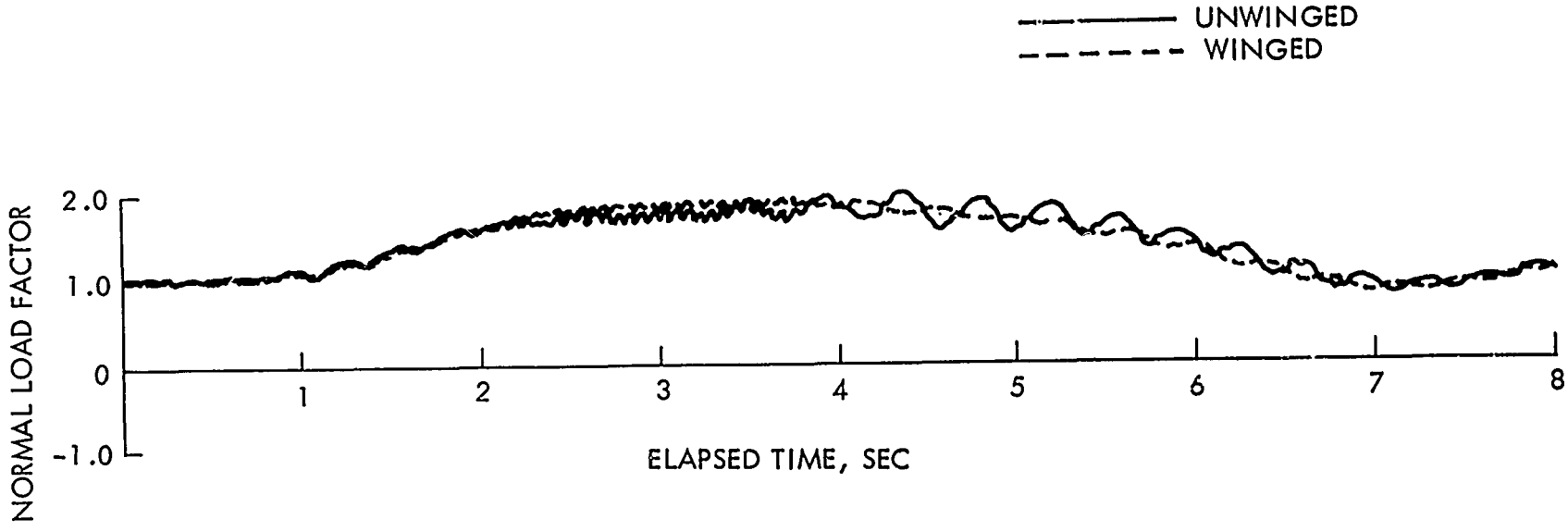

Figure 37. Time Histories of Load Factors Developed by Configurations 3 and 6 Executing Coordinated Turns at 167 KTAS.

Although this rationale offers a plausible explanation, many additional questions can be raised regarding the phenomenon. This suggests that further study should be undertaken prior to the design of helicopters for the flight speeds and maneuver levels represented in Figure 37.

2.3 ROTOR AND WING SIZING AND DESIGN

Various feasible design alternatives have been discussed without special regard to t ir overall system effectiveness. This section evaluates the impact of maneuverability criteria on the design considerations pertaining to each helicopter concept (unwinged and winged) as a class. An attempt is made to arrive at the best balance among accountable factors consisting of physical parameters, system performance and operational characteristics. While these factors are discussed in a particular sequence, they are all interrelated to some extent, partly because of the iterative process involved in designing a system as complex as a helicopter. Because of these interrelationships, some parameters are more meaningful when considered in basic combinations.

2.3.1 Aircraft Weights and Sizes

As noted in 2.2.1, in order to arrive at a realistic size, the fuselage was designed to accommodate the selected basic equipment, crew, troops and fuel to accomplish the UTIAS design mission. For the specified baseline gross weight of 16,000 lb, satisfying the design mission requirements would have required the elimination of some basic equipment. Alternatively, the fixed equipment could be retained and components of the disposable load could be utilized in various combinations. The latter approach was adopted. Table III presents a weight breakdown on the basis of two loading variations of fuel and payload for each configuration.

2.3.2 Engine Size

Early in the study it became apparent that restricting the installed power (as in Reference 1) to the requirement for a 500-ft/min vertical climb would preclude examining other parameters; therefore, the power and engine size were relaxed as constraints early in the study. Upon examining other

limitations during the study, it became evident that safe operations at the design cruise speed would still allow the original premise of power to be used. For the two-engine aircraft used in this study, the uninstalled sea level static Military power ratings per engine range from 1555 to 1673 shp.

2.3.3 Center-of-Gravity Travel

The center-of-gravity envelopes for the principal loading conditions of each configuration are discussed in 2.2.3.

2.3.4 Aerodynamic Trimming Requirements

Aerodynamic trimming is discussed in 2.2.4. Since an irreversible cyclic control system is employed, no maneuver or trim loads would be sensed at the pilot's stick. However, because the nonrotating airframe aerodynamic characteristics are designed to provide stick position stability with speed and with load factor, and since an artificial feel system is provided to produce stick forces proportional to stick displacement, the pilot could be required to resist a steady stick force. The cockpit controls are therefore assumed to include an actuator by means of which the pilot can compensate for the force in steady flight. This actuator would not alter the stick force gradient with speed or load factor, and the stability characteristics would be retained.

2.3.5 Stability and Control Characteristics

As noted in 2.2.5, basic stability is provided by the nonrotating airframe aerodynamic characteristics and the placement of the center-of-gravity envelopes described in 2.2.3.

2.3.6 Rotor Controls and Pilot Maneuver Controls

The rotor controls and pilot maneuver controls, which are suited to both the basic helicopters and the winged helicopters, are described in Section 2.2.6.

2.3.7 Rotor and Flight Controls and Complexity

A pervasive design consideration in synthesizing the various aircraft was simplicity (minimized complexity) of the rotor and flight controls system.

Conventional main collective control and tail rotor yaw and antitorque control are used for all configurations. The basic main rotor cyclic control system employed with the Lockheed hingeless rotor is equally applicable to the unwinged and winged helicopter configurations. There is no need for auxiliary control surfaces in the winged configurations.

The cyclic control system, described in 2.2.6, is designed to make use of the available control power in a manner which is matched to the pilot response capabilities and provides for precision control (see Reference 17) and handling qualities similar to those of fixed-wing aircraft. This system provides excellent damping and handling qualities under turbulent conditions.

If auxiliary control surfaces were to be prescribed, the additional drag due to control displacements would have to be considered in establishing the maneuver propulsive force requirements. Also, the additional structural weight for these components would have to be included.

2.3.8 Rotor Noise Characteristics

The principal aspects of rotor noise pertinent to this study have been discussed in paragraph 2.2.7. Rotational tip speed, the important parameter, was taken as 700 ft/sec.

2.3.9 Rotor Solidity

Since disc loading was presumed constant (6.06 lb/sq ft) in the study, rotor solidity was derived from the blade area and the blade loading coefficient required to achieve a desired maneuver load factor capability. As discussed previously, the required blade loading coefficient depends on the advance ratio (see Figure 4), and is therefore a function of blade tip speed. The influence of these parameters is discussed in detail in paragraph 2.3.10.

Based on an overall assessment of the effects of the various maneuverability criteria on the aircraft design parameters and other areas of concern (discussed in the succeeding sections), preferred rotor solidities were established: 0.12 for the unwinged helicopter, Configuration 2, and 0.10 for the winged helicopter, Configuration 5.

2.3.10 Tip Speed and Advance Ratio

As indicated previously, blade loading coefficient is the foremost parameter influencing maximum thrust (and therefore maneuver load factor) capability. Blade loading coefficient is a function of blade loading, air mass density, and blade tip speed. Since blade loading is a function of solidity for a particular disc loading, and the air mass density is determined by design atmosphere conditions (4000 ft pressure altitude and 95°F ambient temperature in the present study), blade loading coefficient can be considered a function of blade tip speed if solidity is presumed constant.

At a particular forward speed, as tip speed is increased, higher advancing tip Mach numbers and lower advance ratios are encountered (see Figure 26). The gain in practicable blade loading coefficient accompanying a reduction in advance ratio (see Figure 4) is counteracted to some extent by adverse tip speed effects. Higher tip speeds aggravate compressibility effects, and intensify rotor noise radiation. Within practical limitations, tip speed can be traded for solidity to establish a best rotor weight. Based on these trade-off considerations, a tip speed of 700 ft/sec was selected. Figure 38 shows the relationships that exist between forward speed (in terms of KEAS and KTAS), advance ratio, and advancing tip Mach number at this tip speed.

2.3.11 Disc Loading

Since disc loading was presumed constant (6.06 lb/sq ft) for all configurations studied, trade-off considerations involving disc loading were not relevant. As indicated previously, varying disc loading in the range of 6 to 8 lb/sq ft would not be expected to significantly alter maneuvering ability, especially at the higher forward speeds.

2.3.12 Mean Lift Coefficient

Of the several alternative designs studied, Configuration 2 (unwinged) and Configuration 5 (winged) were found to offer the best balance among system design parameters and performance characteristics. Though not necessarily optimal designs, these aircraft exhibit the most favorable characteristics, particularly with respect to relative weight, oscillatory loads, and power compatible with other mission requirements.

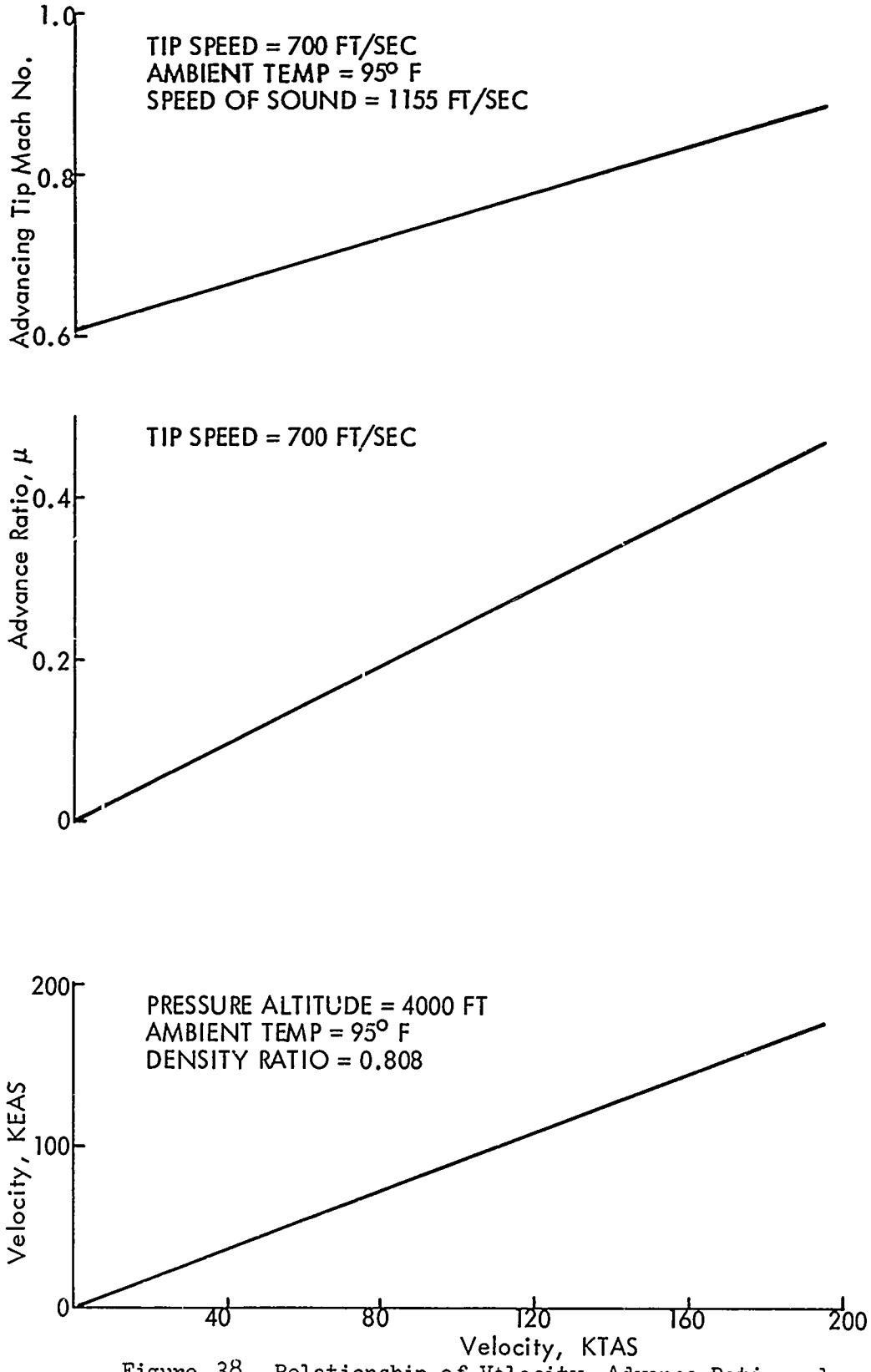

Figure 38. Relationship of Velocity, Advance Ratio and Advancing Tip Mach Number at Design Atmosphere and Tip Speed.

Based on the dual requirements of Configuration 2 to sustain (for 3 sec) a maneuver load factor of 1.75 in a coordinated turn and simultaneously produce sufficient propulsive force to maintain forward speed at 155 KTAS, the preferred blade loading coefficient was taken as 0.094 (at a solidity of 0.12). The corresponding value of mean lift coefficient, which is an alternate form of blade loading coefficient, is 0.56. Trends established from analysis results show that this target load factor would be achieved at 150 KTAS.

The blade loading coefficient (or mean lift coefficient) which was obtained for Configuration 5 was approximately 15 percent greater than that determined for the unwinged helicopter. This permitted trade-offs to be made between decreased rotor lift loading and increased propulsive loading in high-speed maneuvering flight.

2.3.13 Rotor and Wing Lift Sharing Characteristics

Under conditions of level unaccelerated flight, the airframe (nonrotating components of the aircraft) of the unwinged helicopter suffers a download throughout the flight regime,with the maximum levels of download occurring in hovering and high-speed flight (see Figures 39 through 41). The contribution of airframe lift to the total lift developed by Configurations 1, 2, and 3 in coordinated turns is shown in Table XVIII. Table XVIII, which was derived from Table X, shows that the airframe produces progressively more positive lift as the angle of attack increases. The net changes in the ratios of airframe lift to total lift corresponding to the changes in angles of attack between the initial values in level flight and the maximum values attained in the maneuvers are 0.0453, 0.0528 and 0.0665 for Configurations 1, 2 and 3, respectively.

An important consideration affecting the design of the winged helicopters is that the amount of reduction in blade area made possible by the addition of a wing is limited by the increase in rotor propulsive force required due to the drag of the wing. Initially, to facilitate determination of the wing area, collective pitch angle was treated as an invariable quantity and the propulsive-force requirement was suppressed. With this approach, and noting that at low to moderate advance ratios, blade loading coefficient decreases

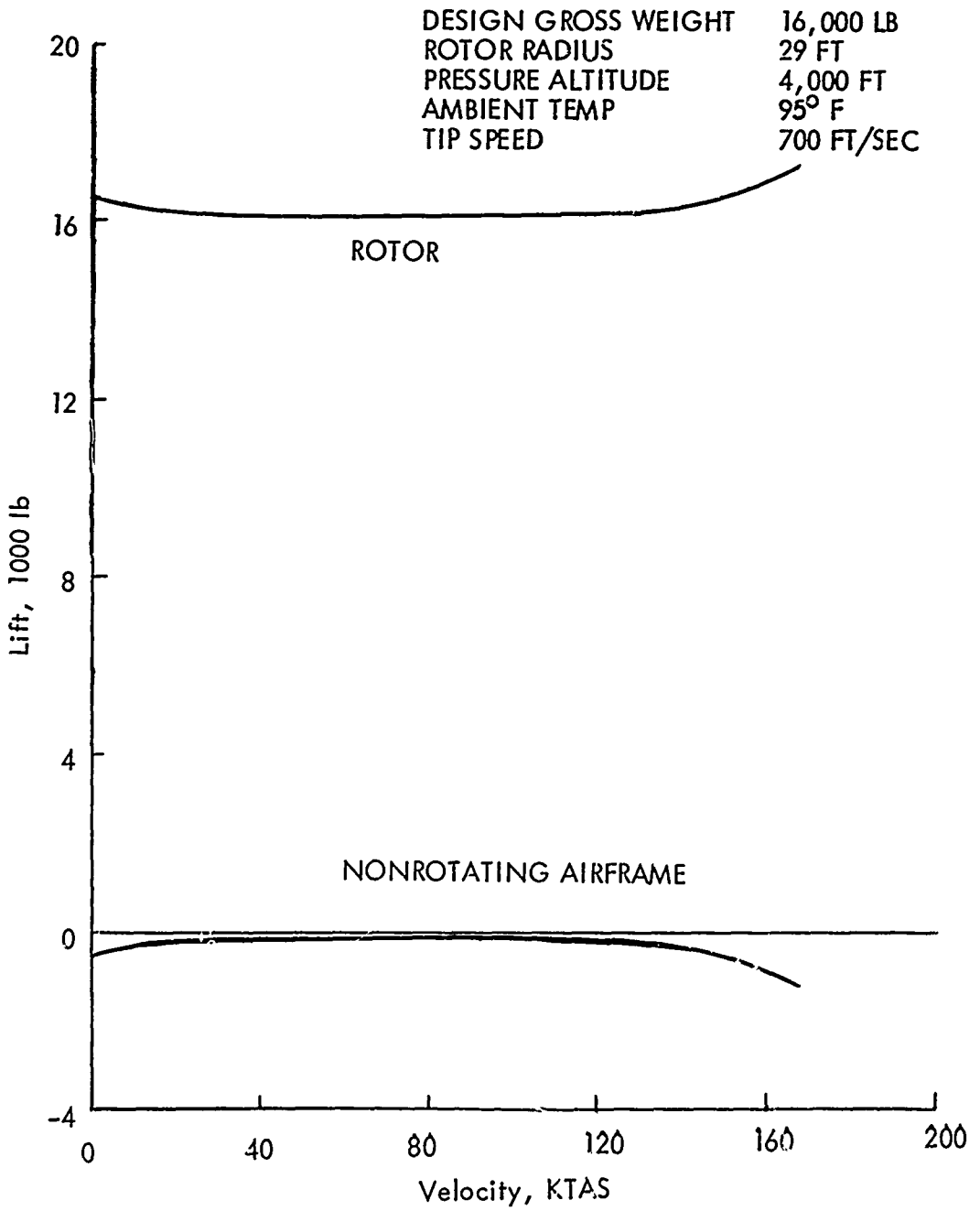

Figure 39. Level Flight (Trim) Lift Sharing for Configuration 1.

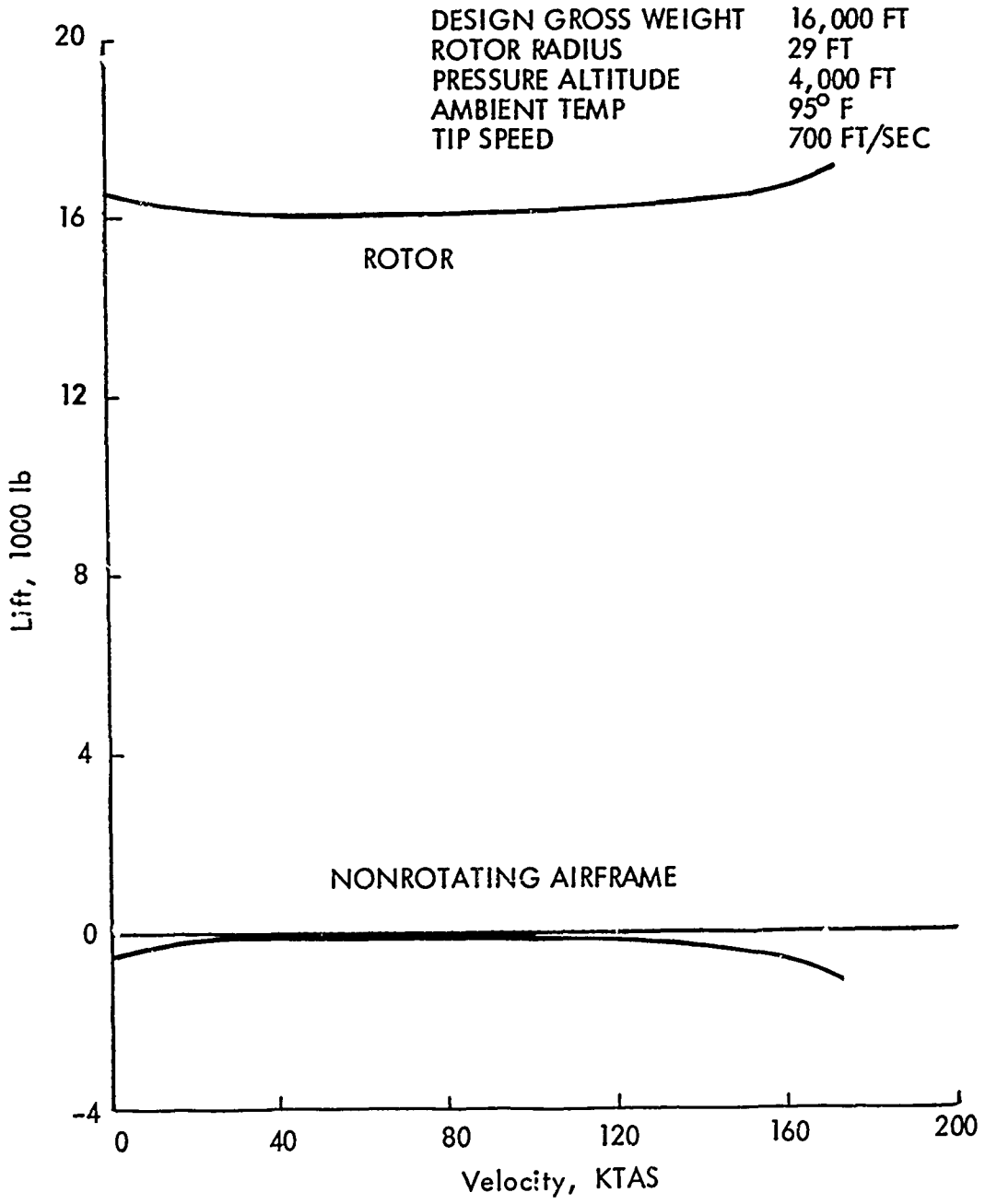

Figure 40. Level Flight (Trim) Lift Sharing for Configuration 2.

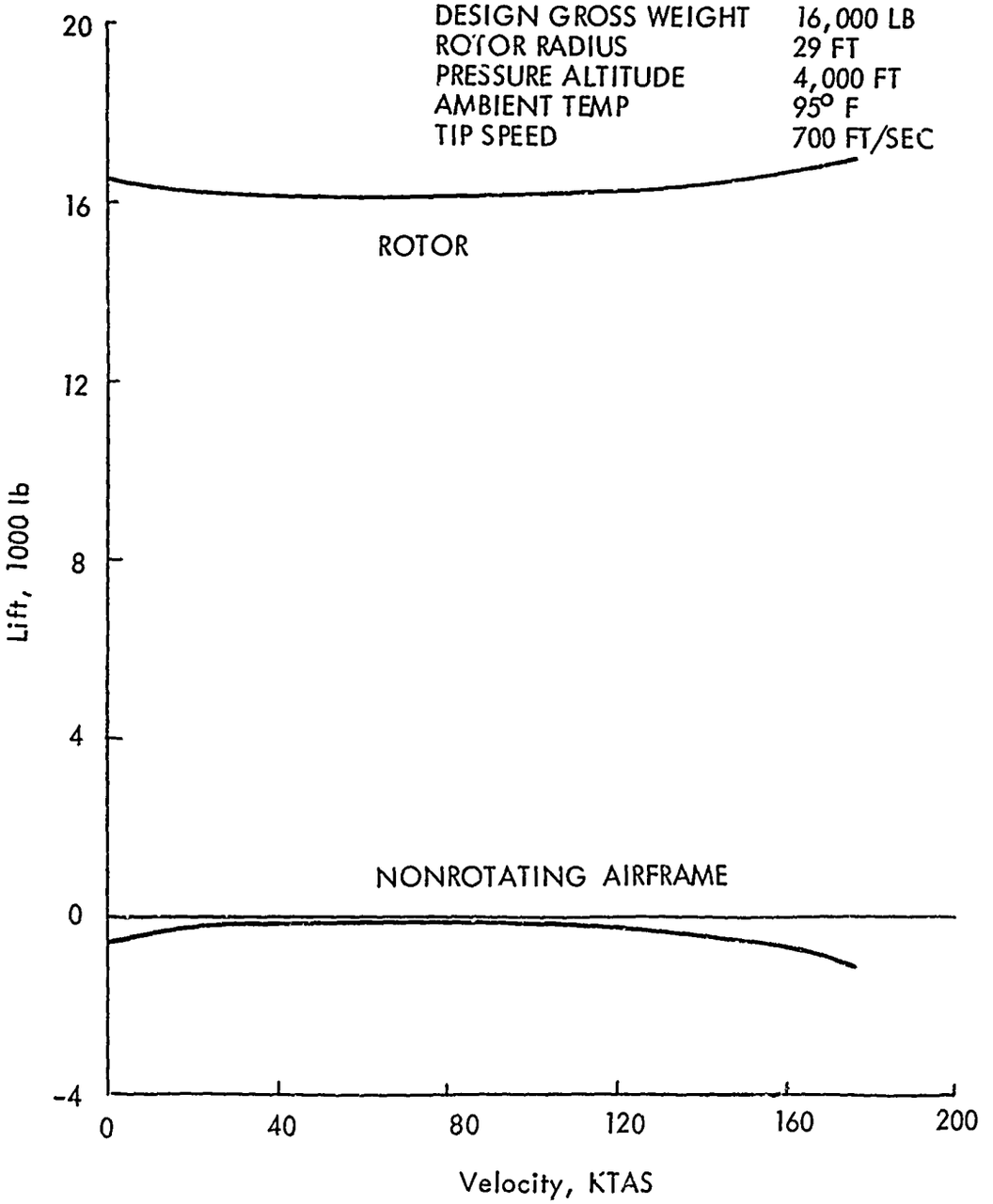

Figure 41. Level Flight (Trim) Lift Sharing for Configuration 3.

TABLE XVIII. HELICOPTER LIFT SHARING CHARACTERISTICS DURING INITIAL LEVEL FLIGHT AND COORDINATED TURNS

Configuration	Initial 1 g Level Flight				Maneuvering Flt., Coordinated Turn					
	Velocity, KTAS	L	$\frac{L_R}{L}$	$\frac{L_A}{L}$	L	$\frac{L_R}{L}^*$	$\frac{L_A}{L}^*$	$\frac{\Delta L_A}{L}$	n^{**} Actual	n Target
1	140	16000	1.022	-0.0219	23040	0.977	+0.0234	0.0453	1.50	1.50
2	155	16000	1.034	-0.0344	25470	0.982	+0.0184	0.0528	1.65	1.75
3	167	16000	1.053	-0.0531	28380	0.987	+0.0134	0.0665	1.75	2.00

*Measured at maximum α_R during maneuver

**Sustained for 3 seconds

with advance ratio in roughly the same manner that dynamic pressure increases with speed, it was tentatively assumed that a wing of the appropriate area operating at a constant lift coefficient throughout the speed regime would compensate for the loss of lift accompanying a reduction in blade area.

But, as implied above, the wing areas established in this manner are not suitable. At the higher speeds, the drag due to the wing imposes an additional propulsive burden on the rotor. Therefore, the wing should be operated at less than its maximum lift coefficient in order to minimize the increment of drag which accompanies an increase in lift. At somewhat lower speeds, where the rotor has adequate propulsive capability, the maximum lift coefficient of the wing can be used to develop the necessary maneuver load. At still lower speeds, a change in collective pitch is necessary to accomplish the more extreme maneuvers. Finally, at the lowest speeds, rotor downwash diminishes the lift coefficient at which the wing would otherwise operate.

This information provides the basis for refinement of the wing design. In designing a winged helicopter for high-speed maneuverability, a wing of relatively large area operating at a moderate lift coefficient (providing for relatively low drag) is preferred; in designing for maneuverability at moderate speeds, a wing of smaller area operating at a higher lift coefficient is preferred.

By tailoring the design of the wing in this manner, it was possible to arrive at conformable maneuver response characteristics for the matching unwinged and winged helicopters.

The hovering download factor used for the unwinged configurations, whose horizontal tails are immersed in the rotor downwash throughout the flight regime, was 3.5 percent of the design gross weight. In the winged configurations, consideration was given to the fact that during hovering and vertical climb, making the ratio of wing span to rotor diameter small minimizes download. Hovering download values which were used for the winged aircraft, Configurations 4, 5 and 6, were 3.9, 4.1 and 4.3 percent, respectively. These values were obtained per the techniques presented in Reference 1. For vertical climb at 500 ft/min, all download factors were increased by approximately 0.2 percent.

In level unaccelerated flight, the distribution of lift between the wing and the rotor is shown by Figures 42 through 44 for Configurations 4, 5 and 6, respectively. The wings begin to contribute positive lift at about 50 KTAS, and this lift increases in a nearly linear manner to speeds of between 140 and 155 KTAS. However, since the wings are designed to be most effective during maneuvering flight, they contribute little lift in level unaccelerated flight, their maximum contribution ranging between 1600 and 1800 lb.

The contribution of wing (airframe) lift to the total lift developed by Configurations 4, 5 and 6 in coordinated turns is shown in Table XIX. Table XIX, which was derived from Table X, also shows the relative lift contributions existing in level unaccelerated flight just prior to execution of the coordinated turns.

It is emphasized that initially available power was not used as a limiting factor in accomplishing the various maneuvers. Rather, the limiting condition of maneuvering ability was the aerodynamic capability of the rotor. As discussed in paragraph 2.2.12, winged Configurations 4, 5 and 6 were limited by rotor propulsive capability at progressively higher speeds. As shown in Table XIX, Configuration 4, which has the lower speed capability, manifests the highest airframe lift coefficient during a coordinated turn.

The net changes in the ratios of nonrotating airframe lift to total lift corresponding to changes in angles of attack between the initial values in level flight and the maximum values attained in the maneuvers are 0.051, 0.079 and 0.067 for Configurations 4, 5 and 6, respectively. These changes are only slightly larger than those obtained for the corresponding unwinged configurations (compare Tables XVIII and XIX). The findings indicate that certain potential advantages that might otherwise accrue to the winged configurations are precluded by rotor propulsive requirements.

2.3.14 Transient Maneuver Flight Path Time Histories

Using the maneuver simulation mathematical model described in Appendix II, time histories of certain quantities having an important bearing on maneuvering flight were calculated and plotted. Appendix V presents reproductions of plots obtained directly from a Calcomp tape plotting system. The various families

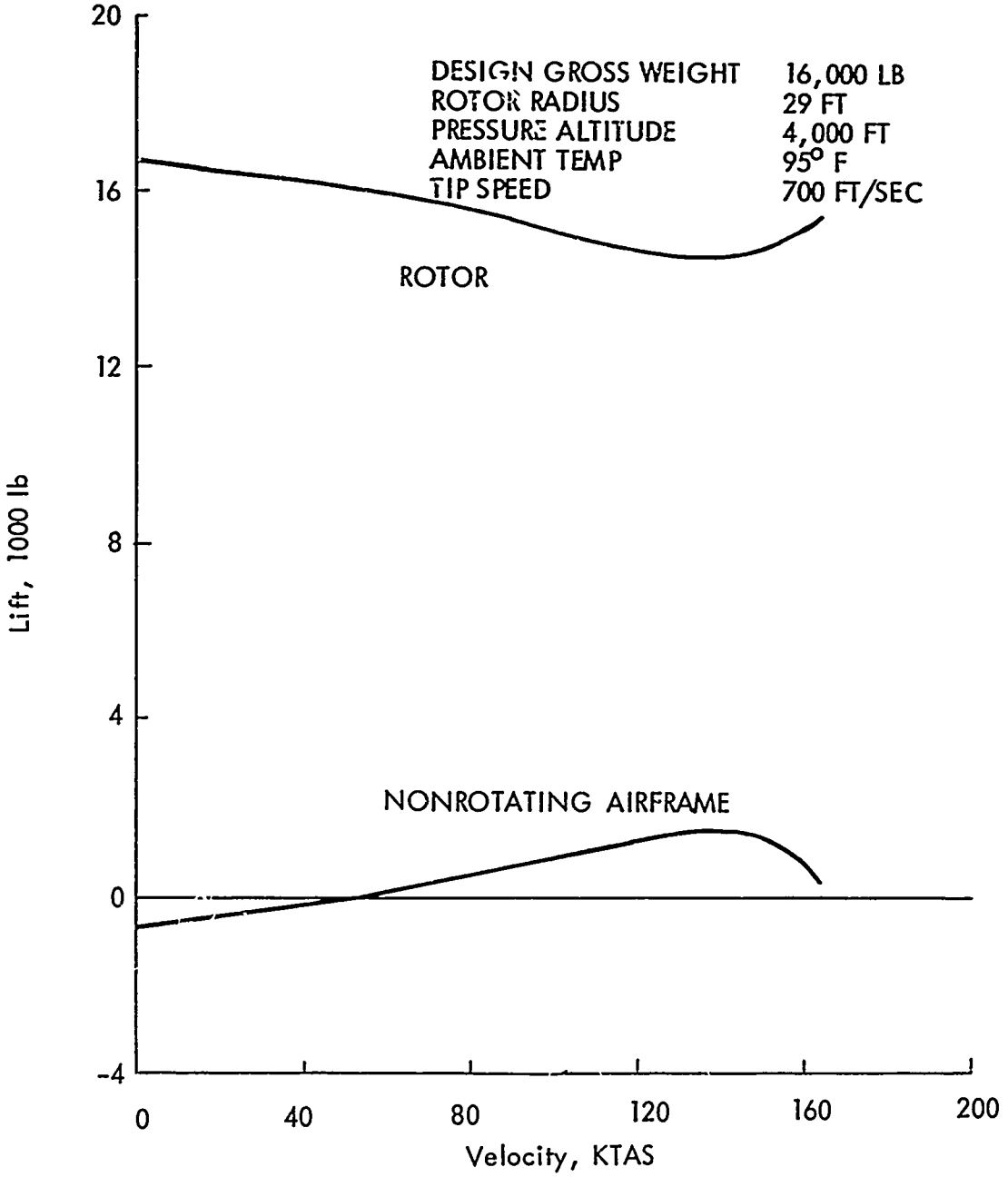

Figure 42. Level Flight (Trim) Lift Sharing for Configuration 4.

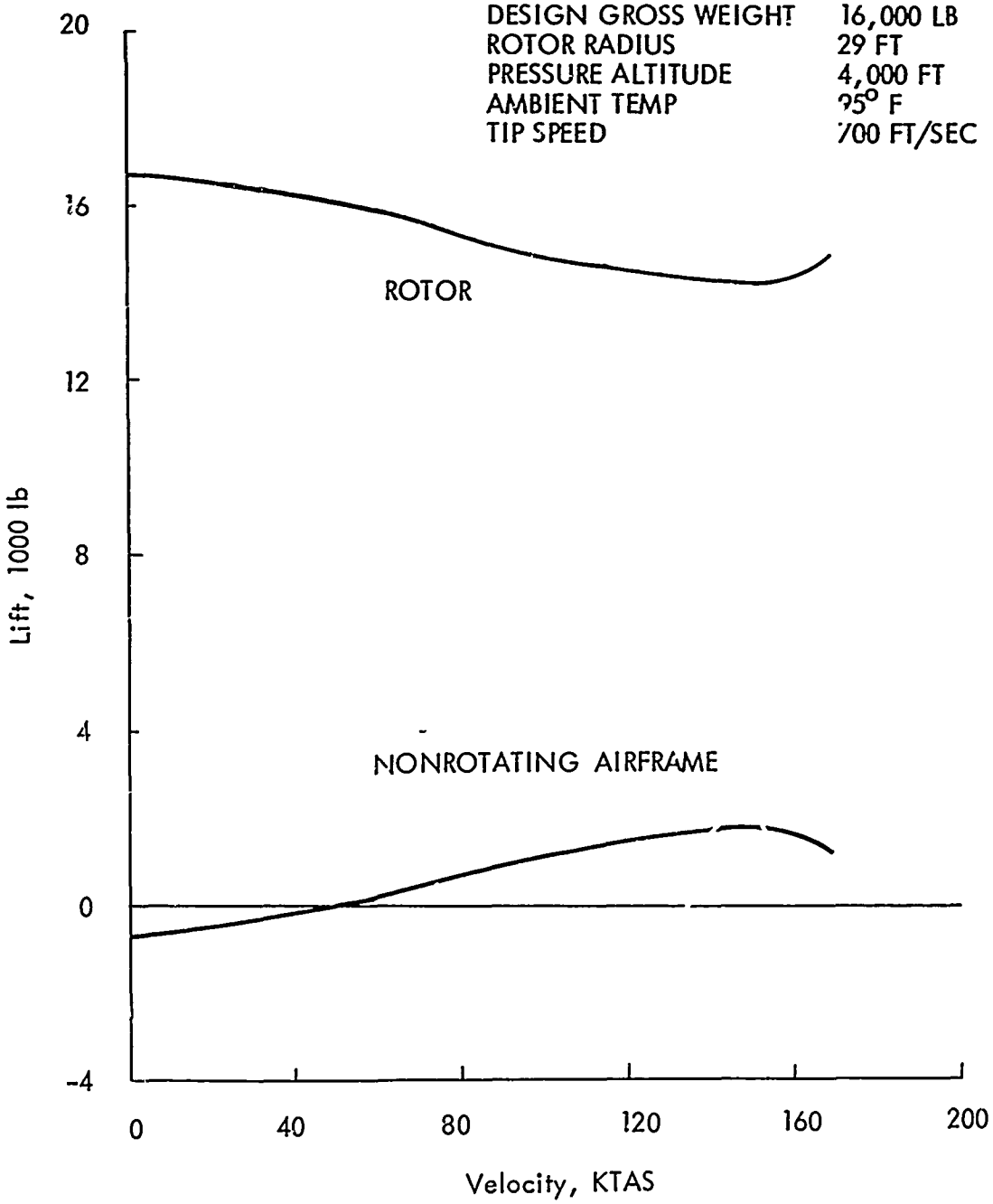

Figure 43. Level Flight (Trim) Lift Sharing for Configuration 5.

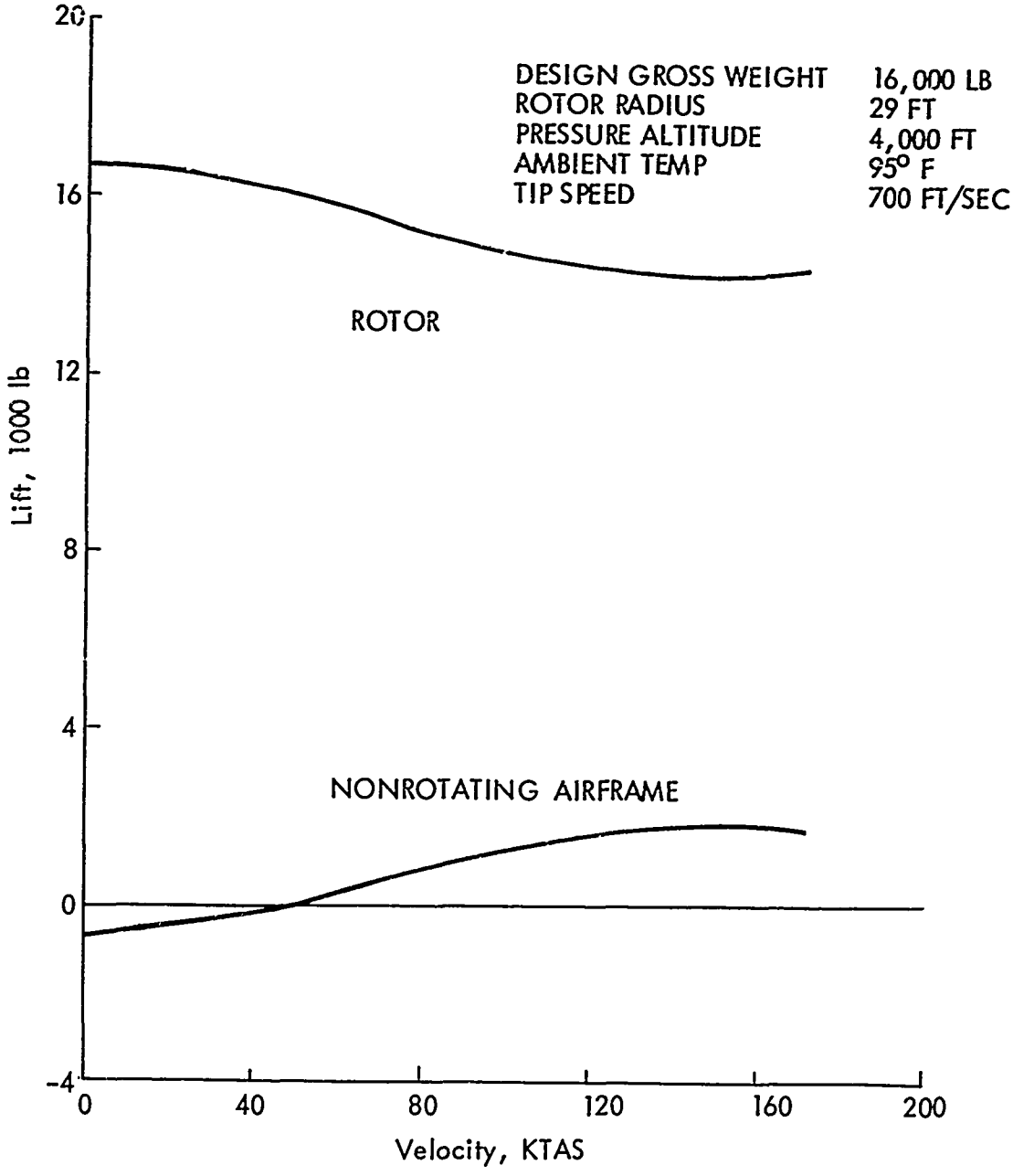

Figure 44. Level Flight (Trim) Lift Sharing for Configuration 6.

TABLE XIX. WINGED HELICOPTER LIFT SHARING CHARACTERISTICS DURING INITIAL FLIGHT AND COORDINATED TURNS

Configuration	Initial 1 g Level Flight					Maneuvering Flight, Coordinated Turn						
	Velocity, KTAS	L	$\frac{L_R}{L}$	$\frac{L_A}{L}$	C_{L_A}	L	$\frac{L_R}{L}^*$	$\frac{L_A}{L}^*$	$C_{L_A}^*$	$\Delta\frac{L_A}{L}$	n^{**} Actual	n Target
4	140	16000	0.900	0.100	0.414	24750	0.849	0.151	1.04	0.051	1.52	1.50
5	155	16000	0.888	0.112	0.285	27200	0.808	0.191	0.89	0.079	1.70	1.75
6	167	16000	0.888	0.112	0.197	32900	0.820	0.179	0.68	0.067	1.80	2.00

*Measured at maximum α_R during maneuver

**Sustained for 3 seconds

of time histories depict the excursions of the flight controls and the behavior of the aircraft after it is disturbed from the trimmed conditions by a maneuver command. Figures 47 and 48 of Appendix III illustrate the commands used to induce a coordinated turn and a height displacement (pull-up and push-over), respectively. Results of the time histories are presented in Tables IX, X, XI, XIII, XIV, and XV.

A review of the transient maneuver normal load factor time histories shows the speeds at which the upper level normal load factors could be accomplished without power limitations. From a rationalization of the trends of the normal load factors which could be accomplished (based on assumed premises for power), and the trends of time required to make 200 ft height changes (at speeds near the design cruise speed), the tentative conclusion is made that the 1.75 normal load factor aircraft has more advantages than the others studied.

2.3.15 Rotor Loads, Stresses, and Weights

Loads, stresses and weights calculated on the six analytic model vehicles are reported in paragraph 2.2.13. Small variations in stresses among the various configurations are due to such variables as extent of retreating blade stall, compressibility losses, and demands on the rotor to produce high propulsive forces at high speeds combined with rotor thrust required for high load factors. Because of the multitude of variables, and since it was not practical to perform a trade-off study of stress influencing parameters within the scope of the reported study, selecting a configuration on the basis of rotor stresses is not practical. A general observation can be made, however: since a major contribution to high rotor loads is the forward propulsion requirement at high forward speeds, the use of an auxiliary propulsion device would prove advantageous in attaining high-speed maneuvering capability without excessively loading the rotor; or, putting it another way, the rotor strength, through the need for propulsive requirement, establishes a limit for maximum speed, particularly if high speed is combined with maneuvers.

It must also be borne in mind when reviewing the loads and stresses given in paragraph 2.2.13 to establish capabilities, that rotor design is an iterative

procedure. That is to say, it is likely that the relative magnitudes of rotor stresses would be improved if more than the one design iteration performed in this study would be made.

2.3.16 Vibrations

The aircraft vibratory characteristics pertinent to this study are described in 2.2.14.

2.4 SELECTED AIRCRAFT CONFIGURATIONS

The exploratory maneuver capability analysis (paragraph 2.2) sought to reveal an adequate range of alternatives. Each alternative has sundry advantages and benefits which can be expected to accrue if it is adopted. The purpose of this section is to establish which of the proffered alternatives of the unwinged and winged helicopter classes is the best design concept, that is, which one appears likely to offer the best means of attaining the desired capabilities.

Each of the alternatives was matched against the spectrum of design requirements. Some judgments were objective and others subjective. When advantages and benefits were more or less equivalent, evaluations hinged on relative levels of confidence regarding the competing alternatives, tempered by experience.

After the evaluations, it was decided which alternatives to adopt. It is again emphasized that the proffered alternatives were the product of preliminary synthesis techniques. It was not practicable to bring them to a better theoretical level within the limit of allotted time.

2.4.1 Maneuver Capability Recommendations

Effective performance of the Utility Tactical Transport Aircraft System (UTTAS) in providing aerial battlefield mobility and rapid logistic support will depend to a great extent on its maneuvering ability. Maneuverability is essential to the performance of low-level, nap-of-the-earth flight to avoid detection, evasive maneuvers to avoid confrontation with superior enemy threats, precise tactical maneuvers, and collision avoidance. A principal

aim of this study was to determine the benefits and penalties ascribable to maneuvering level as it affects high-speed, nap-of-the-earth flight capability.

On the basis of the first iteration study results in the process of design refinement, the recommended maneuver design criterion is a transient normal load factor of 1.75 sustained for 3 seconds in a coordinated turn performed at 150 KTAS. Relative to the higher maneuvering level investigated, this capability at design cruise speed and design atmosphere affords:

- More transient load factor capability for height displacement maneuvers performed in the neighborhood of the design speed (evaluated in Section 2.4.2):
  a. At the moderate increase in empty weight fraction.
  b. Consistent with installed power based on 500 ft/min rate of vertical climb at design atmosphere.
- Moderate to higher (but not major) increase in lift sharing ratio of nonrotating airframe as the aircraft achieves the normal load factor in the high-speed coordinated turn (reviewed in 2.4.2).
- Higher transient load factor with respect to requirements prescribed by nap-of-the-earth terrain models at speeds of 94 KTAS and less, such as described in Reference 17. The aircraft of that reference were not designed to achieve maximum load factor capabilities at the design cruise speed specified for this study.

2.4.2 Configuration Selection Rationale

2.4.2.1 Effect of Load Factor on Empty Weight. A helicopter whose design gross weight is fixed but which is designed to accomplish progressively higher maneuver load factors at high speed shows a corresponding growth in empty weight fraction. This fundamental result is evidenced in Table V wherein the empty weights of unwinged Configurations 1 through 3 and winged Configurations 4 through 6 are seen to increase with a requirement to increase maneuver load factor.

2.4.2.2 Effect of Load Factor on Lift Sharing. It is shown in 2.3.13 that during a maneuver, the nonrotating airframe, with or without a wing, provides an increase in the increment of nonrotating airframe lift to total lift. The

increase occurs in progressing from the level flight speed from which the maneuver is initiated through the maximum angle of attack. The analyses corresponded to the accomplishment of particular transient normal load factors sustained for 3 seconds in coordinated turns as determined by the propulsive capabilities of the rotors prevailing when the maneuvers were initiated. Table XVIII gives the increases in the ratios of nonrotating airframe lift to total lift for Configurations 1, 2 and 3 as 0.0453, 0.0528 and 0.0665, respectively, in accomplishing load factors of 1.50, 1.65, and 1.75 from corresponding initial speeds of 140, 155, and 167 KTAS. Configuration 2 is considered to be capable of effectively achieving a normal load factor of 1.75 at 150 KTAS. The increase on the ratio of nonrotating airframe lift to total lift in executing this maneuver is estimated to be 0.050.

Table XIX gives the increases in the ratios of nonrotating airframe lift to total lift for Configurations 4, 5 and 6 as 0.051, 0.079 and 0.067, respectively, in accomplishing load factors of 1.52, 1.70, and 1.80 from corresponding initial speeds of 140, 155 and 167 KTAS. Configuration 5 is considered to be capable of effectively achieving a normal load factor of 1.75 at 150 KTAS. The increase in ratio of nonrotating airframe lift to total lift in executing this maneuver is estimated to be 0.077.

The winged helicopter configurations show a larger increase in the ratios of nonrotating airframe lift to total lift than the corresponding helicopters. However, as described in 2.3.13, the relative increase is not as large as might be expected due to the higher drag of the winged configurations and the limitation in propulsive capability accompanying the lower rotor solidities of these configurations.

2.4.2.3 Load Factor Compatibility with Other Parameters in Configuration Selection. Figure 45 shows calculated points for initial speeds and transient normal load factors sustained for 3 seconds in coordinated turns as limited by the rotor propulsive capability. Based on experience and simple analysis, the trends of attainable load factor are shown by curves through these points and intersecting 150 KTAS.

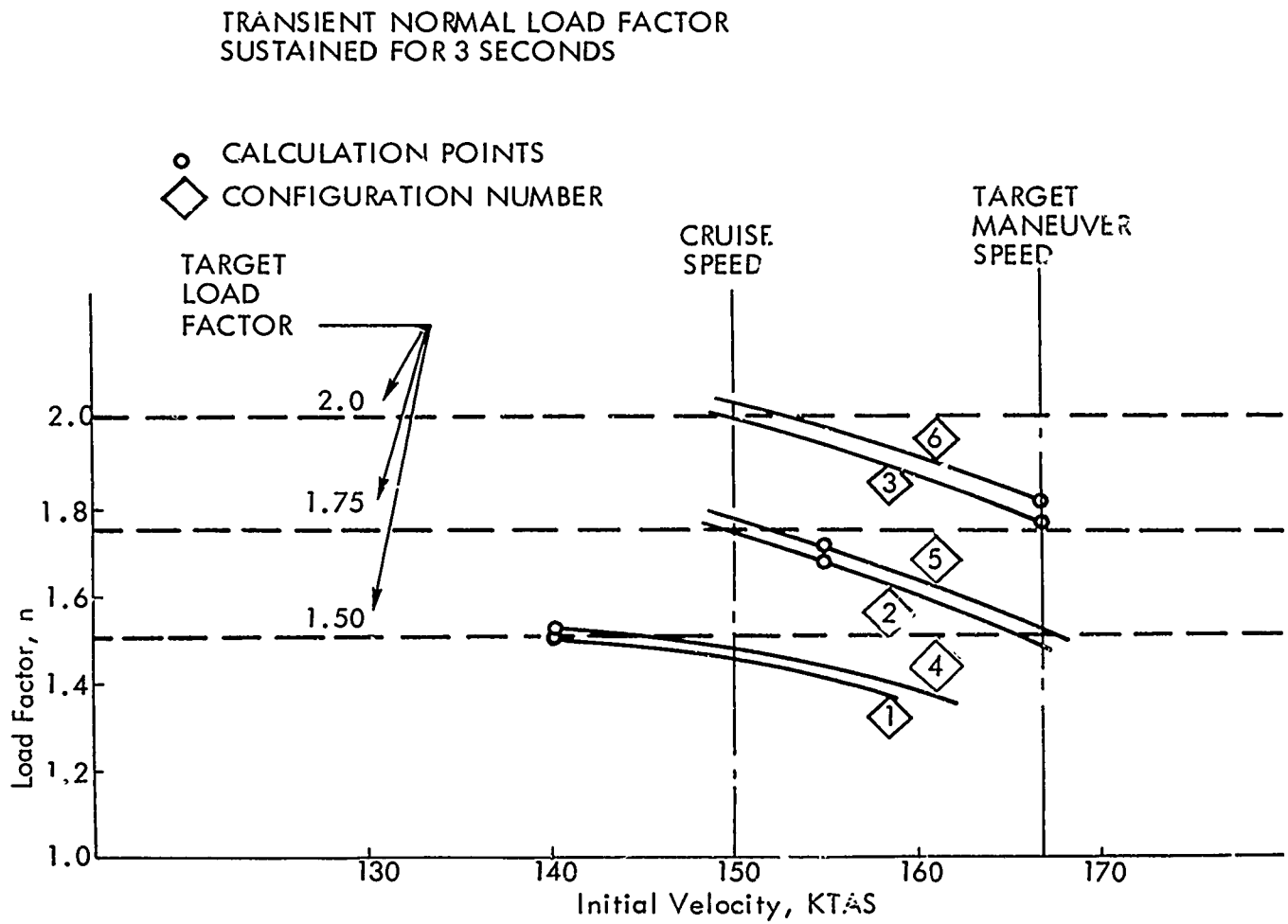

Figure 45. Trends of Analysis Results for Coordinated Turns.

Owing to rotor propulsive force limitations, Configurations 1 and 4 would not be expected to be capable of a sustained normal load factor of 1.5 in a coordinated turn executed at the design cruise speed of 150 KTAS. Configurations 3 and 6, which have adequate propulsive capabilities at 150 KTAS, based on normal load factor and power deficiencies at 167 KTAS, would be expected to be capable of a sustained normal load factor of 2.0 at the design cruise speed. However, they show the largest empty weights, 11,670 and 11,535 lbs , respectively. Configurations 2 and 5, which have adequate propulsive capabilities at 150 KTAS and manifest only moderate load factor and power deficiencies at 155 KTAS, would be expected to be capable of a sustained normal load factor of 1.75 at the design cruise speed. They show intermediate empty weights of 11,281 and 11,135 lbs, respectively, and in the coordinated turn maneuvers initiated at 150 KTAS, these configurations show increases of 0.050 and 0.077, respectively, in the ratios of nonrotating lift to total lift.

Comparison of power required for 200-ft height displacements (Table IV) and power available (Figures 9 through 14) shows that Configurations 1, 2, 4 and 5 have sufficient power to accomplish the 200-ft height displacement maneuvers while Configurations 3 and 6 exhibit power deficiencies with respect to these maneuvers. On the basis of available power (that installed to enable vertical climb at the rate of 500 ft/min), Configurations 2 and 5 are most compatible with the 200-ft height displacement maneuvers. These data are summarized in Table XX .

TABLE XX. POWER AVAILABLE AND REQUIRED FOR 200-FT HEIGHT DISPLACEMENT INITIATED AT SPEED CORRESPONDING TO MANEUVER PROPULSIVE LIMIT*

	Configuration					
	1	2	3	4	5	6
Initial Velocity, KTAS	140	155	167	140	155	167
Power Available, shp	2270	2365	2420	2265	2300	2395
Power Required, shp	1655	2250	2580	1505	1980	2450

*Speed for maneuver propulsive limit based on transient normal load factor for 3 seconds in coordinated turn

As shown in Table XIII, if power limitations are not a consideration, the aircraft having nominal maneuver load factor capabilities of 1.5 at 140 KTAS, Configurations 1 and 4, require approximately 80 ft less distance (measured along a direct "collision heading") to maneuver 200 ft to the side of a point representing an obstacle than do the aircraft having nominal maneuver load factor capabilities of 2.0 at 167 KTAS, Configurations 3 and 6.

Conversely, as shown in Table IX, the lower load factor, lower speed aircraft require slightly greater horizontal distances to accomplish 200-ft height displacements than do the higher load factor, higher speed aircraft.

Thus, so far as overall nap-of-the-earth flight capability is concerned, the aircraft having the intermediate maneuver load factor and speed capabilities, Configurations 2 and 5, represent the best alternatives (among those specifically studied).

The foregoing results are based on complete maneuvers, including recovery segments. This approach, of course, imposes more severe constraints on aircraft design and performance than would partial maneuvers which simply demonstrate the diversionary portion of maneuvers. For example, in the case of the 200-ft height displacement maneuvers simulated, the load factor differential (relative to unit load factor) is greater during the terminal (recovery) portion of a complete maneuver than during the initial portion of the maneuver. Specifically, to accomplish a 200-ft increase in height with Configuration 3 required an initial increase in load factor of 0.58 followed by a 0.72 decrease in load factor (relative to unit load factor) in the process of returning to a load factor of 1.0.

Except for Configurations 1 and 4, the maximum load factors encountered in recovering from negative height displacements equalled or exceeded the mean load factors sustained in the execution of coordinated turns. However, in all cases studied, the peak stresses were developed in the execution of coordinated turns.

No special incompatibilities were observed between upper and lower maneuver load factors for any of the maneuvers analyzed.

2.4.2.4 Supplementary Comments in Unwinged and Winged Configurations. In accordance with design intent of the transient maneuver time histories (see 2.2.12), unwinged and winged configurations of corresponding maneuver load factor capabilities manifested reasonably conformable performance characteristics. A significant advantage of one concept over the other was that the winged helicopters evidenced generally lower oscillatory loads.

As shown in Table V, Configurations 1 and 4 have nearly identical empty weights whereas winged Configurations 5 and 6 have slightly lower empty weights than the corresponding unwinged Configurations 2 and 3, with Configuration 5 offering the greatest reduction in empty weight over its unwinged counterpart.

From the standpoints of oscillatory loads and empty weight fractions, the winged helicopters slightly surpass their unwinged counterparts. Since Configuration 5 is characterized by the largest decrease in empty weight fraction and somewhat less severe oscillatory loads and stresses, it might be selected as the single most-preferred configuration within the scope of the work performed.

2.4.3 Aircraft Configuration Details

The basic hypothetical aircraft synthesized for this study were derived from the baseline features listed in Table I and the mission requirements which led to the development of the CL 1100, the UTTAS design concept described in Reference 1.

The general arrangements of the most promising helicopter and winged helicopter design concepts, Configurations 2 and 5, are shown in Figures 1 and 2, respectively. Salient physical characteristics are given in Table II.

2.4.4 Maneuvering Flight Time Histories

The transient responses of Configurations 2 and 5 to coordinated-turn commands are depicted by Figures 55 and 58 of Appendix V, respectively. Derived information concerning the quality of these maneuvers and the power expenditures required to accomplish them are given in Table XIII. The transient

responses of Configurations 2 and 5 to ascending and descending 200-ft height-change commands (pull-ups and push-overs) are depicted by Figures 59 and 60 and 65 and 66, respectively. A comparison of these symmetrical maneuvers is given in Table IV.

2.5 RISK AREAS AND RECOMMENDATIONS

The study revealed that several areas need further development of technology in order to extend the speed/load factor envelope beyond that generally flown by helicopters today. A brief discussion on each of several items is given in the following subsections. One risk area is identified: a winged helicopter can experience flight regimes where inadequate control moment is available (when the rotor is unloaded by the wing) unless airplane-type control surfaces are added, or unless a hingeless rotor is used. This risk area identification did not emerge from the study since a hingeless rotor was used in each of the analysis models.

2.5.1 Speed and Load Factor Limits

Attempts to accomplish (analytically) maneuvers where load factors were sustained for long periods, say 3 seconds, at the analysis target speed of 150 KEAS (167 KTAS) and the analysis target load factor of 2.0 were unsuccessful with all the model configurations. Load factors of 1.75 and 1.80 at this speed were sustained with two of the configurations: an unwinged helicopter (Configuration 3) and a winged helicopter (Configuration 6) respectively. The rotor loads for these two cases were relatively high, although it is expected that with additional design iterations, the rotor loads could have been improved. The general conclusion is that the limit was pushed for design of a helicopter which must provide forward propulsions through a component of rotor thrust. The conclusion suggests that winged and unwinged helicopters must be designed to perform maneuvers at speeds less than 150 KEAS, unless they are compounded (that is, provided with auxiliary propulsion to relieve the rotor of the propulsive function).

2.5.2 Dynamic Effects due to Control System Stiffness

It became evident in reviewing the results of computations that rotor and control system stiffnesses are important ingredients in establishing criteria for configuring aircraft to have maneuver speed capabilities. Although the importance of stiffnesses, per se, is no surprise, limitations were identified only through the use of comprehensive analytical techniques which reflect stiffness effects when analyzing maneuvers.

2.5.3 Effects of Wing Size

While it was shown that the addition of a wing provides some benefit in attaining load factor capability, it was also shown that the wing imposes limitations. For example, while aiding the rotor by providing part of the lift required to perform a maneuver, the wing conversely tends to load the rotor by demanding a propulsive component of rotor thrust, to offset wing drag: this situation is aggravated as speed is increased in level flight. Some indication of influence of wing size resulted from the study, but since it was limited in scope, additional studies could prove beneficial. These additional studies could provide further insight as to optimum wing size, and could be extended to investigate if any net gain could be achieved from use of lift devices on wings (lift, drag, and mechanical complexity of devices will be offsetting).

It is recognized that the wing can adversely affect autorotation characteristics of aircraft. This effect is of minimal concern for a UTTAS multiengine configuration, but can be identified as a risk area if a wing is added to a helicopter.

3.0 CONCLUSIONS

The development of maneuver simulation techniques has lagged behind the development of high performance helicopters. Lockheed's digital flight simulation computer program, REXOR, proved to be especially suited to provide time histories of aircraft and rotor system behavior during steady and transient maneuvers. The maneuver capabilities of three helicopters and three matching (on the basis of maneuvering level) winged helicopters were investigated, from which the following conclusions are drawn:

- The levels of blade loading coefficient demonstrated in many experimental maneuverability studies are not necessarily indicative of maximum maneuver load factors, such as might be required in a high-speed coordinated turn sustained for some period of time such as 3 seconds. Flight test data might pertain to blade loading coefficient levels achieved in short-duration maneuvers. Sustained maneuvers are associated with blade loading coefficients which are lower than those indicated by test data which were examined in this study.
- In high-speed maneuvering flight, the propulsive capability of the rotor can be extended by unloading the rotor lift with a wing. Since the propulsive capability of the rotor must also compensate for the drag due to the wing, the extent to which rotor solidity can be reduced by adding a wing is limited.
- Merits of the winged helicopter, relative to an unwinged helicopter of the same maneuvering capability, are:
  - The presence of the wing had a beneficial effect on oscillatory loads and vibration level during maneuvers for those configurations which were analyzed.
  - Slightly lower empty weight fractions are possible at high design maneuver load factors.
  - Slightly lower power (based on the power required to climb vertically at 500 ft/min) is needed; however, higher power is required to achieve maximum speed in level flight.

The advantages are small, and are based on a first design iteration of each model.

- In all cases studied, maximum stresses were developed in coordinated turns rather than in push-over and pull-up maneuvers.
- No incompatibilities were observed to exist between upper ($n > 1.0$) and lower ($0 < n < 1.0$) load factors during any maneuver.
- High maneuvering levels at speeds much above 150 KTAS would benefit from propulsive unloading of the rotor by the addition of an auxiliary propulsion system.
- Collective pitch control would be required (in addition to cyclic pitch) below speeds of 100 to 120 KTAS in order to achieve the maximum maneuver load factors specified as targets.
- The degree of blade stall and the region of the rotor disc operating in stall strongly influence rotor propulsive force capability and affect steady-state load factor capability more than highly transitory maneuver load factor capability. Maneuvers enduring approximately 3 seconds are judged to fall between these extremes. The use of profile power coefficient as an index of permissible penetration into stall, while adequate under steady-state conditions, leads to unduly conservative predictions in transient maneuvers. Consequently, a rigorous, particularized approach to the analysis of rotor propulsive capability is required in dealing with transient maneuvers.
- Within the scope of work performed, a maneuver load factor of 1.75 at a design cruise speed of 150 KTAS is most compatible with all performance and mission requirements which were considered.

LITERATURE CITED

1. UTILITY TACTICAL TRANSPORT AIRCRAFT SYSTEM PRELIMINARY DESIGN STUDY, FINAL REPORT, VOLUME 1, TECHNICAL CHARACTERISTICS, BOOK 1 - TECHNICAL DESCRIPTION, LR 21785-1, Lockheed-California Company, Burbank, California, October 1968.

2. Gessow, Alfred, and Myers, Gary C. Jr., AERODYNAMICS OF THE HELICOPTER, New York, The Macmillan Co., 1952, pp 250-267.

3. Amer, Kenneth B., EFFECT OF BLADE STALLING AND DRAG DIVERGENCE ON POWER REQUIRED BY A HELICOPTER AT HIGH FORWARD SPEED, American Helicopter Society Proceedings of the Eleventh Annual National Forum, Washington, D.C., April 1955, pp. 100-109.

4. McCloud III, John L., and McCullough, George B., COMPARISON OF CALCULATED AND MEASURED STALL BOUNDARIES OF A HELICOPTER ROTOR AT ADVANCE RATIOS FROM 0.3 to 0.4, Ames Research Center; NASA Technical Note D-73, National Aeronautics and Space Administration, Washington, D.C., September 1959.

5. Fradenburgh, Evan A., AERODYNAMIC EFFICIENCY POTENTIALS OF ROTARY WING AIRCRAFT, American Helicopter Society Proceedings of the Sixteenth Annual National Forum, Washington, D.C., May 1960, pp. 20-30.

6. Sweet, George E., Jenkins, Julian L. Jr., and Winston, Mathew M., WIND TUNNEL MEASUREMENTS OF A LIFTING ROTOR AT HIGH THRUST COEFFICIENTS AND HIGH TIP SPEED RATIOS, Langley Research Center; NASA Technical Note D-2462, National Aeronautics and Space Administration, Washington, D.C., September 1964.

7. Tanner, Watson H., CHARTS FOR ESTIMATING ROTARY WING PERFORMANCE IN HOVER AND AT HIGH FORWARD SPEEDS, United Aircraft Corporation, NASA Contract Report CR-114, National Aeronautics and Space Administration, Washington, D.C., November 1964.

8. Harris, Franklin D., and Pruyn, Richard R., BLADE STALL - HALF FACT, HALF FICTION, Proceedings of the American Helicopter Society 23rd Annual National Forum, Paper No. 101, Washington, D.C., May 1967.

9. Harris, Franklin D., Tarzanin, Frank J. Jr., and Fisher, Richard K. Jr., ROTOR HIGH SPEED PERFORMANCE, THEORY VS TEST, Journal of the American Helicopter Society, Vol. 15, No. 3, July 1970, pp. 35-44.

10. Prouty, R. W., ACHIEVING HELCIOPTER STABILITY WITH THE LOCKHEED RIGID ROTOR SYSTEM, Paper Presented at Symposium on Education in Creative Engineering, Massachusetts Institute of Technology, April 1969.

11. HELICOPTER FLYING AND GROUND HANDLING QUALITIES: GENERAL REQUIREMENTS FOR, MILITARY SPECIFICATION H-8501A, Department of Defense, Washington, D.C., September 7, 1961.

12. Arndt, Roger E. A., and Borgman, Dean C., NOISE RADIATION FROM HELICOPTER ROTOR OPERATING AT HIGH TIP MACH NUMBER, Proceedings of the 26th Annual National Forum of the American Helicopter Society, Preprint No. 402, Washington, D.C., June 1970.

13. Cox, C. R., ROTOR NOISE MEASUREMENTS IN WIND TUNNELS, Proceedings of the Third CAL/AVLABS Symposium, Vol. 1, Buffalo, N. Y., June 1969.

14. King, Robert J., and Schlegel, Ronald G., PREDICTION METHODS AND TRENDS FOR HELICOPTER ROTOR NOISE, Proceedings of the Third CAL/AVLABS Symposium, Vol. 1, Buffalo, N. Y., June 1969.

15. Kelley, Henry L., Pegg, Robert J., and Champine, Robert A., FLYING QUALITY FACTORS CURRENTLY LIMITING HELICOPTER NAP-OF-THE-EARTH MANEUVERABILITY AS IDENTIFIED BY FLIGHT INVESTIGATION, Langley Research Center, NASA Technical Note D-4931, National Aeronautics & Space Administration, Washington, D.C., December 1968.

APPENDIX I

DEVELOPMENT OF ROTOR STRUCTURAL PARAMETERS

In order to provide a realistic dynamic representation, the dynamic properties of the CL-1120 rotor blades were designed to simulate those of the AH-56A compound helicopter. The airfoil sections, however, are different. This appendix describes the methods used to achieve dynamic similarity. The mass properties of the rotor system were determined from equations presented in Reference 1 and are in conformity with those of the AH-56A.

The following dimensionless scale factors were used to determine the dimensional magnitudes of the inertia and flexibility distributions as well as the deformation mode shapes:

$$\text{Rotor Blade Mass Ratio}, \eta = \frac{\text{CL 1120 Rotor Weight}}{\text{AH-56A Rotor Weight}}$$

$$\text{Rotor Blade Radius Ratio}, \nu = \frac{\text{CL 1120 Rotor Radius}}{\text{AH-56A Rotor Radius}}$$

$$\text{Rotor Blade Chord Ratio}, \xi = \frac{\text{AH-56A Rotor Chord}}{\text{CL 1120 Rotor Chord}}$$

$$\text{Rotor Stiffness Ratio}, K_r = \frac{\text{CL 1120 Flexural Rigidity}}{\text{AH-56A Flexural Rigidity}}$$

The dimensional properties which were designed into the CL 1120 rotor system were derived from the following expressions, where the subscript 1 refers to values for the CL 1120. The blade stations were computed from

$$x_1(i) = x(i)\nu$$

Similarly, the distributions of mass density, pitching moment of inertia and the location of the elastic axis were obtained, respectively, from

$$m_1(i) = m(i)\eta/\nu$$

$$I_1 (i) = I (i)\, \eta/\xi^2 \upsilon$$

$$y_{c_1} (i) = y_c (i)/\xi$$

To compute the natural modes and frequencies of free vibrations of the rotor blades, Equation (8), Appendix II, is written as

$$-M_g \ddot{q} + K_g q = -M_g \ddot{q} + \left(C - \Omega^2 B\right) q = 0 \tag{1}$$

where

C = generalized structural stiffness

ΩB = generalized centrifugal stiffness

Assuming simple harmonic motion, $\ddot{q} = -\omega^2 q$.

In terms of the CL 1120 rotor system, Equation (1) becomes

$$-\omega_{r_1}{}^2 M_{g_1} + C_1 - \Omega_1{}^2 B_1 = 0 \tag{2}$$

where ω_r denotes the natural frequency of the rotating blades. In the case of nonrotating blades, Equation (2) reduces to

$$-\omega_{n_1}{}^2 M_{g_1} + C_1 = 0 \tag{3}$$

The deformation modes of the CL 1120 rotor blades were derived from those characterizing the AH-56A rotor blades by applying the radius ratio, υ, and maintaining the same relative deflection slopes.

Applying the mass ratio, η, the generalized mass properties of the CL 1120 rotor blades are given by

$$M_{g_1} = M_g\, \eta \upsilon^2 \tag{4}$$

The generalized centrifugal stiffness parameter B may be expressed in terms of AH-56A rotor blade dynamic quantities as

$$B = \left(C - M_g \omega_r^2\right) / \Omega^2 = M_g \left(\omega_n^2 - \omega_r^2\right) / \Omega^2 \qquad (5)$$

Since this parameter is proportional to the mass and the square of the dimension characterizing deformation mode of the rotor blades, the generalized centrifugal stiffness properties of the CL 1120 rotor blades are given by

$$B_1 = B\eta v^2 \qquad (6)$$

The generalized structural stiffness properties may be expressed in terms of the dimensionless ratio of flexural rigidities and the radius ratio:

$$C_1 = \left(C / v^2\right) v K_r = C K_r / v \qquad (7)$$

(Note that for equivalent lateral displacements, the curvature is scaled by $1/v^2$ because the displacement equals the double integral of the curvature over the blade radius.) Introducing expressions (6) and (7) and the relation $\omega_{r_1} = \omega_r(\Omega_1/\Omega)$ into Equation (2) defines the rotor blade stiffness ratio:

$$K_r = v \left(\Omega_1^2 B_1 + M_{g_1} \omega_{r_1}^2\right)/C$$

APPENDIX II

FLIGHT SIMULATION MATHEMATICAL MODEL (REXOR)

The REXOR method of analysis, a digital flight simulation technique, is especially suited to provide time histories of steady and transient maneuver characteristics and handling qualities. This method embodies 21 degrees of freedom: 6 rigid body coordinates; first and second flapwise bending and first chord bending modes for each of four independently acting rotor blades; and gyro pitch, roll and plunge.

The method is based on the superposition of a finite number of assumed modes. Each assumed deformation shape or mode represents a degree of freedom, and the multiplier that determines the amount of its contribution to any general deformation represents the generalized coordinate corresponding to that mode.

The aerodynamic loads imposed on the rotor are represented by two-dimensional airfoil data (lift, drag and moment coefficients) which take into consideration variation in airfoil section. Compressibility, stall and reverse-flow effects are taken into account by using airfoil data corresponding to full ranges of Mach numbers and angles of attack.

The dynamic response of the helicopter in flight can vary in an arbitrary manner with time, depending upon the initial conditions, the character of the applied forces, and the response properties of the helicopter.

The twelve equations of motion of the rotor blades are represented by

$$- M_g \ddot{q} + K_g q = F_g \tag{8}$$

where

M_g = generalized mass

K_g = generalized stiffness

F_g = generalized external force, including damping

q = generalized coordinate

Orthogonal modes of the blades are employed which allow separate solution of the individual equations of motion. In accordance with finite-difference techniques, the coefficients of Equations (8) may be considered transitorily constant and the equations themselves may be regarded as the equations of motion for free vibrations. Thus, the solutions of Equations (8) are found by substitution of $K_g = \omega_n^2 M_g$.

The solutions are of the form

$$q = q_c \cos \omega t + q_s \sin \omega t + q_0 \tag{9}$$

from which the expressions for accelerations may be obtained directly by differentiation:

$$\ddot{q} = -\omega^2 \left(q_c \cos \omega t + q_s \sin \omega t \right) \tag{10}$$

Substitution of Equations (9) and (10) into (8) gives

$$q_0 = \bar{F}_g / \omega_n^2 M_g \tag{11}$$

The arbitrary constants q_c and q_s adapt the solution to the prevailing set of initial conditions. At time $\tau = 0$,

$$\begin{aligned} q(0) &= q_c + q_0 \\ \dot{q}(0) &= \omega q_s \end{aligned} \tag{12}$$

or

$$\begin{aligned} q_c &= q_0 - q(0) \\ q_s &= \dot{q}(0)/\omega \end{aligned} \tag{13}$$

Using the preceding expressions, the time histories of q, $\dot{q}$ and $\ddot{q}$ are found by means of numerical analysis.

Loads imposed on the helicopter body include motion-dependent aerodynamics, gyroscopic loads arising from combinations of rolling, pitching and yawing rates, and loads imparted by the rotor. The control gyro is subjected to feedback moments from the rotor blades, gyroscopic moments, spring and damper forces (arising from relative motion between the body and gyro), friction forces, and control inputs.

Time histories of the rigid-body motions of the gyro and body are obtained by computing (on a finite-difference basis) the accelerations

$$\ddot{q} = F_g / M_g \tag{14}$$

and then integrating to obtain velocities and displacements. To accommodate longer time intervals (corresponding to a rotor angular displacement of 6 degrees), polynomial interpolation and prediction are used in performing the preceding integration.

Since it was desirable to have the maneuvers commence from conditions of trimmed level flight, it is necessary to find the combination of collective and cyclic pitch angles, vehicle pitch and roll displacements, and tail rotor pitch angles which result in trimmed level flight. In addition, it is desirable that the rotor blade motions be devoid of transients. An iterative procedure is used to establish trimmed flight. Reiterated control angles and body displacements are based on time-averaged accelerations of the body. The iteration process is continued until no angular displacement exceeds 0.001 rad. By the time this condition has been satisfied, transient motions of the rotor blades will normally have subsided.

APPENDIX III

ANALYTIC AUTOPILOT

An analytic autopilot was used to represent the pilot in executing the maneuvers of the helicopters considered in this study. The autopilot provides rational control system displacements and corresponding maneuver command inputs and aircraft responses. The purpose of the autopilot was to perform a series of coordinated turns and a series of symmetrical pull-up and push-over maneuvers under various flight conditions for each of the helicopter configurations. These maneuvers were performed in a manner consistent with good pilot technique.

The autopilot is shown in Figure 46. A list of gains and filter characteristics is shown in Table XXI. This autopilot uses body pitch, yaw and roll rate and attitude as well as altitude, height, vertical velocity and normal acceleration sensors to determine control displacements to comply with input commands and to adjust for vehicle disturbances. Input commands include main rotor collective blade angle, aircraft pitch and roll attitudes, height, and normal load factor. Control displacements can be applied through the main rotor cyclic stick, the main rotor collective angle, and the tail rotor blade angle. Typical command histories for coordinated turn and height change (pull-up and push-over) maneuvers are shown in Figures 47 and 48, respectively.

The command rate used to execute the pull-up maneuver, shown on Figure 48, appears slow if compared to a command rate that might be expected of a pilot in an emergency situation where he is avoiding an obstacle. The rate used was based on a first approximation to comply with the prescribed analysis criterion that the helicopter must perform the entire maneuver without exceeding a total height change of approximately 200 feet. This criterion, and a review of human factors studies to establish realism in the pilot response rates, were used as bases for selecting feedback filtering, forward path filtering, and gain levels used in designing the analytic pilot. Had the scope of the program permitted additional iterations, it is expected that tighter maneuvers could have been shown. The result of this approximation is discussed in Section 2.2.12.

The oasic autopilot provided for main rotor control variation from level unaccelerated flight by means of cyclic control only. Collective pitch control was added to allow the accomplishment of high normal load factor maneuvers at low flight speeds. The mechanization of this portion of the autopilot is indicated in Figure 46 by the dashed signal flow paths.

The aim of the analytic autopilot was that of simulating pilot behavior and providing a simple command history format rather than providing a true automatic pilot to perform the usual pilot relief functions.

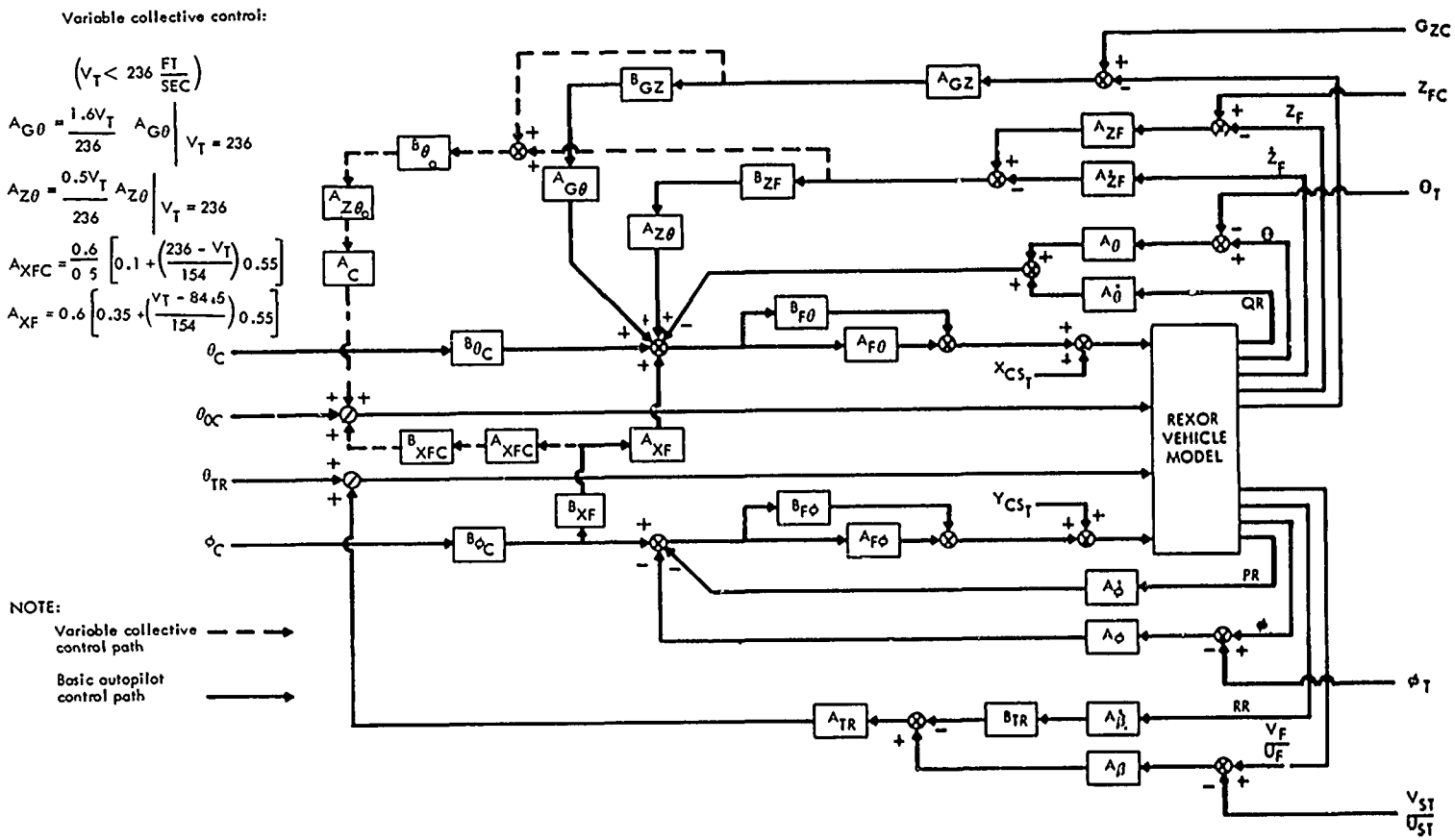

Figure 46. Analytic Autopilot Block Diagram.

TABLE XXI. AUTOPILOT GAIN SCHEDULE (BASIC AUTOFILOT)

Symbol	Gain	
	Coordinated turn	Pull-up* and Push-over
A_{θ}	0.0	-
$A_{\dot{\theta}}$	0.8	-
A_{ϕ}	1.0	-
$A_{\dot{\phi}}$	1.3	-
A_{β}	0.6	-
$A_{\dot{\beta}}$	0.4	-
A_{C}	0.0	-
$A_{F\theta}$	0.5	-
$A_{F\phi}$	0.036	-
$A_{G\theta}$	1.0	-
A_{GZ}	0.029	0.00
A_{TR}	1.0	-
A_{XF}	0.165	-
A_{XFC}	0.0	-
A_{ZF}	0.0018	0.001
$A_{\dot{Z}F}$	0.0018	-
$A_{Z\theta}$	1.0	-
$A_{Z\theta_0}$	(See Variable Collective Control, Figure 46)	-
$B_{F\theta}$	1/S	-
$B_{F\phi}$	0.16/S	-
B_{GZ}	1.0	-
B_{TR}	0.5	-
B_{XF}	1.0	-
B_{XFC}	0.2	-
B_{ZF}	16.0	-
$B_{\theta C}$	3.33	-
$B_{\theta 0}$	0.6	-
$B_{\phi C}$	5.0	

*Gains for pull-up and push-over maneuvers are the same as the coordinated turn gains, except as noted.

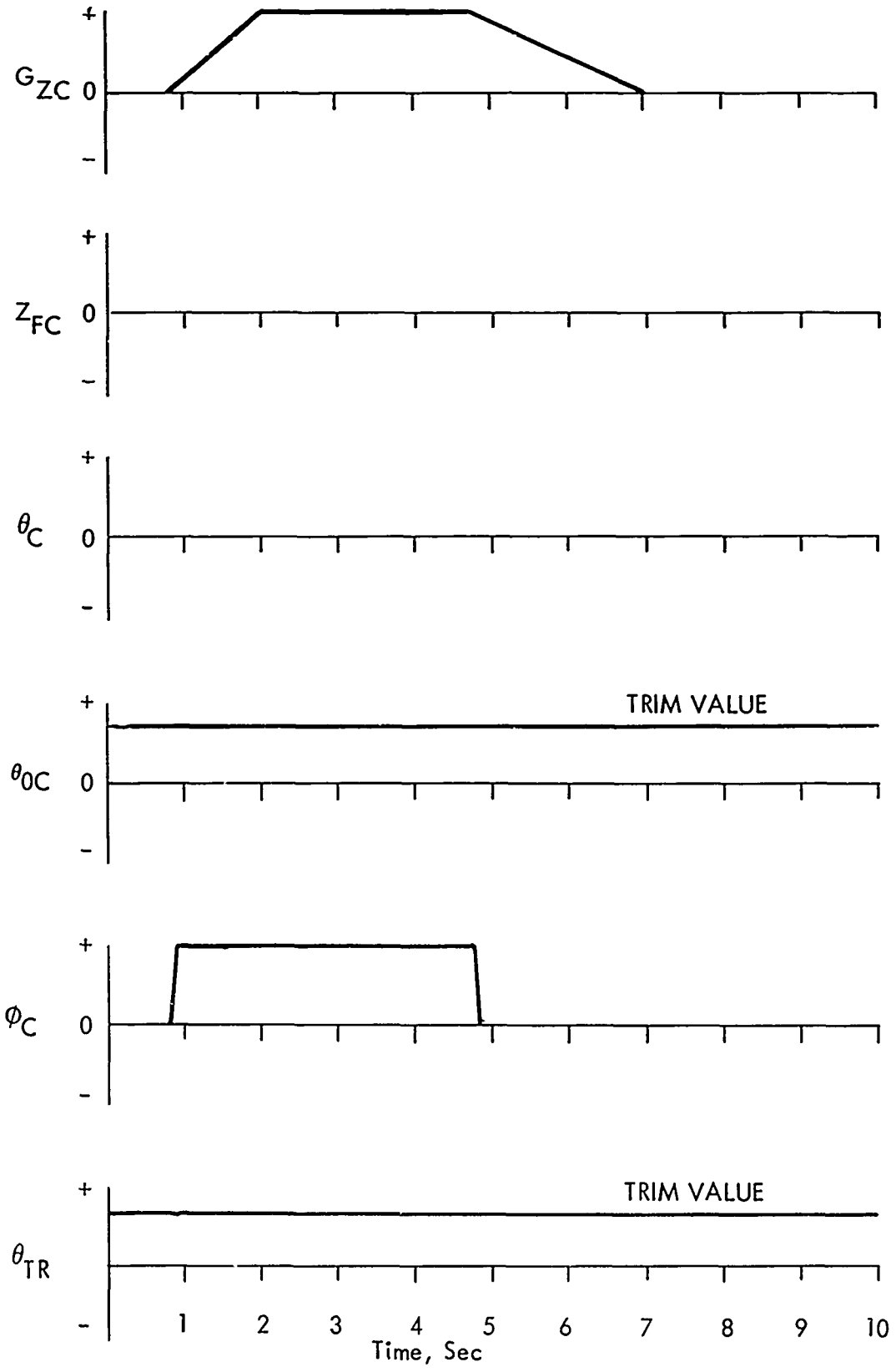

Figure 47. Coordinated-Turn Command History.

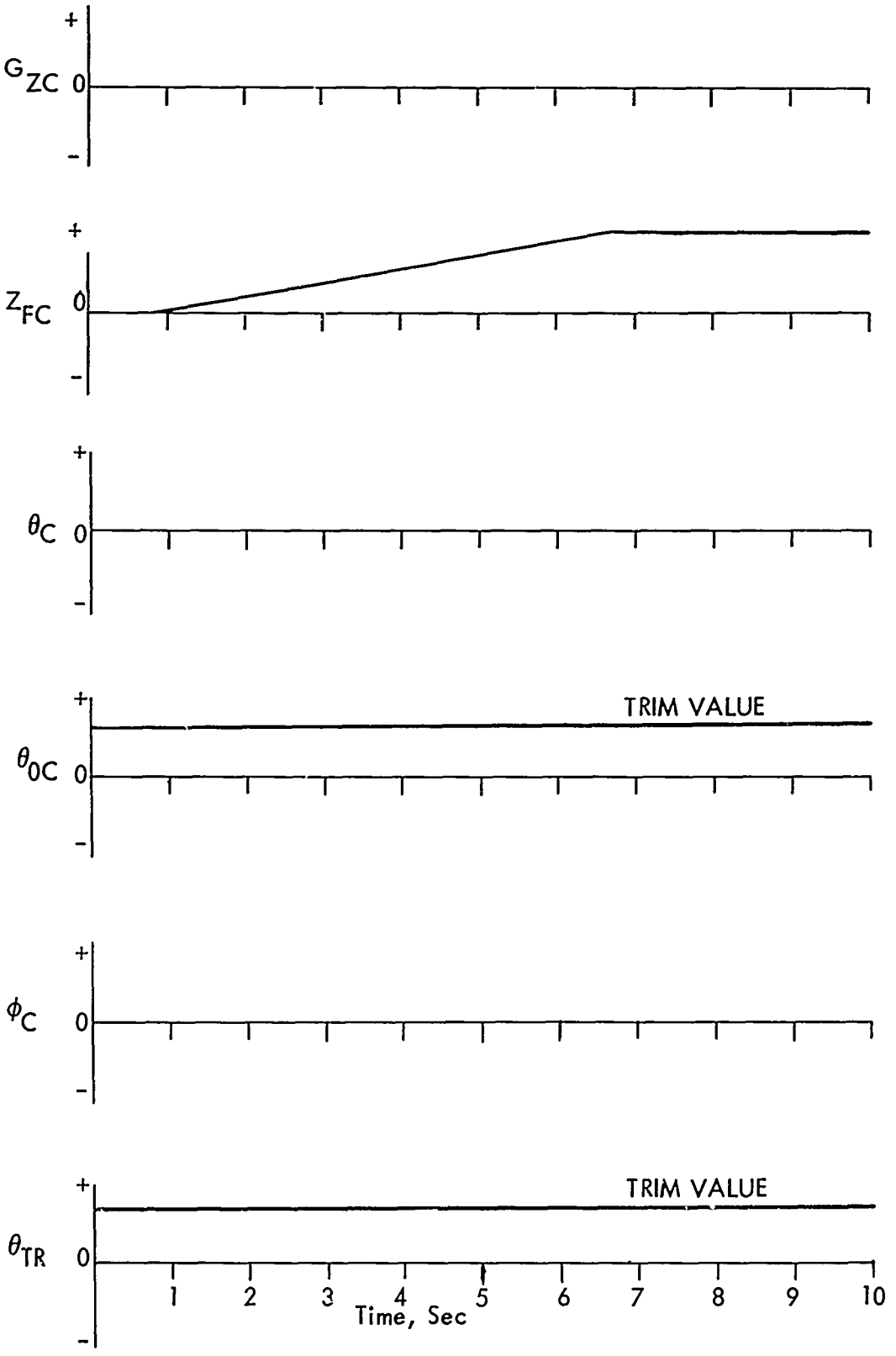

Figure 48. Pull-Up and Push-Over Command History.

APPENDIX IV

REMARKS CONCERNING DYNAMIC STABILITY

During preliminary efforts, it was observed that at certain combinations of rotor solidity and blade stiffness, there was a dynamic instability at high advance ratios. The mathematical model employed in this study does not permit quasi-stable solutions (that is, no solutions can be found for the equations of motion of an unstable system). Hence, aside from the problems of flight stability, successful prediction of the maneuver response characteristics requires that the helicopter system be stable. It was found that the instability could be eliminated by effecting a slight increase in blade flapping frequency. (See Figures 49 and 50.)

In order to better understand the instability phenomenon and to explain the beneficial effect of increasing the blade flapping stiffness, the flight stability of an unwinged helicopter configuration involving a solidity of 0.16 and operating at a flight speed of 167 KTAS was studied in some detail. Typical time histories of the divergent oscillations ensuing following a disturbance from trimmed level flight are shown in Figures 51, 52 and 53.

The frequency of oscillation of the vehicle (in body coordinates) is 0.83 cycle per revolution, or 3.3 cyc/sec. At this frequency, a single-amplitude variation in rotor axial shaft load of approximately 15,000 lb can be observed. Examination of parts (c) and (d) of Figure 51 indicates that approximately 8000 lb of this variation can be attributed to the collective flapping inertia of the rotor blades. Time histories of the relative blade displacements are shown in Figures 52 and 53. It is found that the collective displacements of the tips reflect the contribution of the collective flapping inertia of the rotor blades to the shaft loads. In addition, it is shown that the pitching motion of the tip-path plane is in phase with collective flapping motion, the pitching moment on the shaft, and the variation in rotor axial load. The largest flapping displacements arise in the forward portion of the rotor disc. This occurs because of a negative "aerodynamic spring" effect on the forward portion of the rotor disc. The strength of this

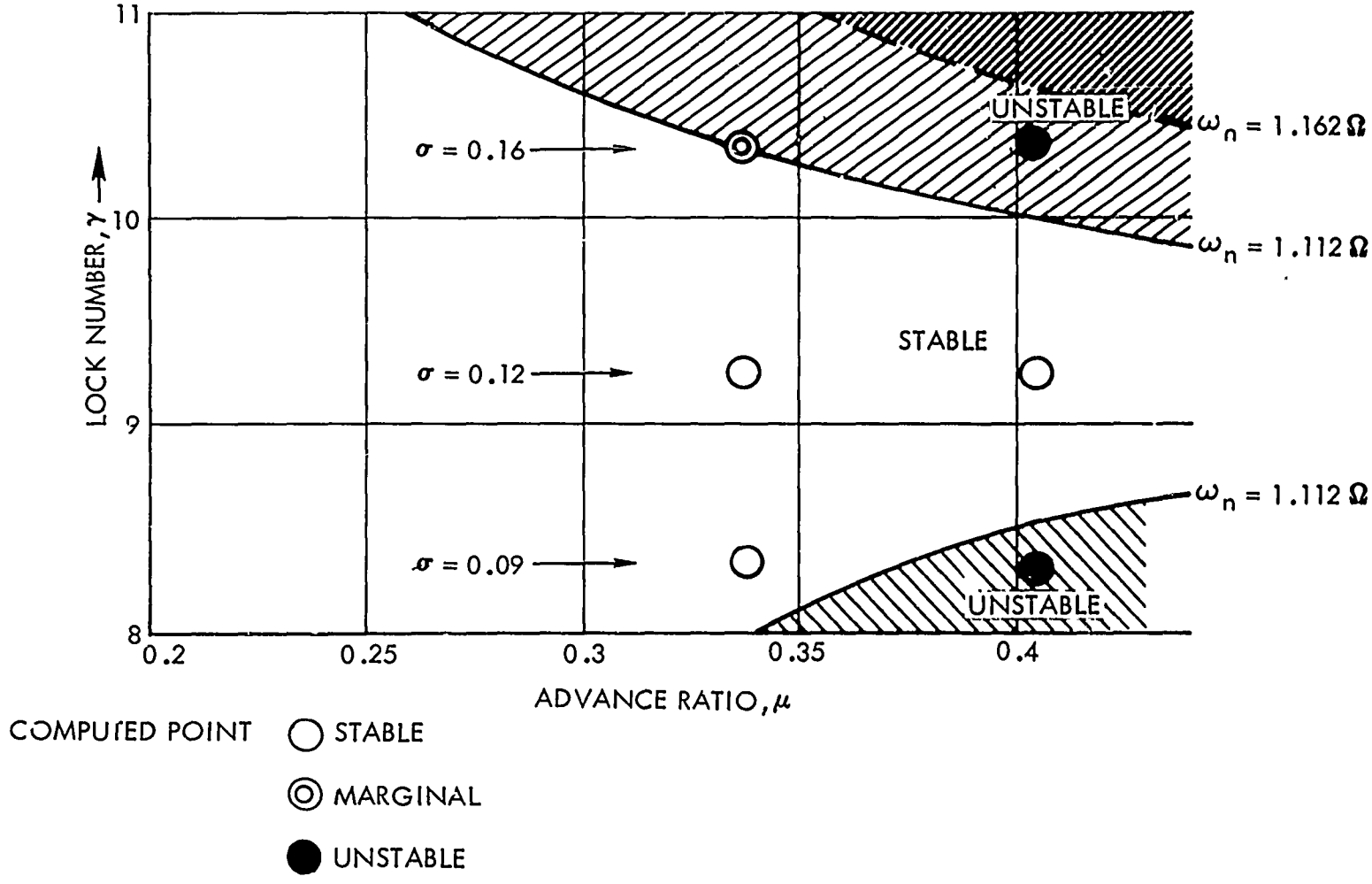

Figure 49. Estimated Stability Boundaries for Blade First Flapping Natural Frequencies, ω_n.

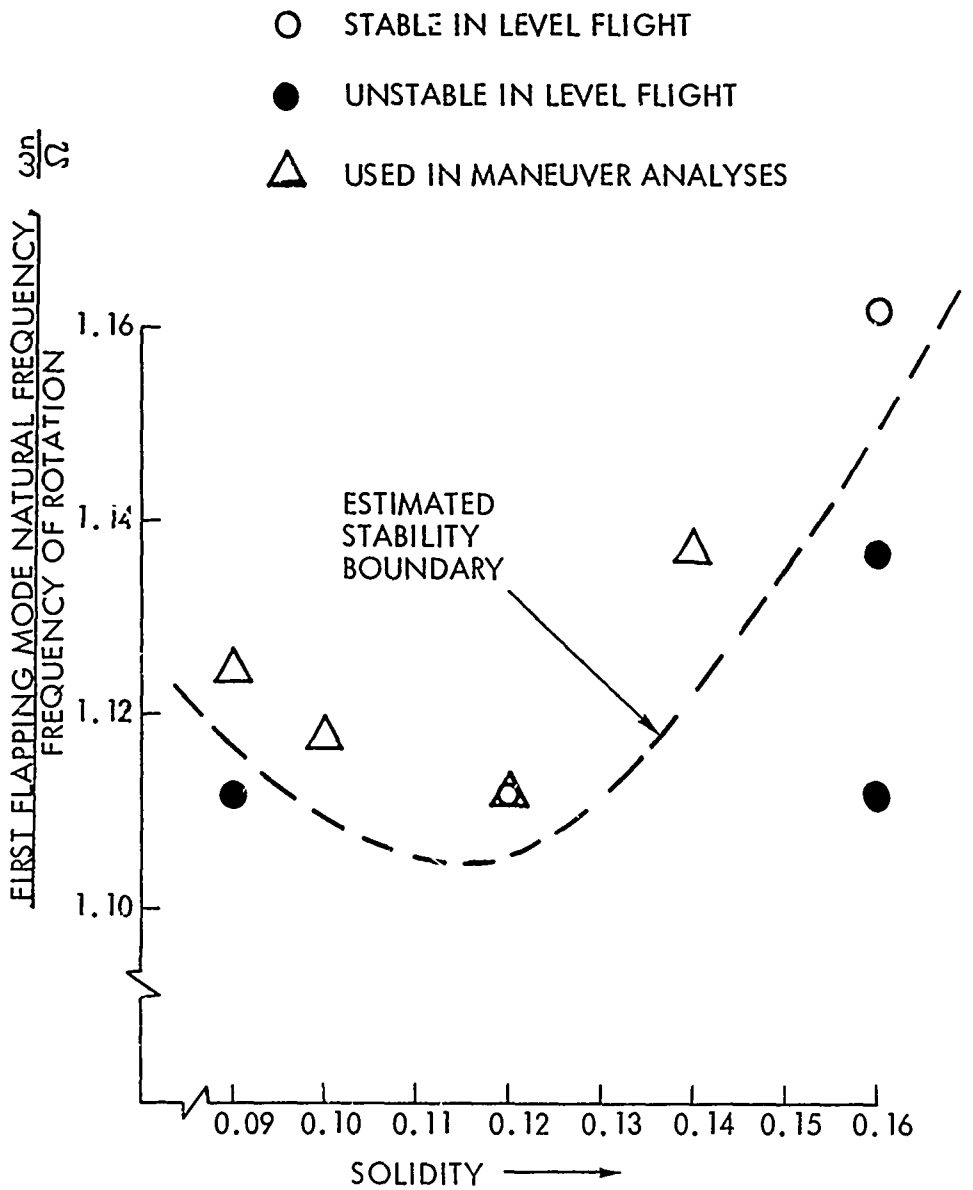

Figure 50. Effect of Blade Solidity and Stiffness on Vehicle Stability at 167 KTAS.

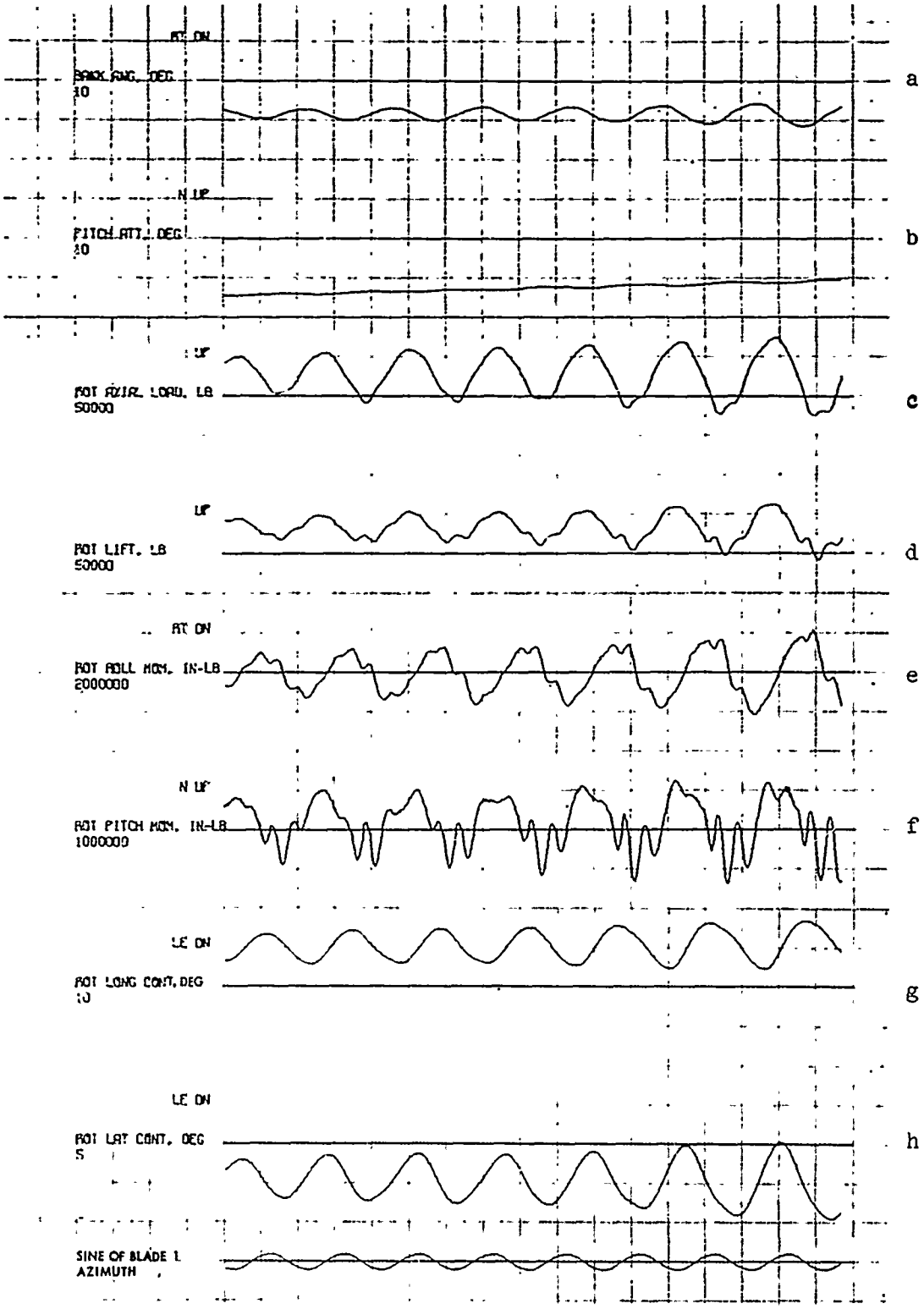

Figure 51. Buildup of Oscillations for an Unstable Condition: $\sigma = 0.16$; $\omega_n = 1.112\Omega$; V = 167 KTAS.

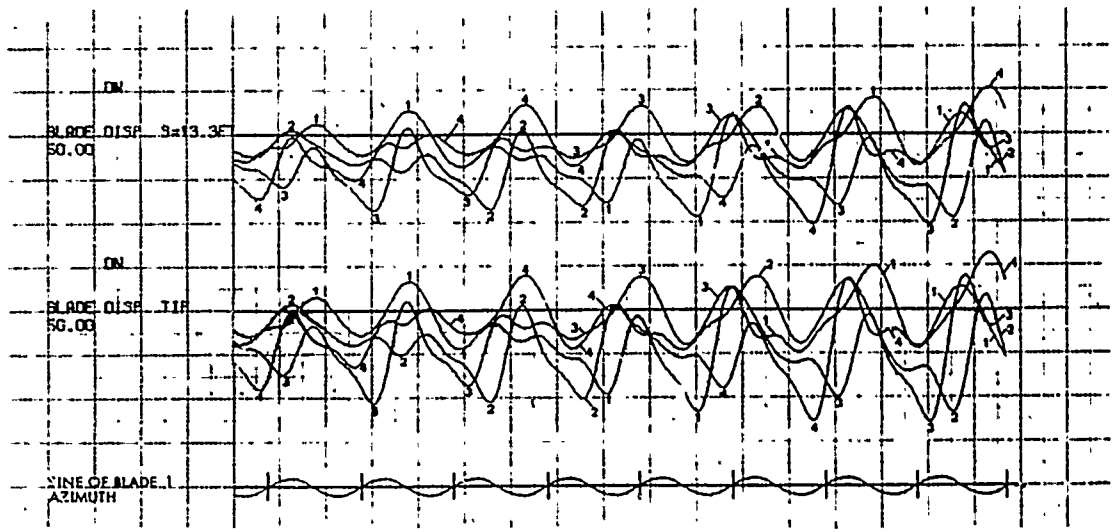

Figure 52. Composite of Blade Displacements for an Unstable Condition: $\sigma = 0.16$; $\omega_n = 1.112\ \Omega$; V = 167 KTAS.

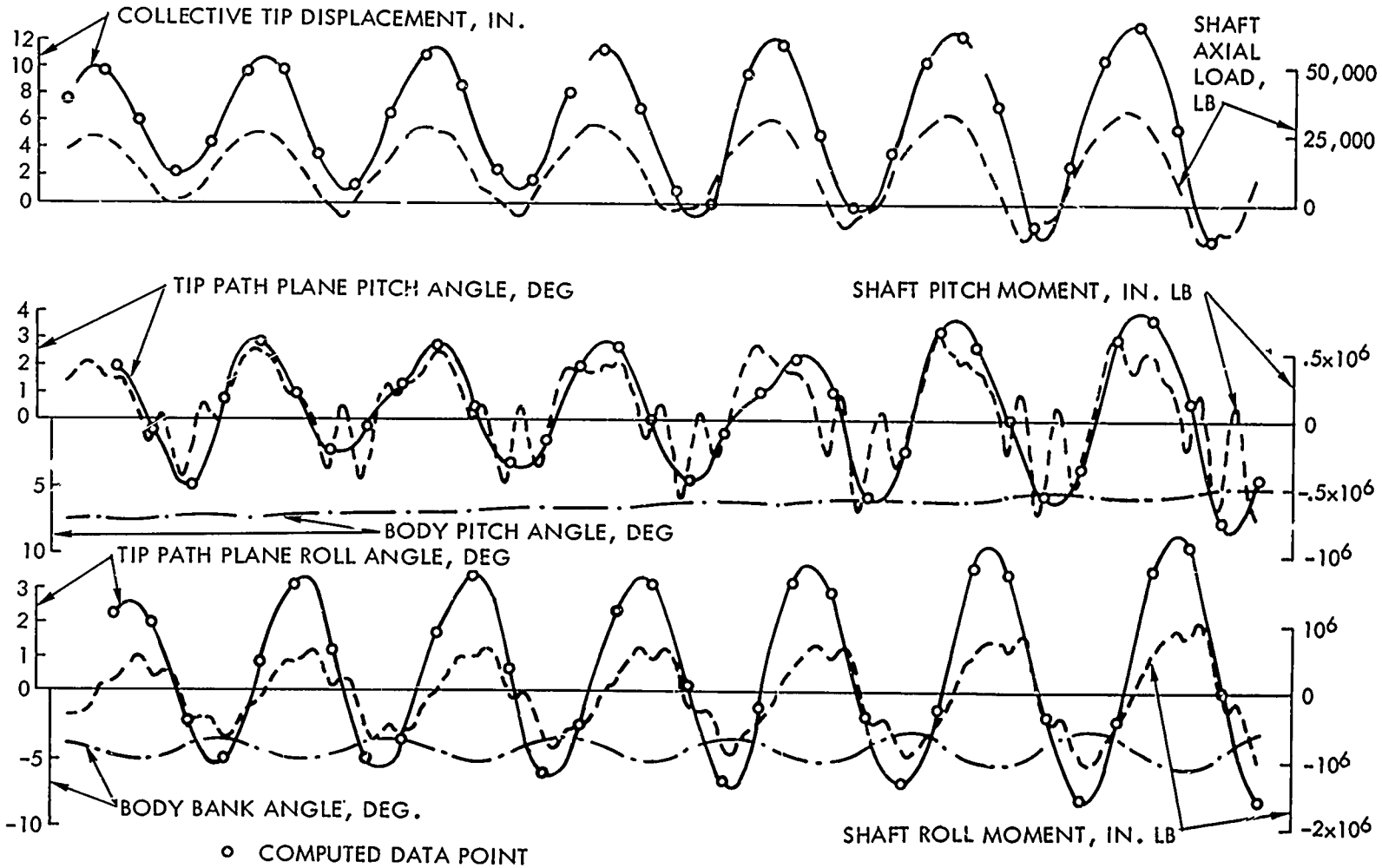

Figure 53. Comparison of Loads and Displacements for an Unstable Condition: $\sigma = 0.16$; $\omega_n = 1.112\ \Omega$; V = 167 KTAS.

spring is found to be rougnly proportional to the square of the advance ratio. (The same configuration is dynamically stable at a speed of 140 KCAS.) Based on the rotor blade tip displacements, it is estimated that the pitching amplitude of the tip-path plane is approximately 3 deg. The aerodynamic rotor thrust variation accompanying this pitching motion of the rotor plane accounts for an additional 7000-lb variation in rotor axial shaft load. The rolling motion of the body is in opposition to that of the rotor plane, indicating that the source of the dynamic behavior described is not a fundamental rolling mode of the helicopter but rather a more complex deformation mode of the rotor and body.

APPENDIX V

TIME HISTORIES

DEFINITIONS OF NOTATIONS APPLIED IN TIME HISTORIES

General Information

The vehicle reference axes for these graphs consist of longitudinal and lateral axes parallel to the main rotor shaft normal plane and of a vertical axis along the main rotor shaft, all intersecting at the reference cg. Table XXII defines the various labels associated with the time history plots.

Cycles of Rotor Rotation

With each group of graphs shown for the figure letter (a, b, c, etc.) above the label "time, sec," there is an unlabelled curve which indicates cycles of rotor rotation. This curve is provided to permit measuring comparative frequencies of vibratory motion which may appear on other curves of the group. The unmarked curve shows the sine of the azimuth angle of one blade sweeping through the rotor plane of rotation from the zero (downwind) position.

Elements of the Labels for Each Graph

To the left of each graph, there are three elements of the plot label:

- The basic name of the graph and the units of measure for the ordinate are noted horizontally in line with the abscissa for the individual graph.
- The number under the name of the graph represents the number of units per major division (tick mark) along the ordinate.
- The positive sense of the graph is shown by a brief notation above the plot name and next to the ordinate.

TABLE XXII. DEFINITIONS OF NOTATIONS USED IN TIME HISTORY PLOTS

Figure Letter	Plot Name and Units	Description	Note For Positive Sense	Description
a	COLL ST POS. IN	Collective stick position, in.	PLUS	Upward stick displacement
	DIR PED POS. IN	Directional pedal position, in.	RT PED	Right pedal displacement
	LAT ST POS. IN	Lateral cyclic stick position, in.	RT	Right displacement
	LONG ST POS. IN	Longitudinal stick position, in.	AFT	Aft displacement
b	PITCH ATT. DEG	Vehicle longitudinal axis pitch attitude with respect to horizon, deg	N UP	Nose up
	VERT VEL. FPS	Vertical velocity of vehicle with respect to horizon, ft per sec	UP	Upward velocity
	HEIGHT DISP. FT	Height displacement of vehicle from initial condition, normal to horizontal, ft	UP	Upward displacement
	NORM LOAD FACTOR	Force of vehicle along vehicle vertical axis, multiples of gravity force	UP	Upward force

TABLE XXII. DEFINITIONS OF NOTATIONS USED IN TIME HISTORY PLOTS (Continued)

Figure Letter	Plot Name and Units	Description	Note For Positive Sense	Description
c	BANK ANG. DEG	Vehicle lateral axis bank angle with respect to horizon, deg	RT DN	Right side down
	SIDESLIP ANG. DEG	Sideslip angle, vehicle longitudinal axis sideward angular displacement from relative wind, deg	RT	Velocity component of vehicle along lateral axis to the right into the relative wind
	INC FLT PATH V. KTAS	Increment of flight path velocity from initial condition, KTAS	PLUS	Increase in flight path velocity
	FLT PATH VEL. KTAS	Flight path velocity, KTAS	FWD	Forward velocity
d	LAT DISP. FT	Lateral displacement of vehicle from initial condition, parallel to horizon, ft	RT	Displacement to the right
	T R COLL CONT. DEG	Tail rotor blade collective pitch angle, deg	LE RT	Blade leading edge displaced to the right
	INC TOTAL POWER. HP	Increment of total shaft power required, measured from initial condition, shp	PLUS	Increase in power required
	TOTAL POWER. HP	Total shaft power required, shp	PLUS	Power greater than zero

TABLE XXII. DEFINITIONS OF NOTATIONS USED IN TIME HISTORY PLOTS (Continued)

Figure Letter	Plot Name and Units	Description	Note For Positive Sense	Description
e	ROLL RATE. DPS	Vehicle lateral axis roll rate with respect to horizon, deg per sec	RT DN	Angular velocity of right side downward
	PITCH RATE. DPS	Pitch rate of vehicle about vehicle lateral axis, deg per sec	N UP	Nose-up angular rate
	ROT LONG INPL LD. LB.	Rotor longitudinal inplane load, including rotor weight component in steady flight, and inertia contribution in acceleration, lb	AFT	Aftward force
	ROT COLL CONT. DEG	Rotor collective control, blade collective pitch setting at centerline of rotor, deg	LE UP	Blade leading edge up
f	*N R AIRFR AOA. DEG	Nonrotating airframe angle of attack based on shaft normal plane angle to local relative wind which includes rotor downwash angle, deg	N UP	Nose-up angular displacement

*Shown only for winged configurations

TABLE XXII. DEFINITIONS OF NOTATIONS USED IN TIME HISTORY PLOTS (Continued)

Figure Letter	Plot Name and Units	Description	Note for Positive Sense	Description
f (Continued)	N R AIRFR LIFT. LB	Nonrotating airframe lift normal to freestream relative wind, lb	UP	Upward force
	*N R AIRFR CL	Nonrotating airframe lift coefficient, based on wing area and on shaft normal plane angle to local relative wind which includes rotor downwash angle	UP	Upward force
	N R AIRFR DRAG. LB	Nonrotating airframe drag along freestream relative wind, lb	AFT	Aftward force
g	ROT LIFT. LB	Rotor lift normal to freestream relative wind, lb	UP	Upward force
	ROT AOA. DEG	Rotor angle of attack shaft normal plane, to freestream relative wind, deg	N UP	Nose-up angular displacement
	ROT DRAG. LB	Rotor drag along freestream relative wind, lb	AFT	Aftward force (basically negative in the rotor propulsive mode)

*Shown only for winged configurations

TABLE XXII. DEFINITIONS OF NOTATIONS USED IN TIME HISTORY PLOTS (Continued)

Figure Letter	Plot Name and Units	Description	Note For Positive Sense	Description
h	ROT LONG CONT. DEG	Rotor longitudinal cyclic control, blade cyclic pitch setting, B_{ls}, deg	LE DN	Blade leading edge down
	ROT LAT CONT. DEG	Rotor lateral cyclic control, blade cyclic pitch setting, A_{ls}, deg	LE DN	Blade leading edge down
	ROT PITCH MOM. IN-LB	Rotor hub pitching moment, in-lb	N UP	Nose-up moment
	ROT ROLL MOM. IN-LB	Rotor hub rolling moment, in-lb	RT DN	Right side downward moment
i	BL ST 16 AOA. DEG	Blade station 16 (93.6% rotor radius) local angle of attack, deg	LE UP	Blade leading edge up from local relative wind
	ROT TIP FL DISP. FT	Rotor tip flapping displacement, ft	TIP UP	Tip up from shaft normal plane
	BL ST 17 MACH NO.	Blade station 17 (tip 100% rotor radius) Mach number	PLUS	Mach number measured from zero
j	BL ST 16 CL	Blade station 16 (93.6% rotor radius) local lift coefficient	UP	Upward force

TABLE XXII. DEFINITIONS OF NOTATIONS USED IN TIME HISTORY PLOTS (Continued)

Figure Letter	Plot Name and Units	Description	Note For Positive Sense	Description
j (Continued)	BL RT FLAP MOM. IN-LB	Blade root (zero % rotor radius) flapping moment	TIP UP	Tip up moment
k	BL RT INPL MOM. IN-LB	Blade root (zero % rotor radius) in-plane moment	TIP AFT	Tip aft moment (clockwise viewed from above)

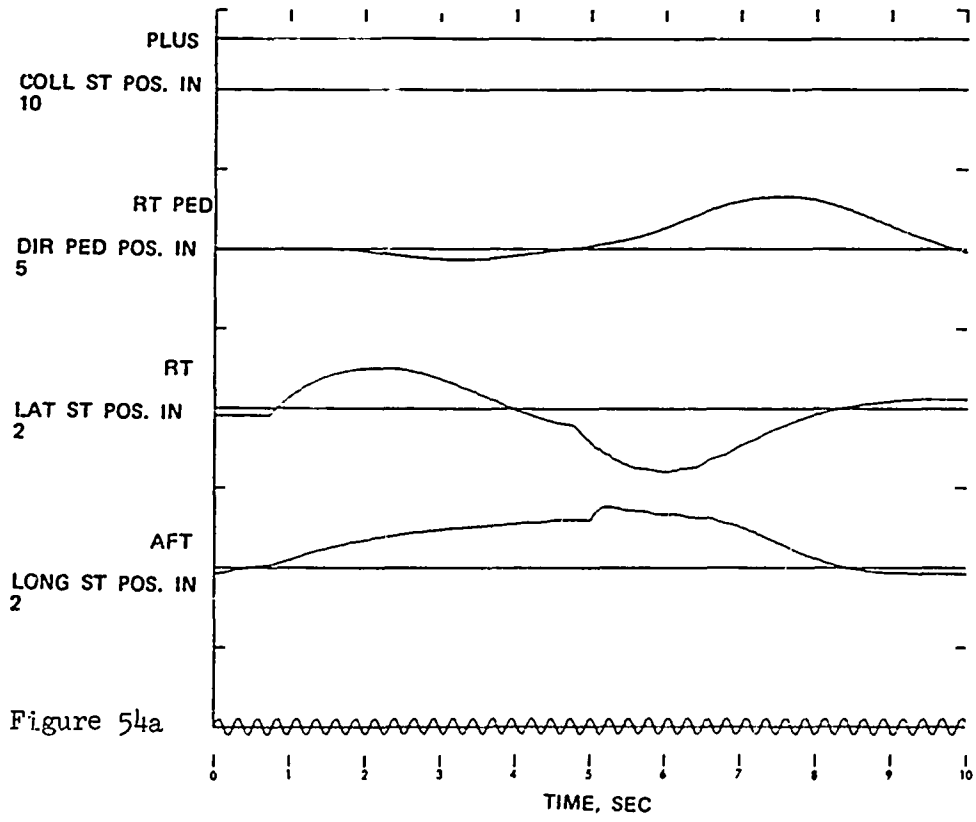

Figure 54a

Figure 54. Time Histories Showing the Effects of Coordinated Turn: Configuration 1; Maneuver Initiated at 140 KTAS.

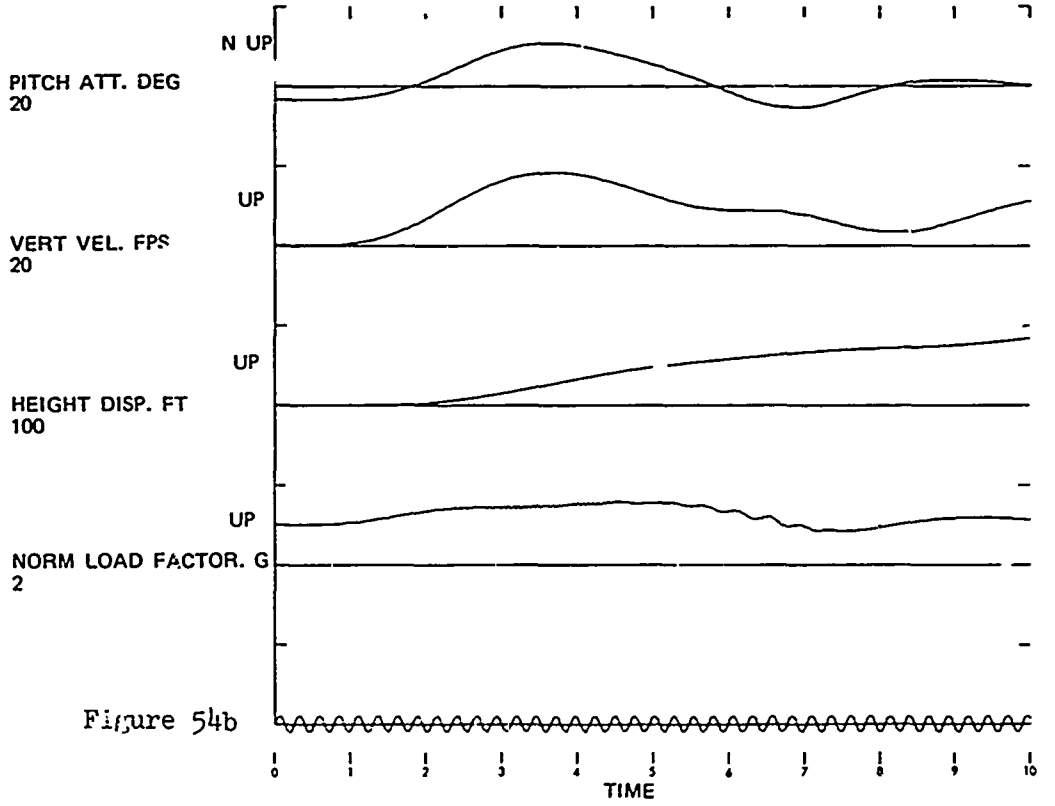

Figure 54b

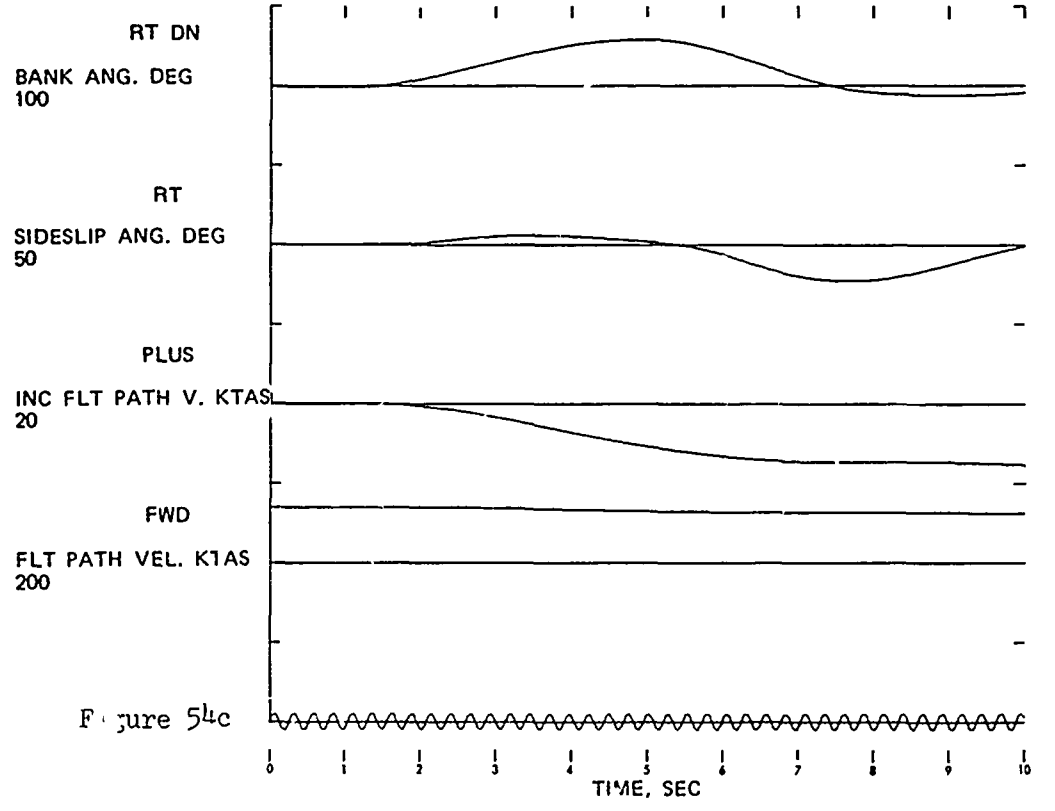

Figure 54c

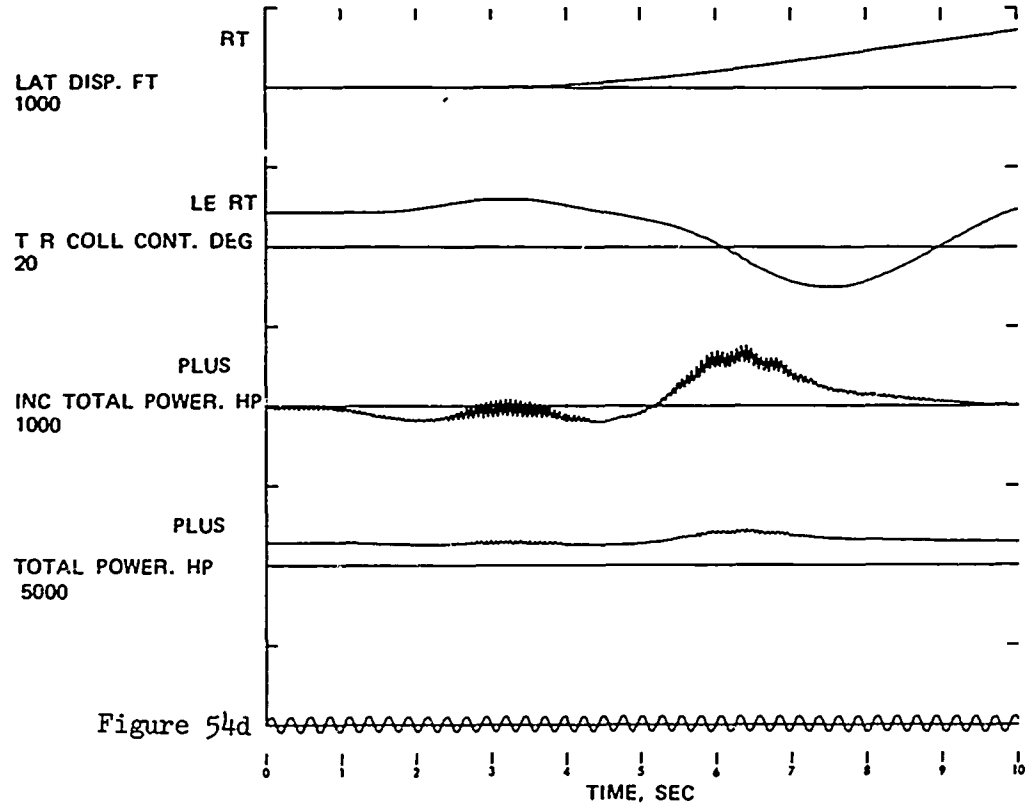

Figure 54d

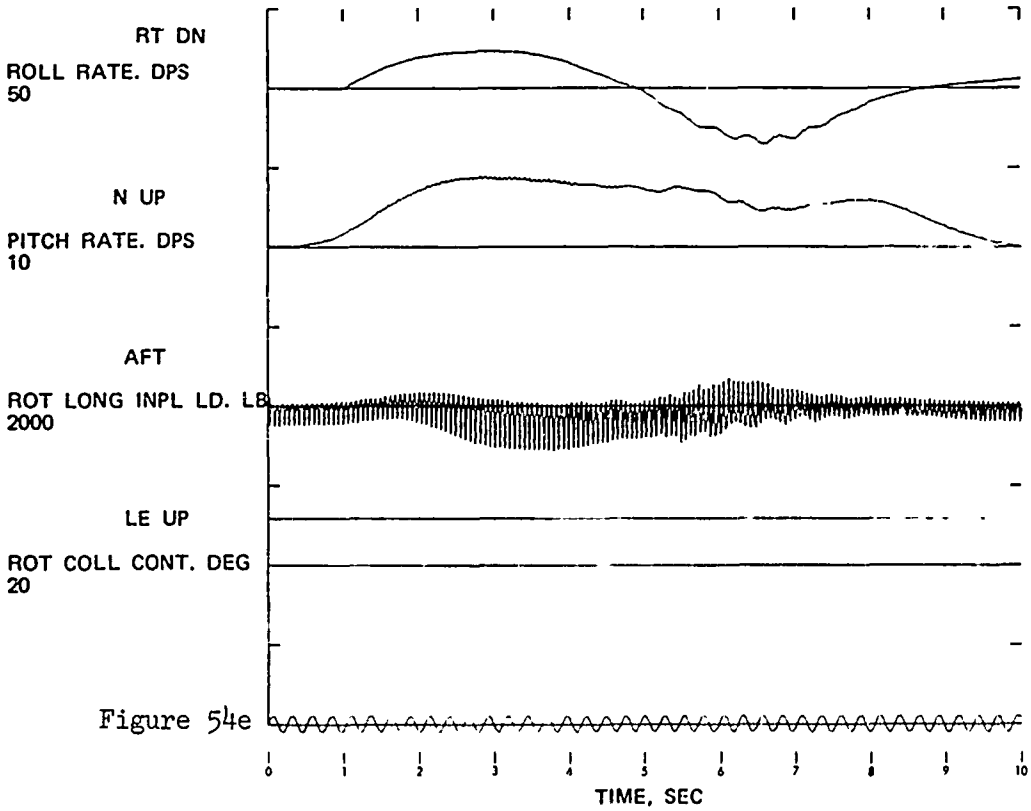

Figure 54e

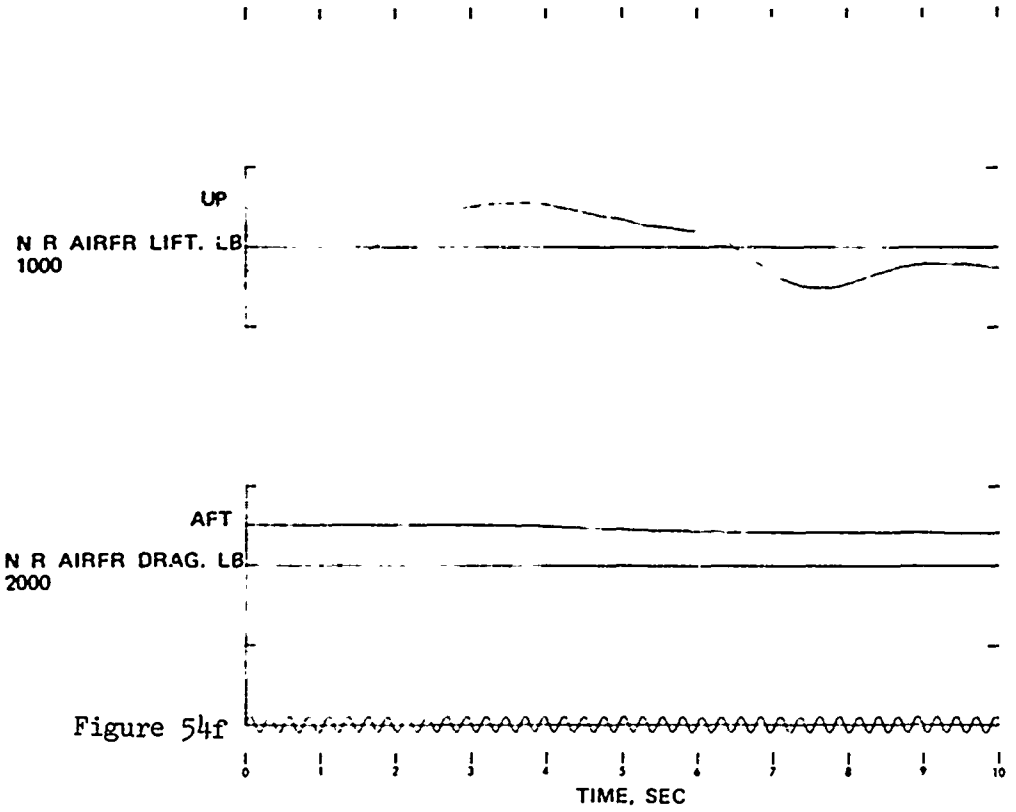

Figure 54f

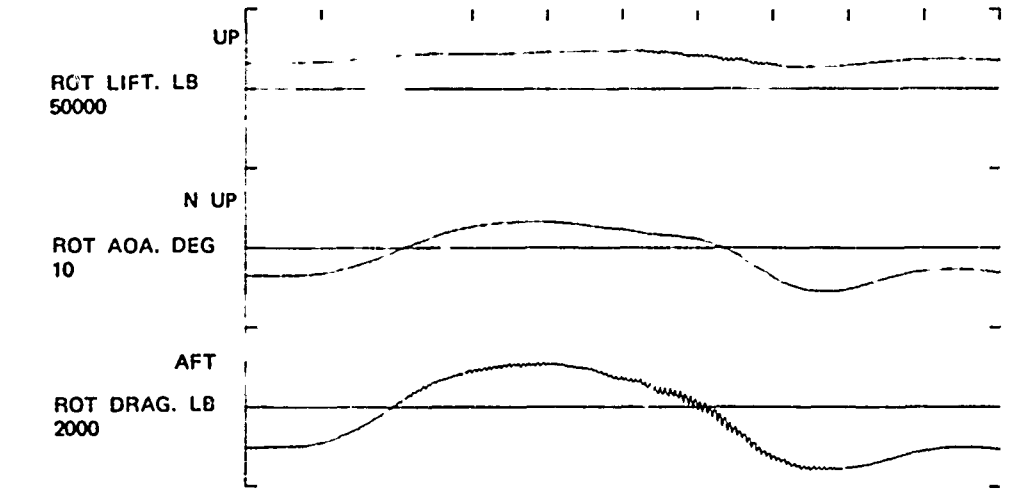

Figure 54g

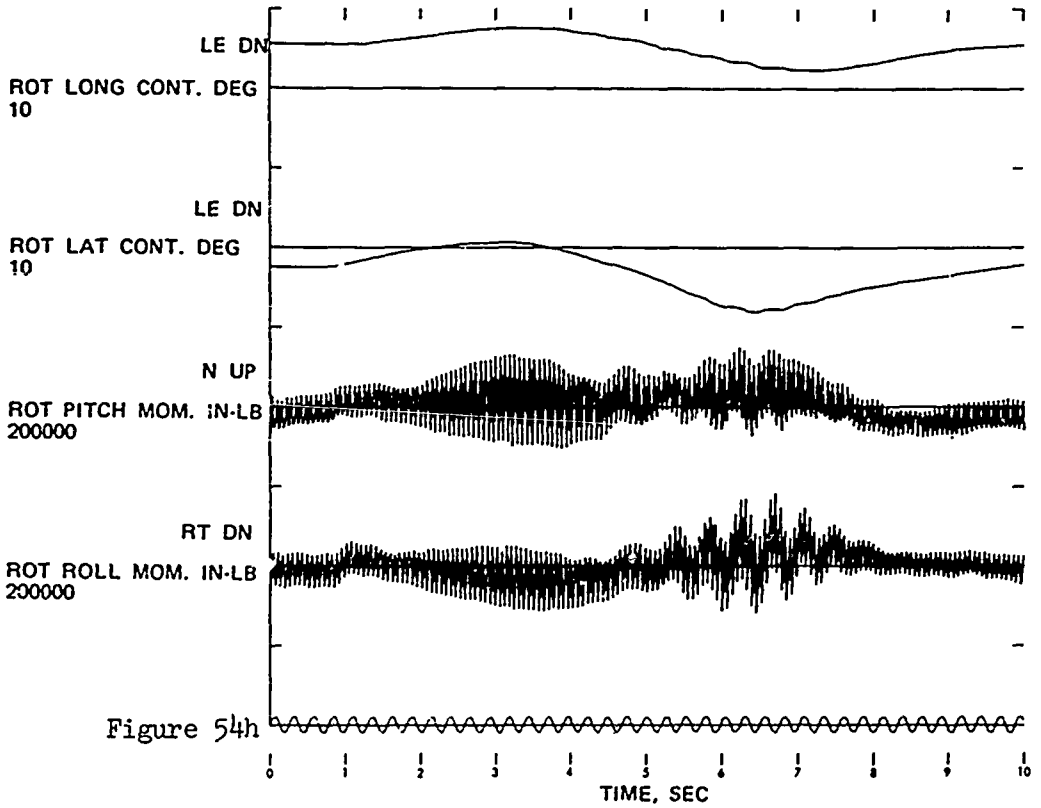

Figure 54h

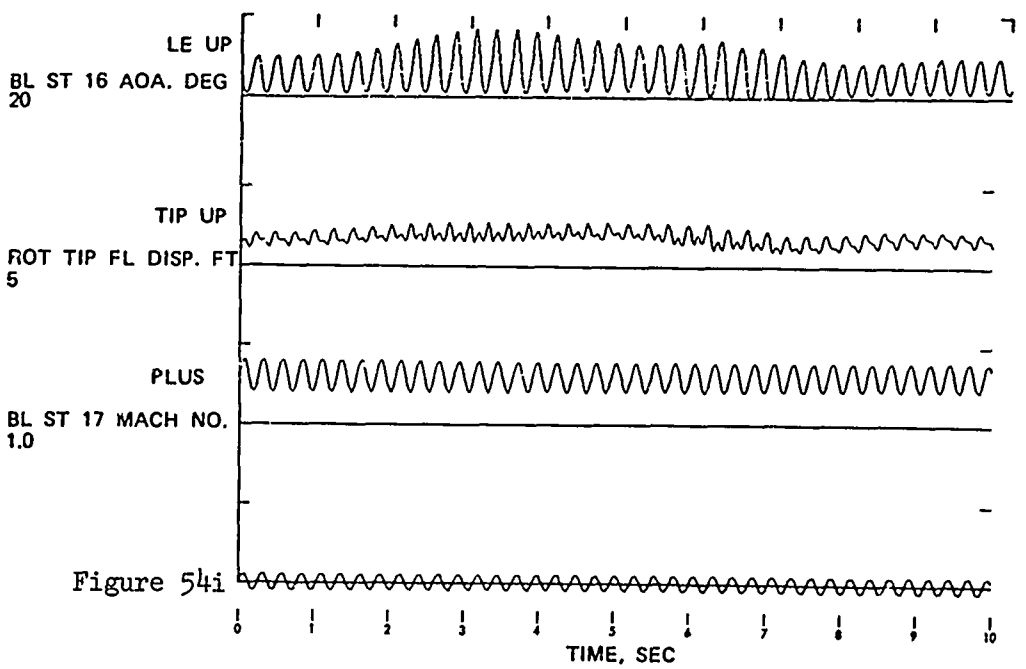

Figure 54i

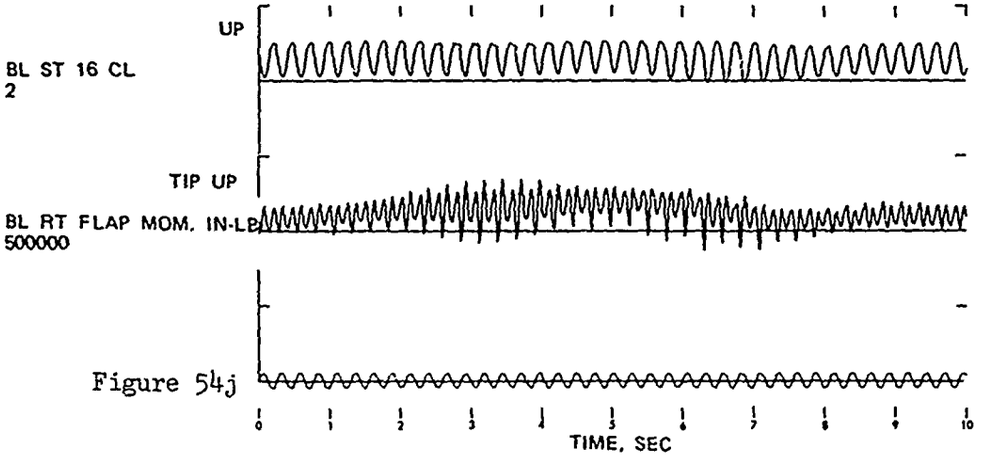

Figure 54j

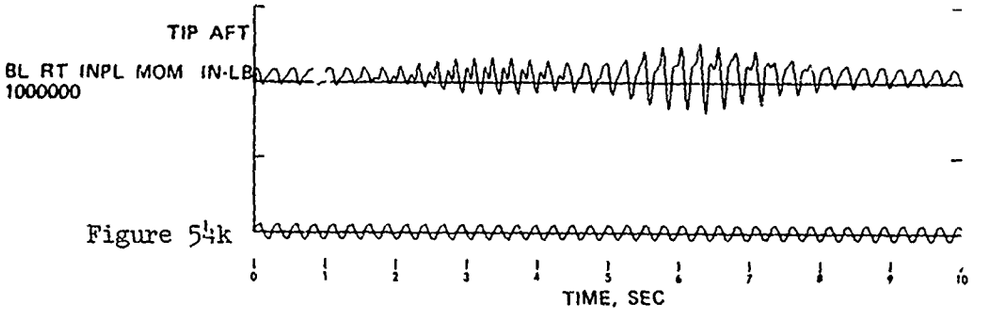

Figure 54k

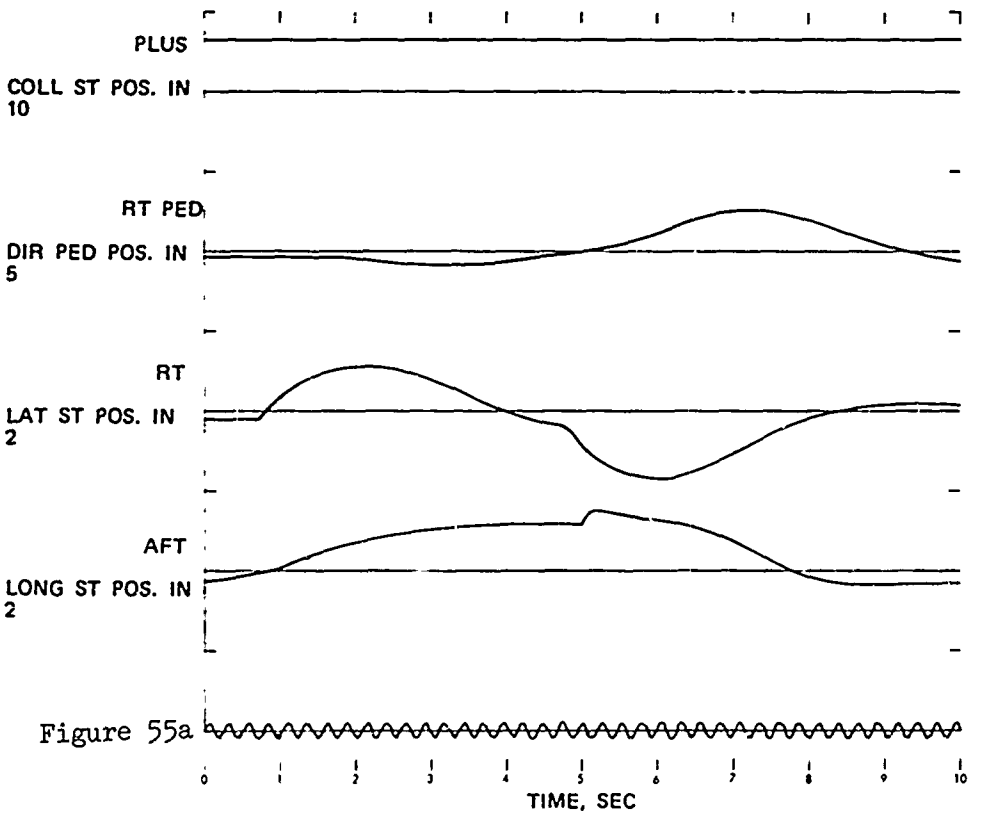

Figure 55a

Figure 55. Time Histories Showing the Effects of Coordinated Turn: Configuration 2; Maneuver Initiated at 155 KTAS.

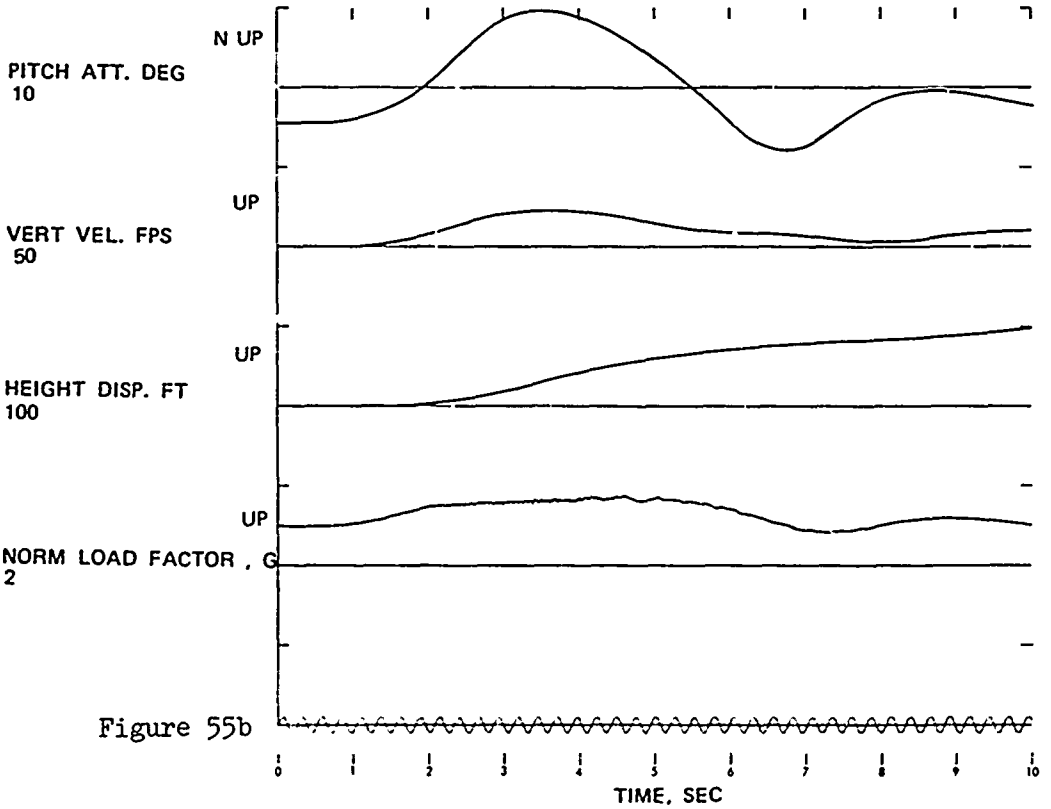

Figure 55b

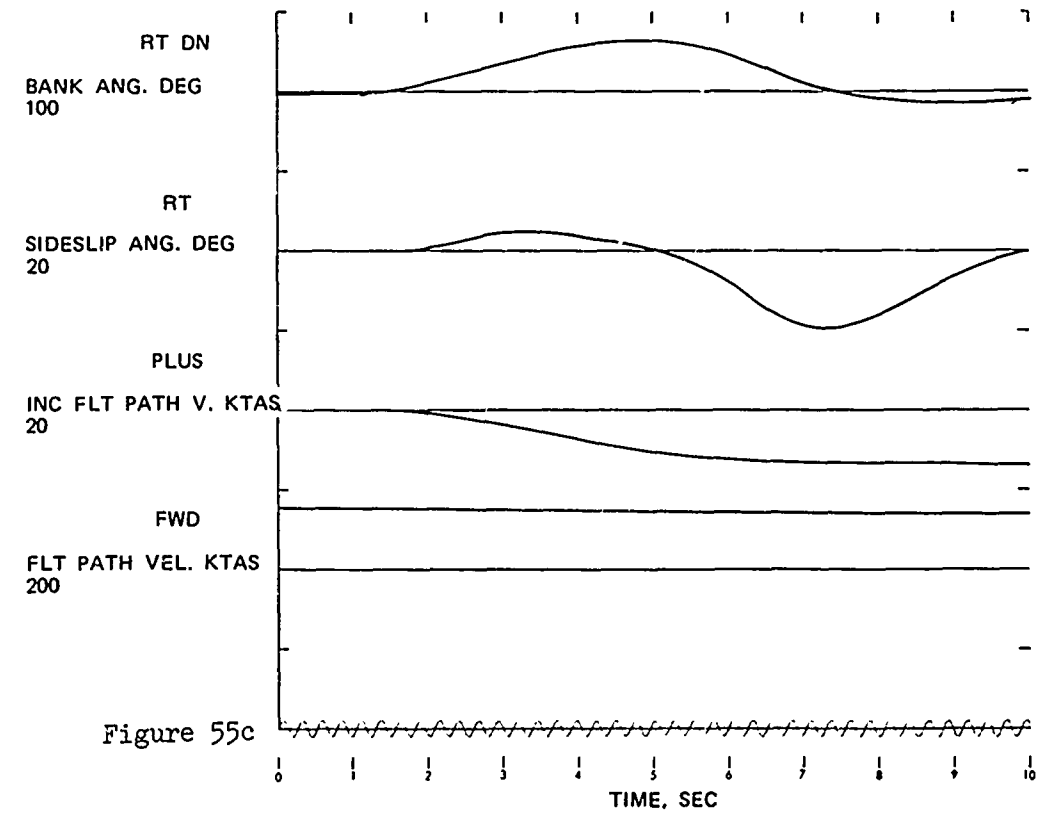

Figure 55c

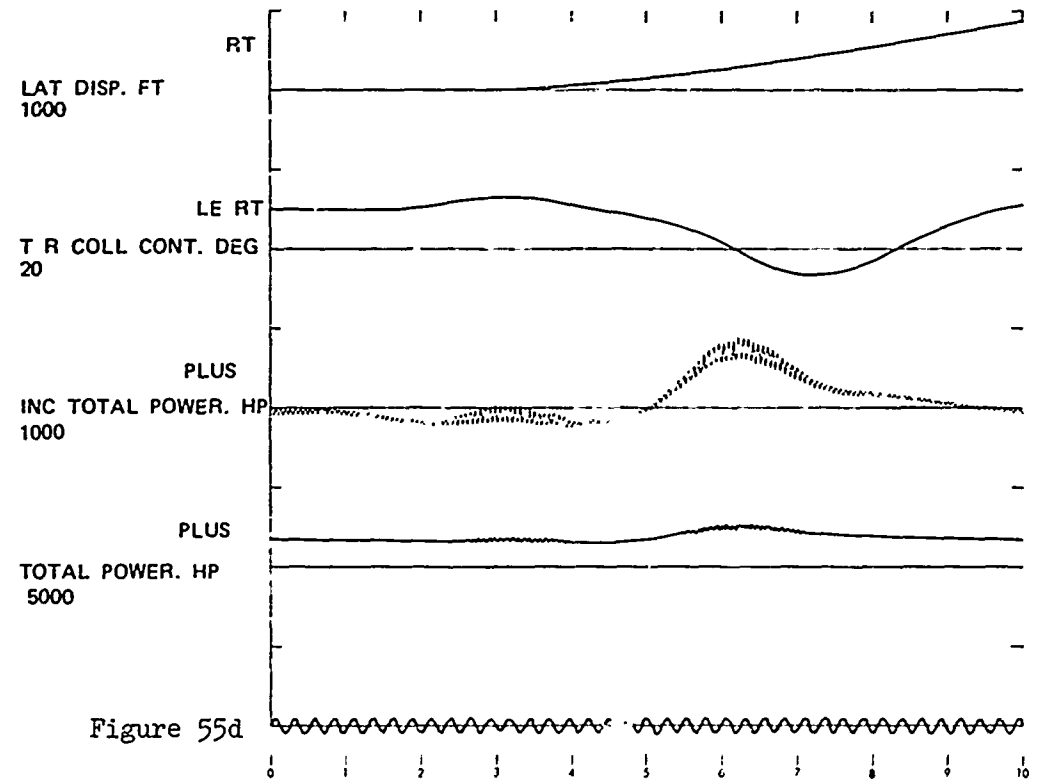

Figure 55d

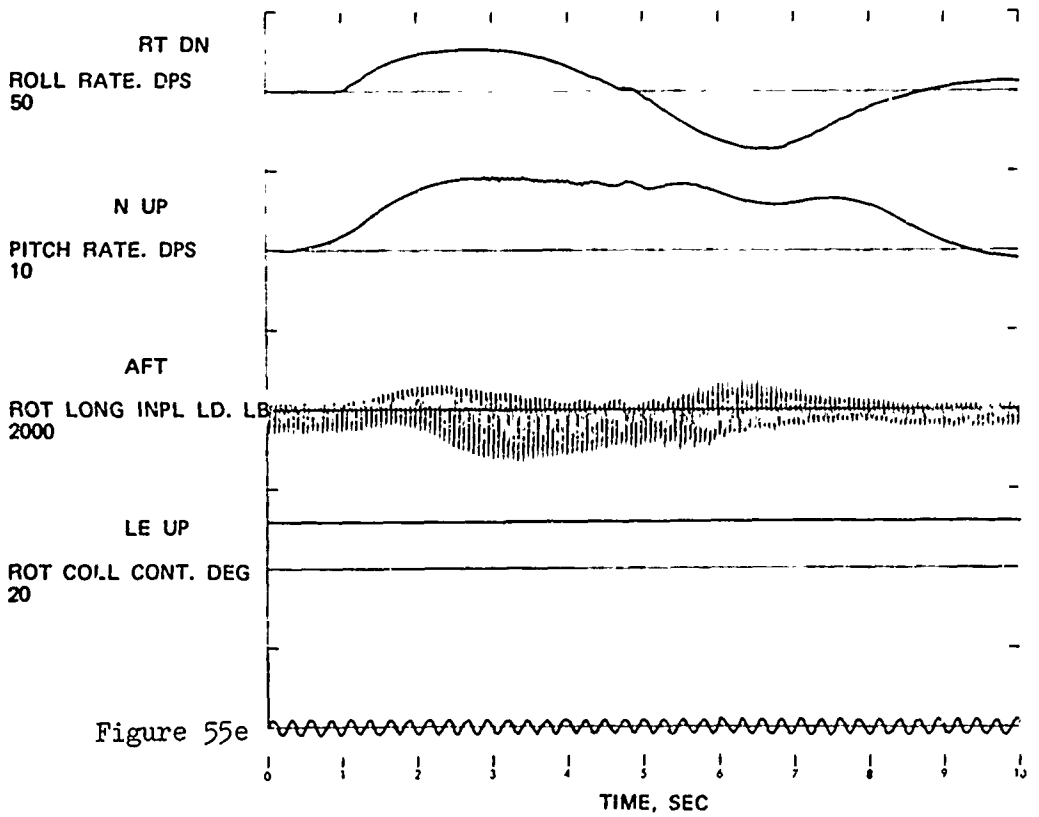

Figure 55e

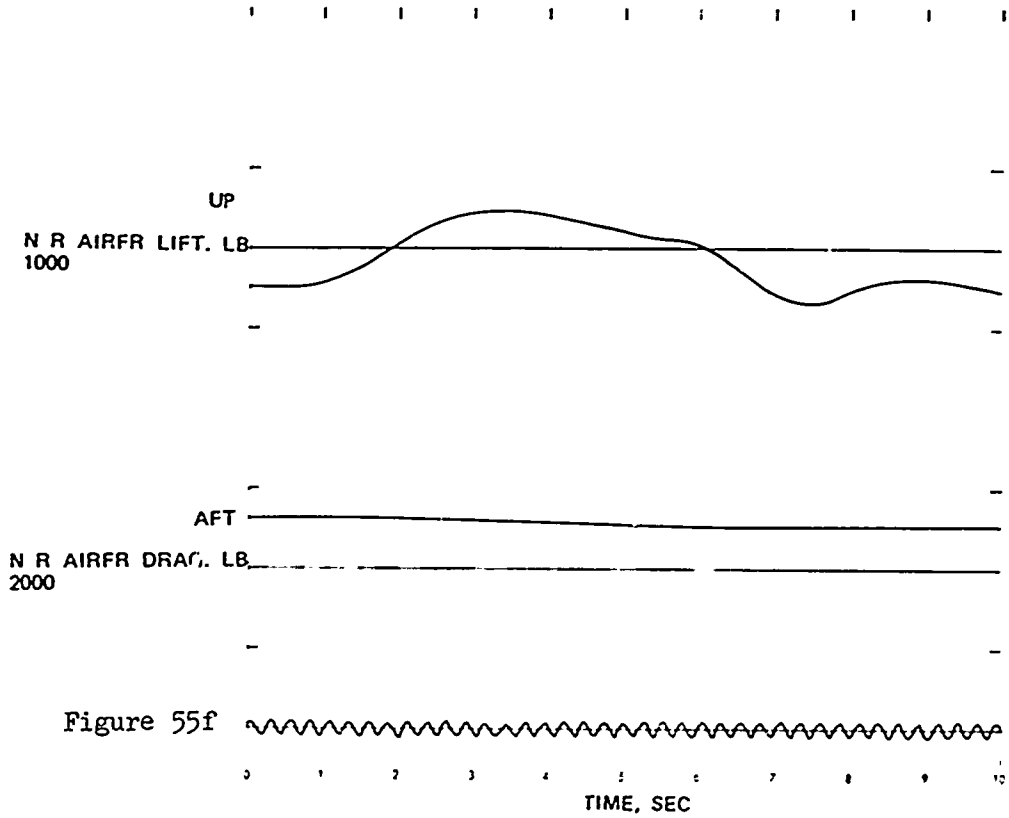

Figure 55f

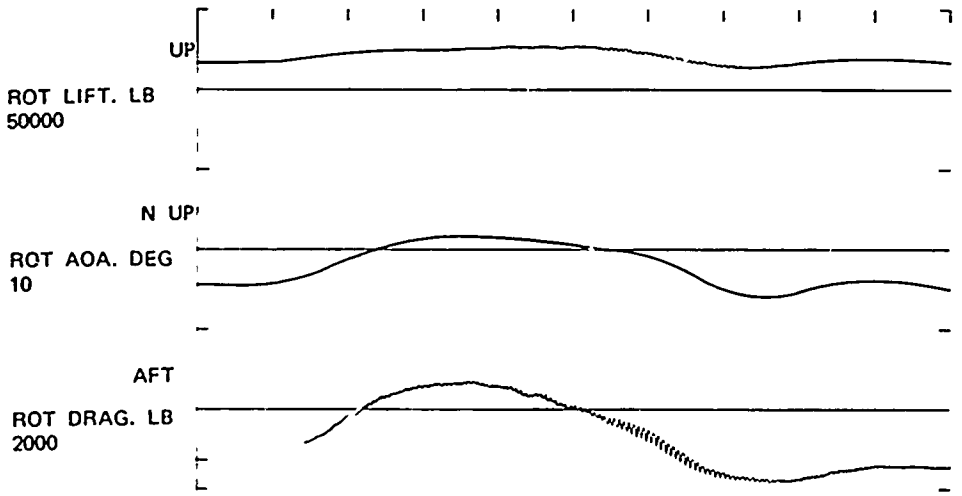

Figure 55g

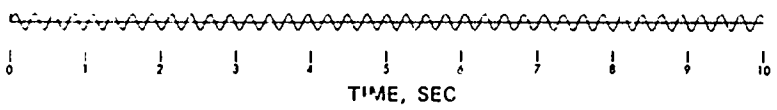

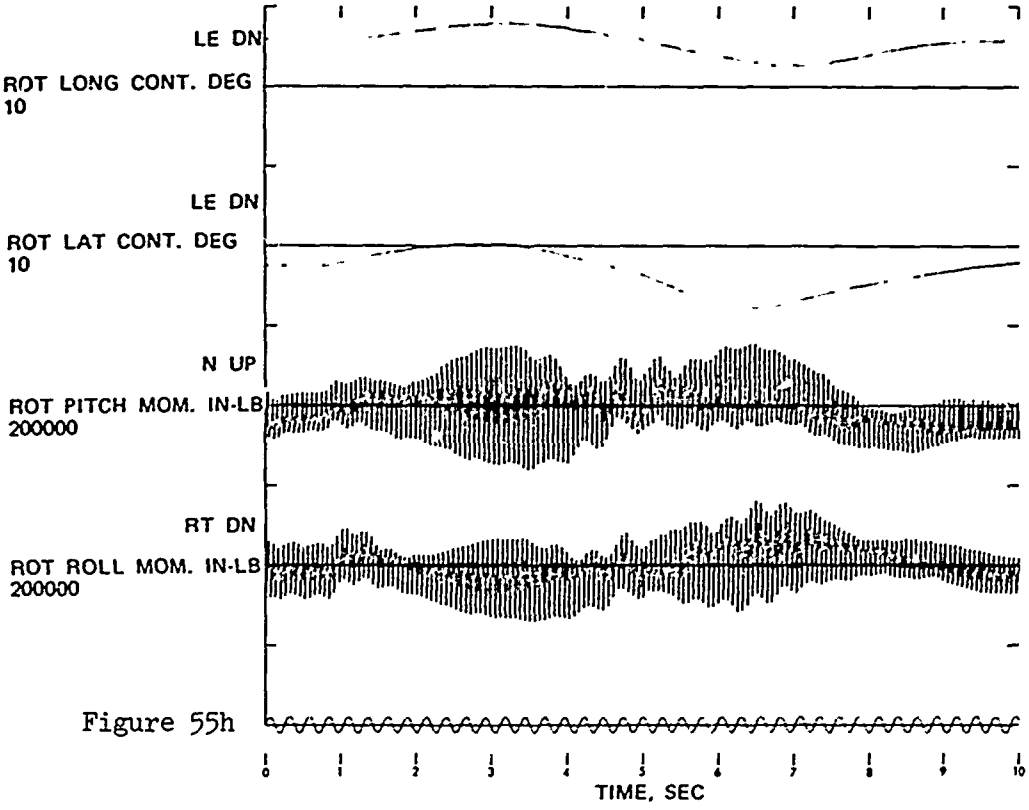

Figure 55h

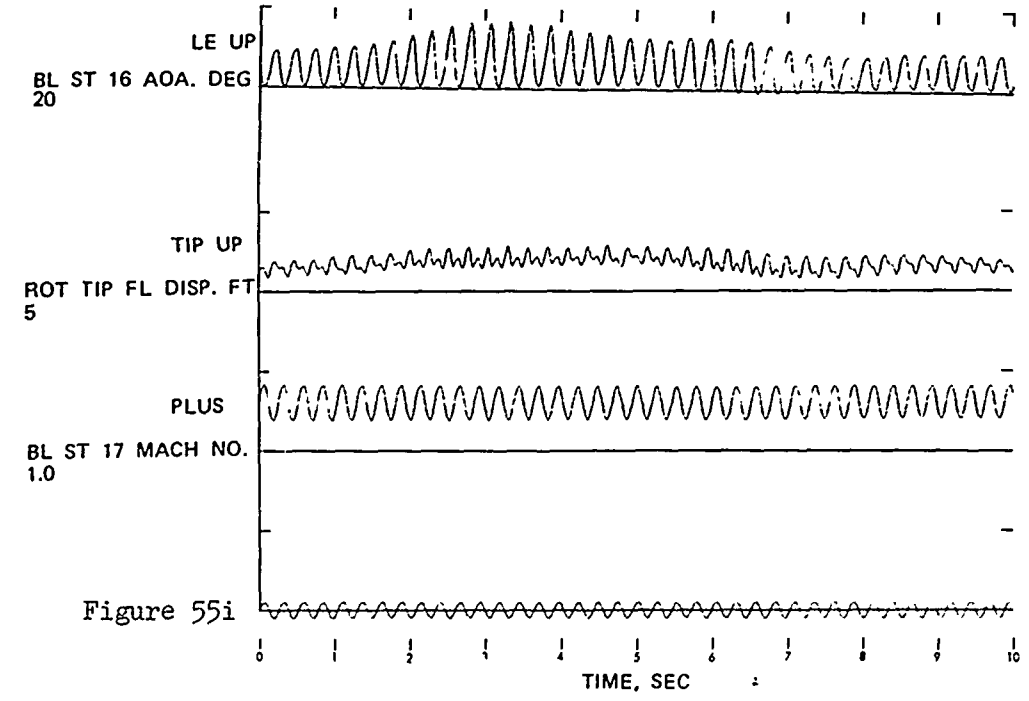

Figure 55i

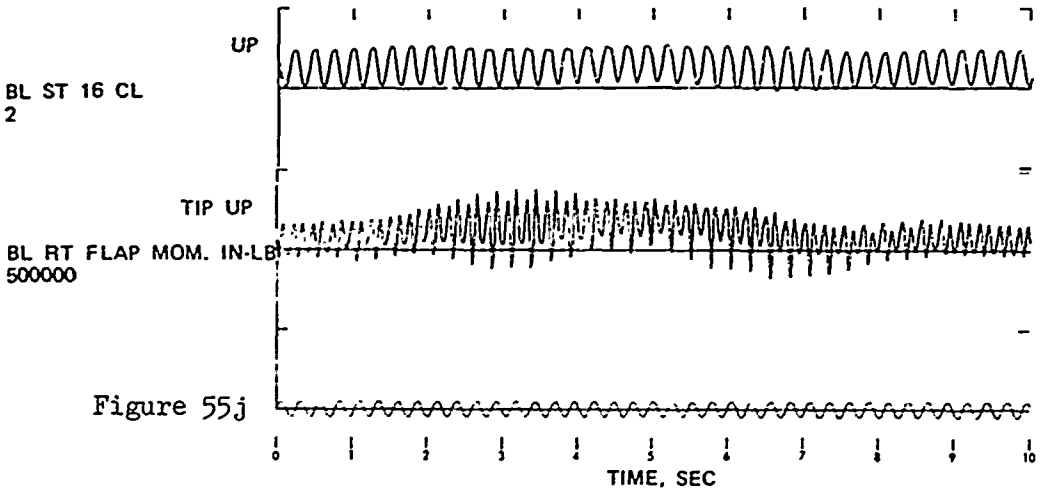

Figure 55j

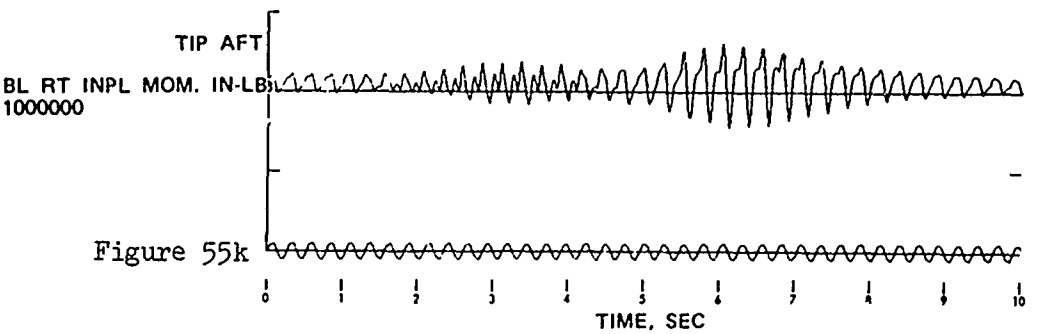

Figure 55k

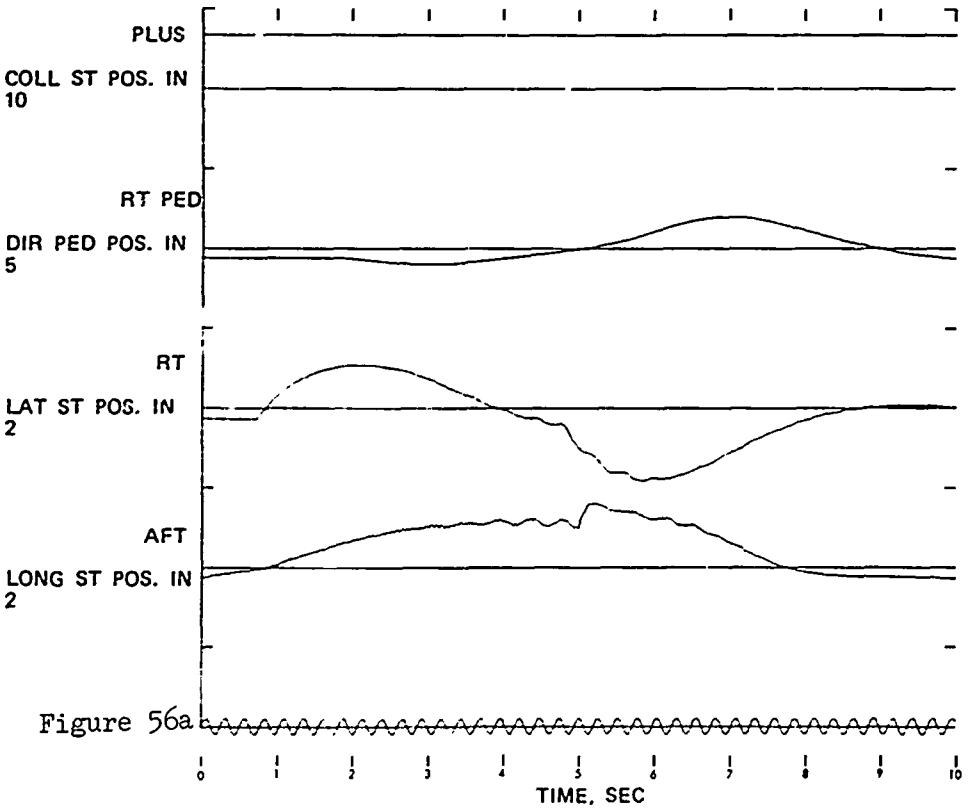

Figure 56. Time Histories Showing the Effects of Coordinated Turn: Configuration 3; Maneuver Initiated at 167 KTAS.

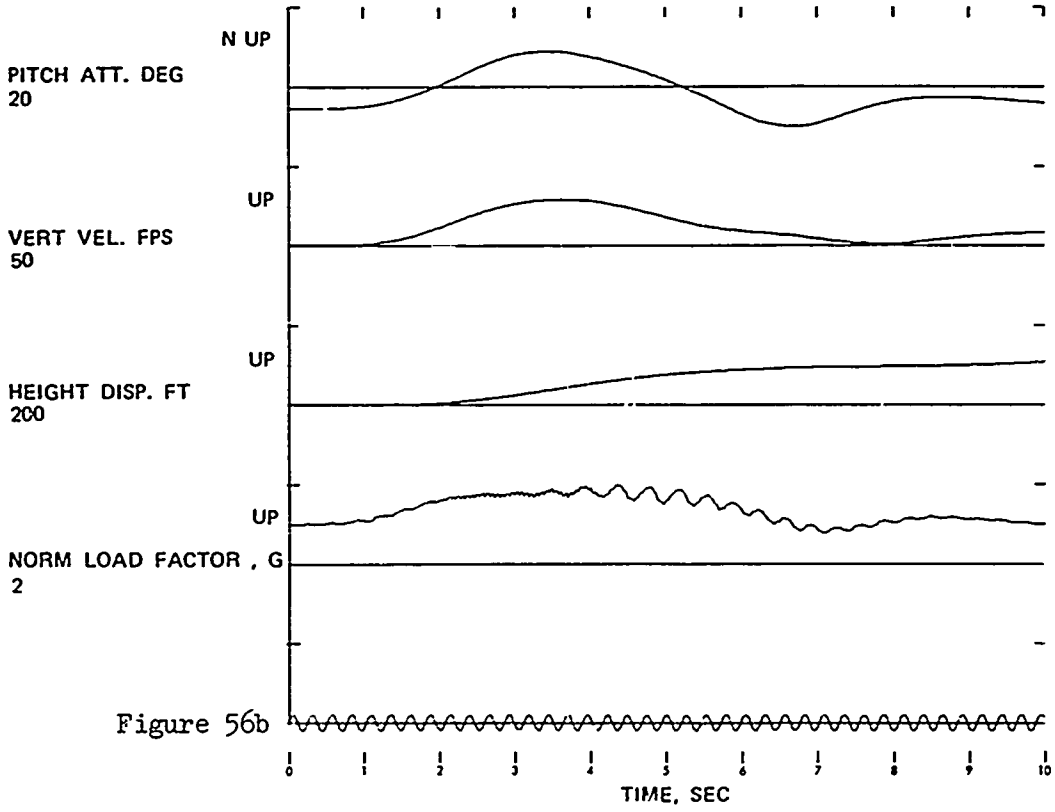

Figure 56b

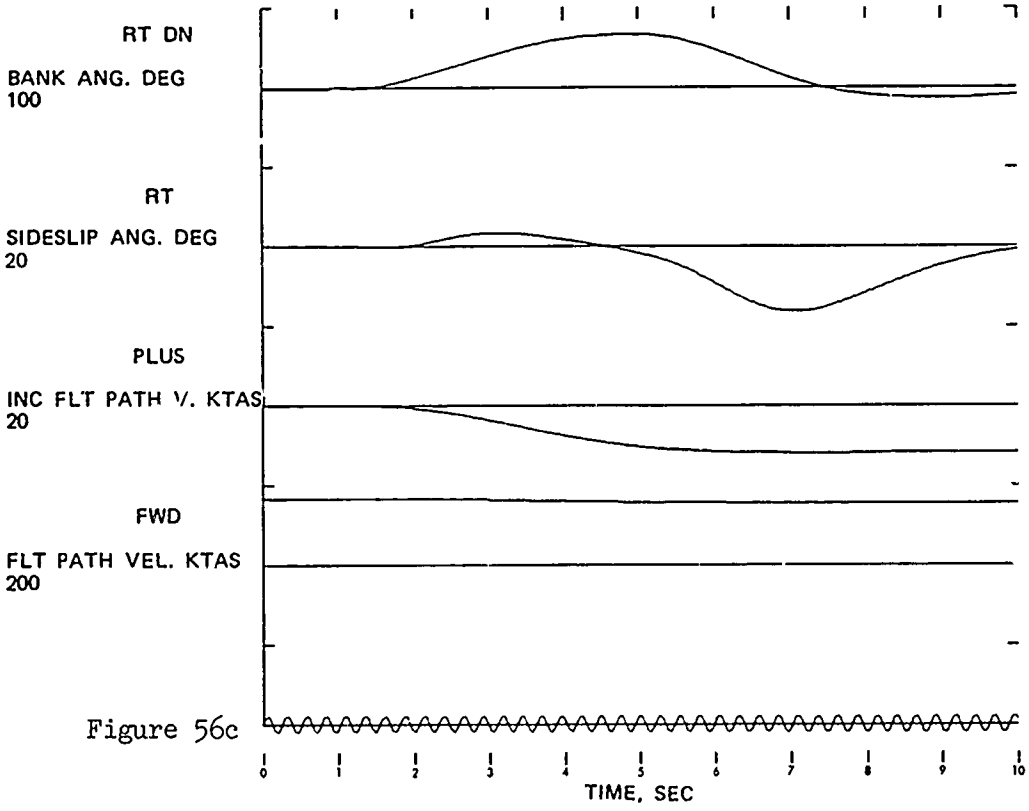

Figure 56c

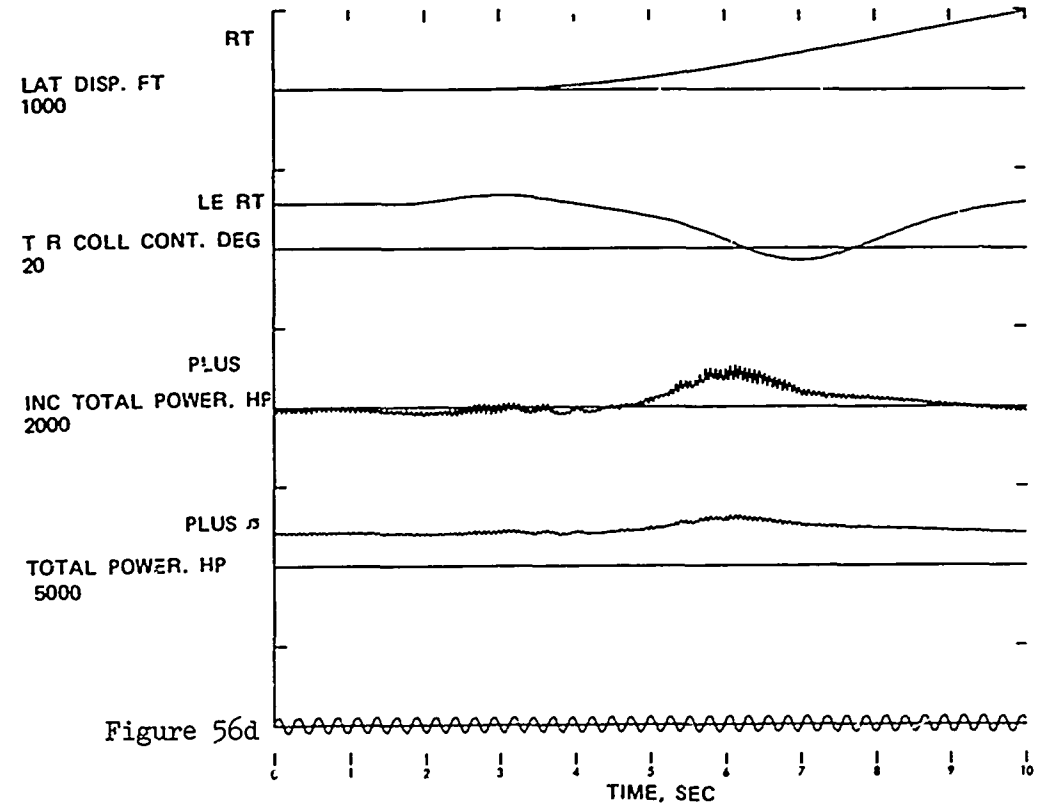

Figure 56d

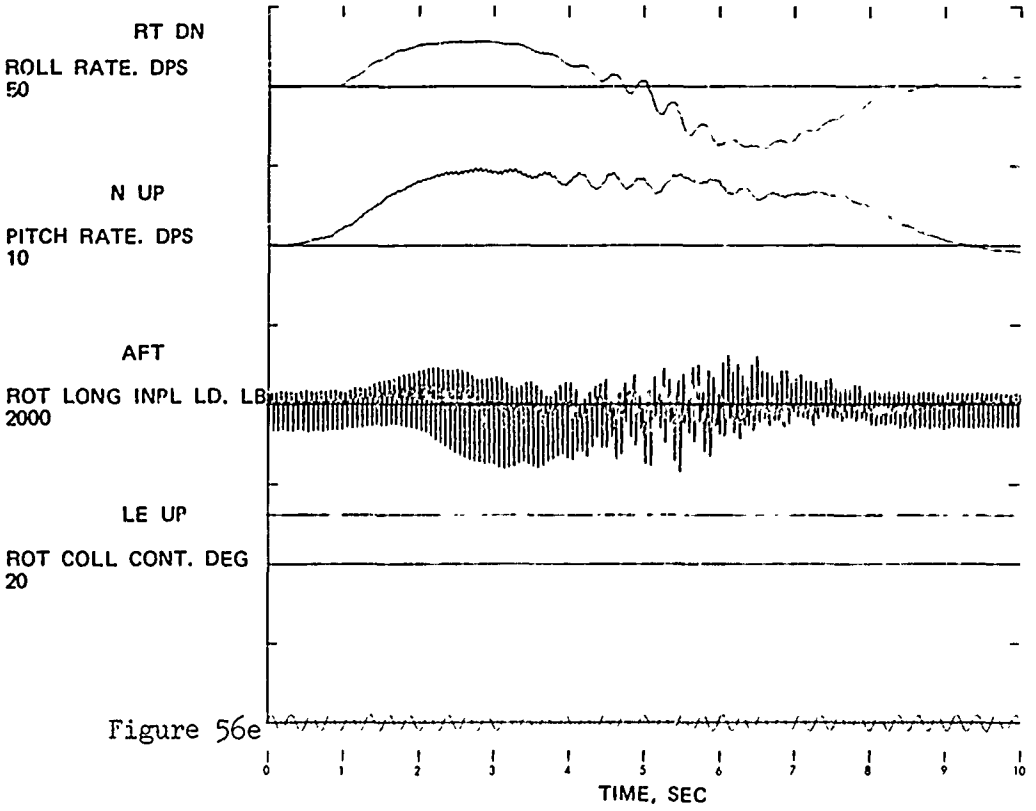

Figure 56e

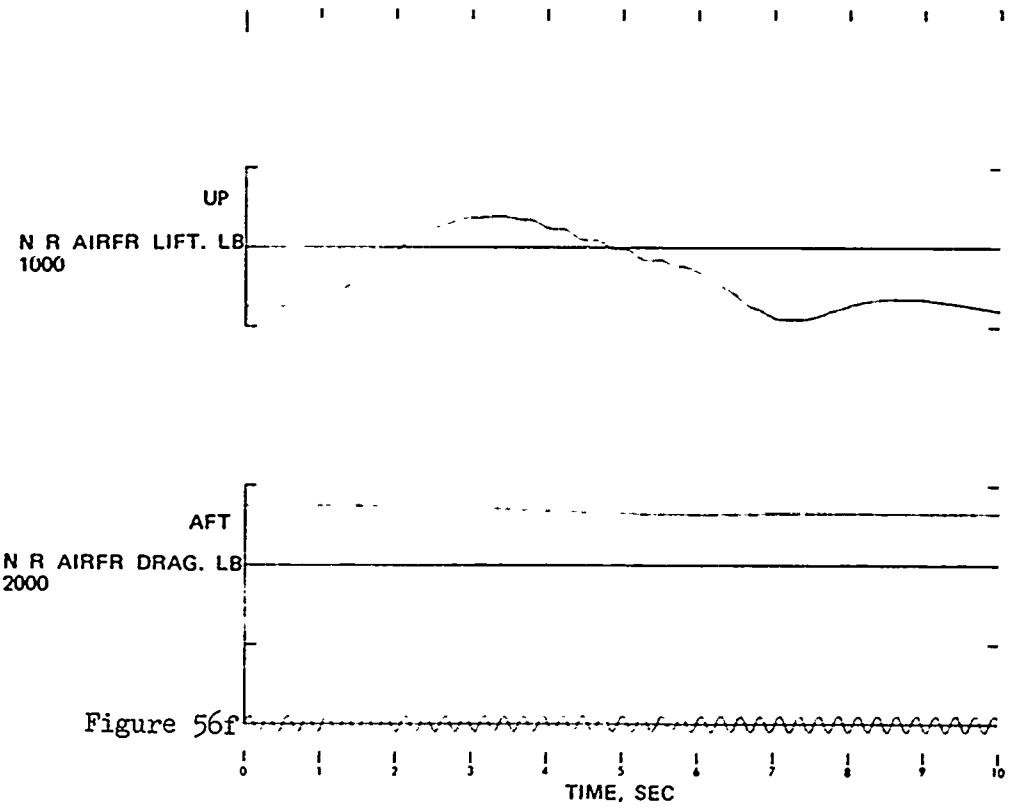

Figure 56f

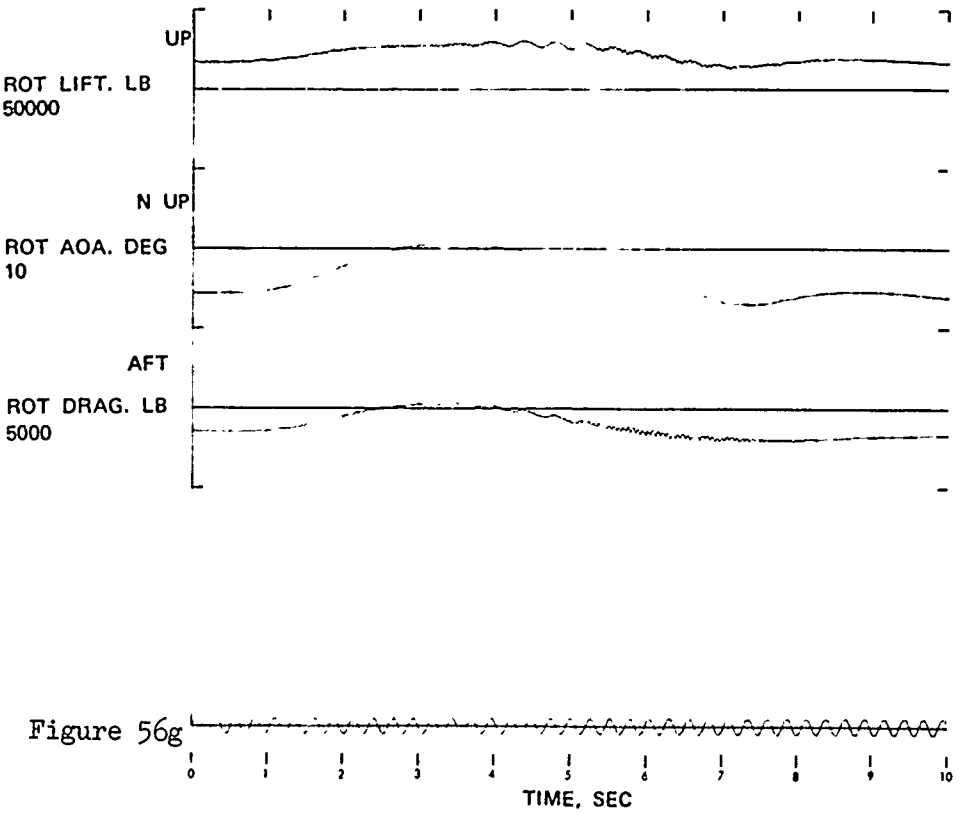

Figure 56g

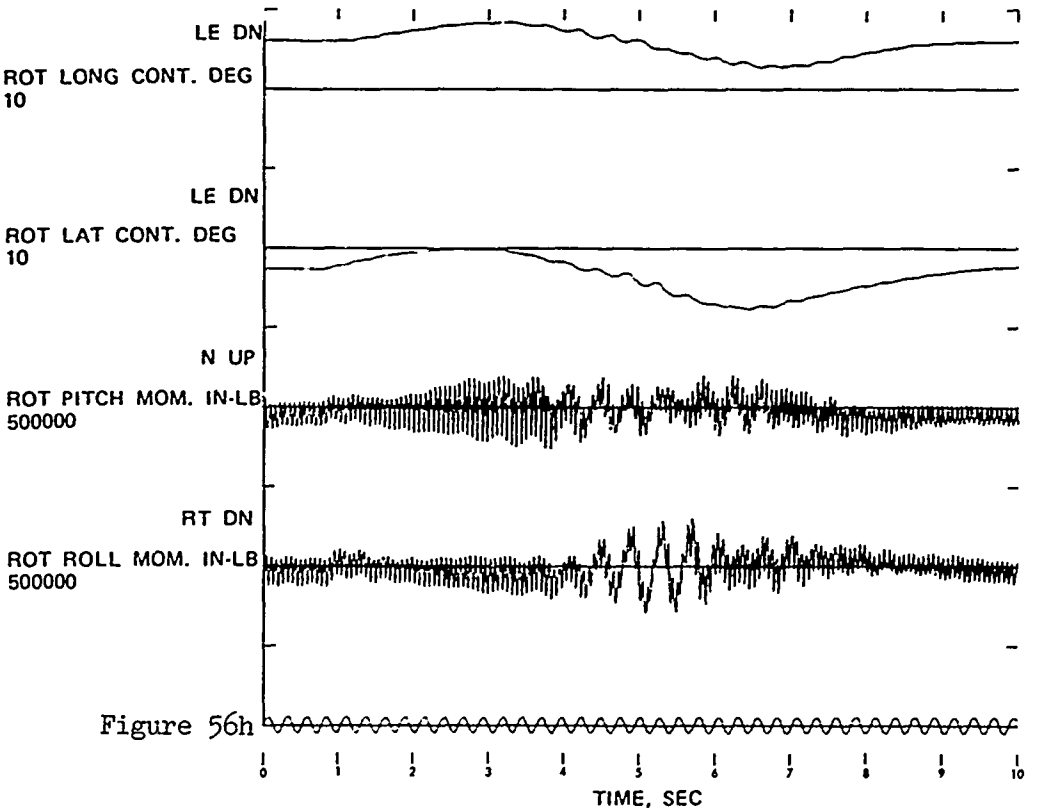

Figure 56h

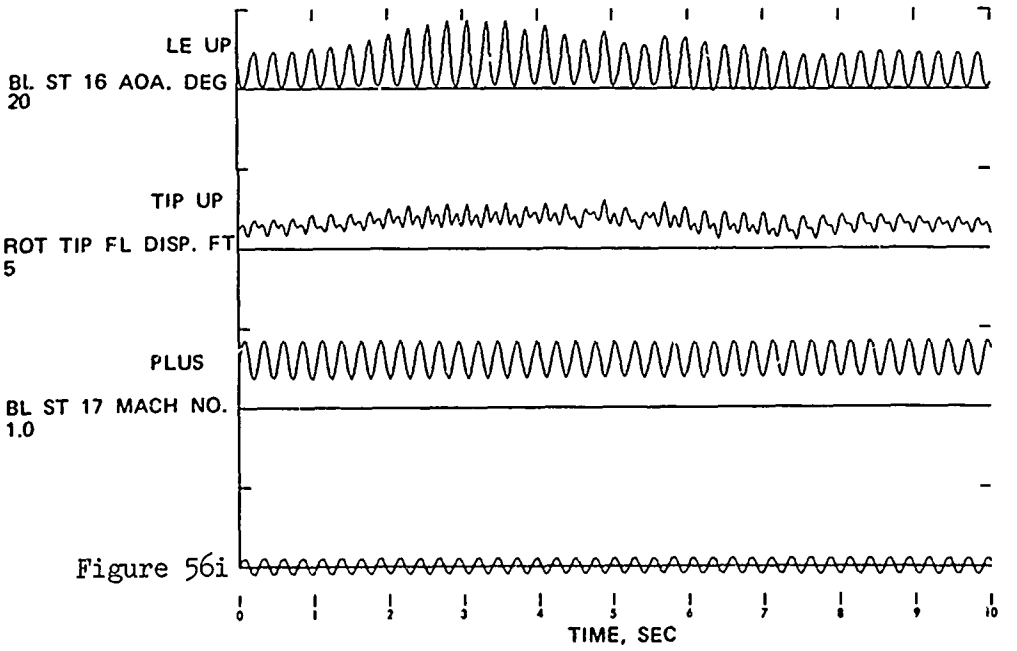

Figure 56i

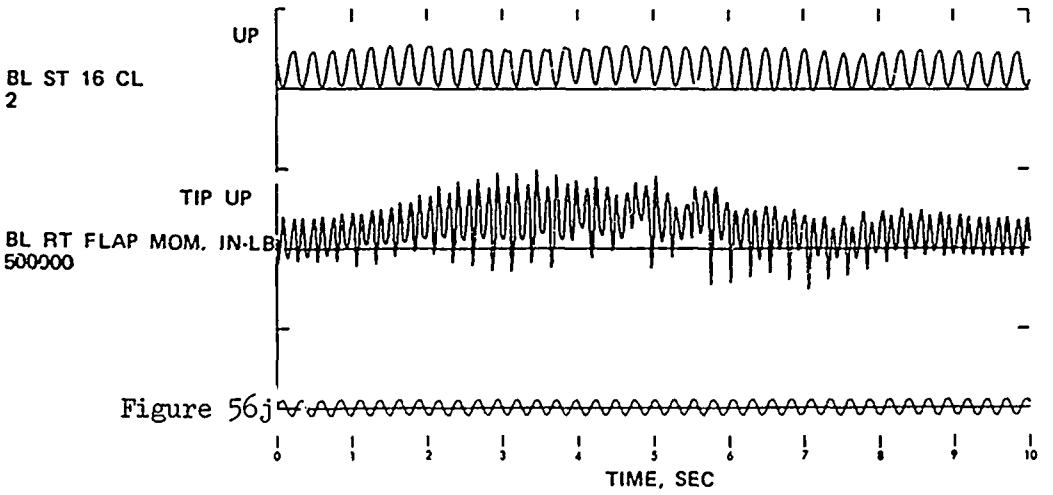

Figure 56j

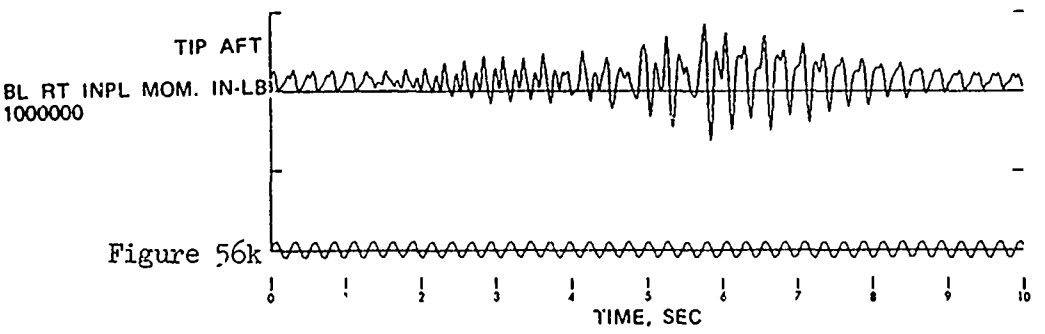

Figure 56k

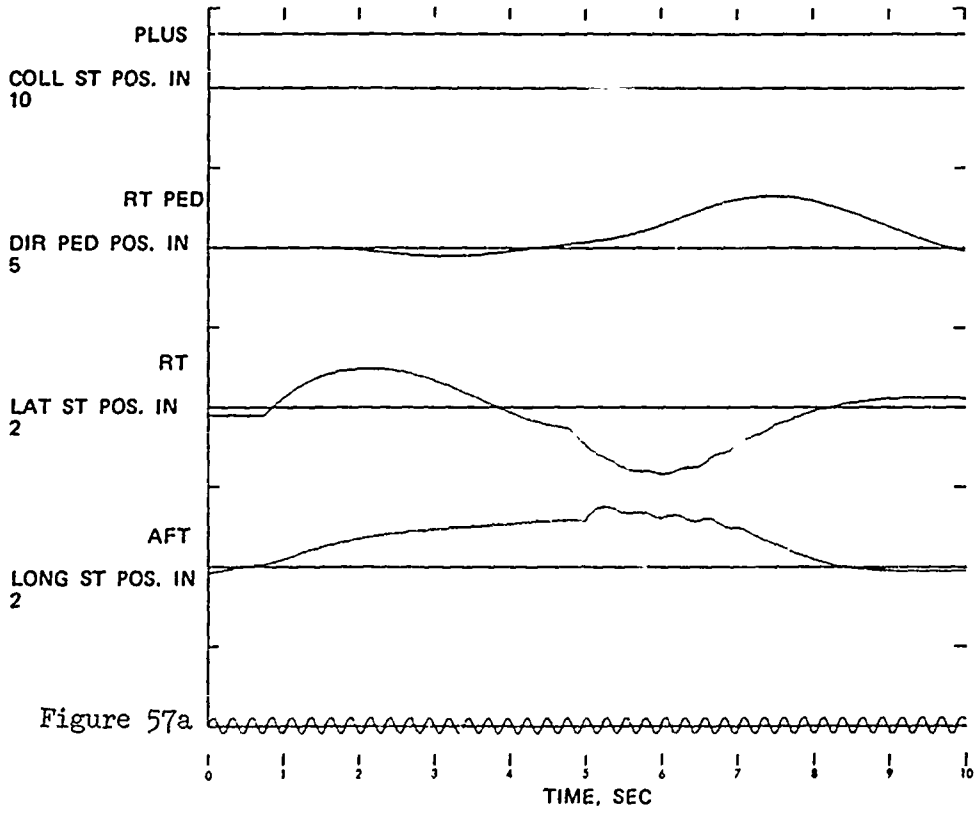

Figure 57a

Figure 57. Time Histories Showing the Effects of Coordinated Turn: Configuration 4; Maneuver Initiated at 140 KTAS.

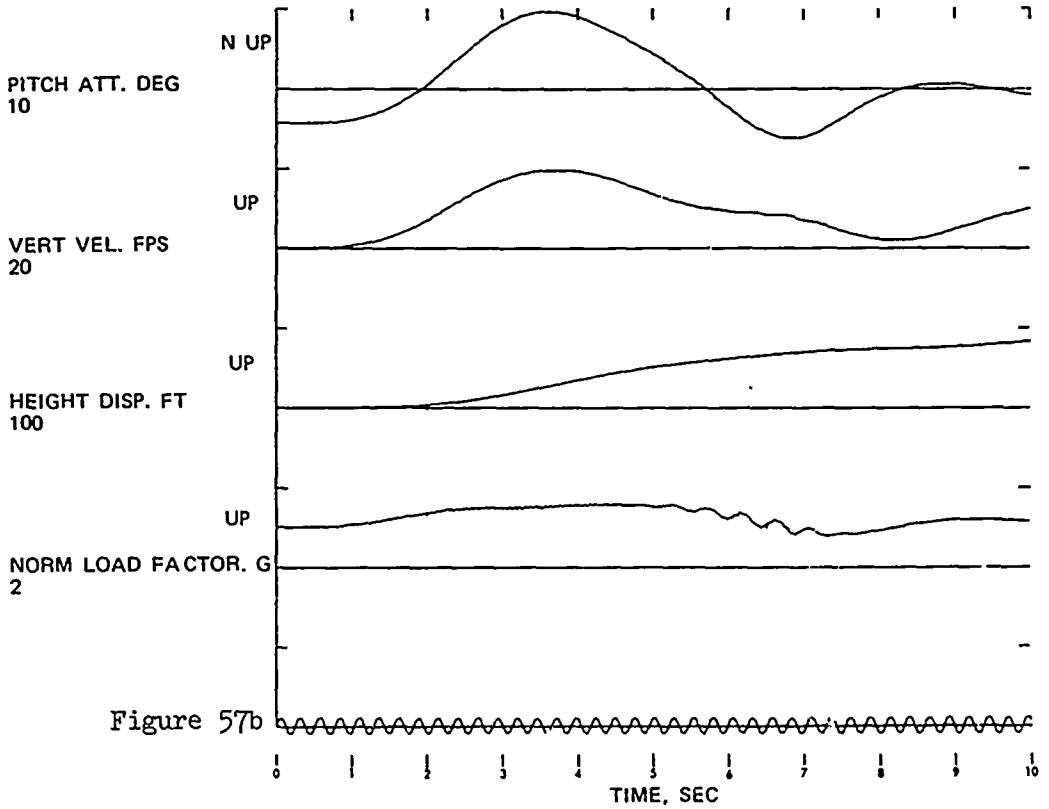

Figure 57b

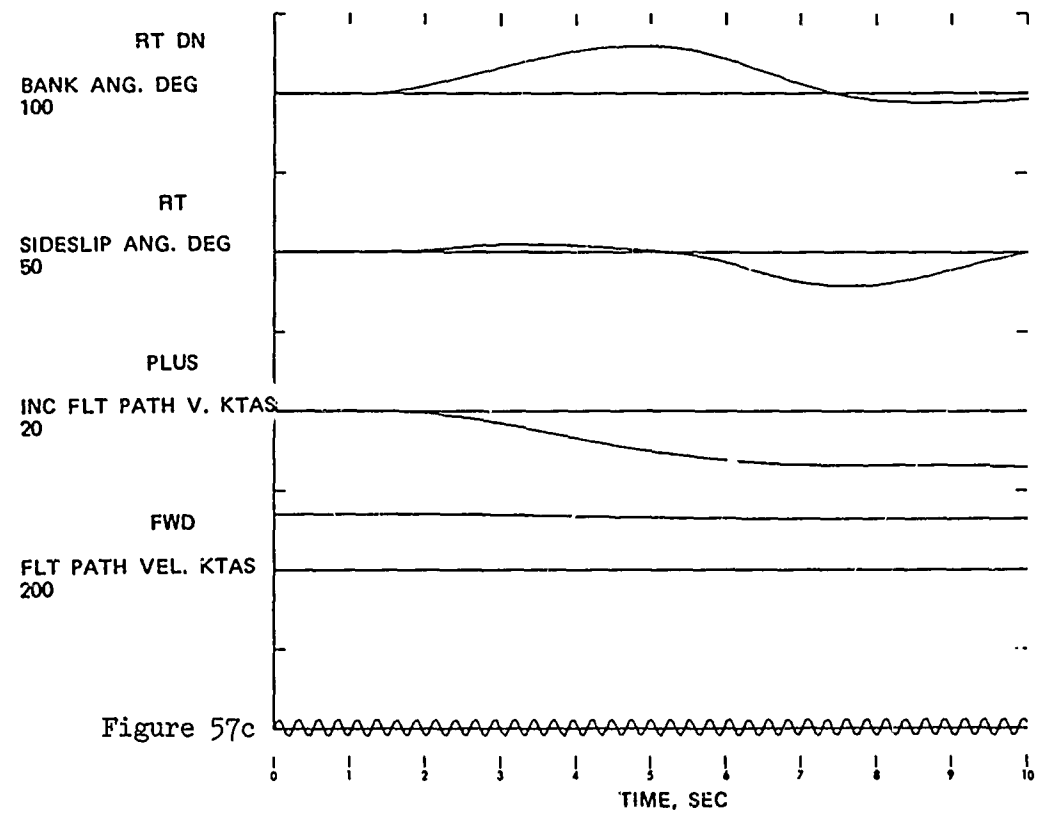

Figure 57c

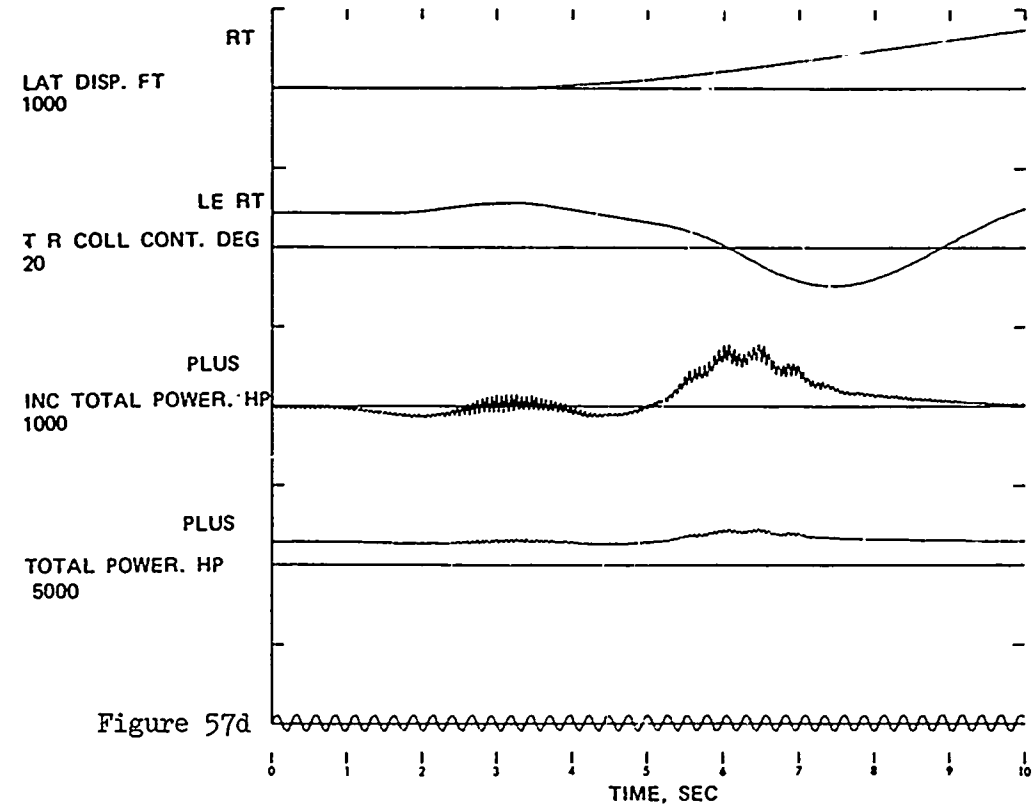

Figure 57d

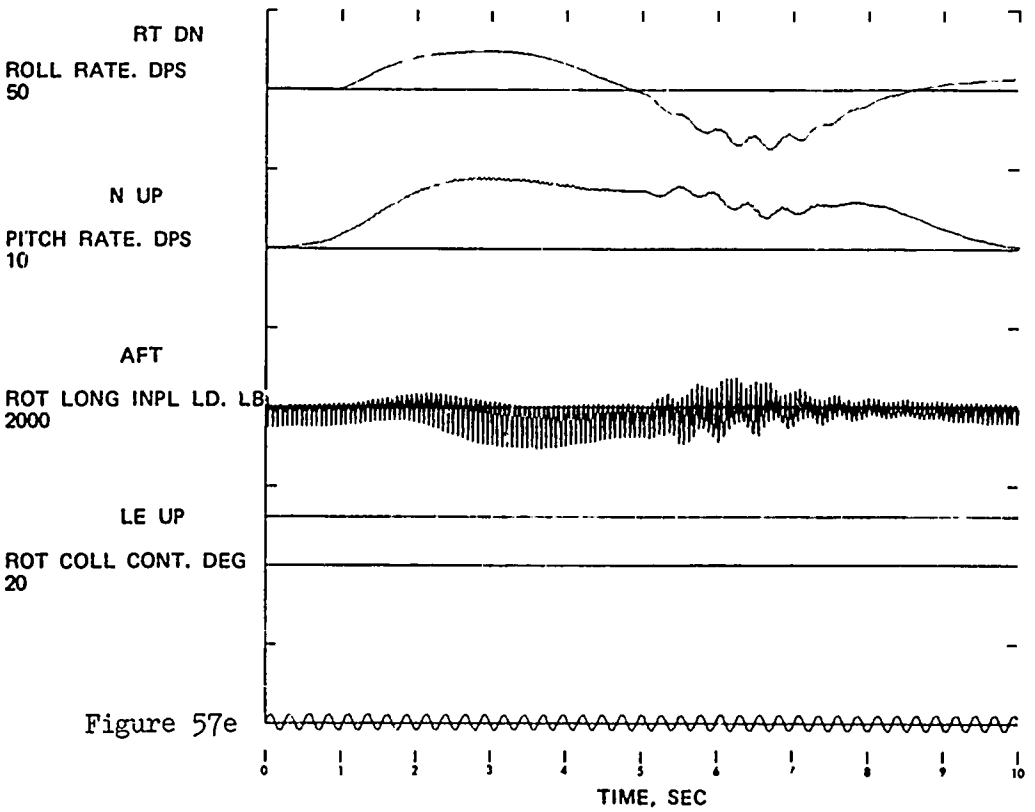

Figure 57e

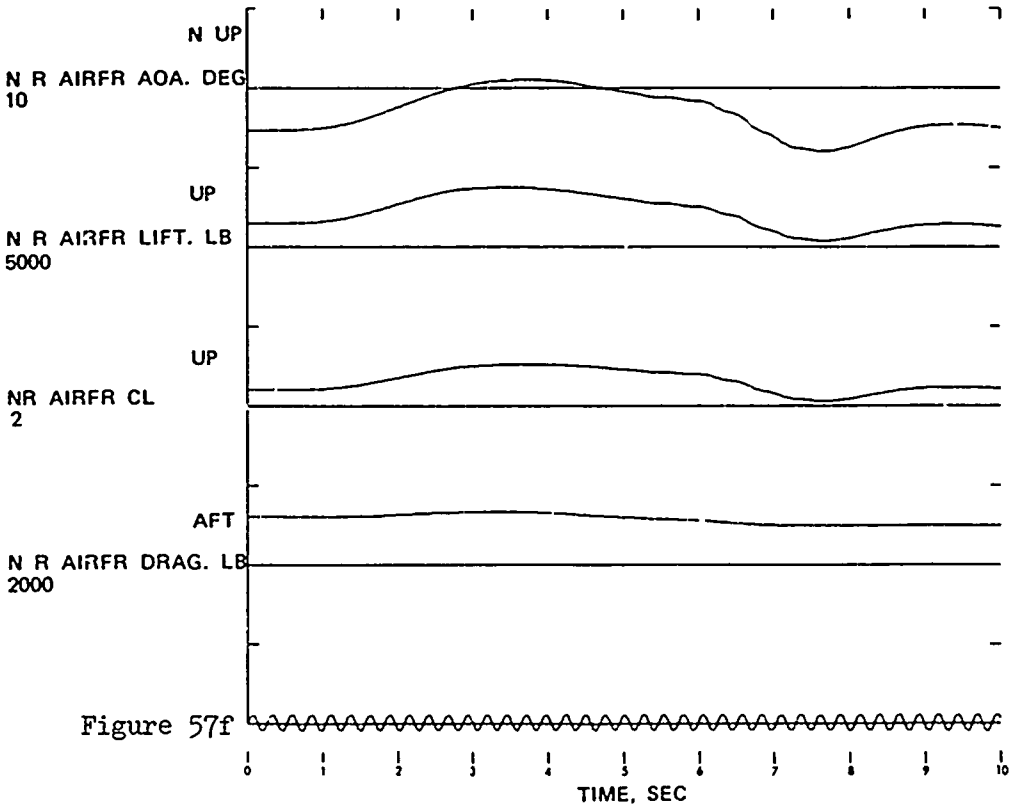

Figure 57f

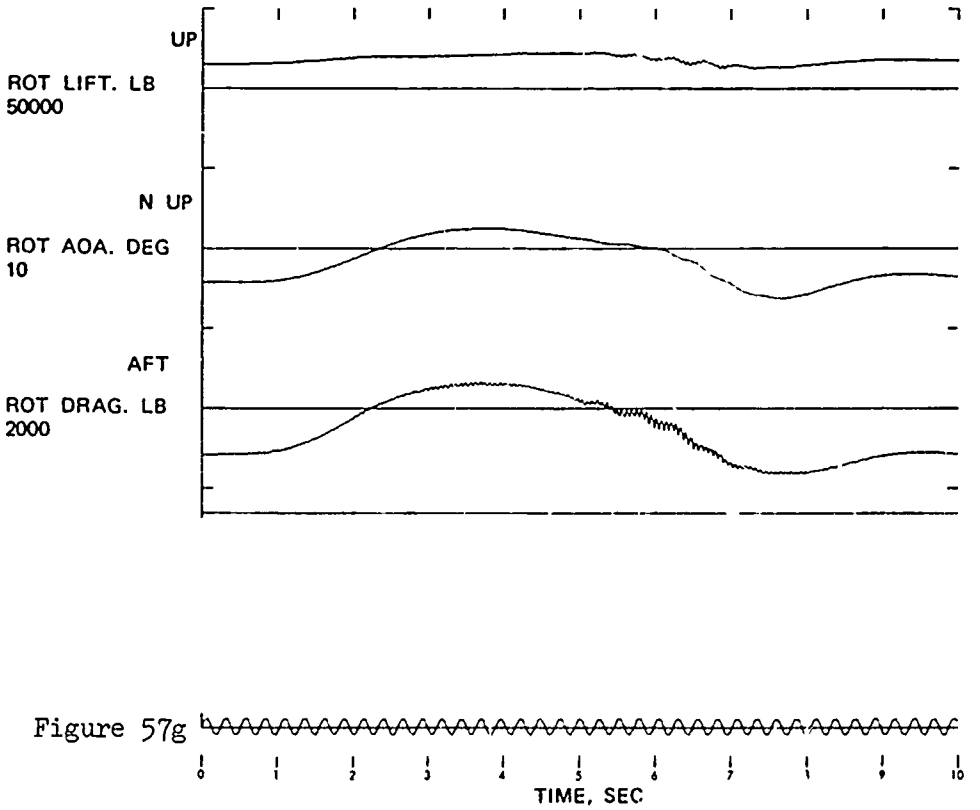

Figure 57g

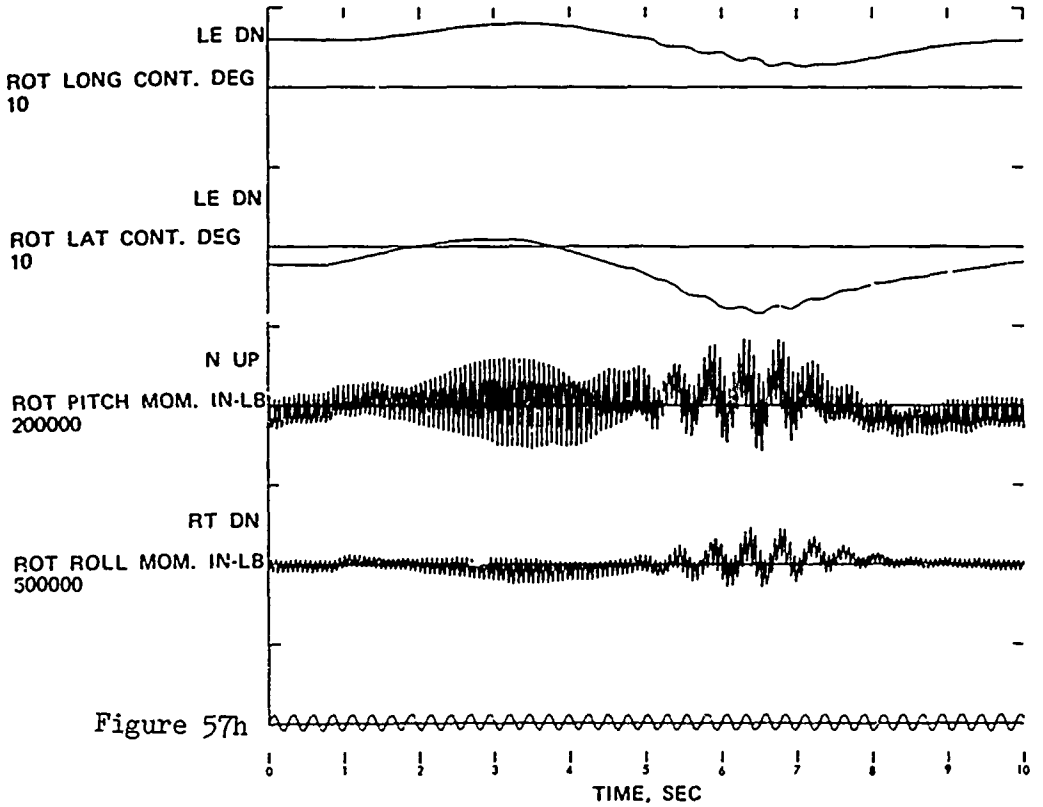

Figure 57h

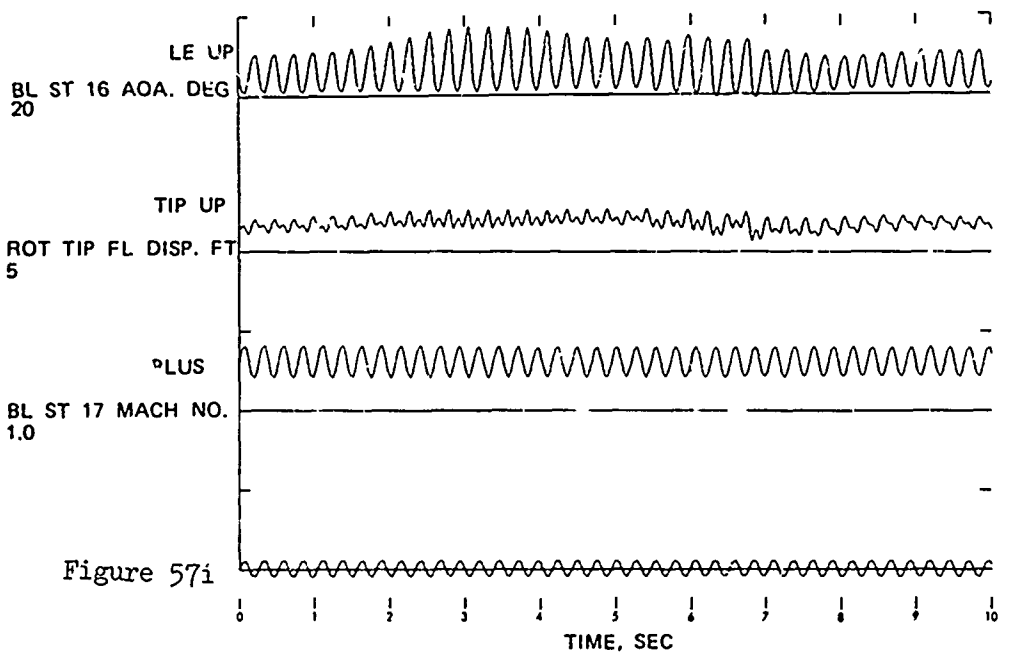

Figure 57i

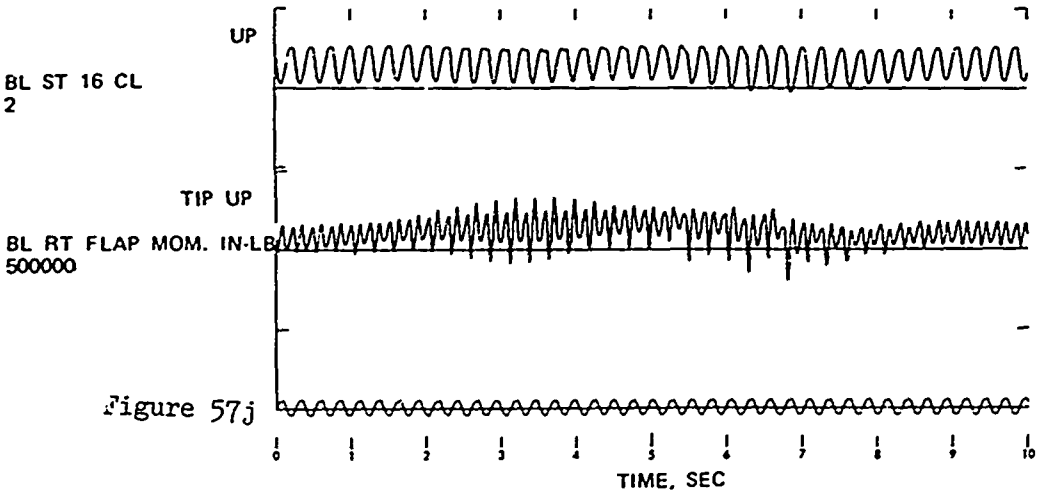

Figure 57j

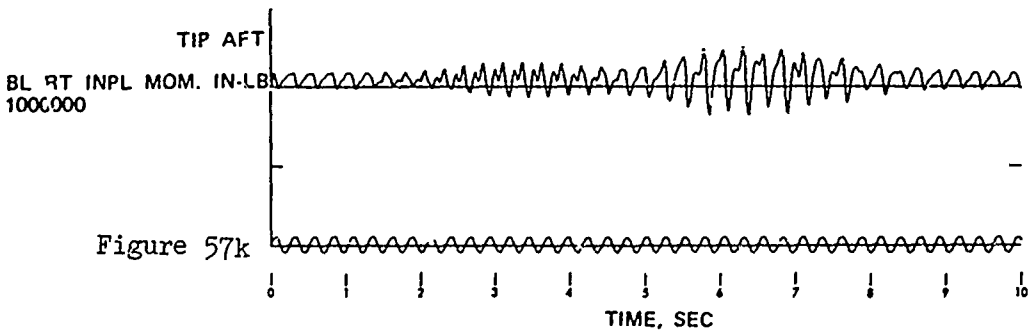

Figure 57k

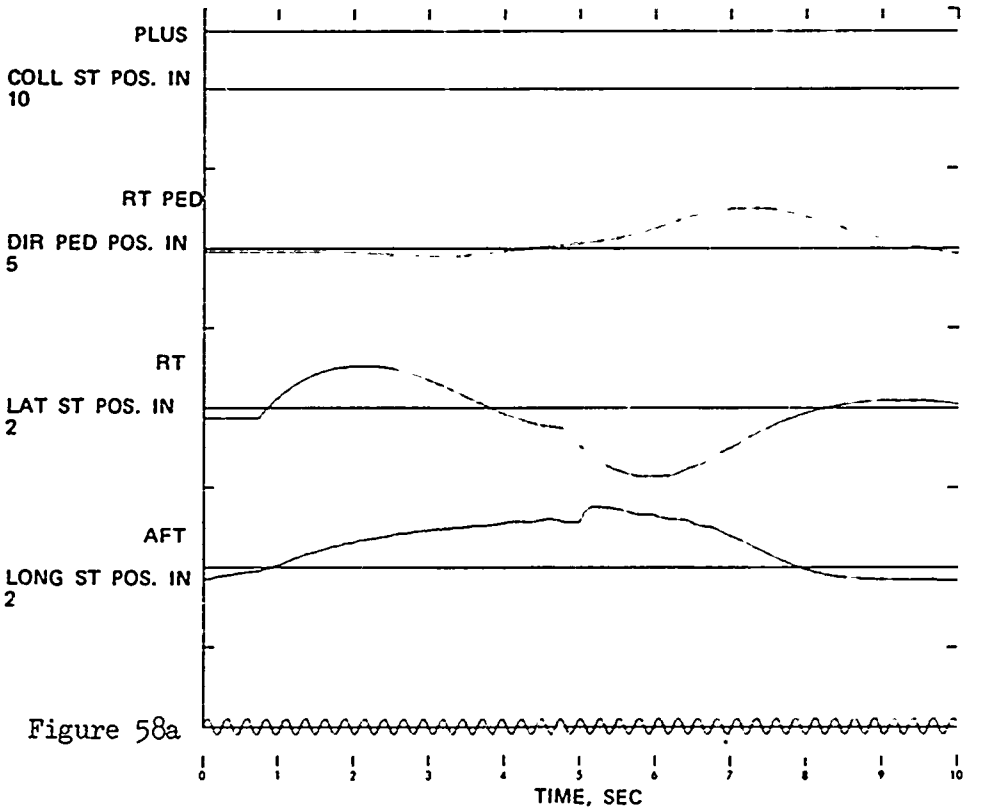

Figure 58a

Figure 58 . Time Histories Showing the Effects of Coordinated Turn: Configuration 5; Maneuver Initiated at 1.5 KTAS.

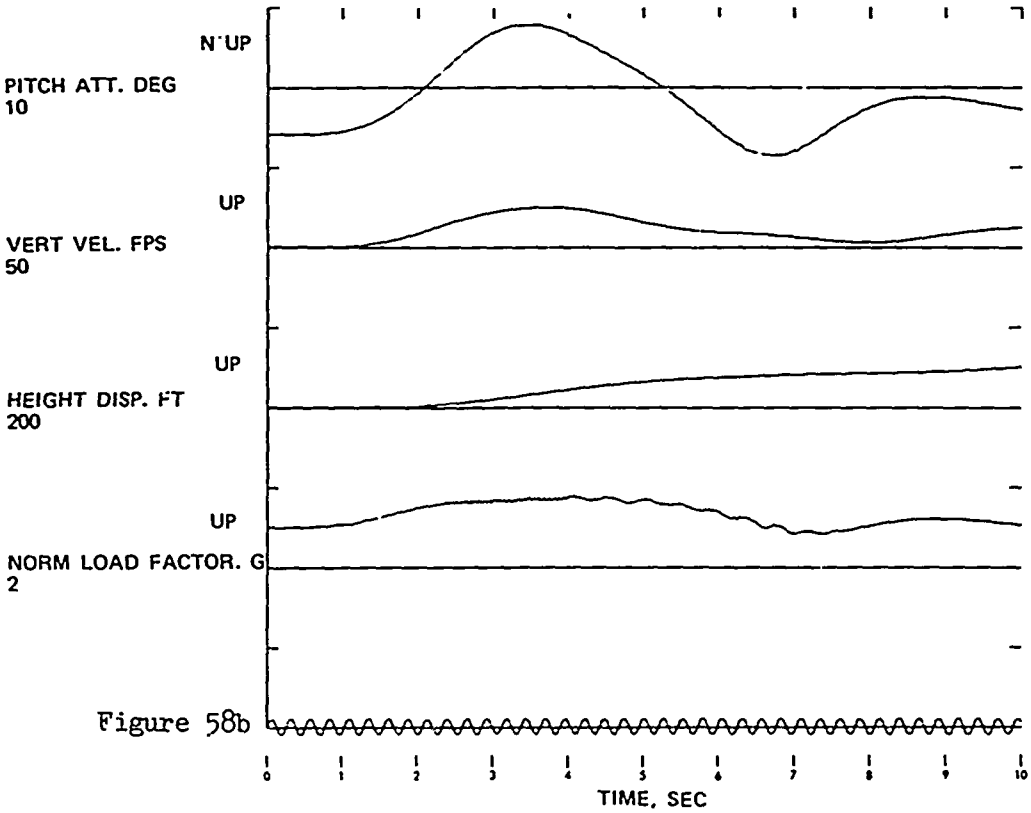

Figure 58b

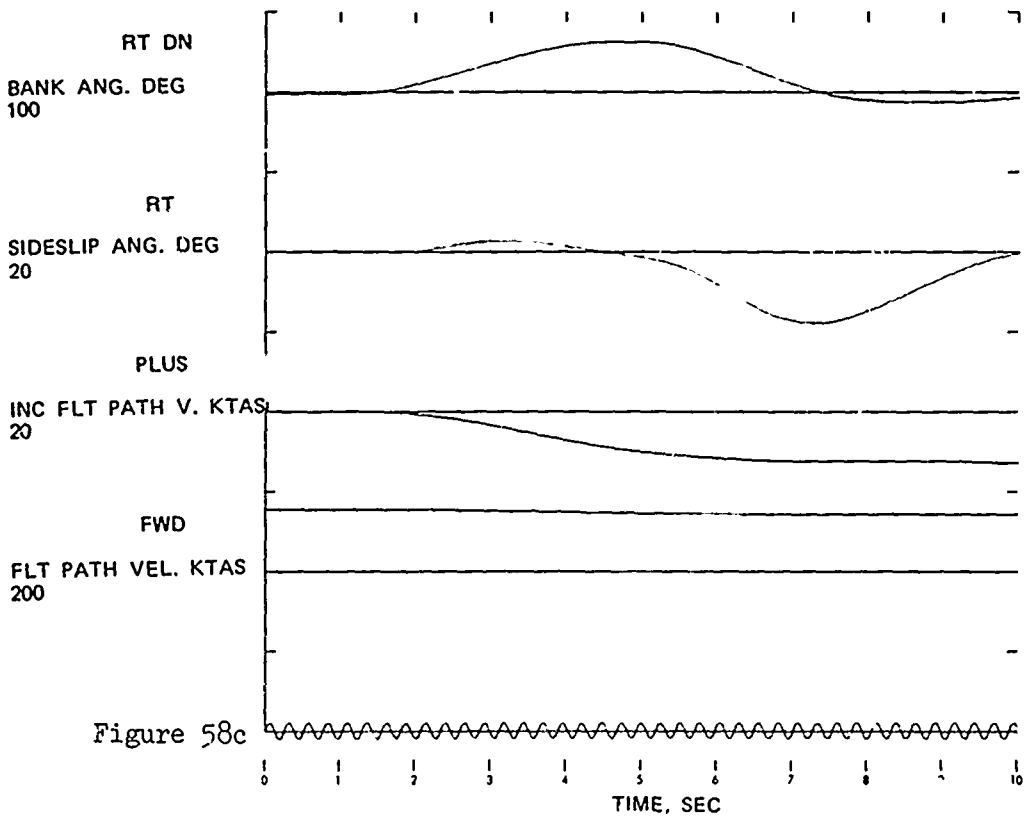

Figure 58c

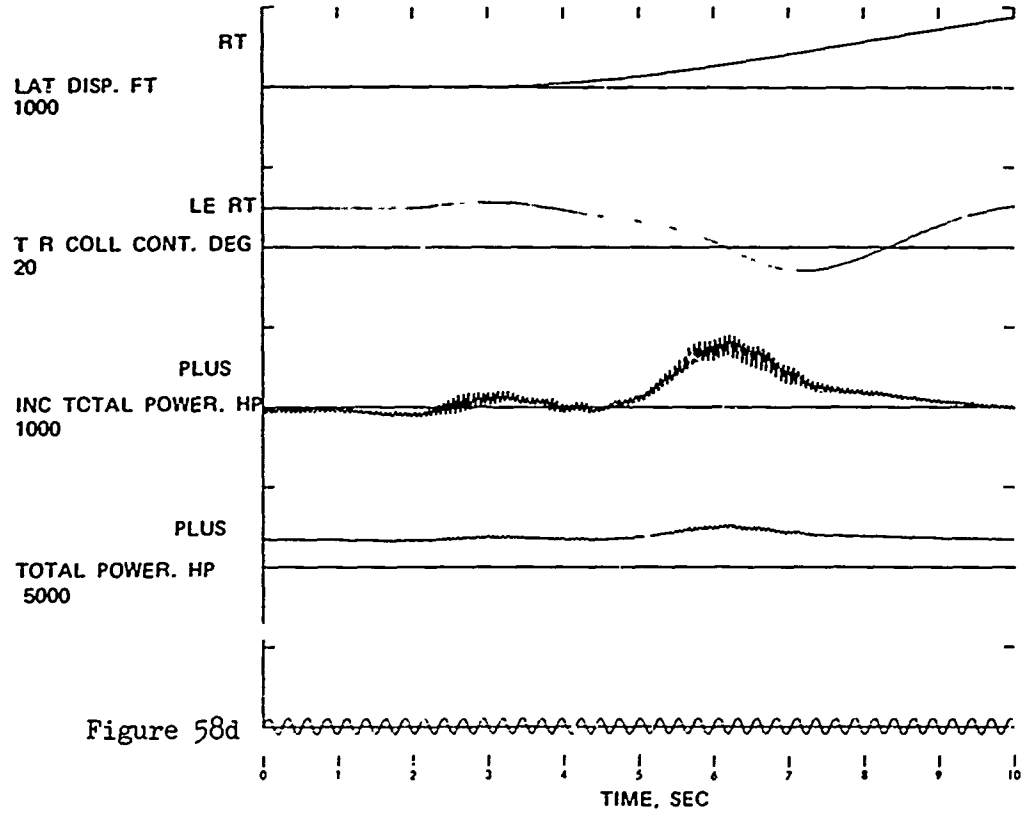

Figure 58d

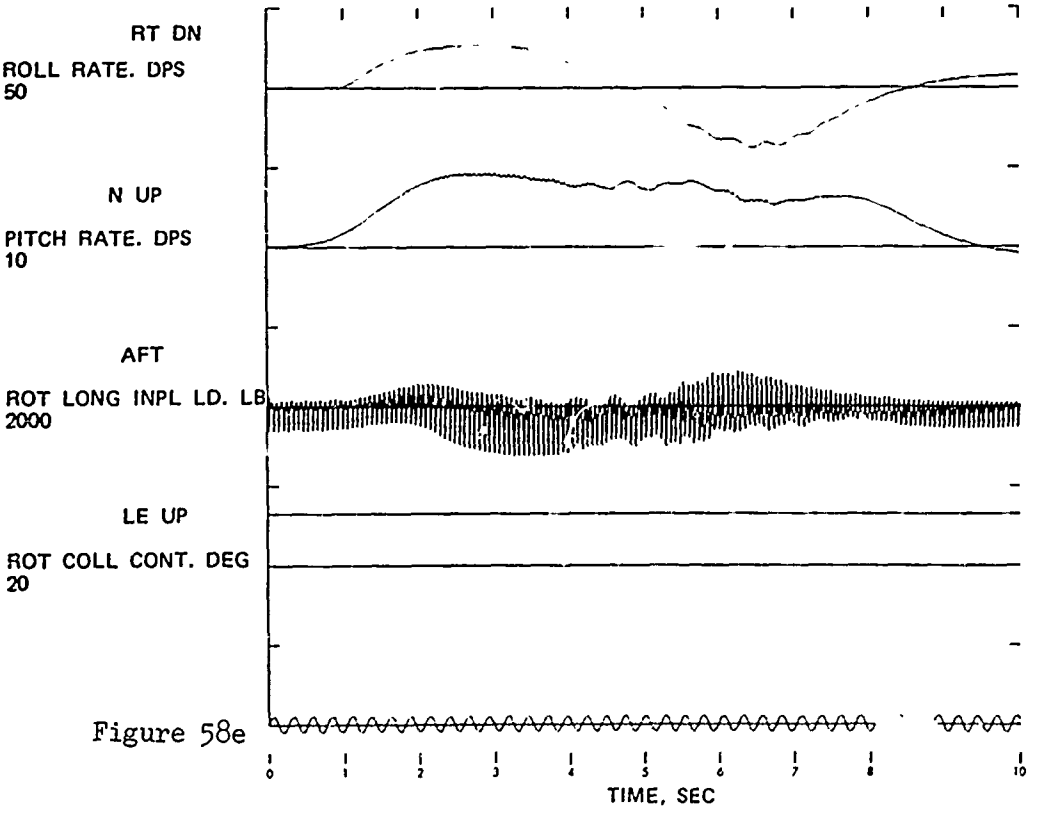

Figure 58e

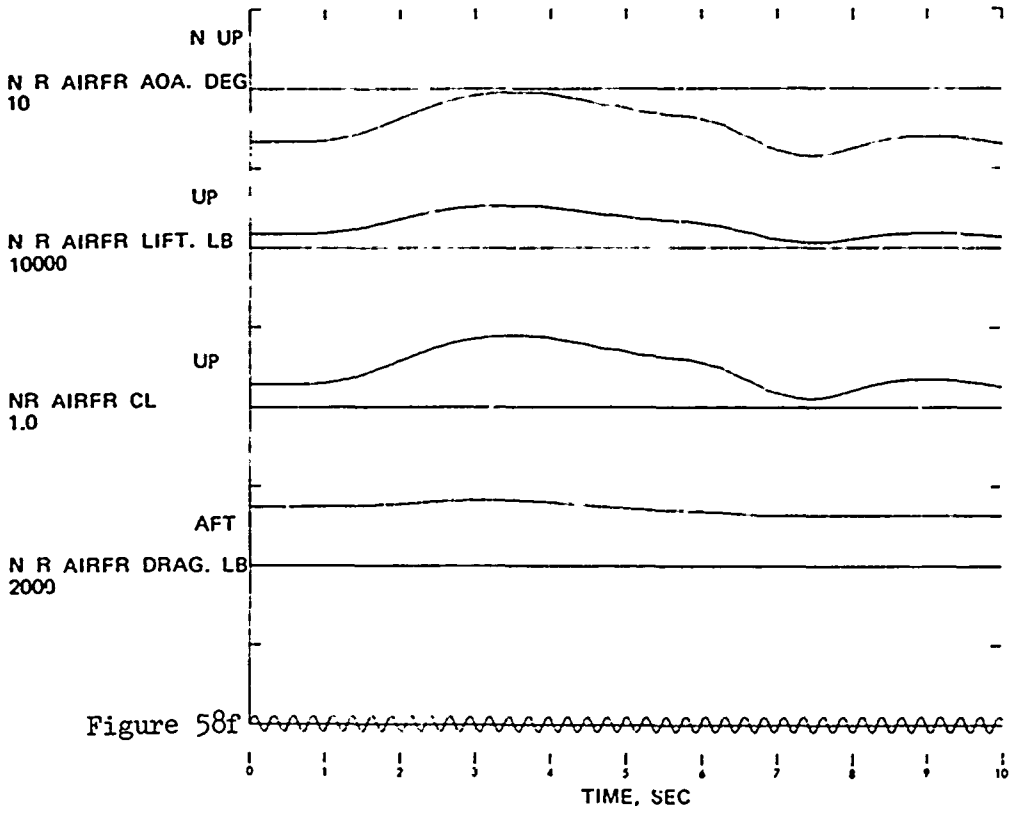

Figure 58f

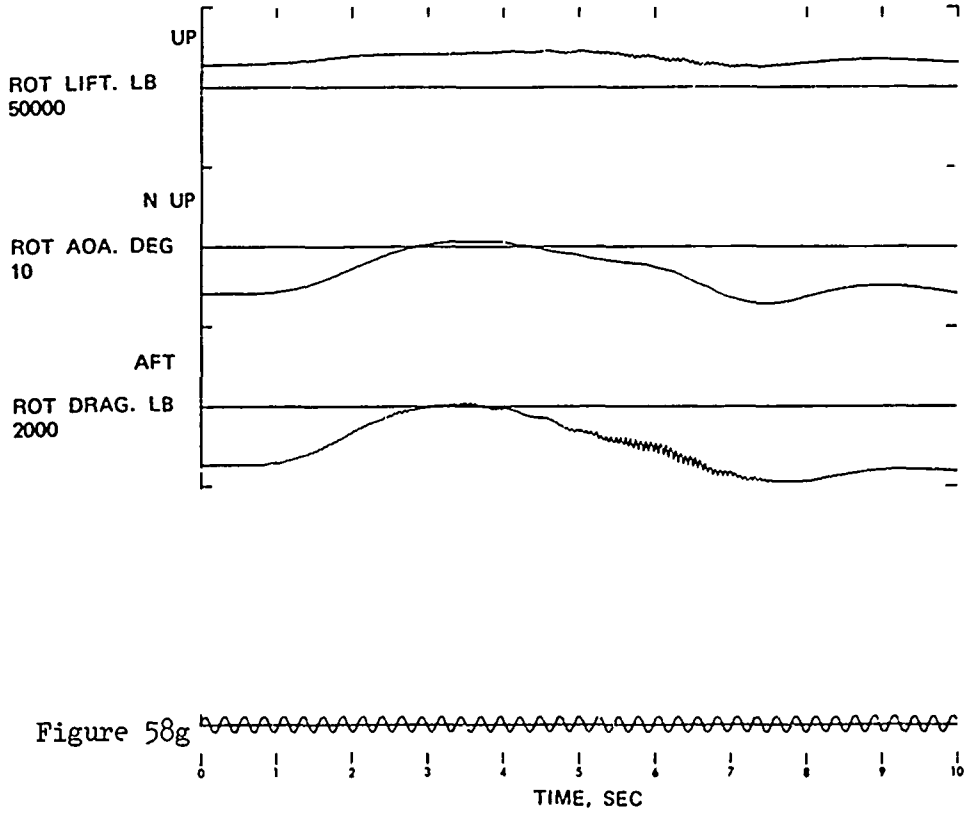

Figure 58g

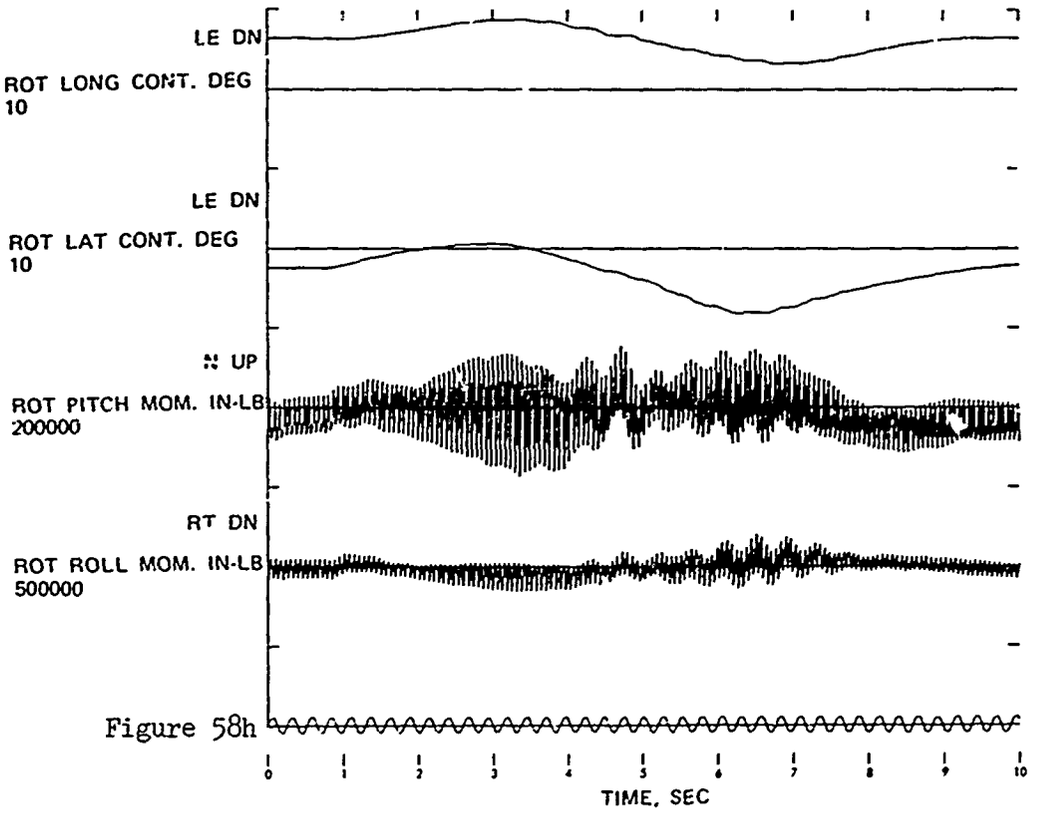

Figure 58h

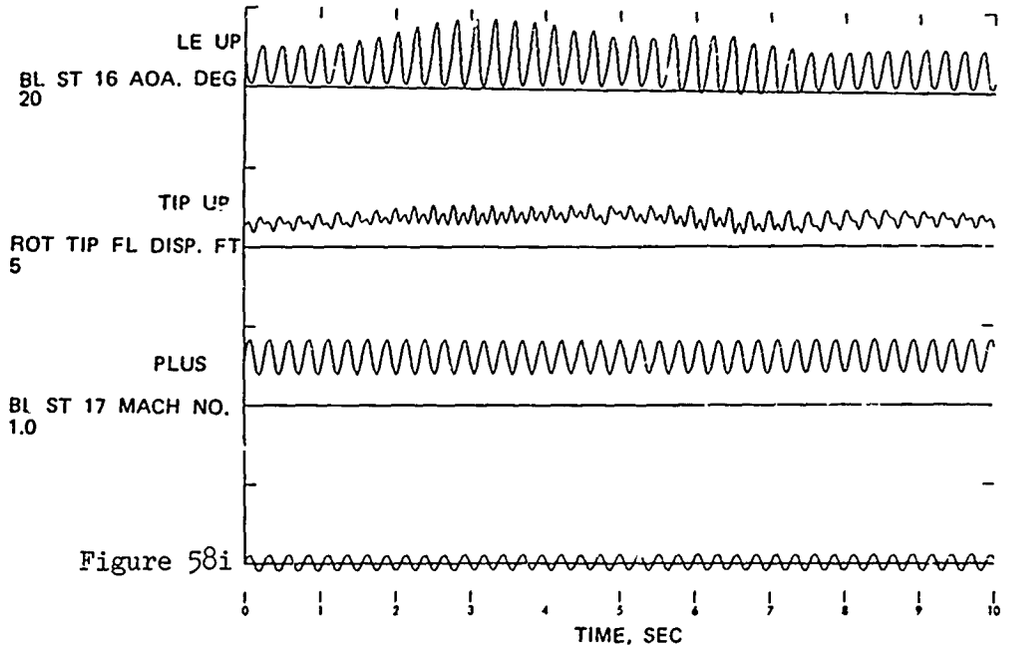

Figure 58i

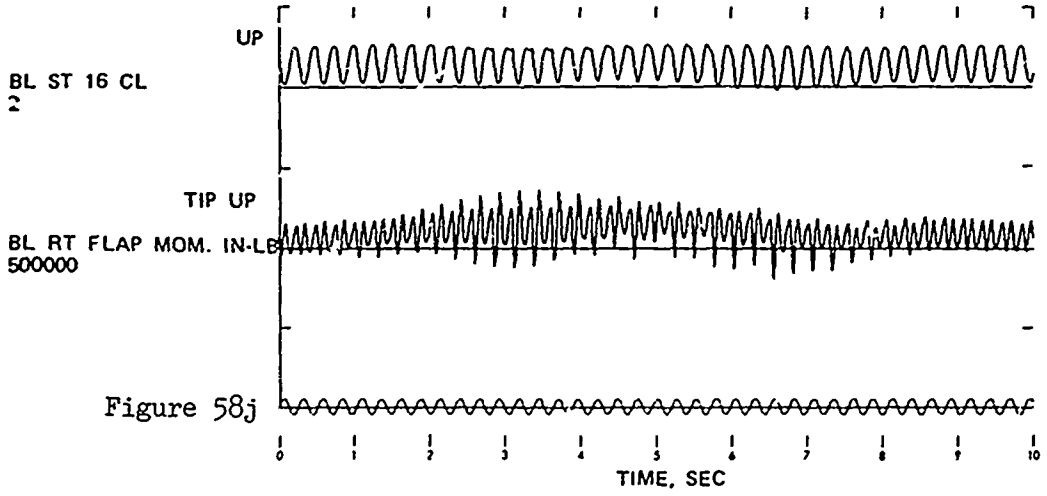

Figure 58j

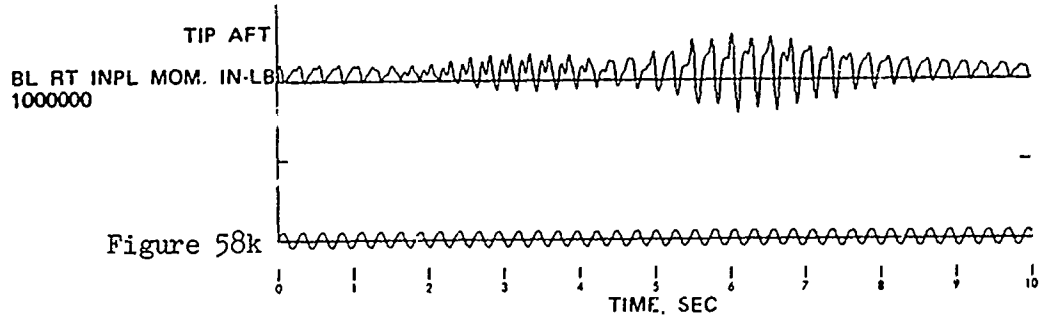

Figure 58k

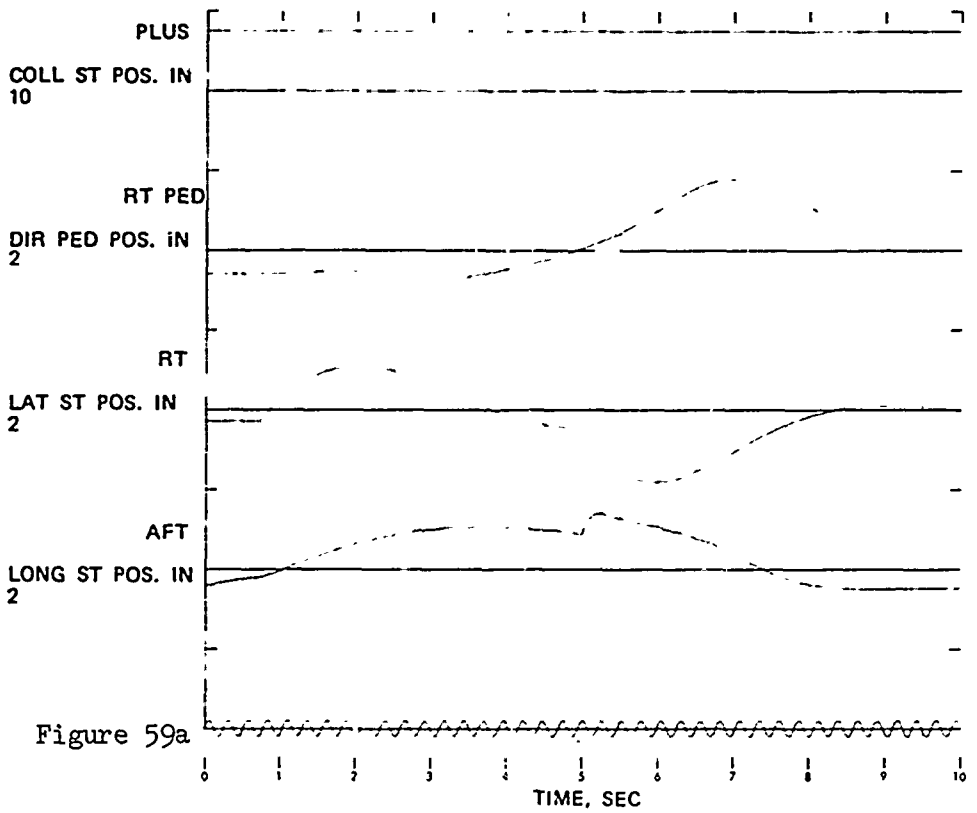

Figure 59a

Figure 59 . Time Histories Showing the Effects of Coordinated Turn: Configuration 6; Maneuver Initiated at 167 KTAS.

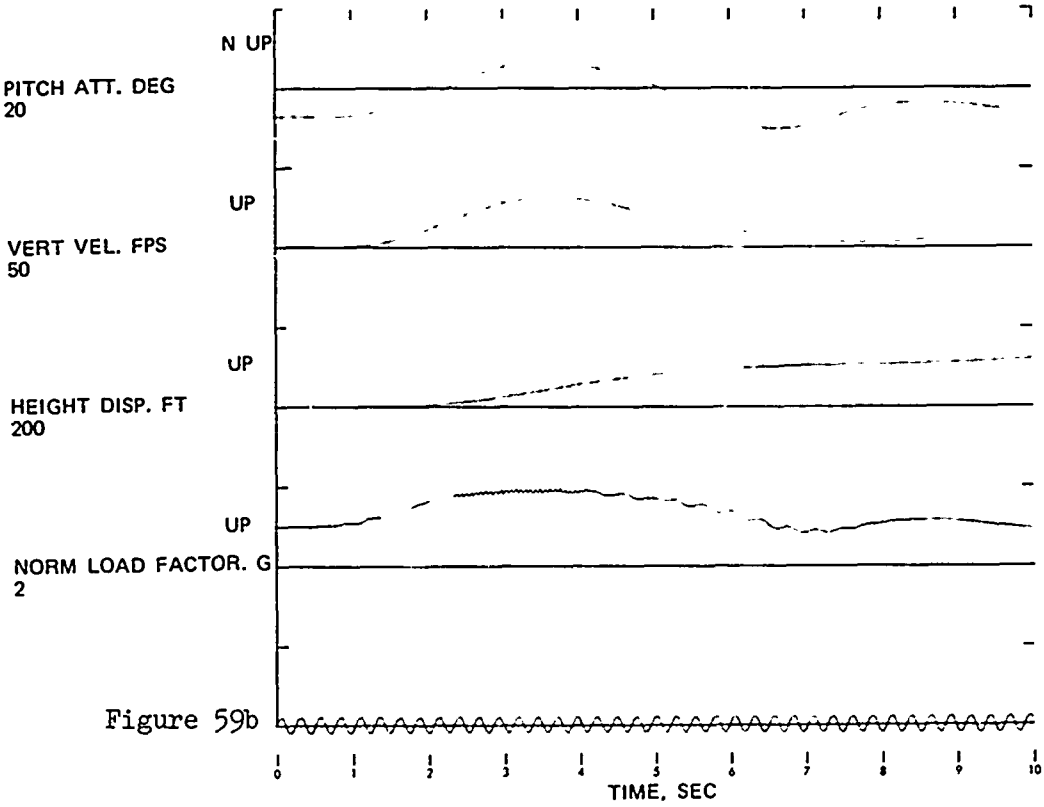

Figure 59b

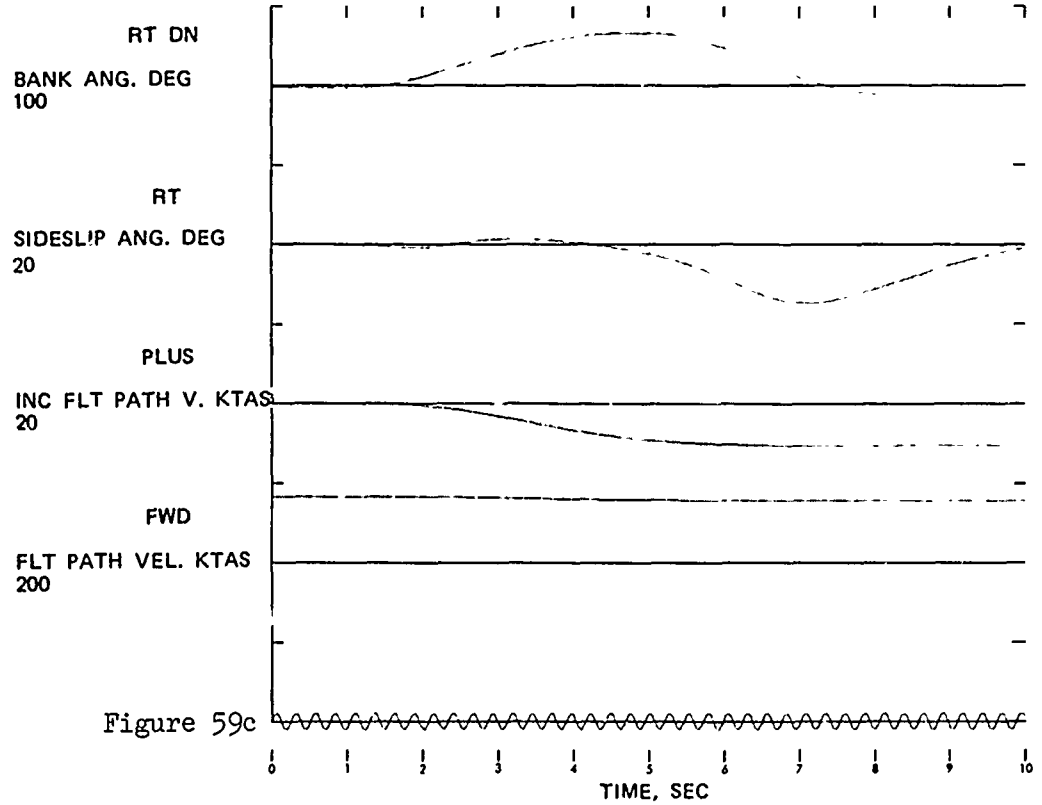

Figure 59c

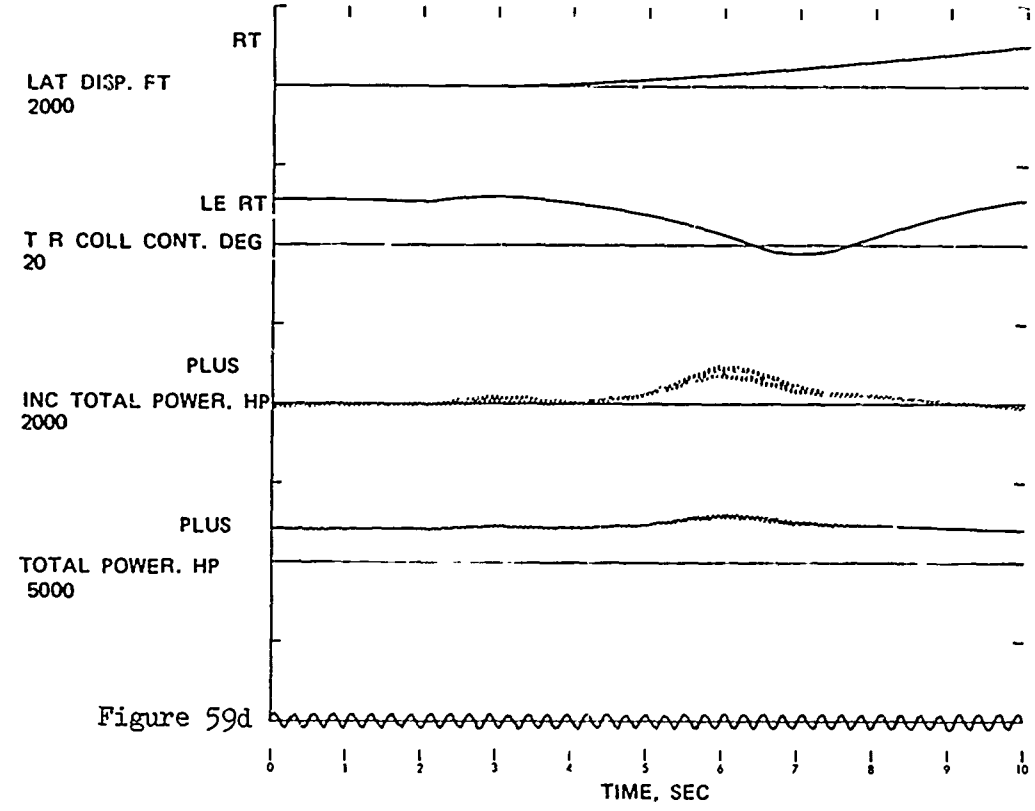

Figure 59d

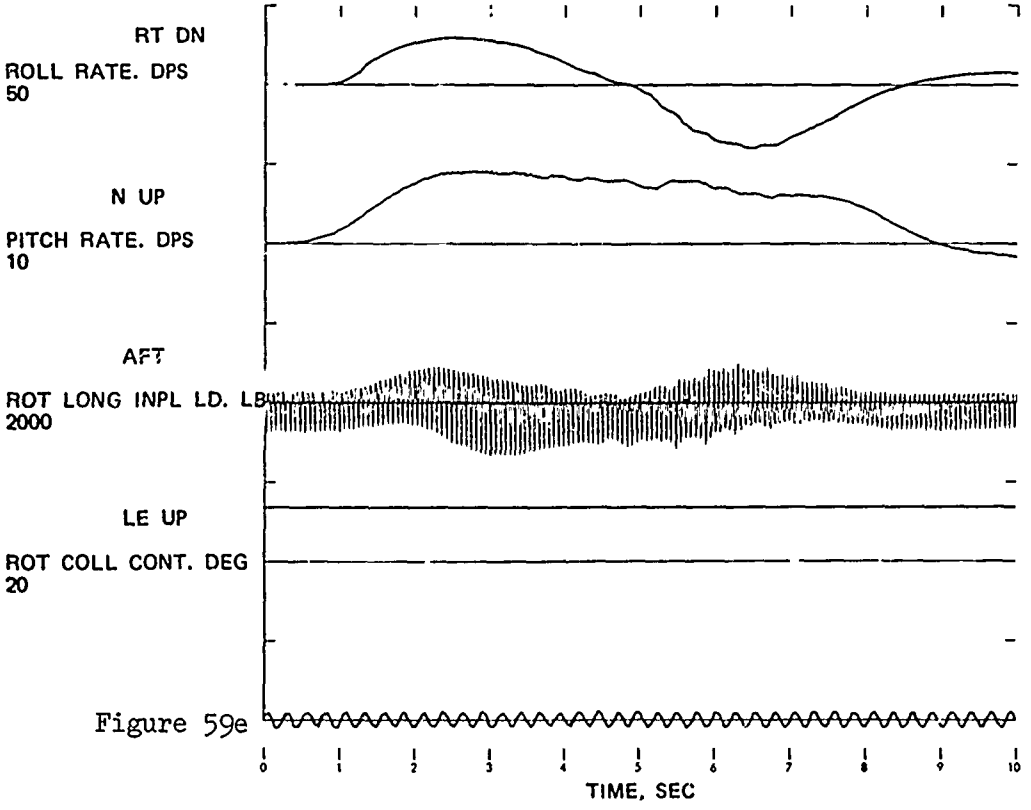

Figure 59e

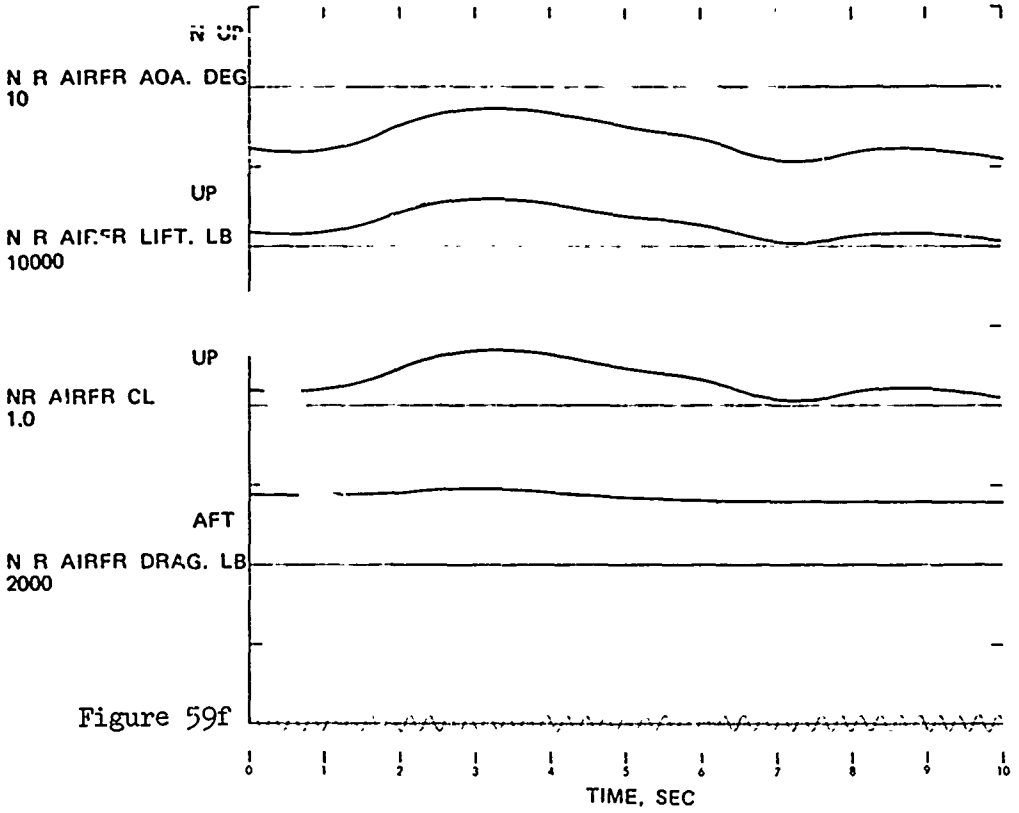

Figure 59f

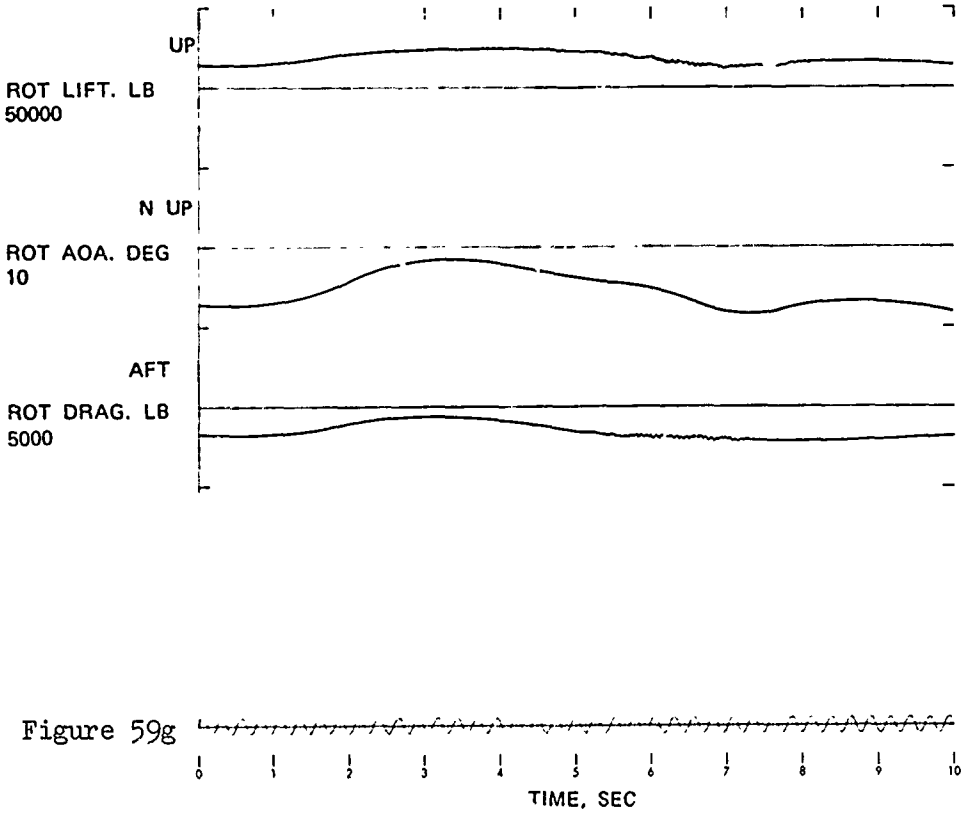

Figure 59g

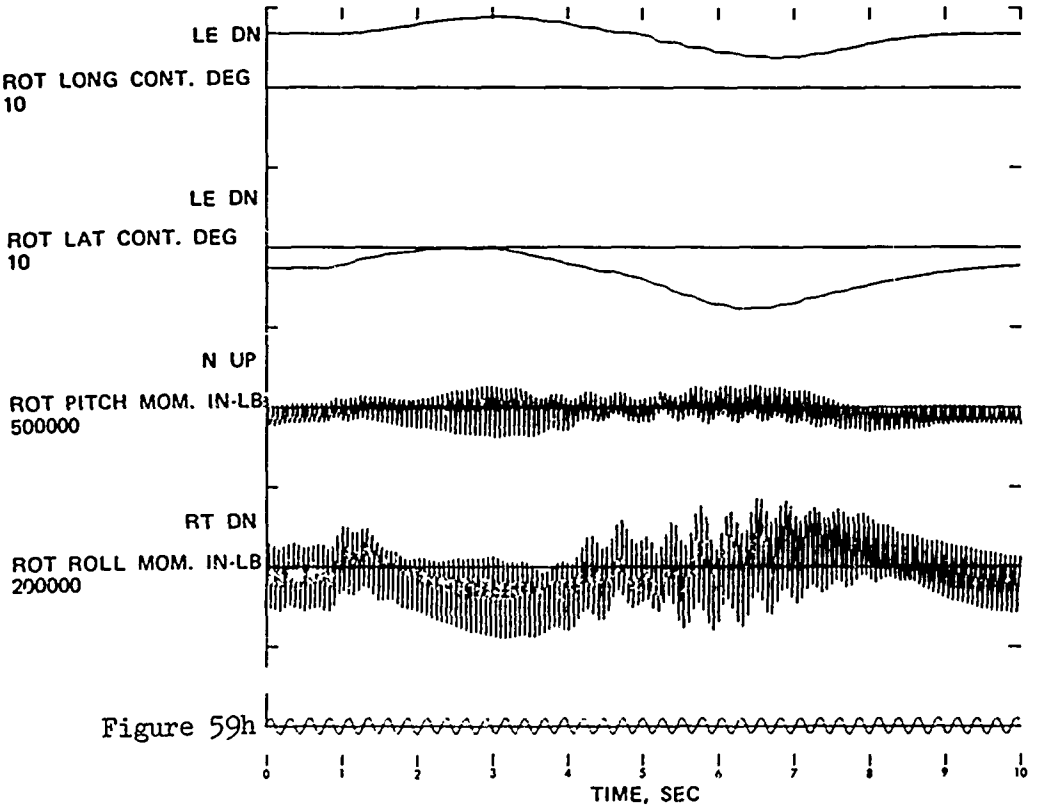

Figure 59h

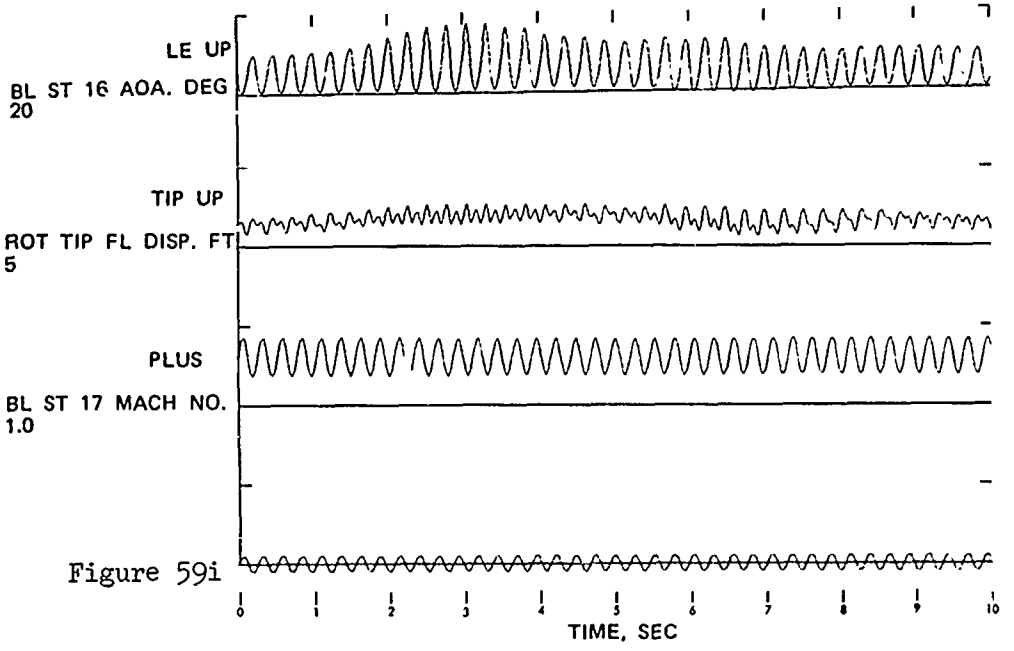

Figure 59i

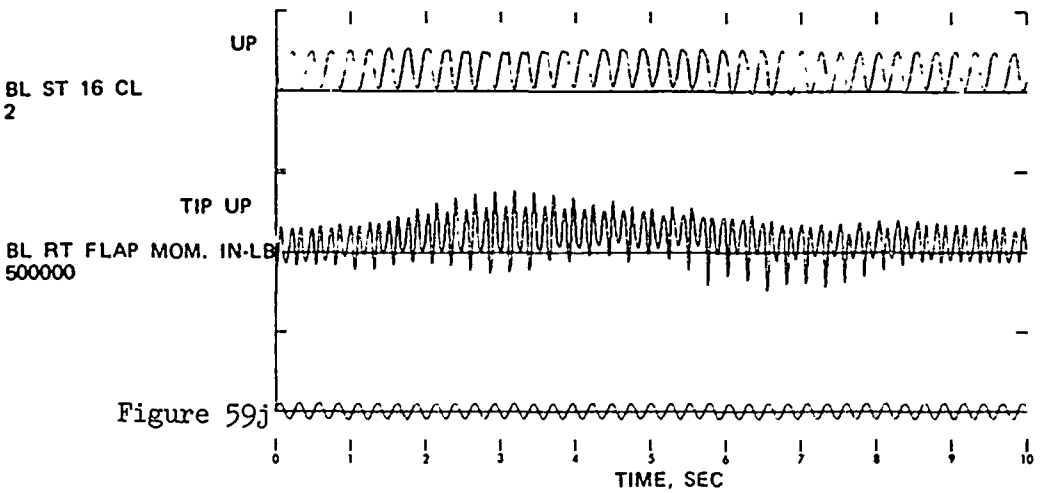

Figure 59j

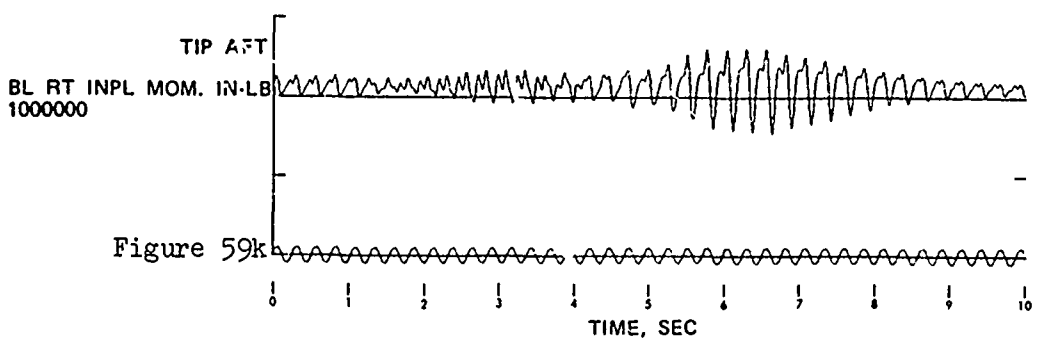

Figure 59k

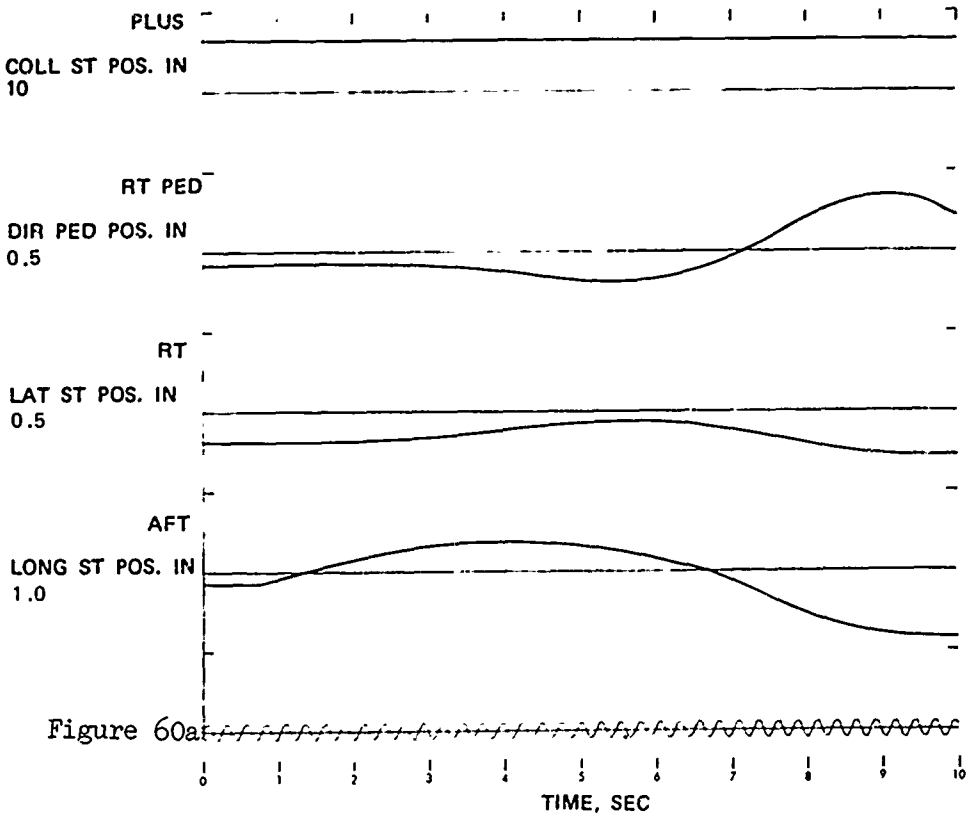

Figure 60a

Figure 60 . Time Histories Showing the Effects of Symmetrical Pull-up and Push-over: Configuration 1; Maneuver Initiated at 140 KTAS; Height Increase .

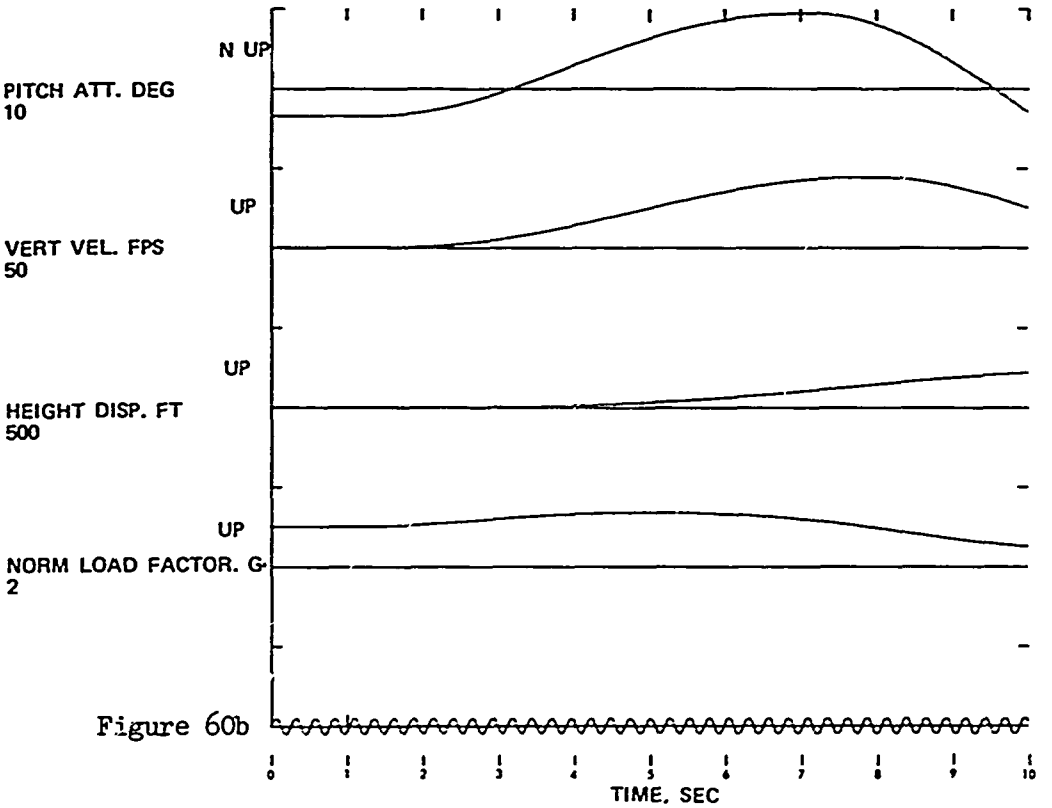

Figure 60b

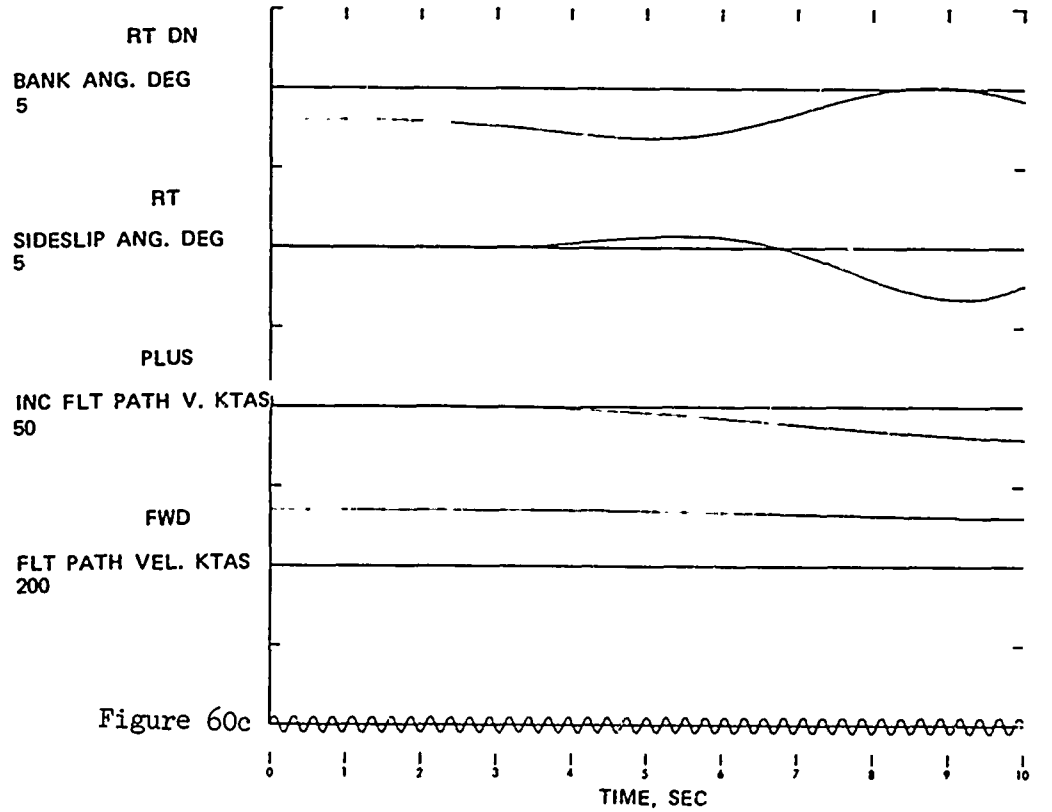

Figure 60c

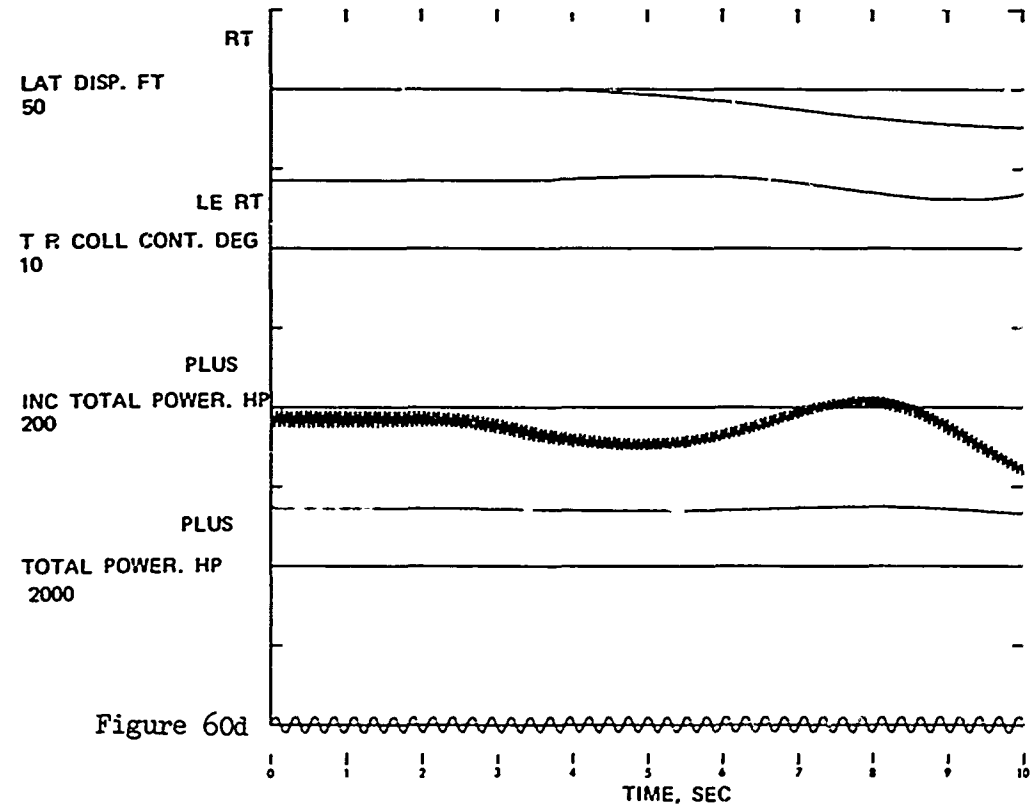

Figure 60d

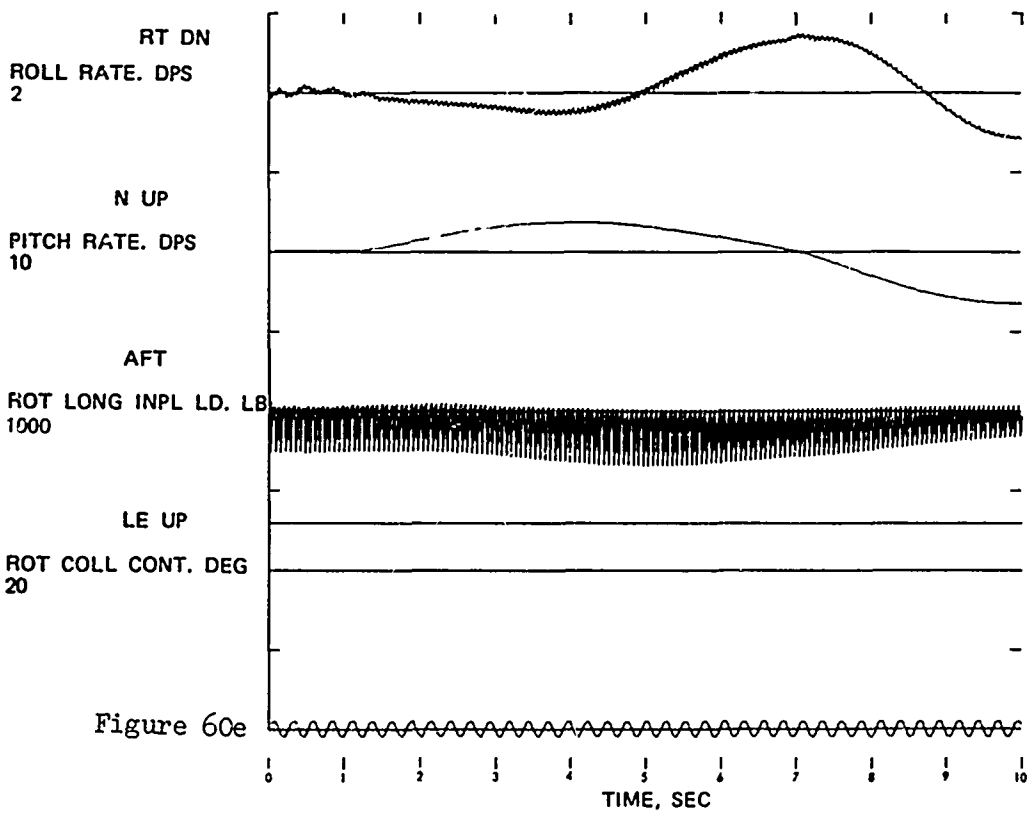

Figure 60e

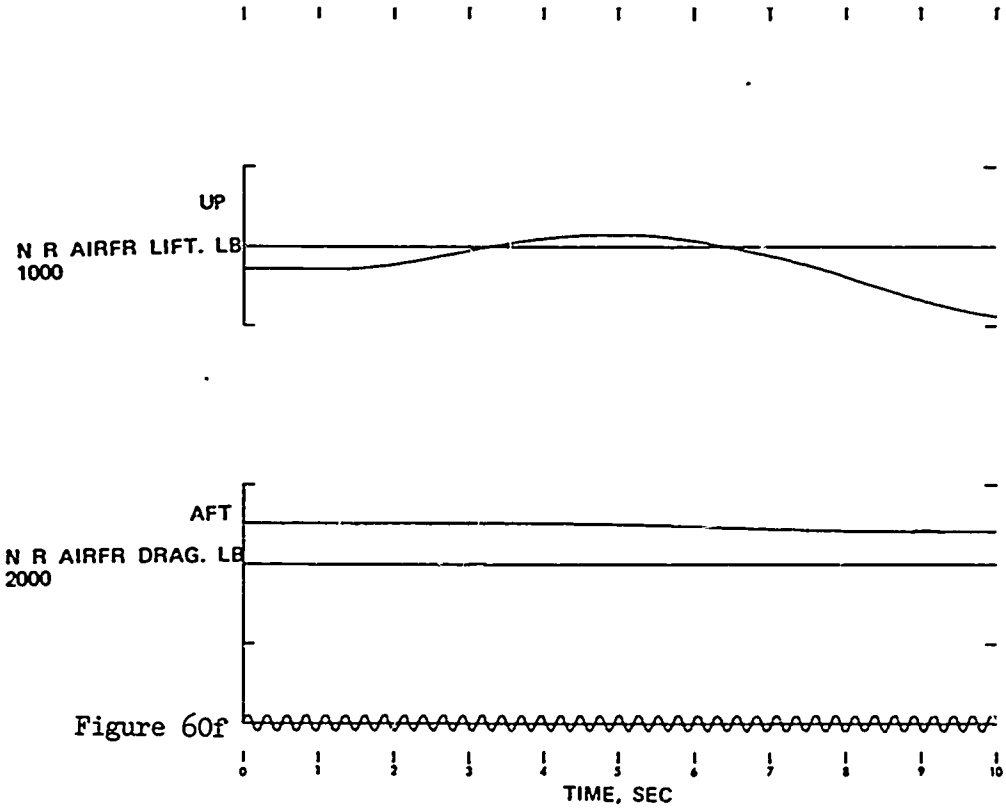

Figure 60f

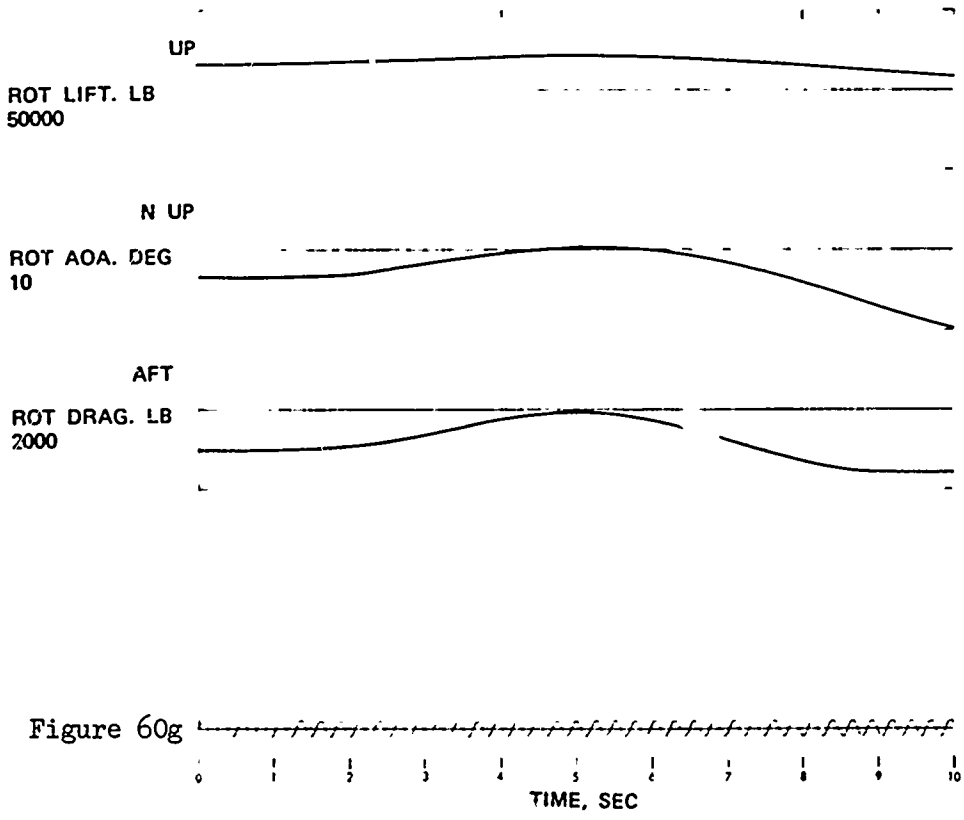

Figure 60g

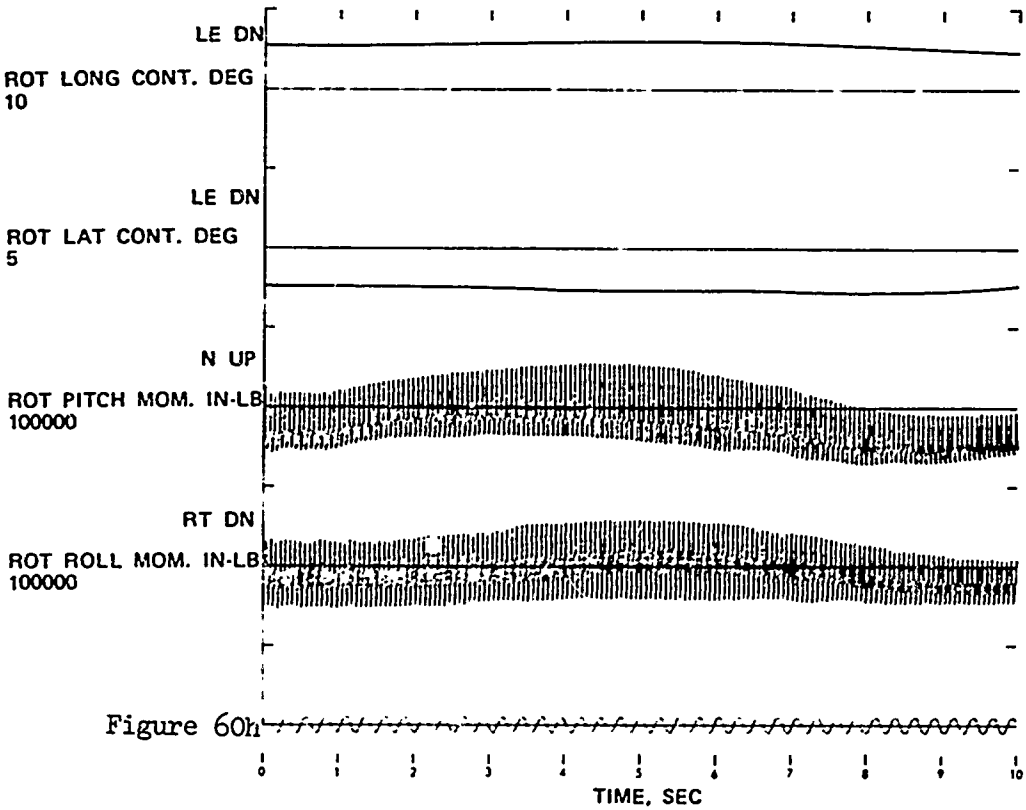

Figure 60h

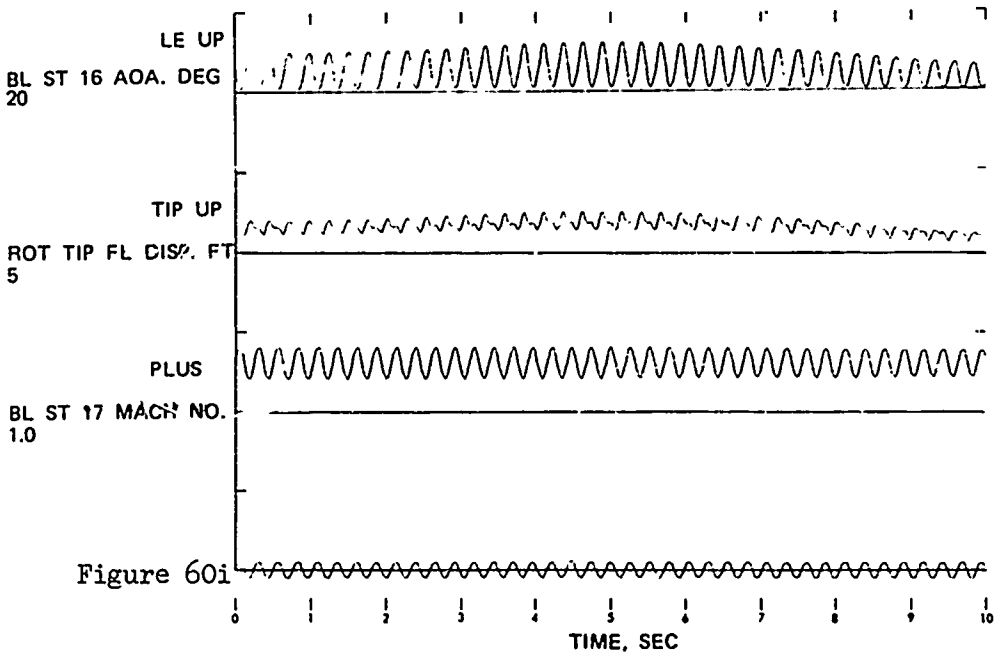

Figure 60i

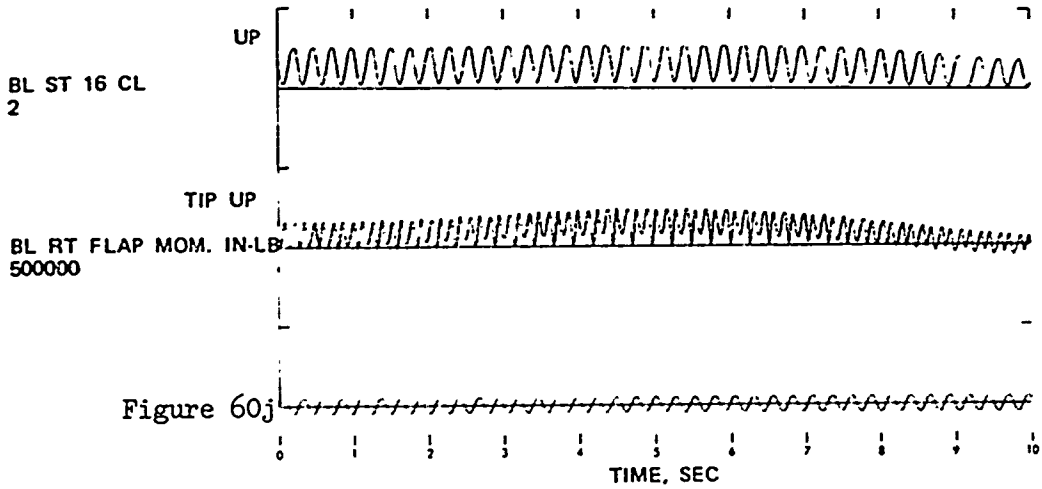

Figure 60j

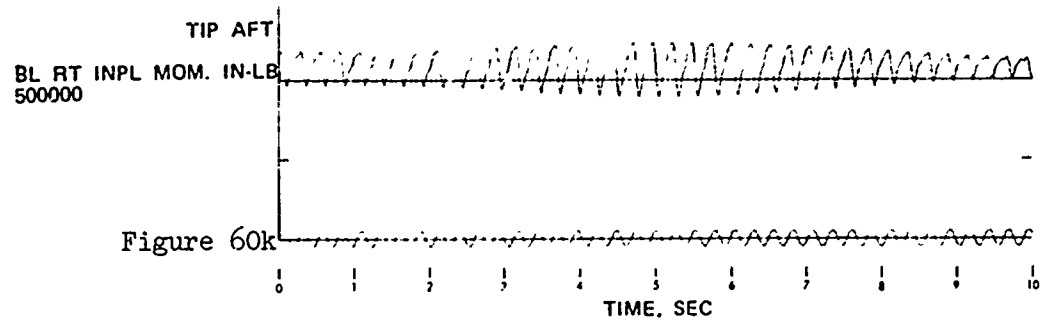

Figure 60k

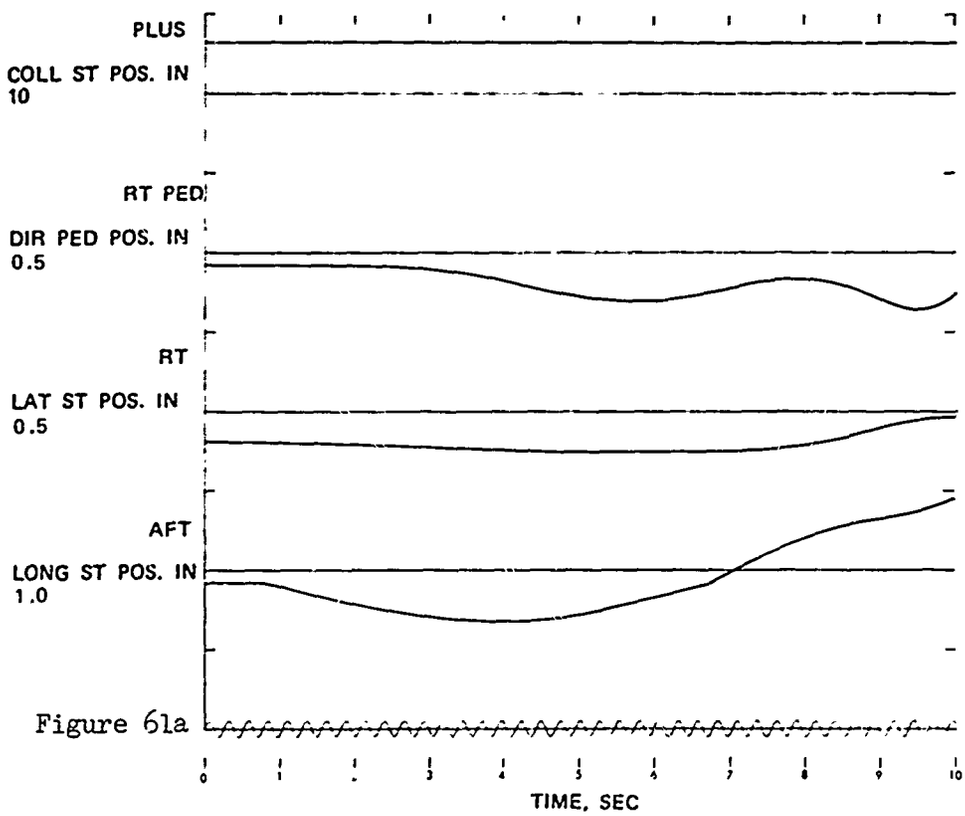

Figure 61 . Time Histories Showing the Effects of Symmetrical Push-over and Pull-up: Configuration 1; Maneuver Initiated at 140 KTAS; Height Decrease.

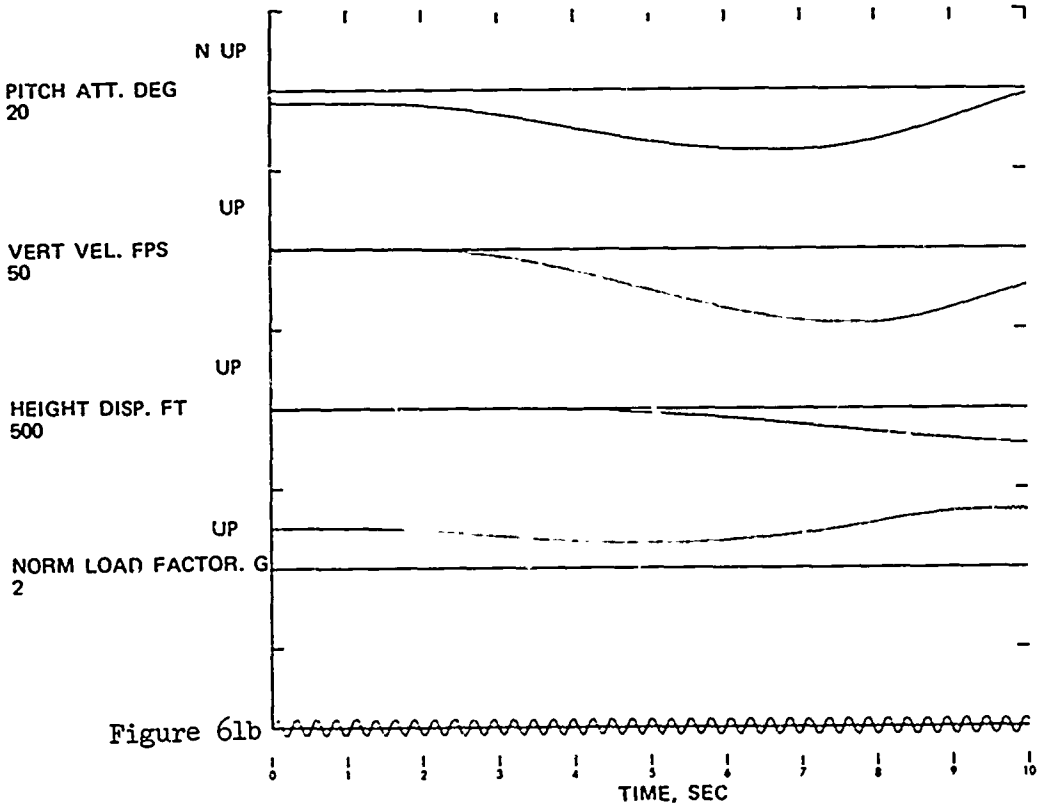

Figure 61b

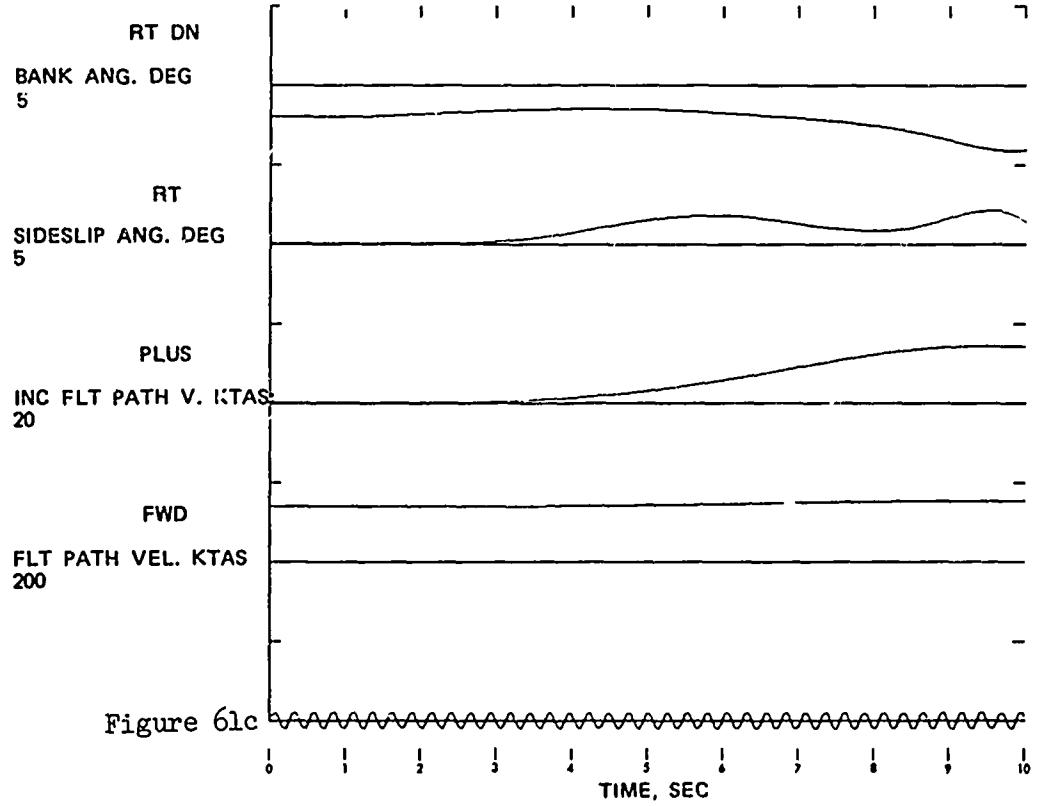

Figure 61c

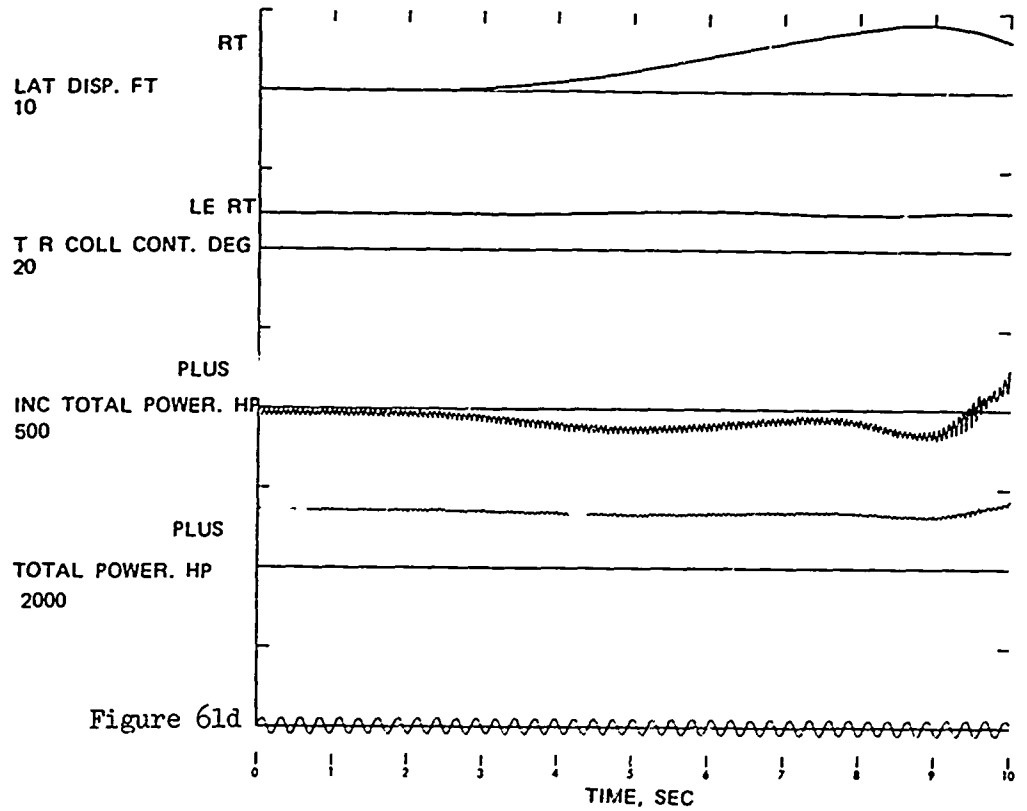

Figure 61d

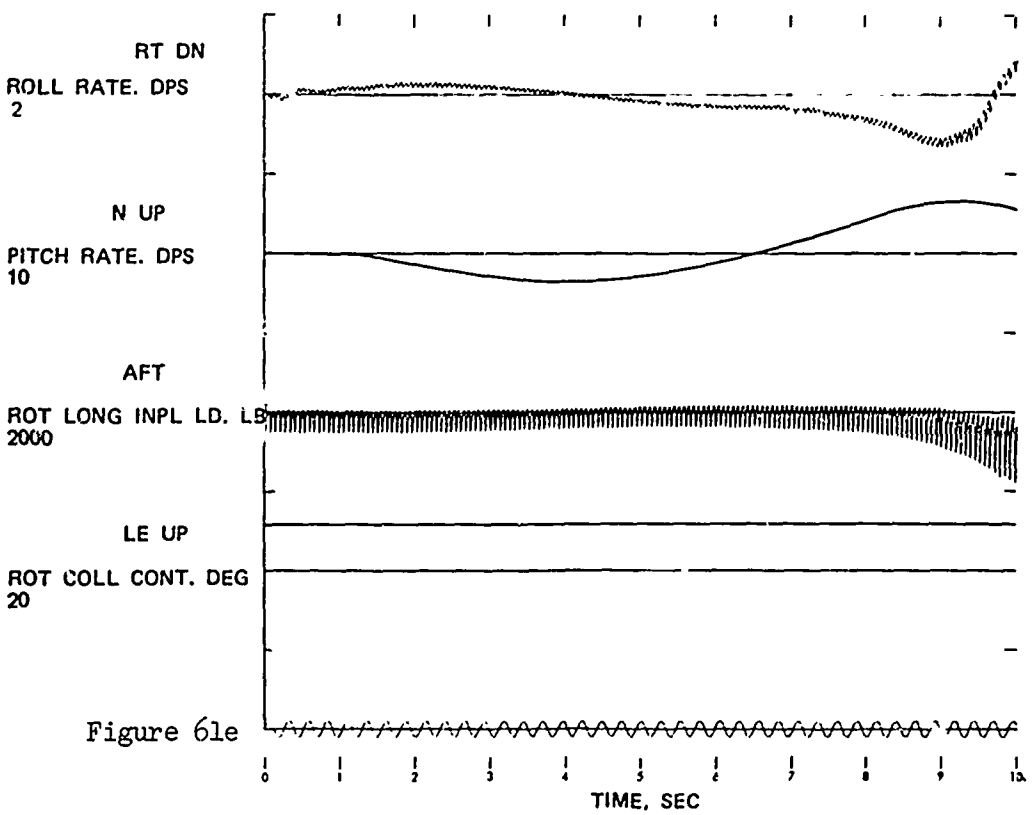

Figure 61e

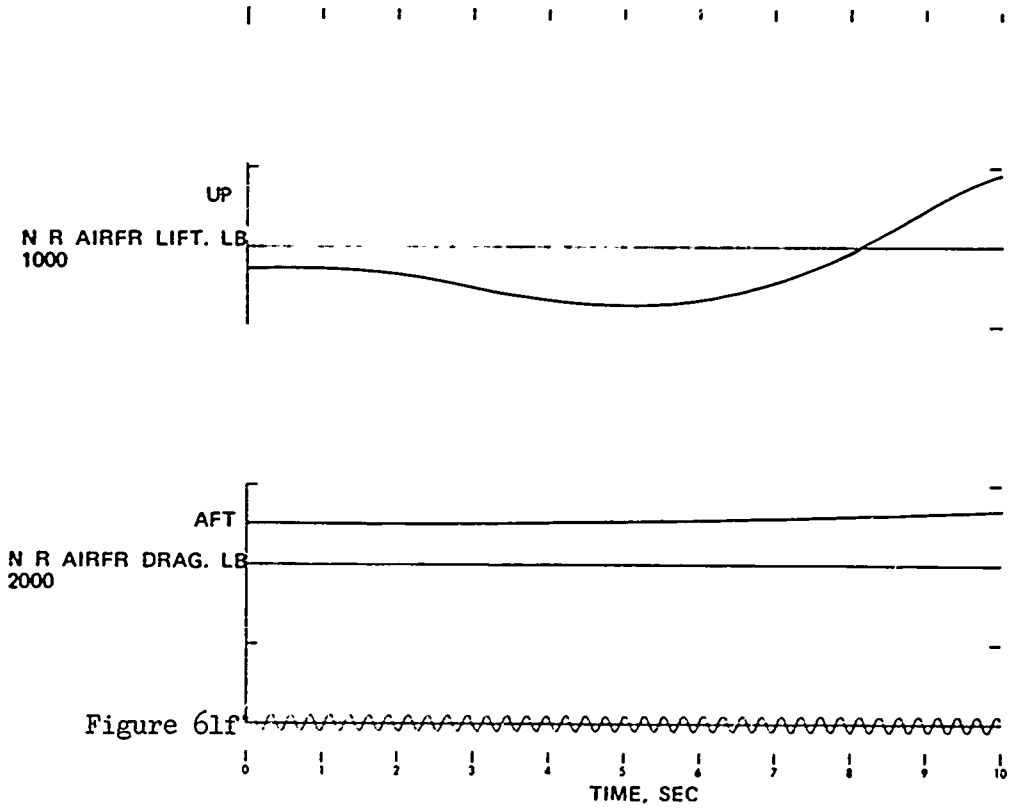

Figure 61f

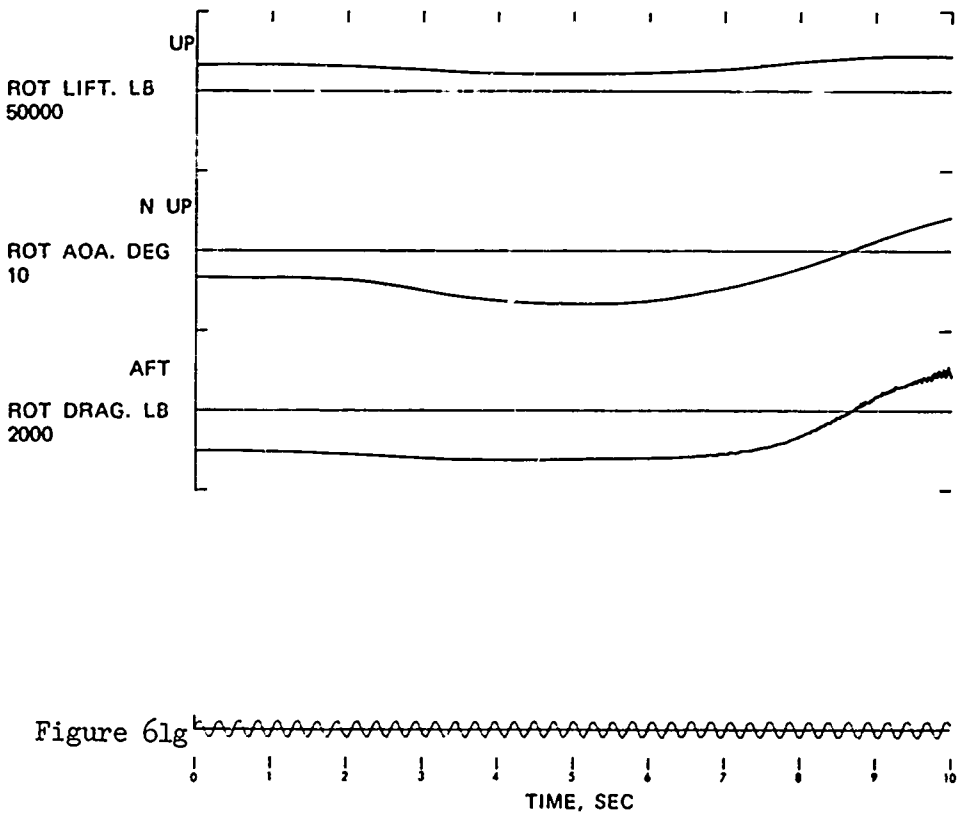

Figure 61g

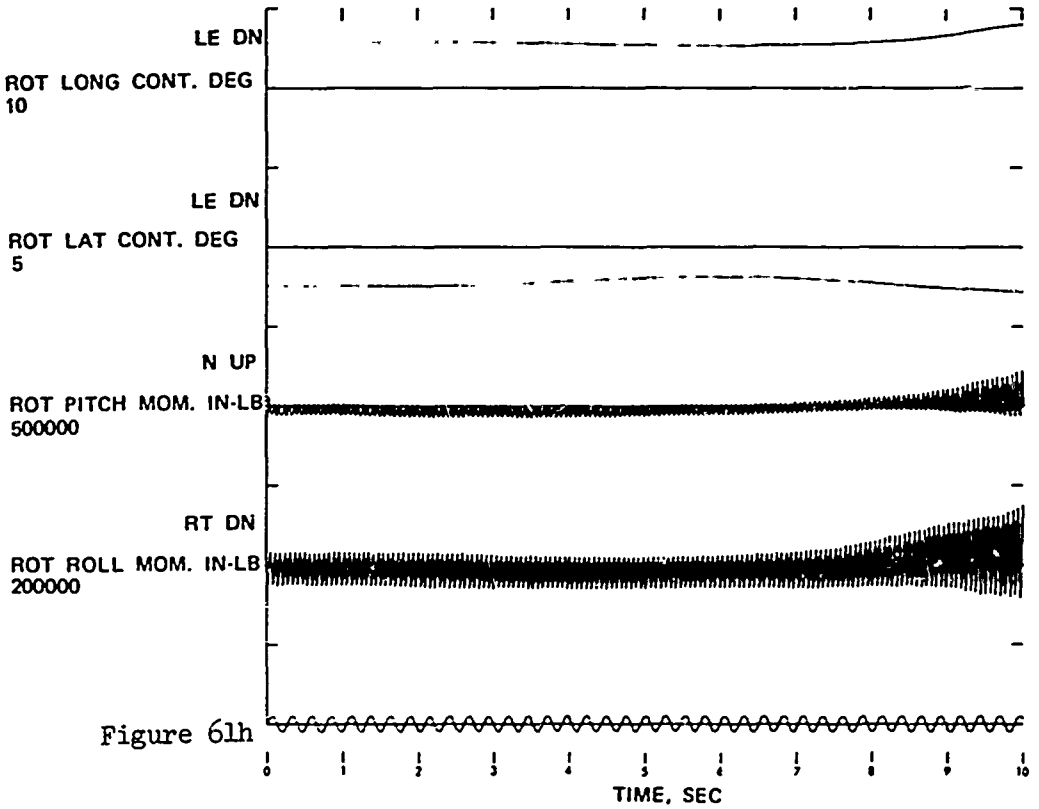

Figure 61h

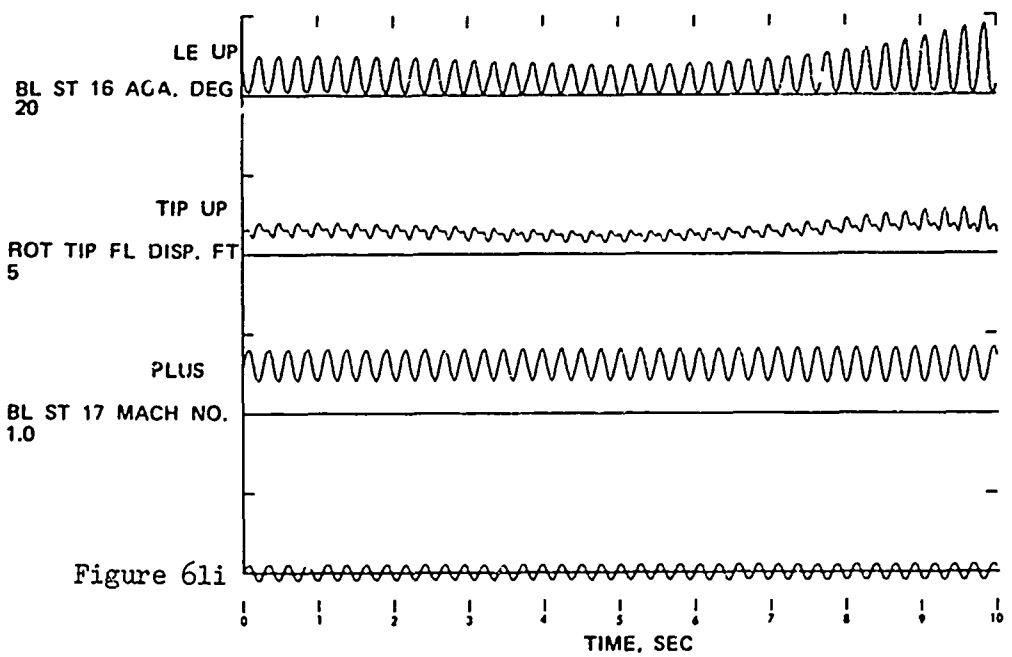

Figure 61i

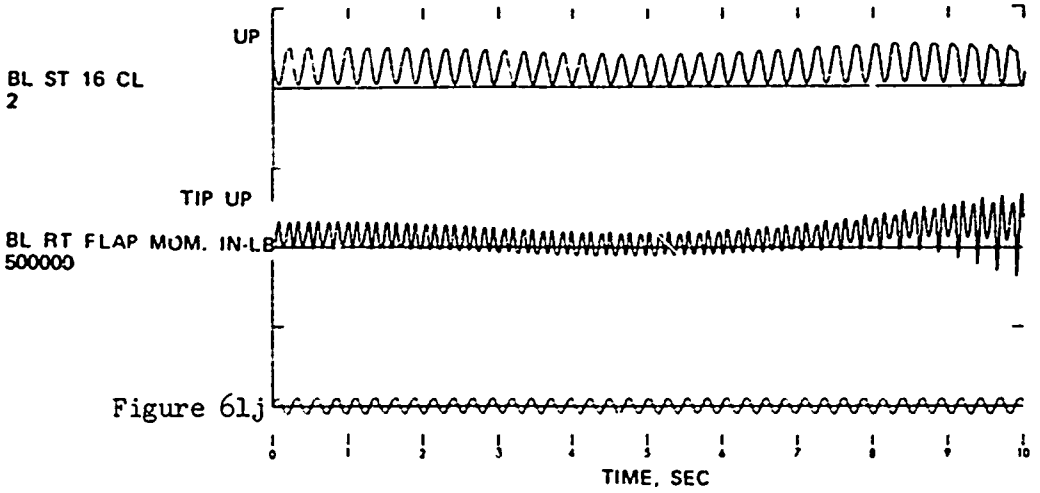

Figure 61j

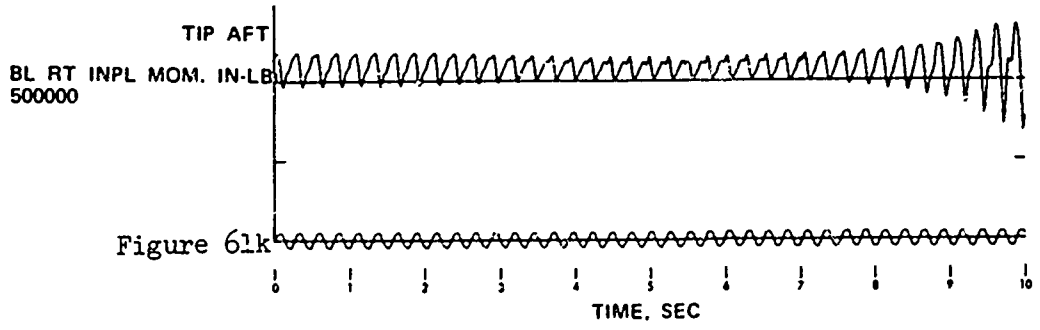

Figure 61k

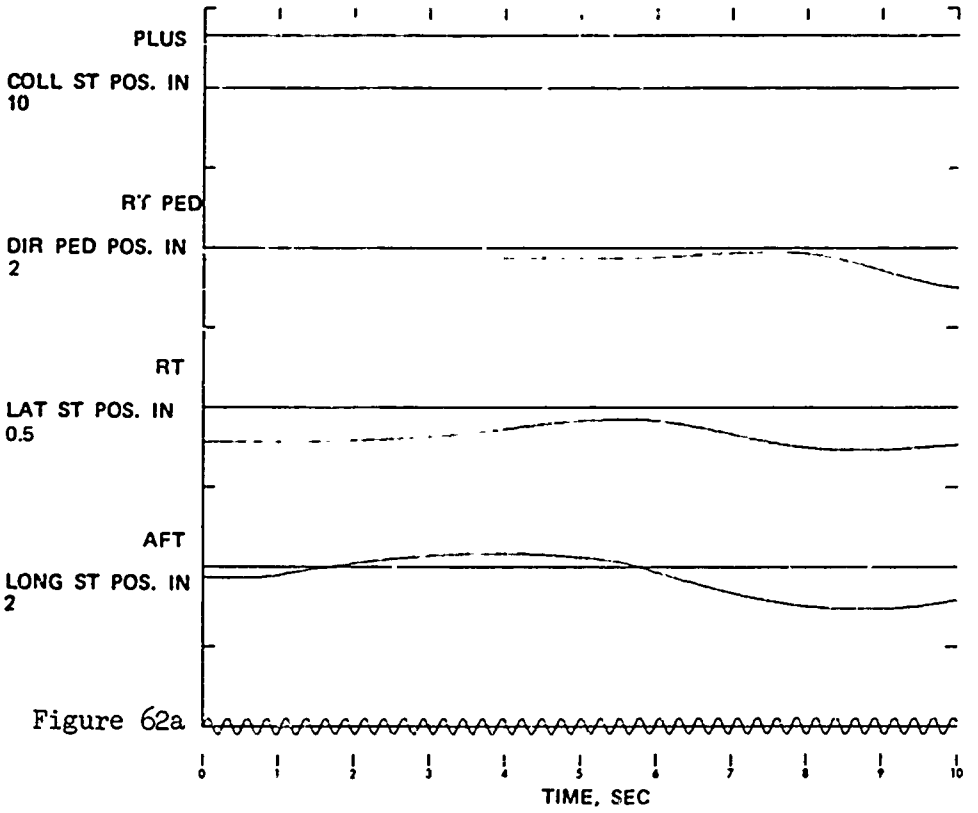

Figure 62a

Figure 62 . Time Histories Showing the Effects of Symmetrical Pull-up and Push-over: Configuration 2; Maneuver Initiated at 155 KTAS; Height Increase.

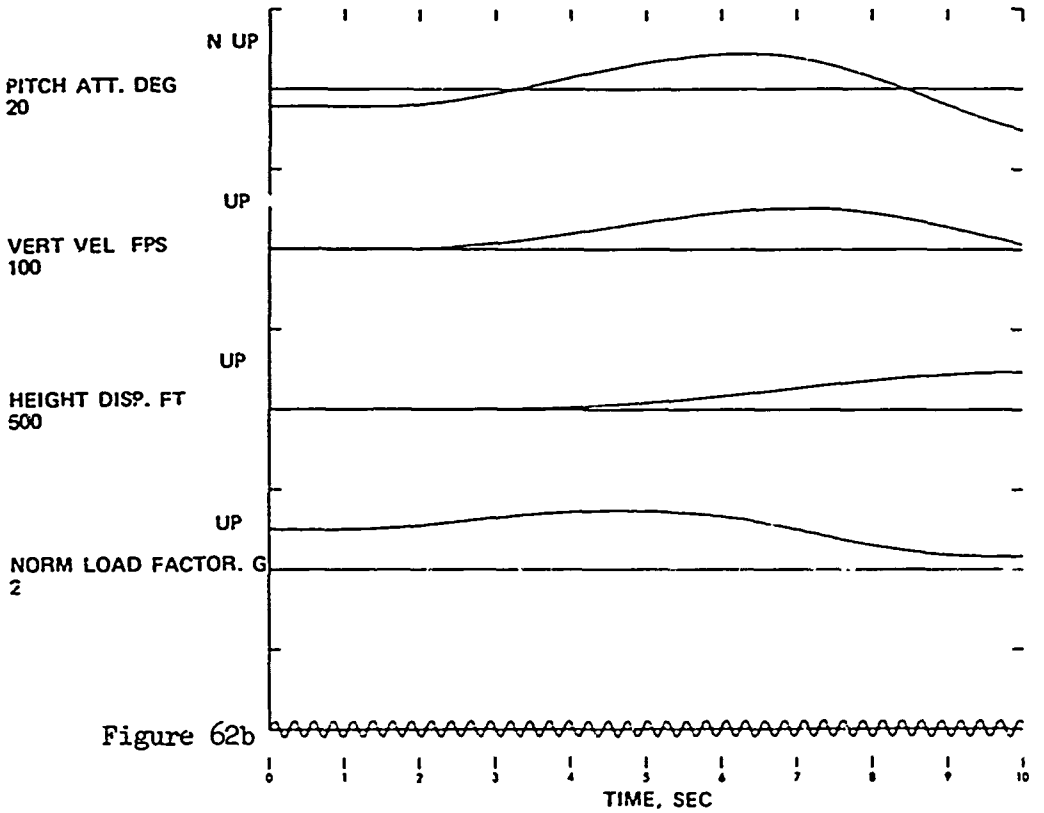

Figure 62b

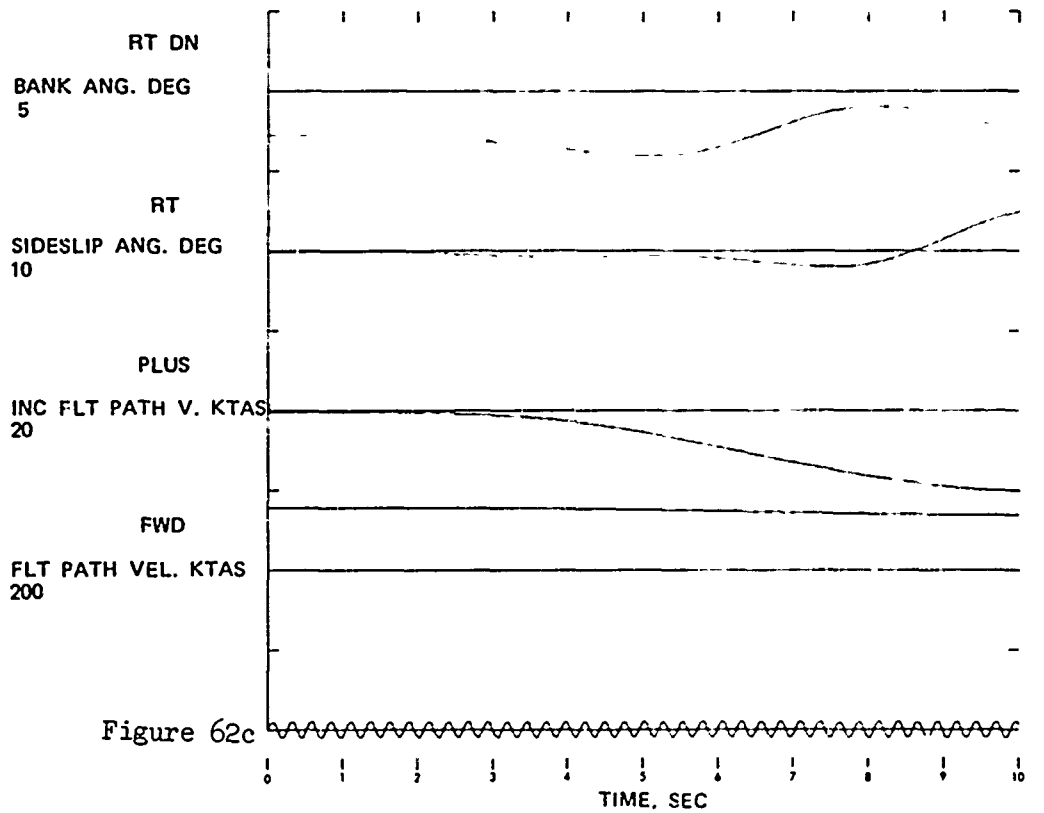

Figure 62c

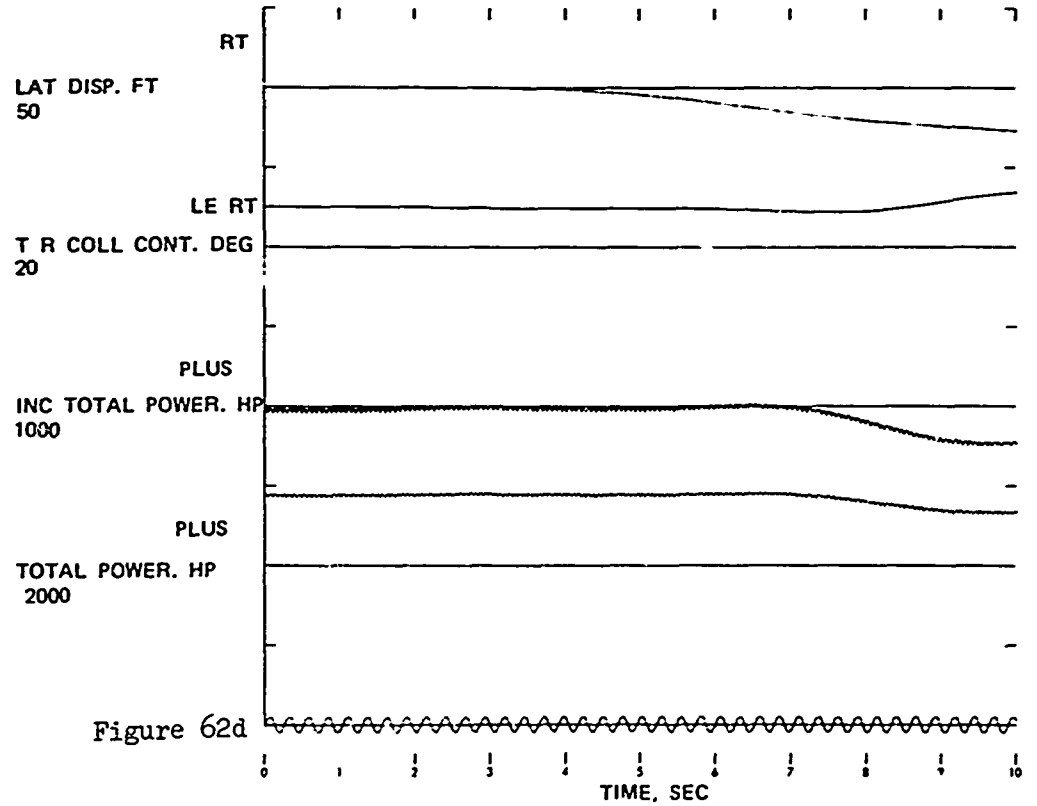

Figure 62d

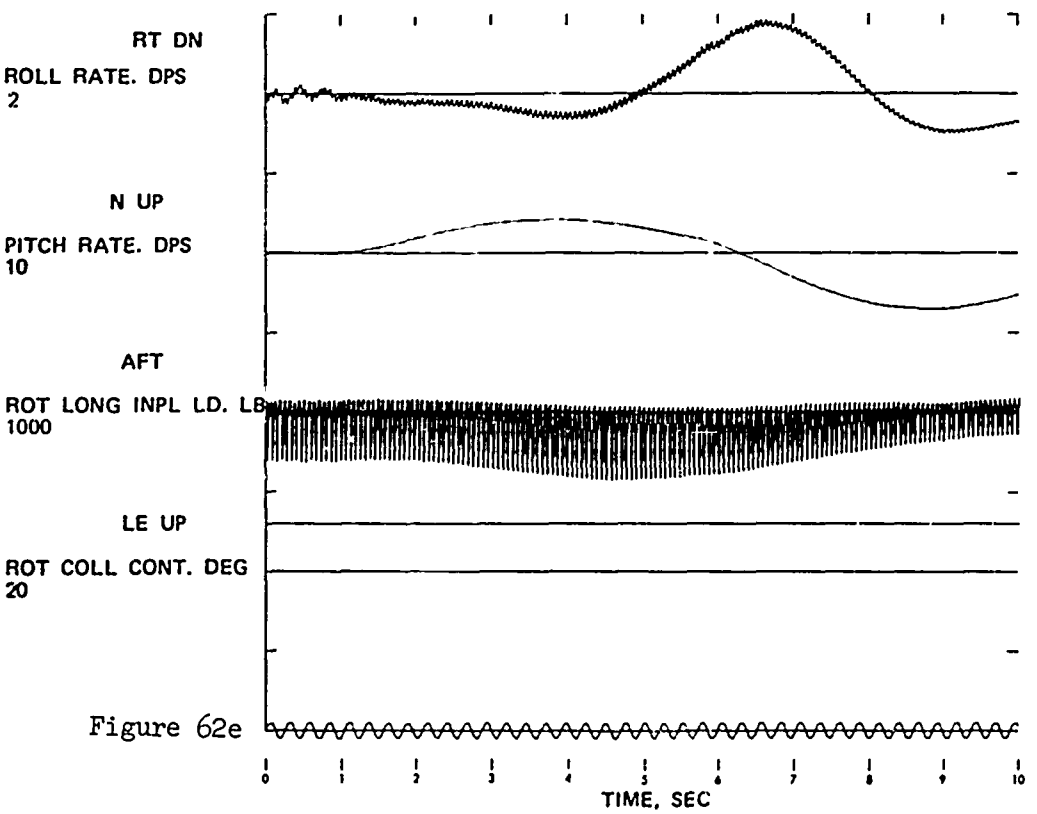

Figure 62e

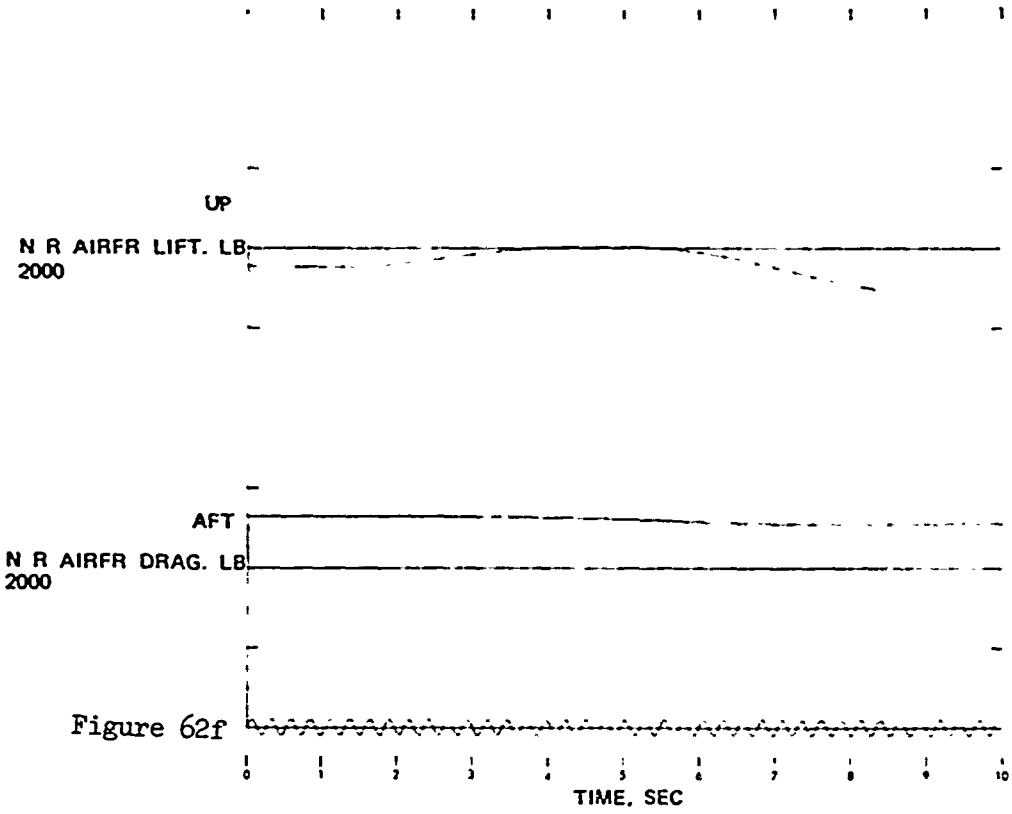

Figure 62f

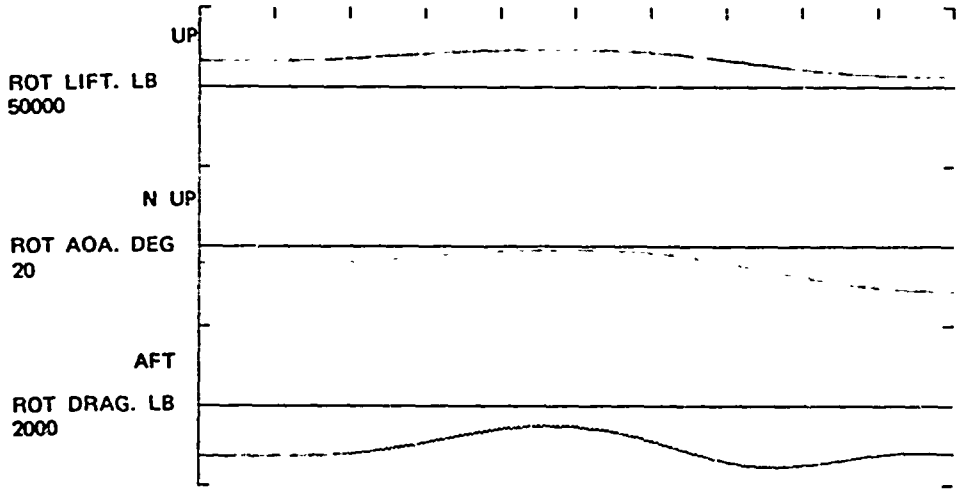

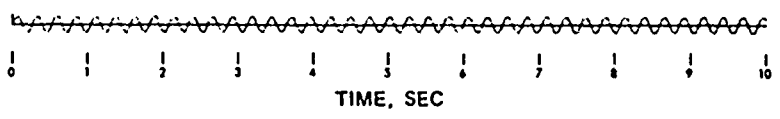

Figure 62g

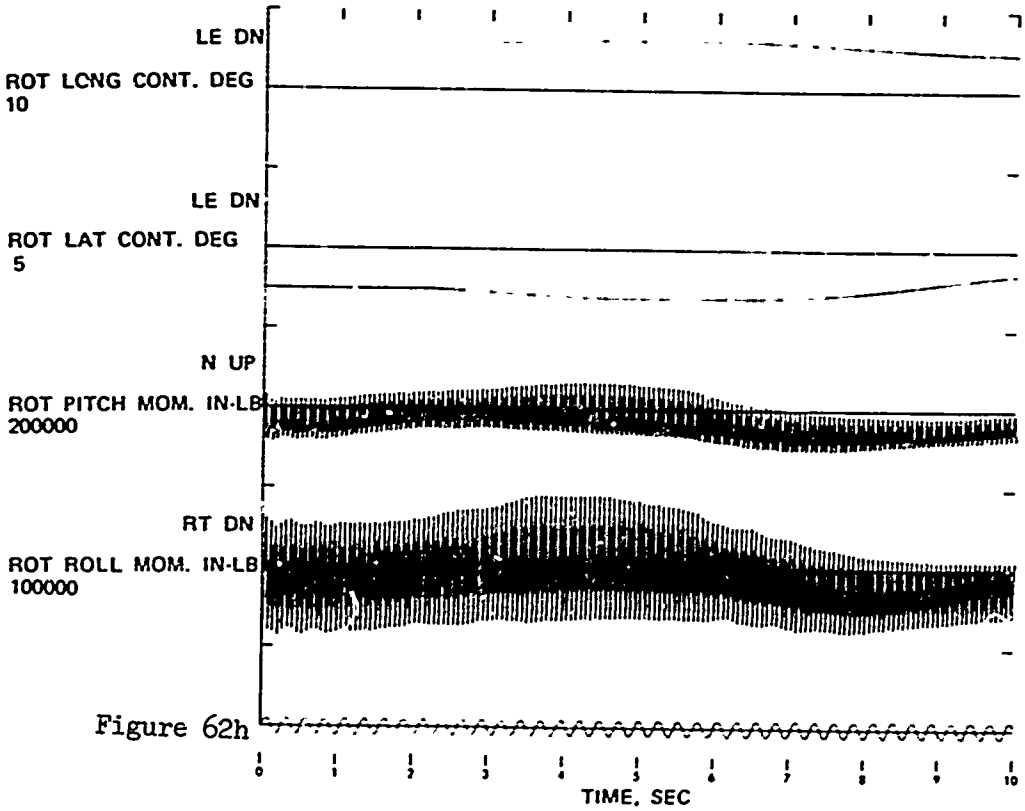

Figure 62h

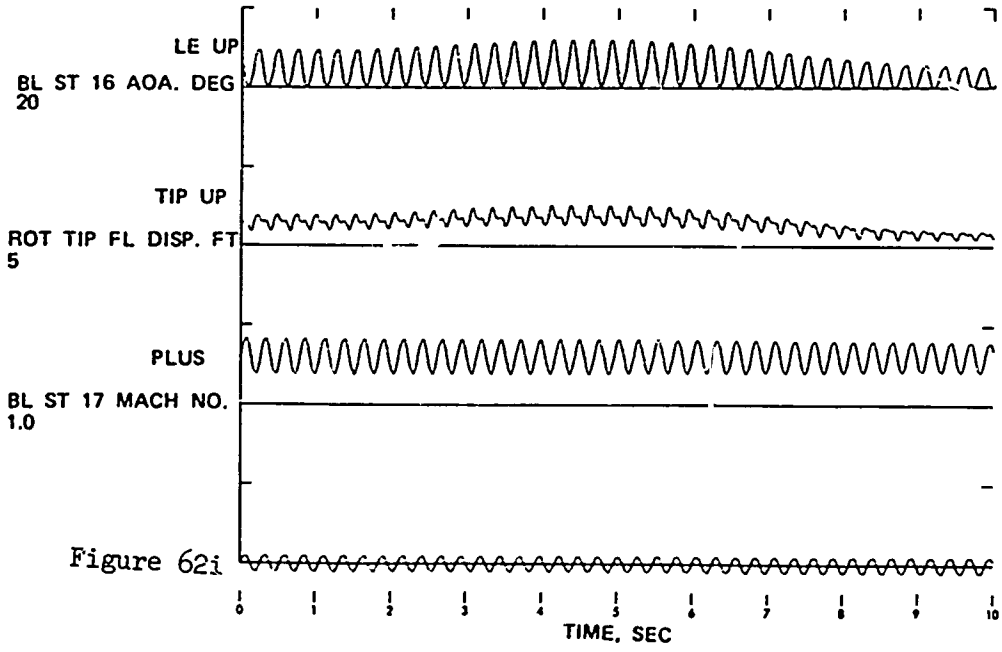

Figure 62i

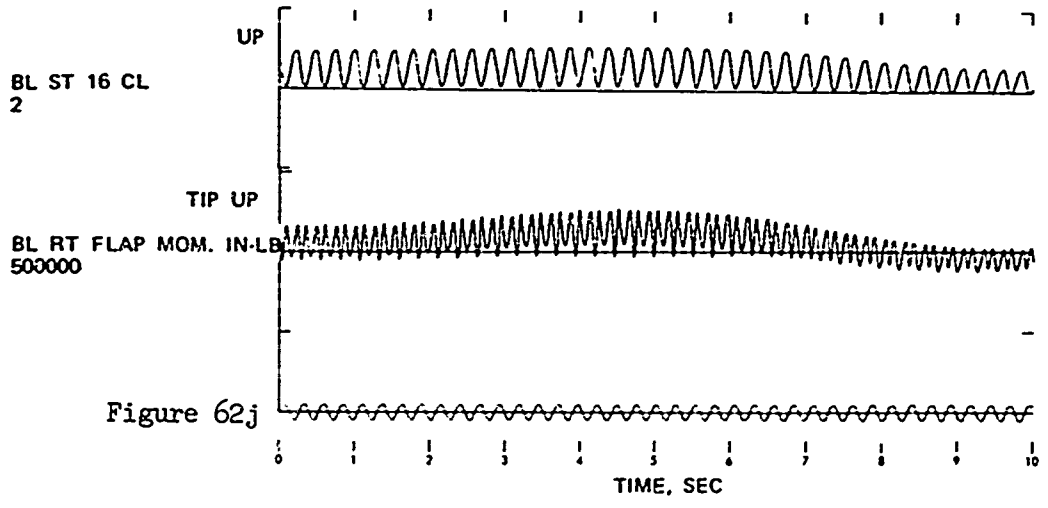

Figure 62j

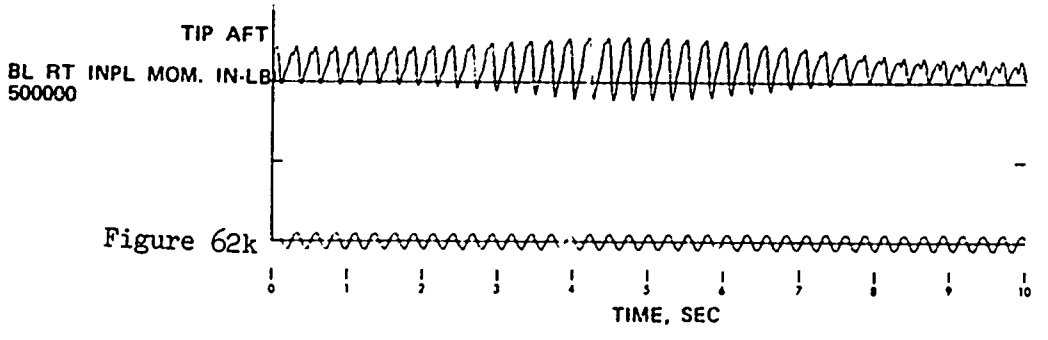

Figure 62k

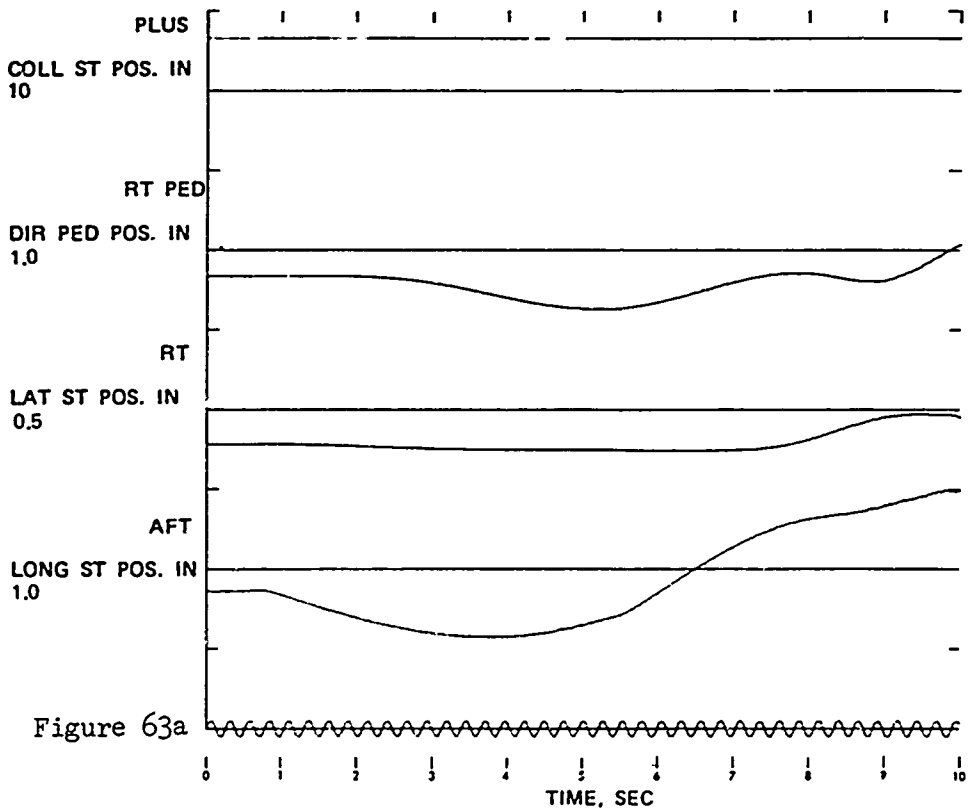

Figure 63a

Figure 63 . Time Histories Showing the Effects of Symmetrical Push-over and Pull-up: Configuration 2; Maneuver Initiated at 155 KTAS; Height Decrease .

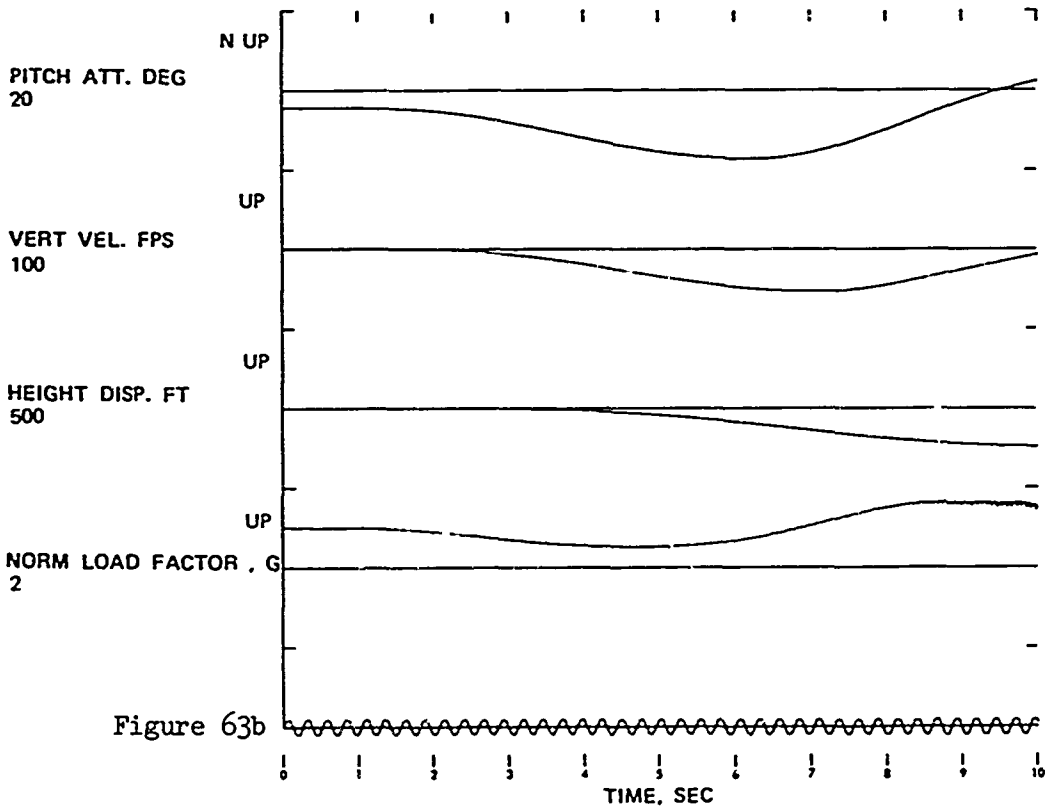

Figure 63b

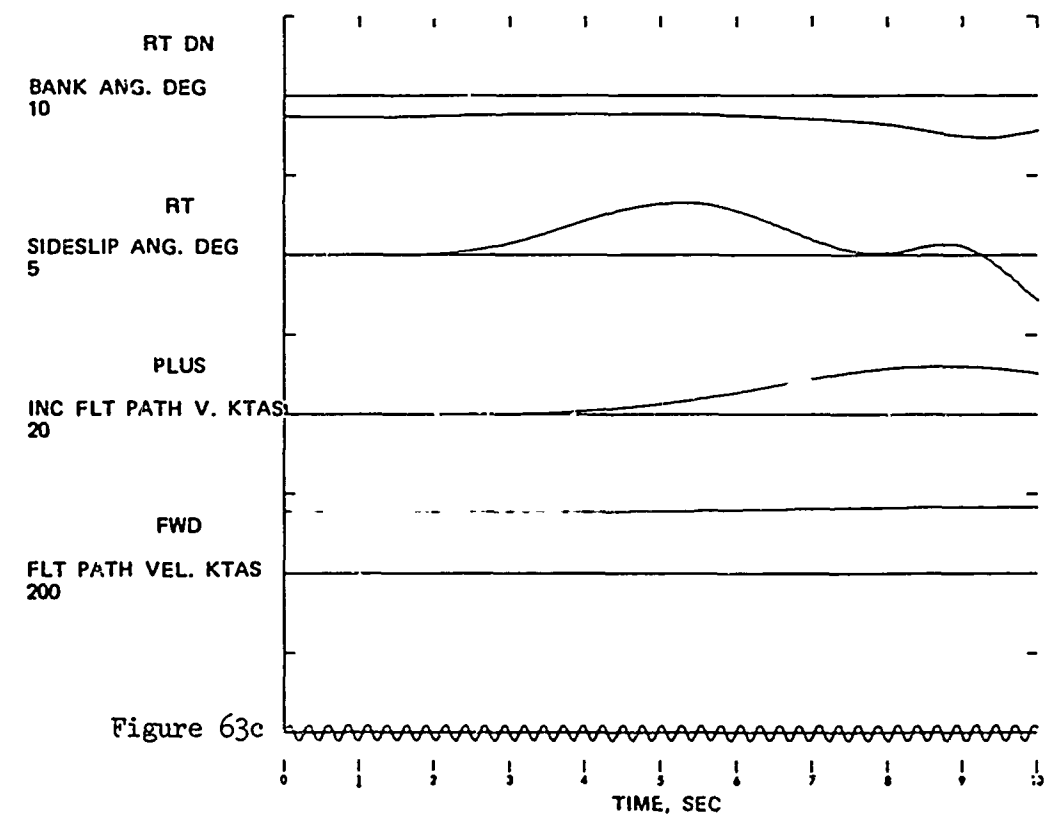

Figure 63c

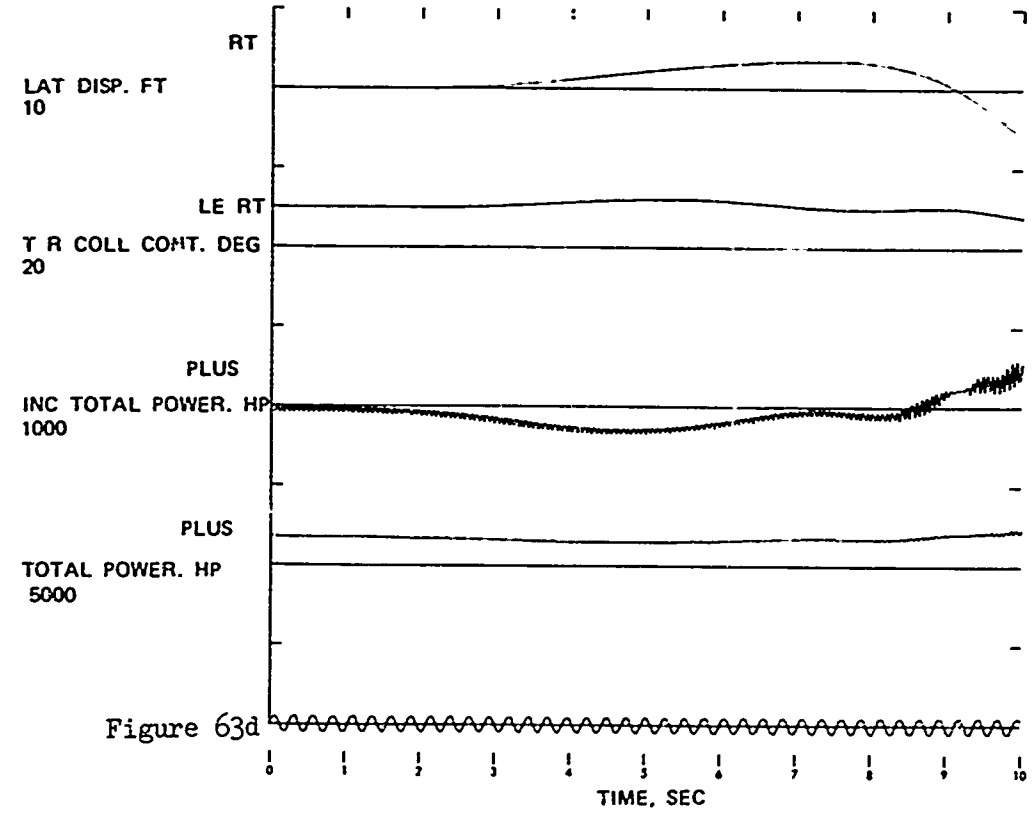

Figure 63d

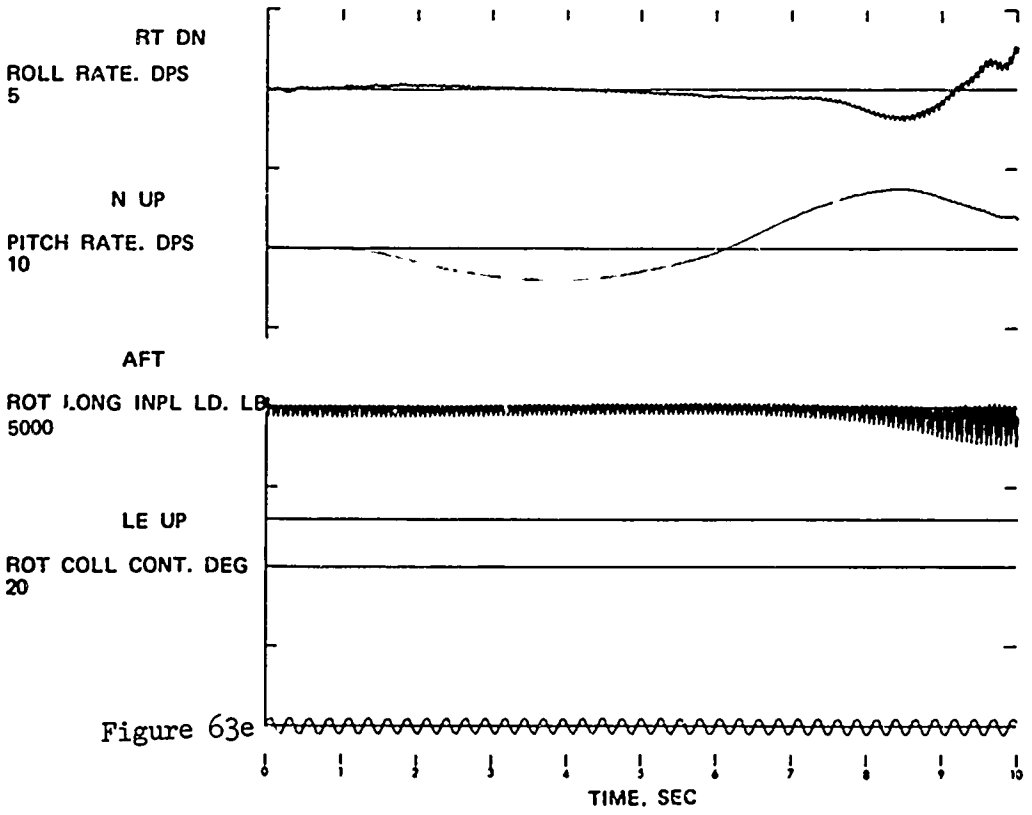

Figure 63e

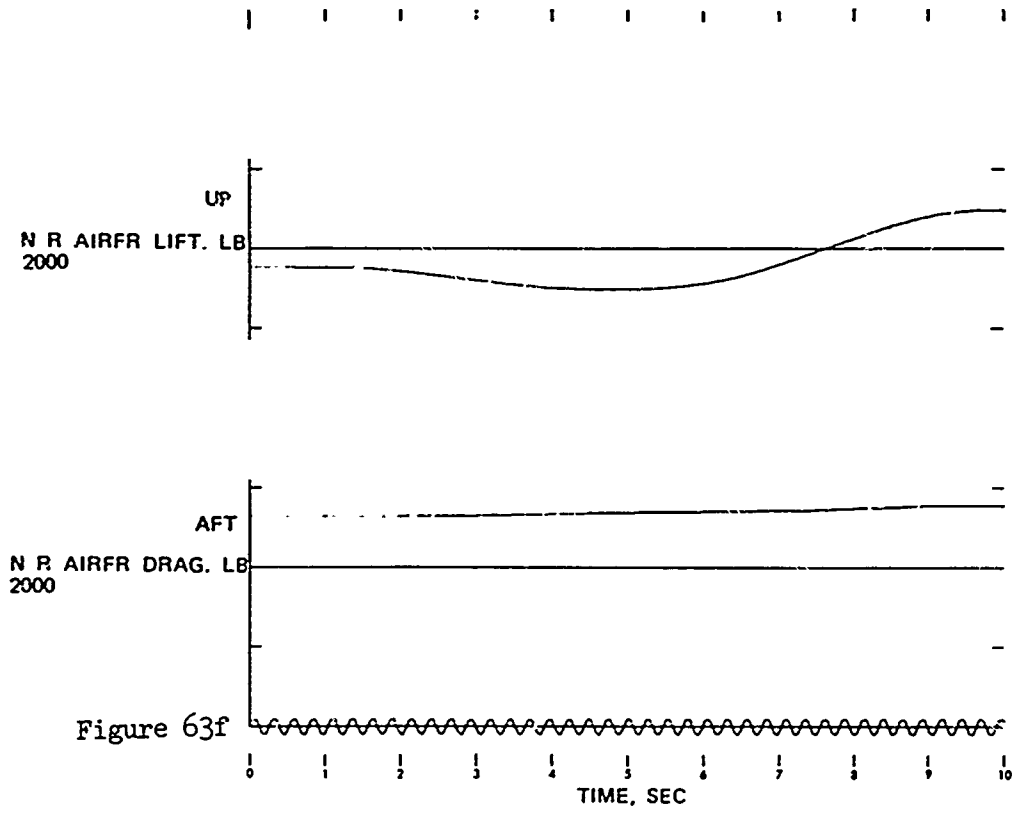

Figure 63f

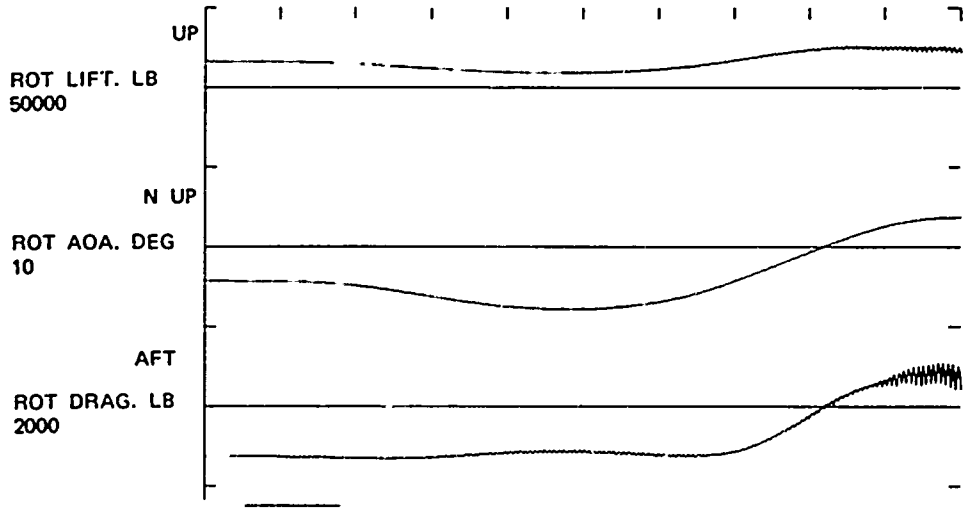

Figure 63g

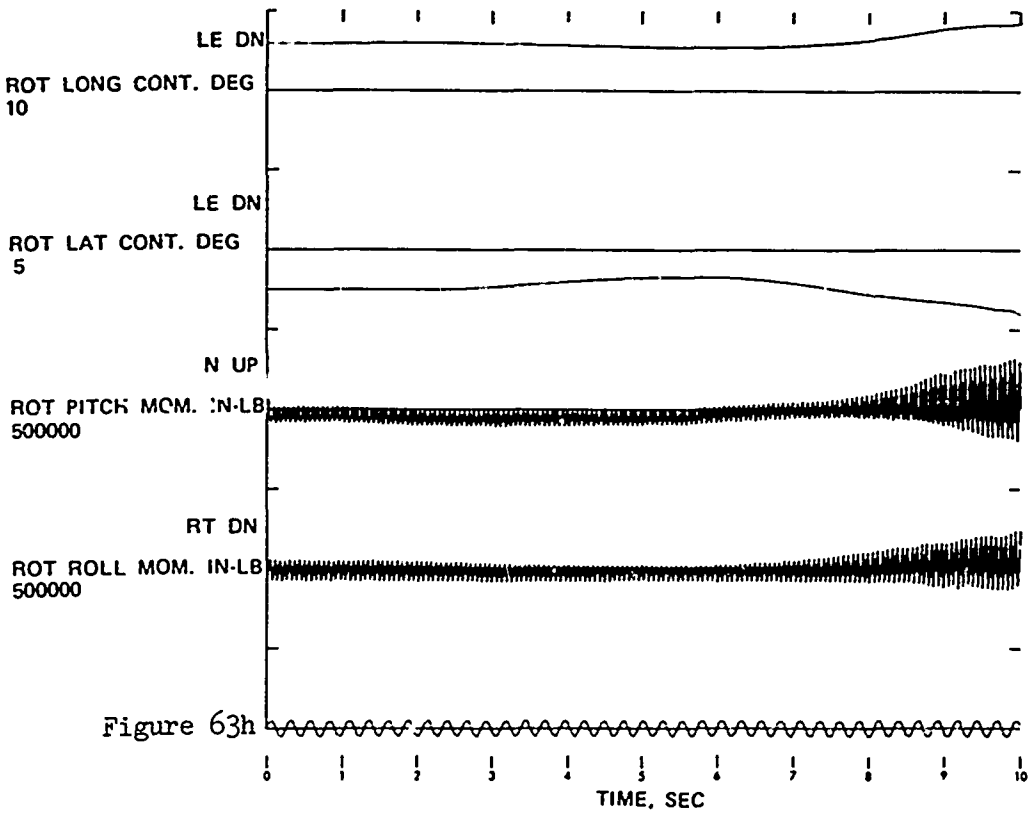

Figure 63h

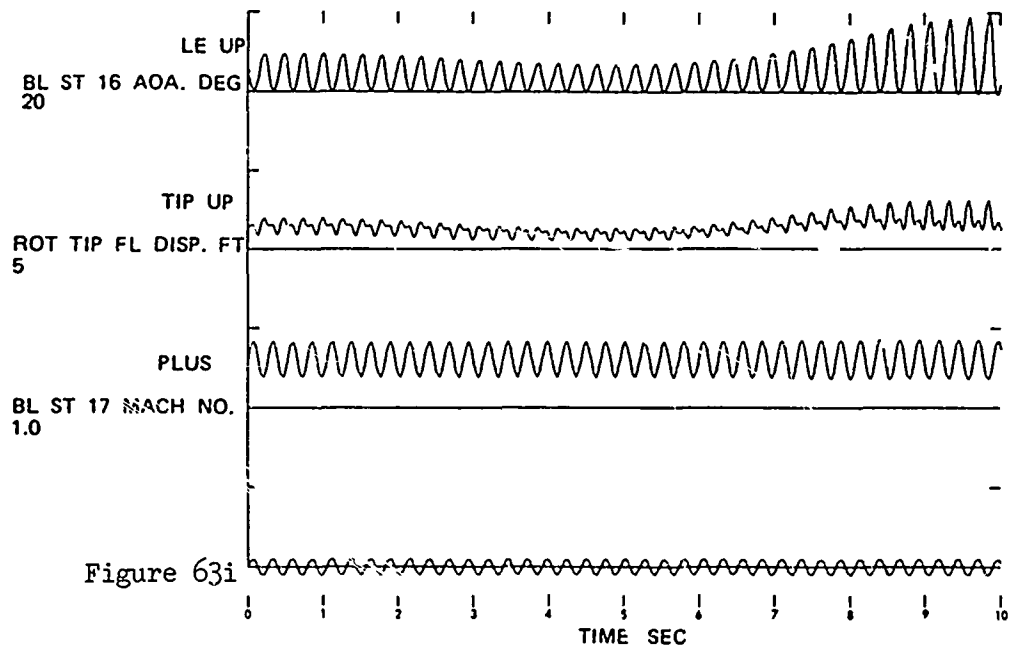

Figure 63i

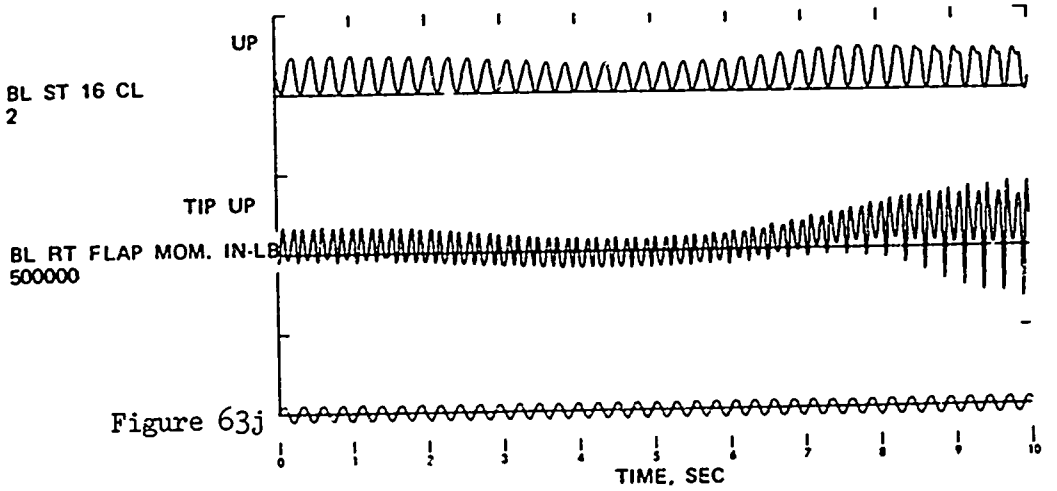

Figure 63j

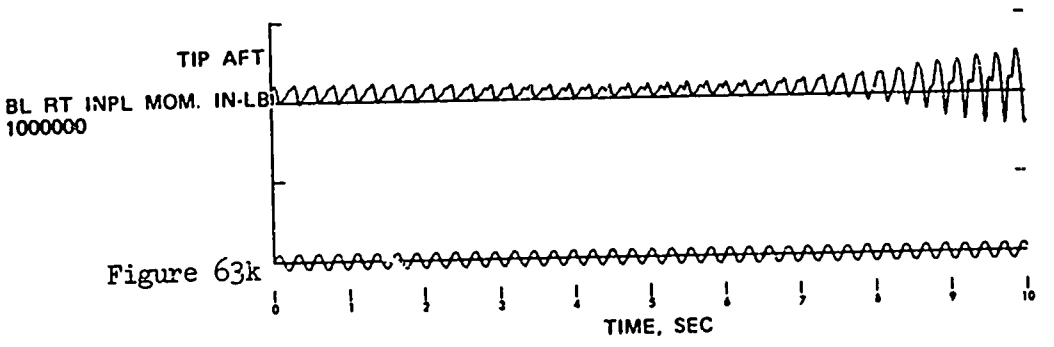

Figure 63k

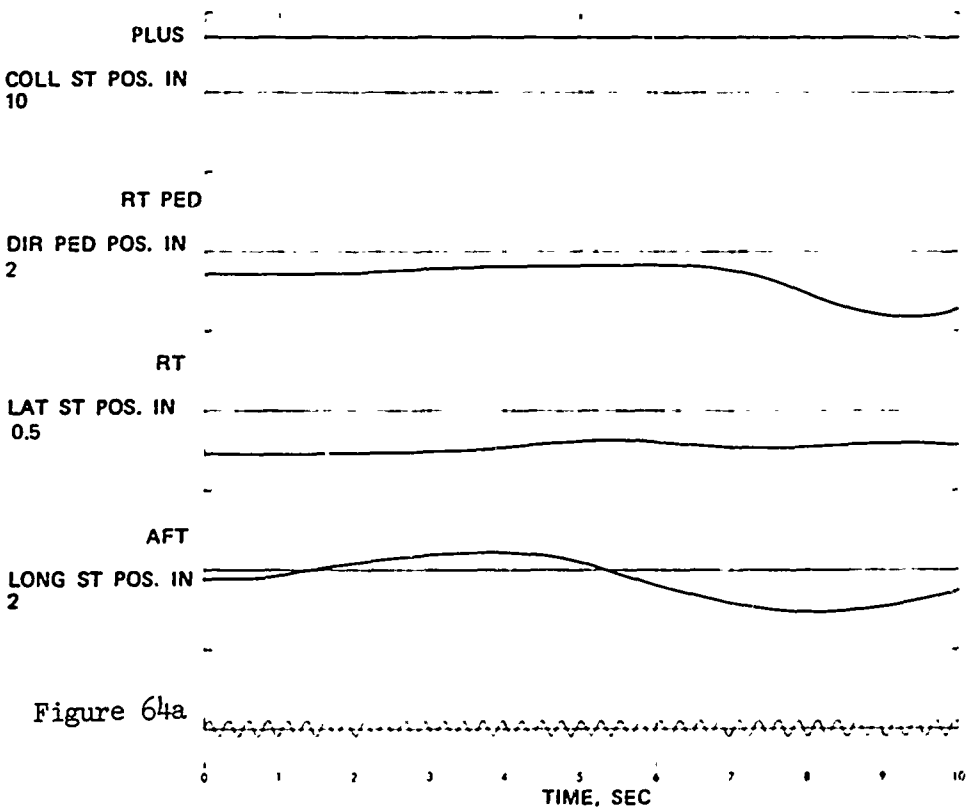

Figure 64a

Figure 64 . Time Histories Showing the Effects of Symmetrical Pull-up and Push-over: Configuration 3; Maneuver Initiated at 167 KTAS: Height Increase .

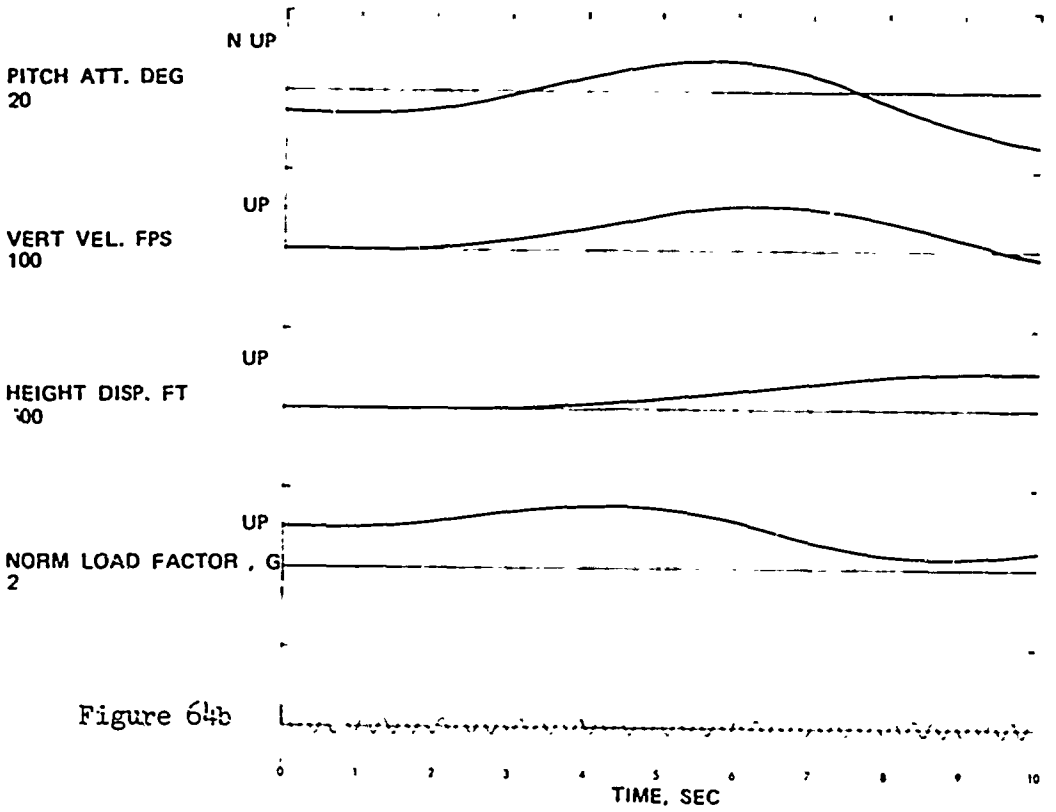

Figure 64b

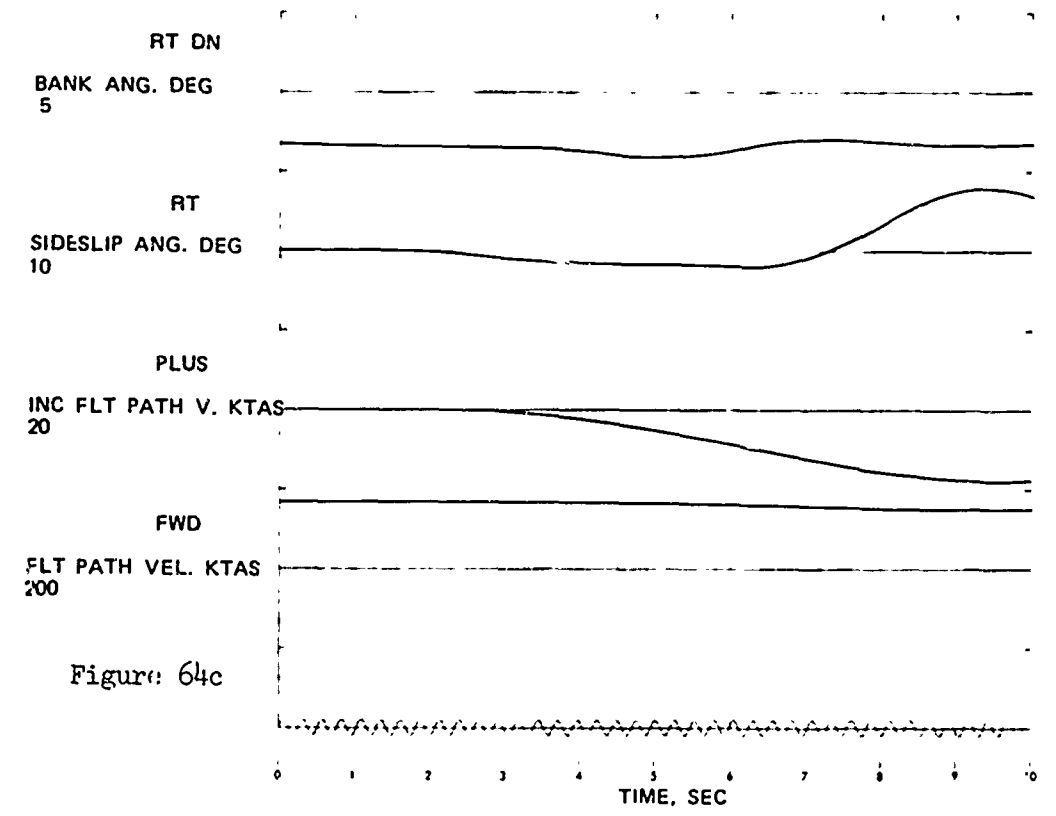

Figure 64c

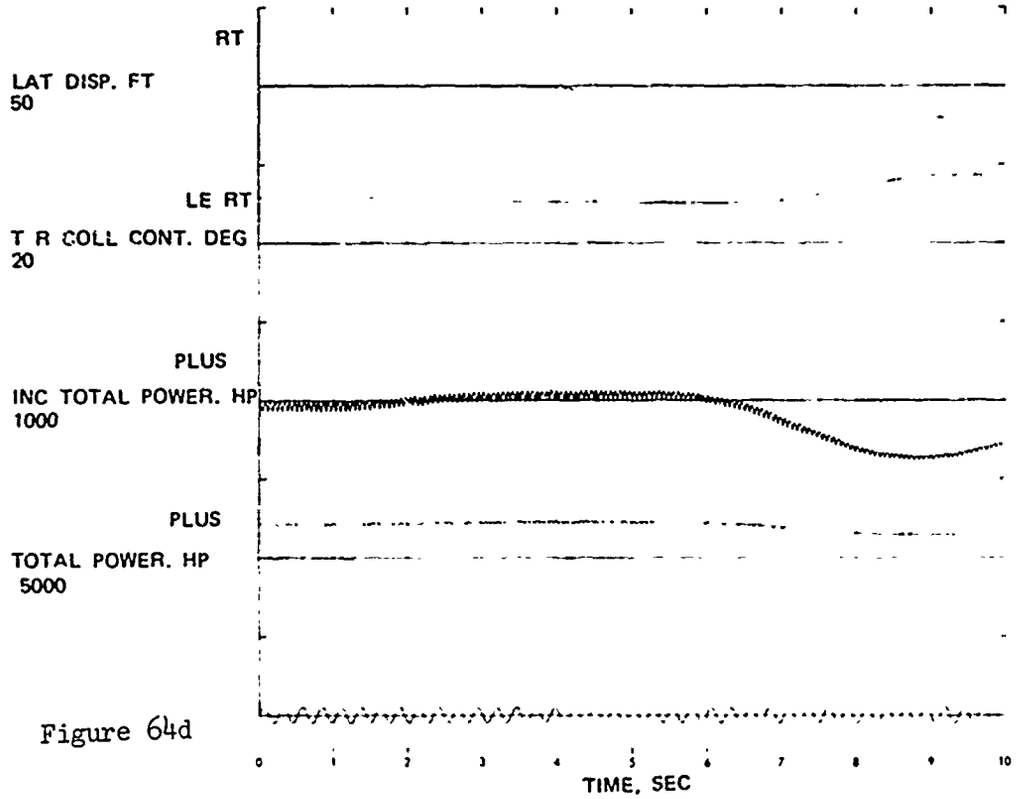

Figure 64d

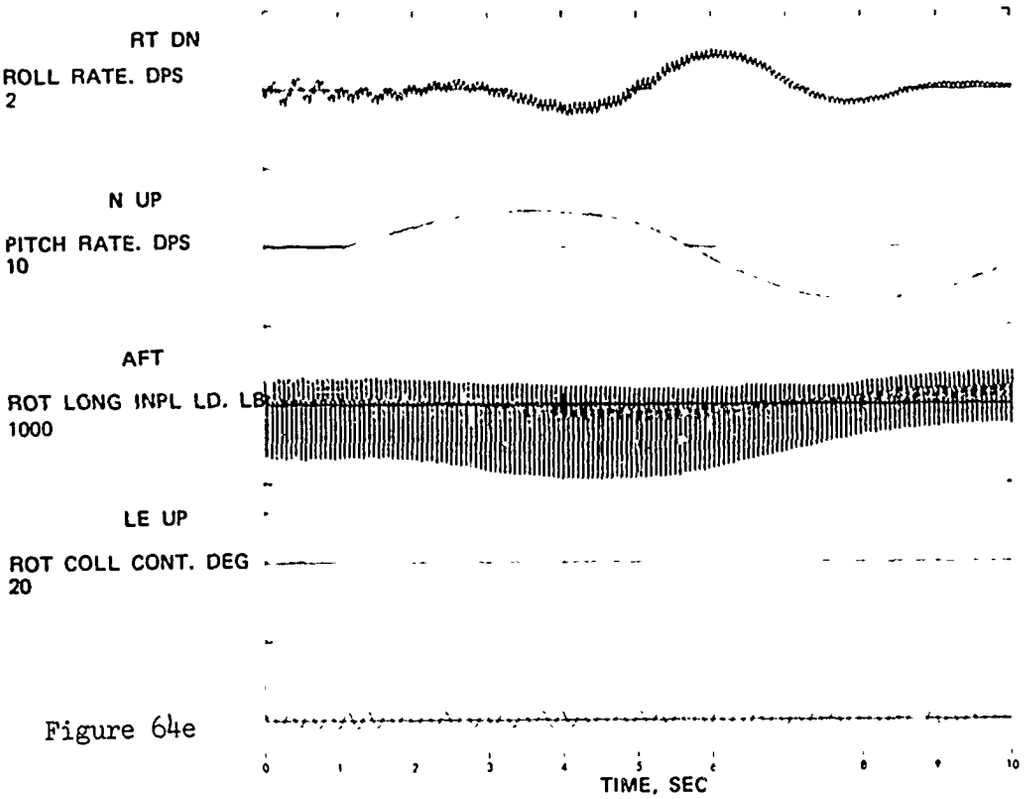

Figure 64e

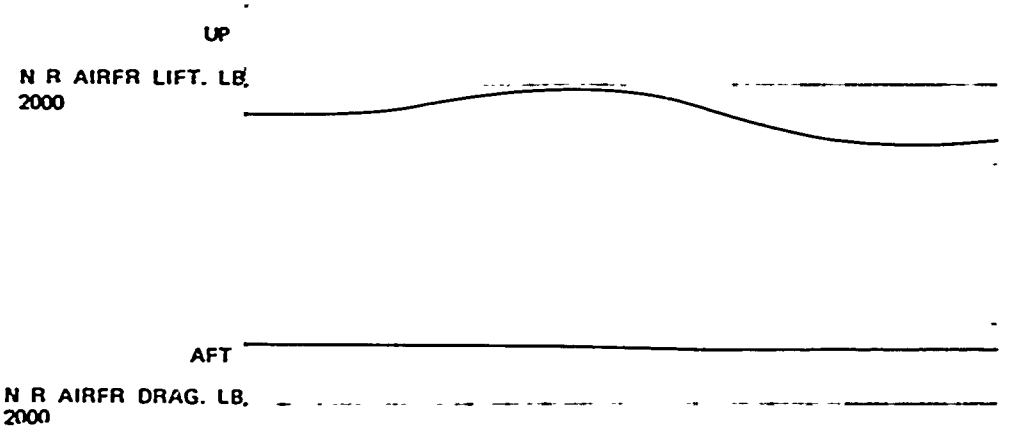

Figure 64f

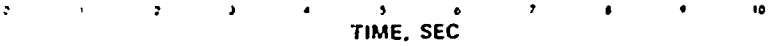

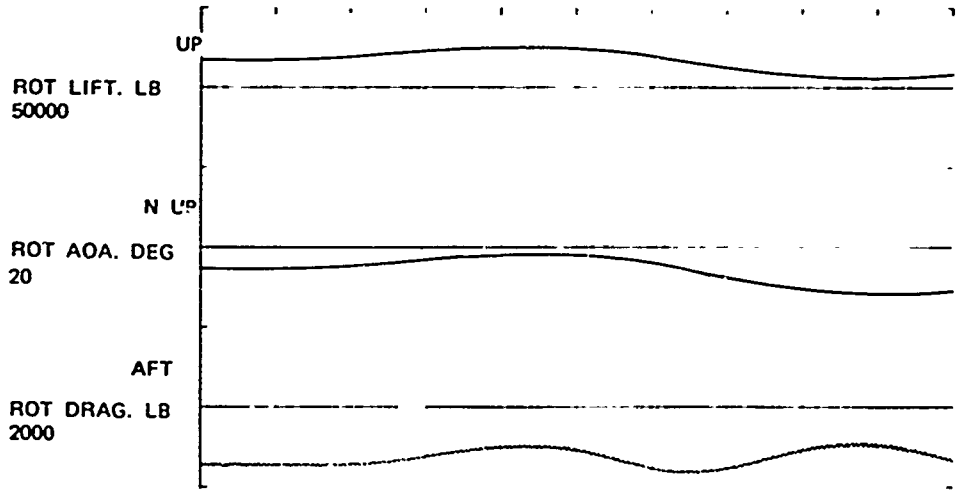

Figure 64g

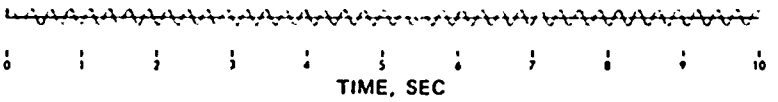

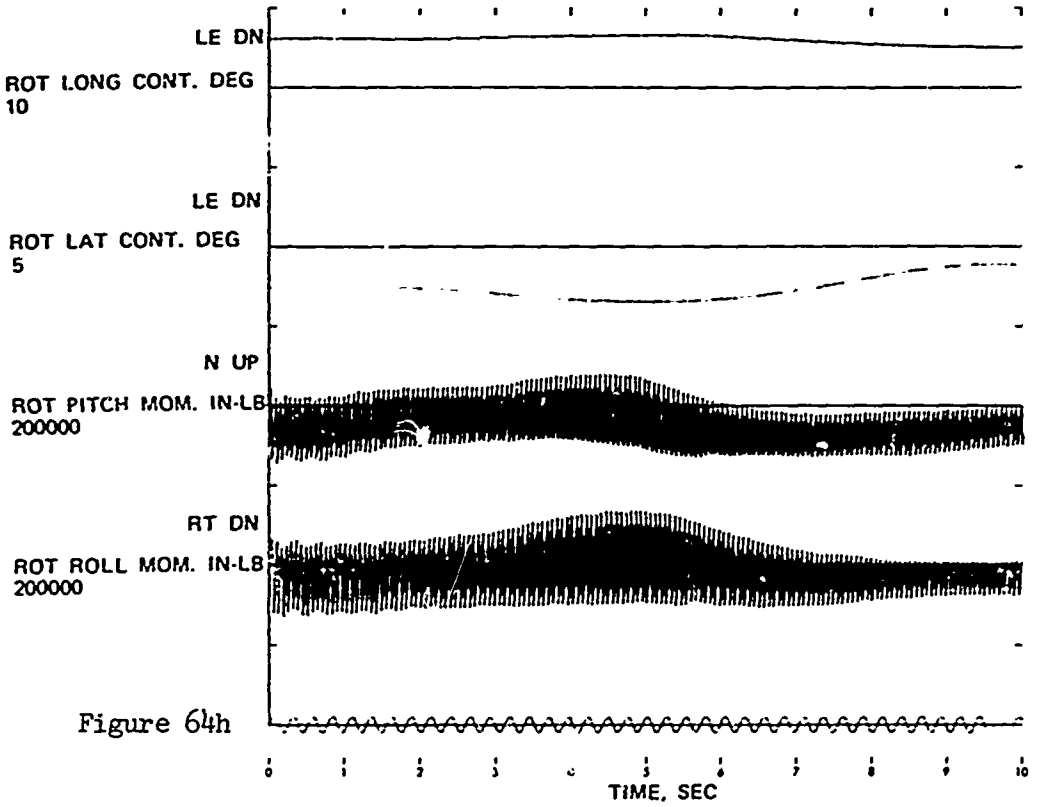

Figure 64h

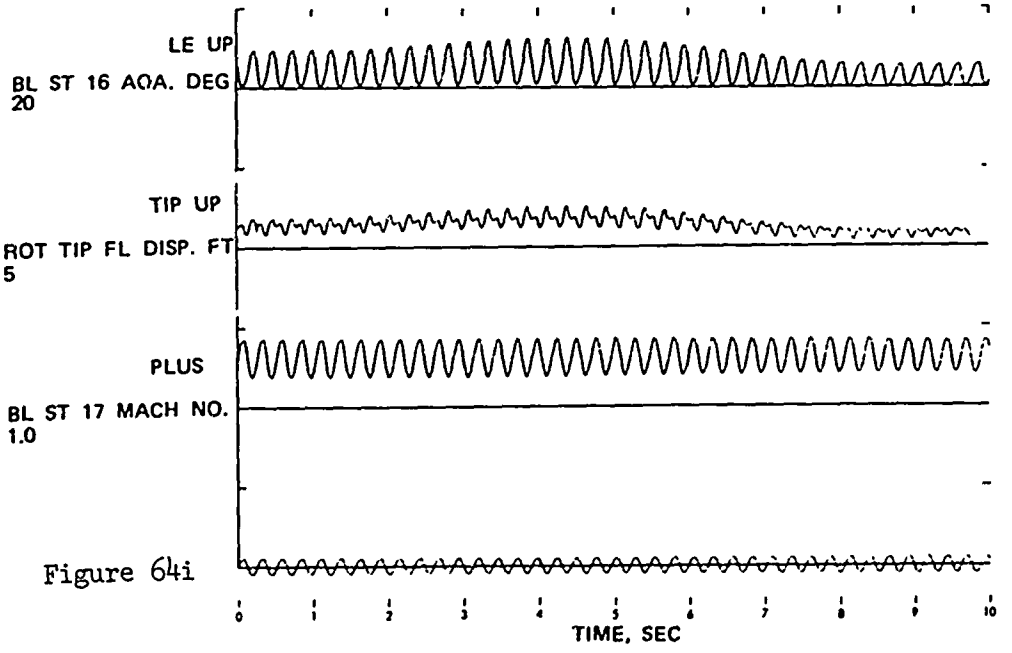

Figure 64i

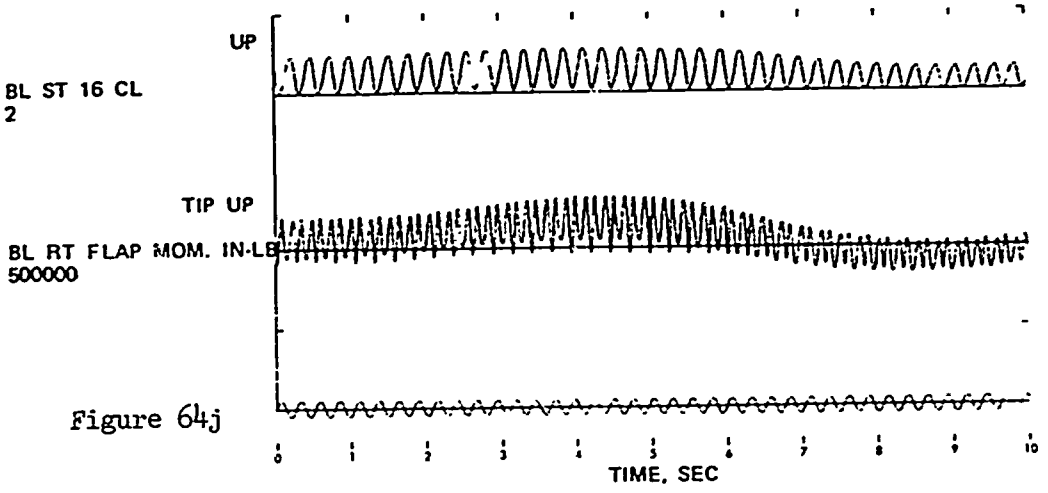

Figure 64j

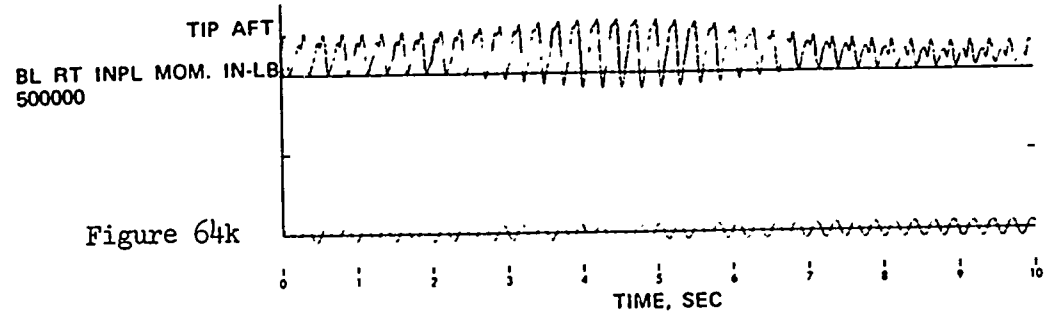

Figure 64k

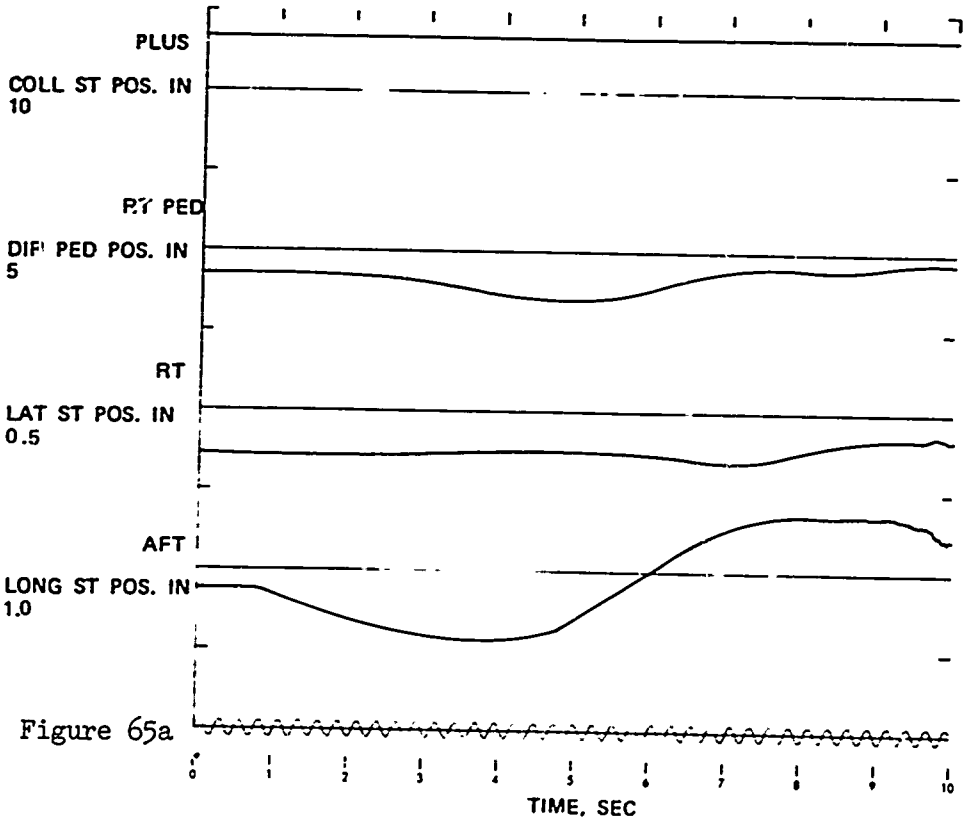

Figure 65a

Figure 65 . Time Histories Showing the Effects of Symmetrical Push-over and Pull-up: Configuration 3; Maneuver Initiated at 167 KTAS; Height Decrease .

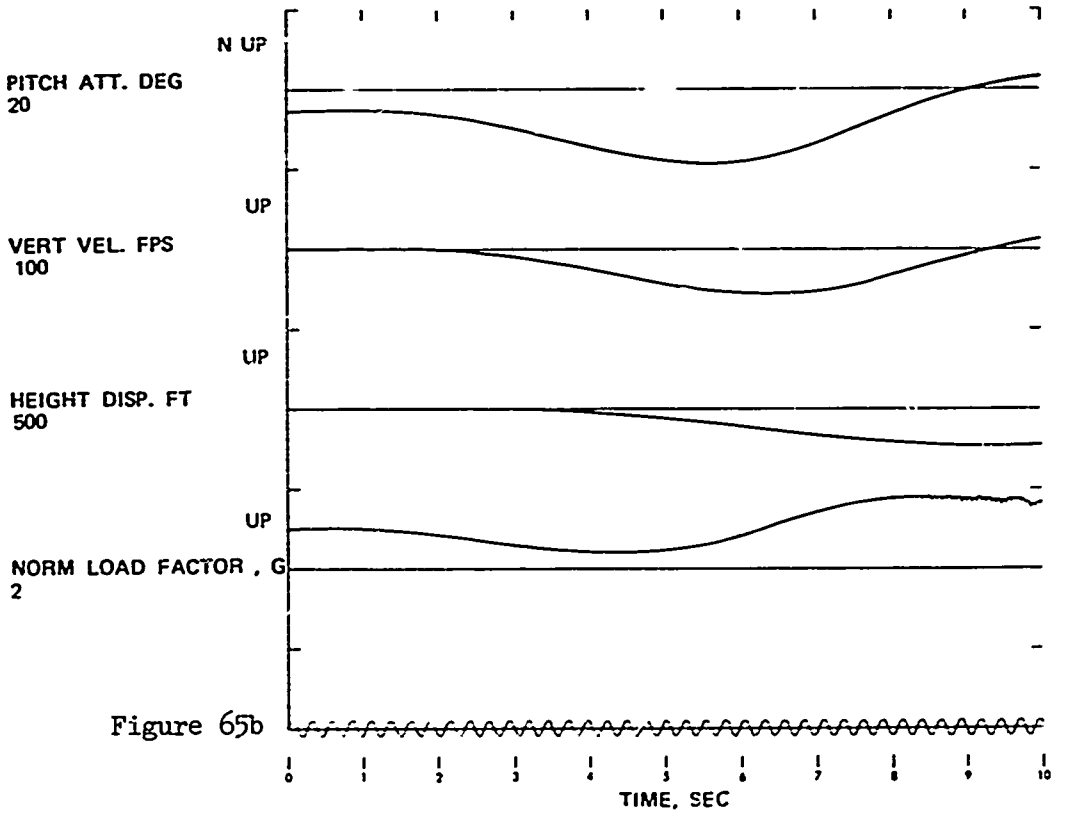

Figure 65b

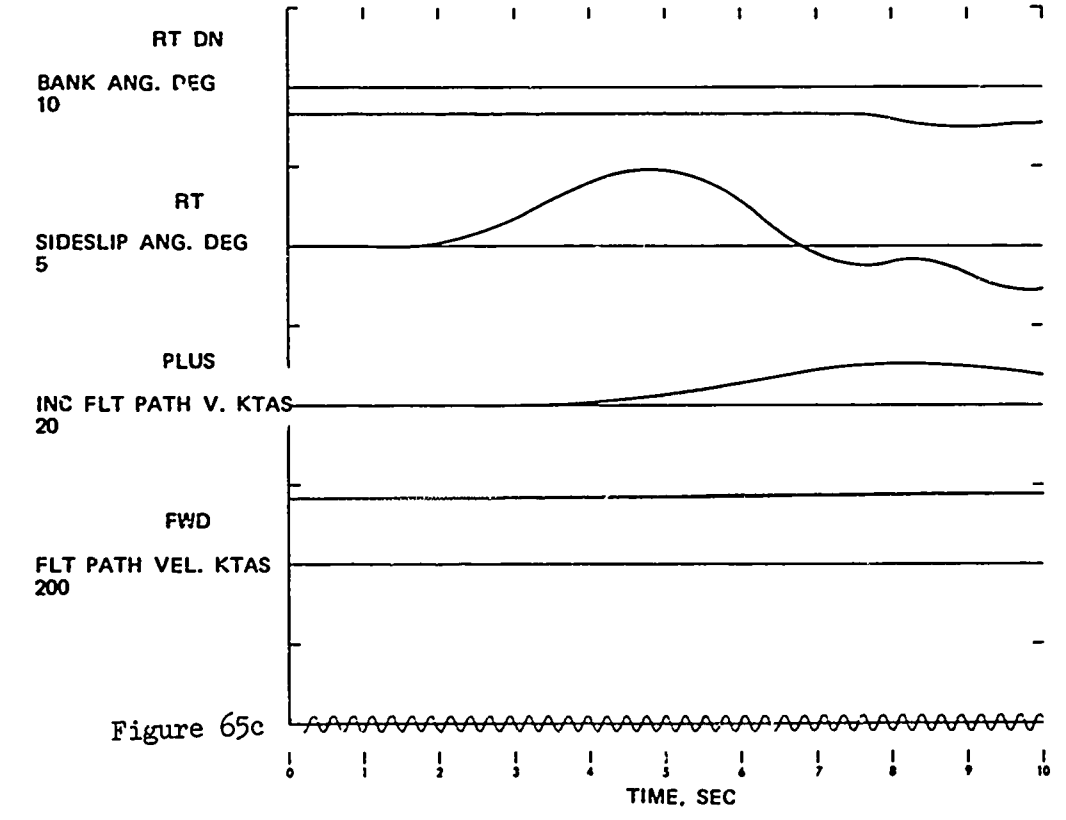

Figure 65c

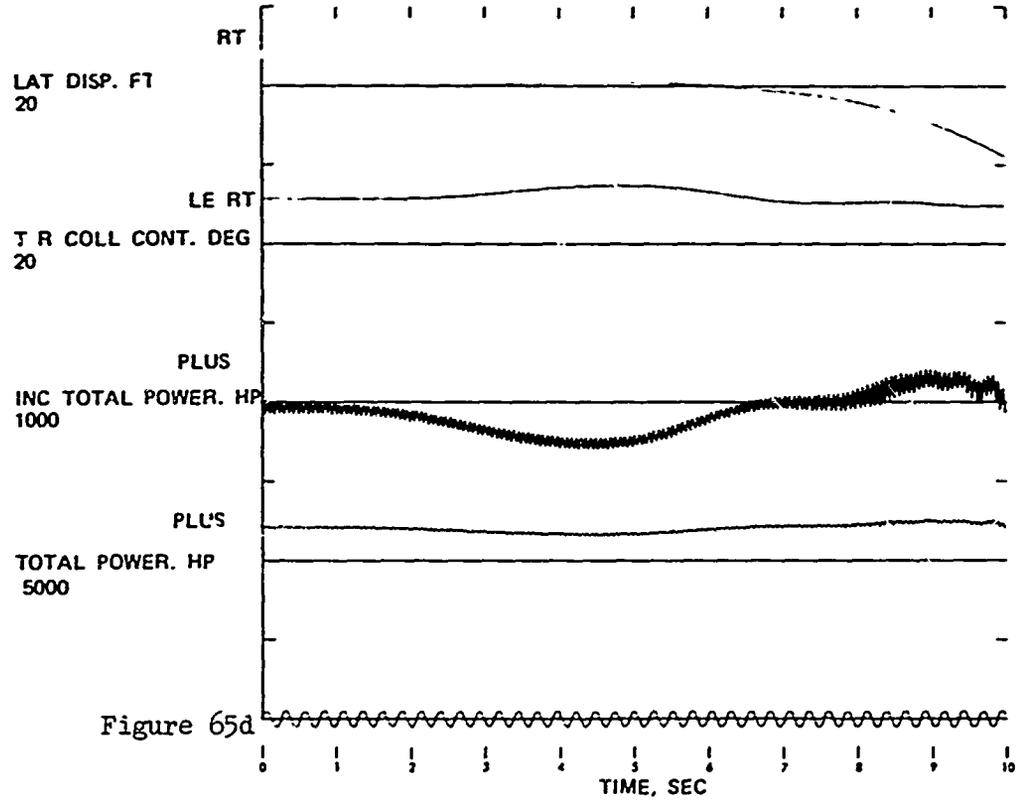

Figure 65d

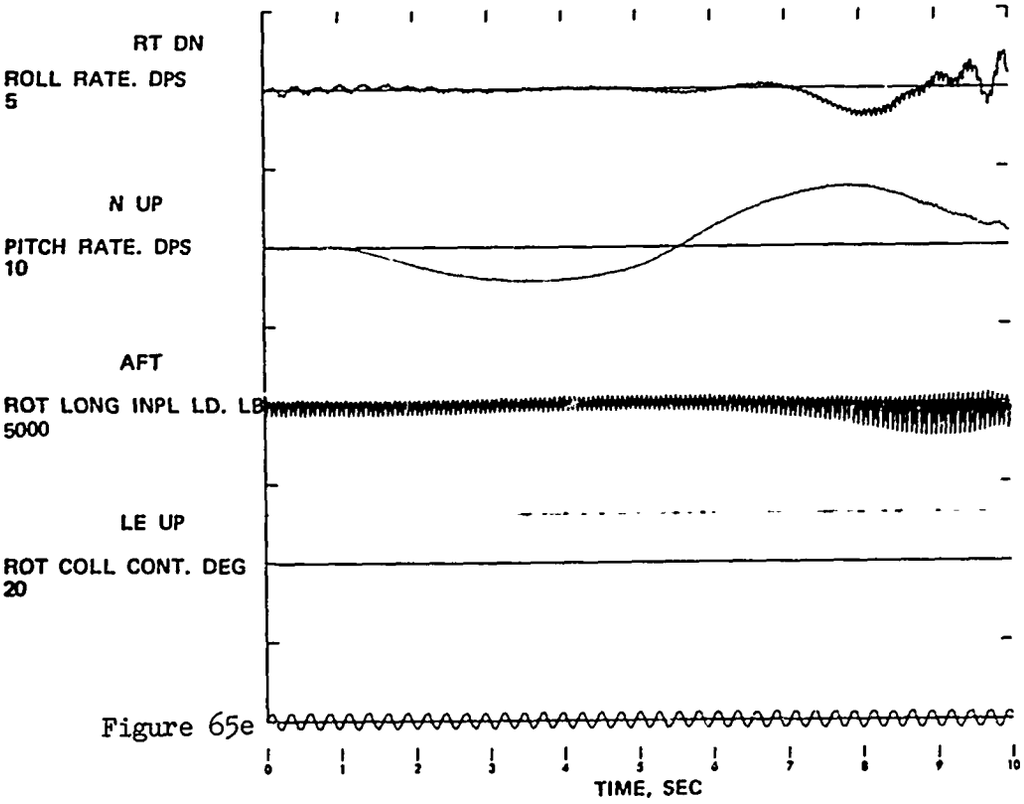

Figure 65e

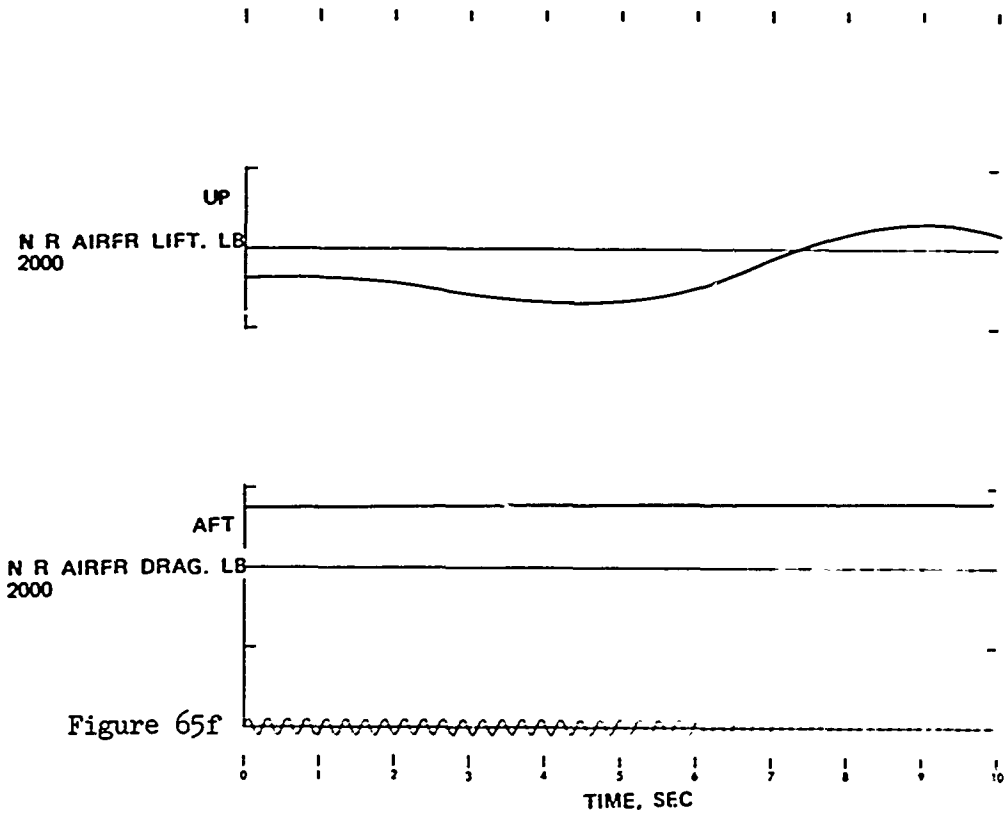

Figure 65f

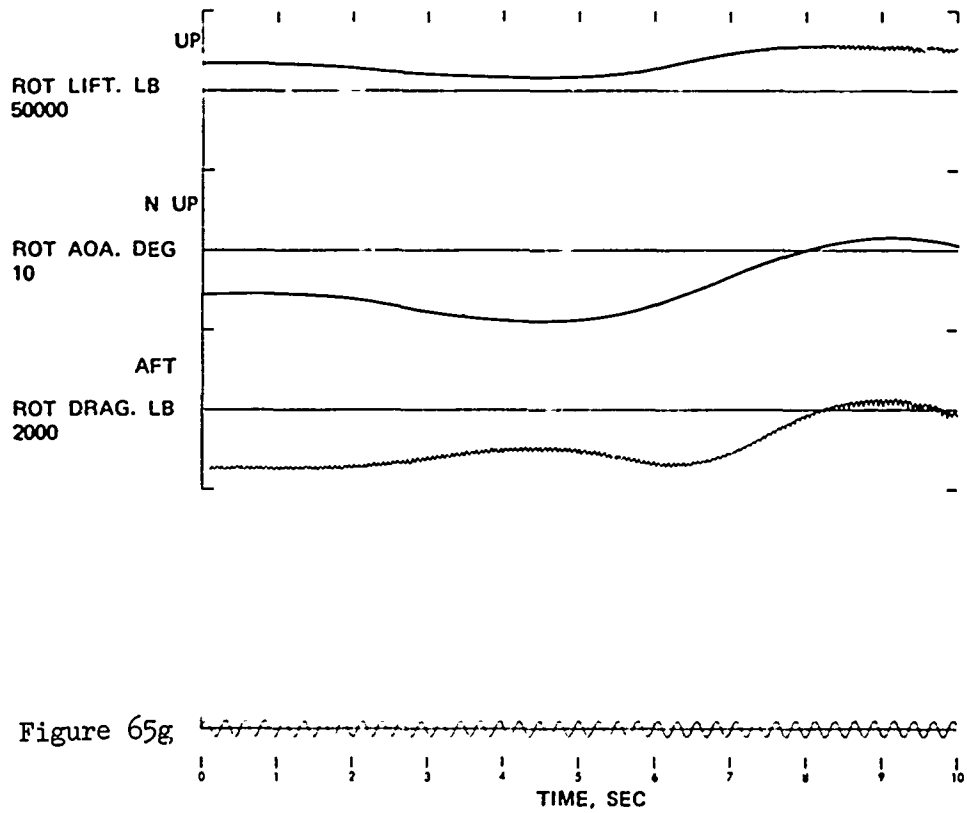

Figure 65g

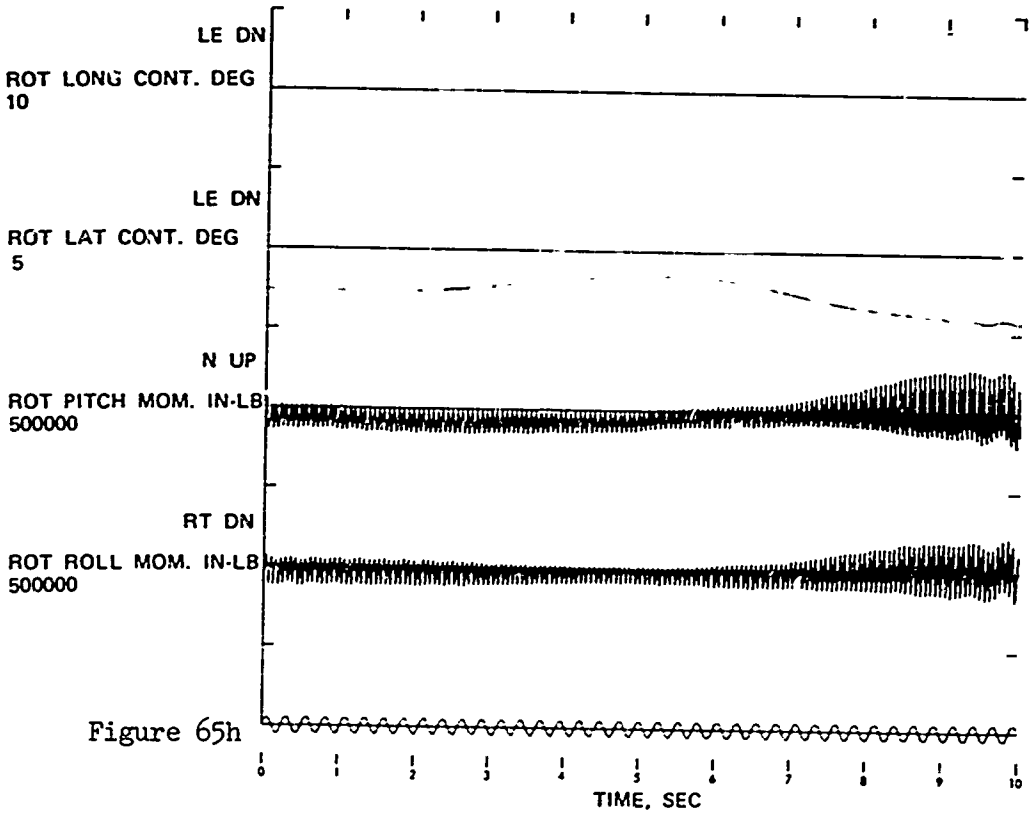

Figure 65h

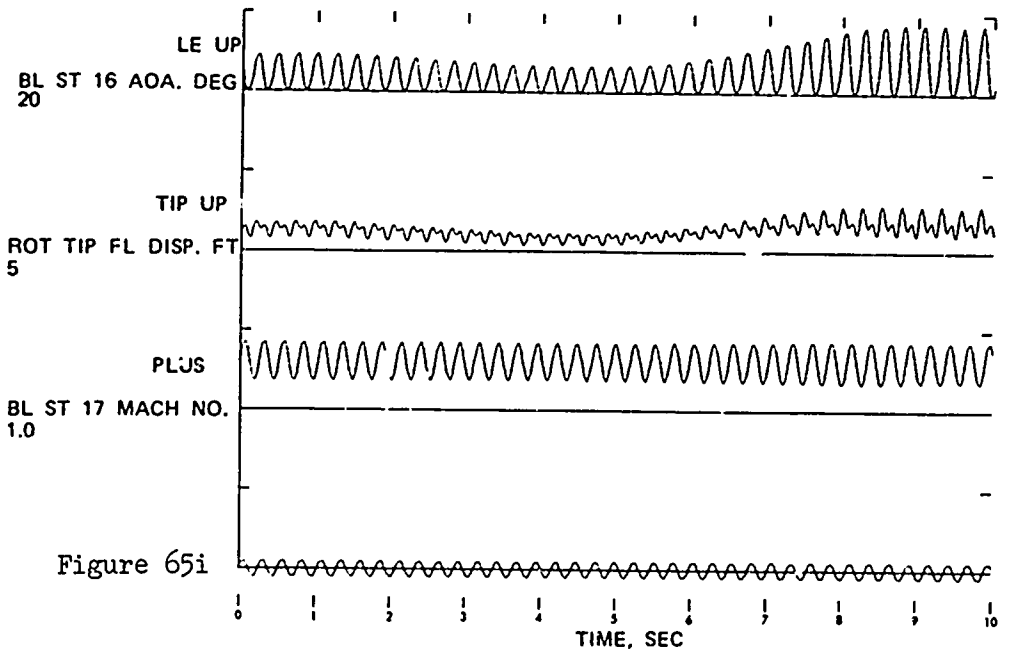

Figure 65i

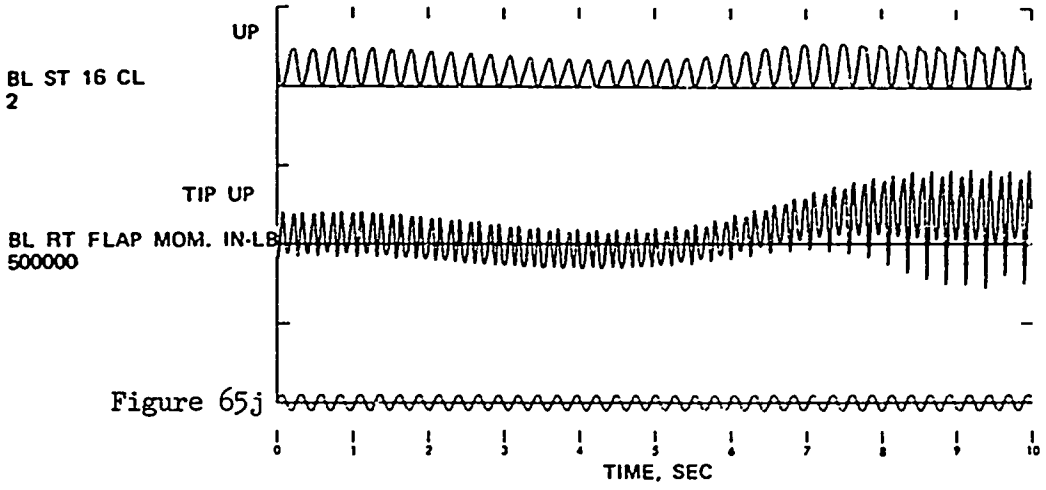

Figure 65j

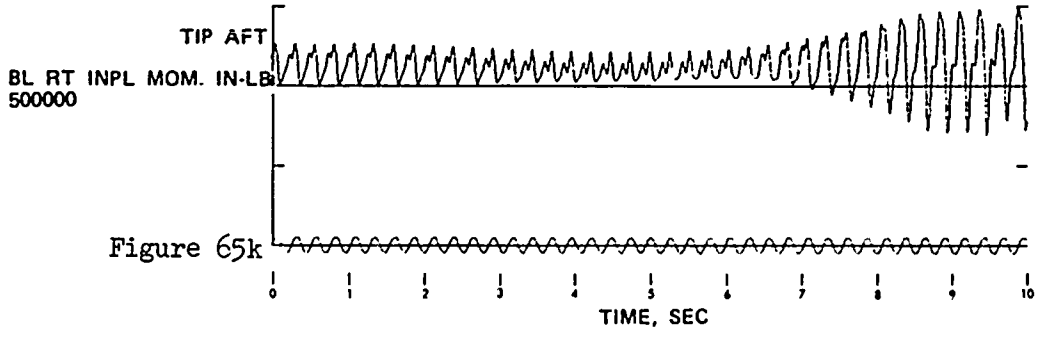

Figure 65k

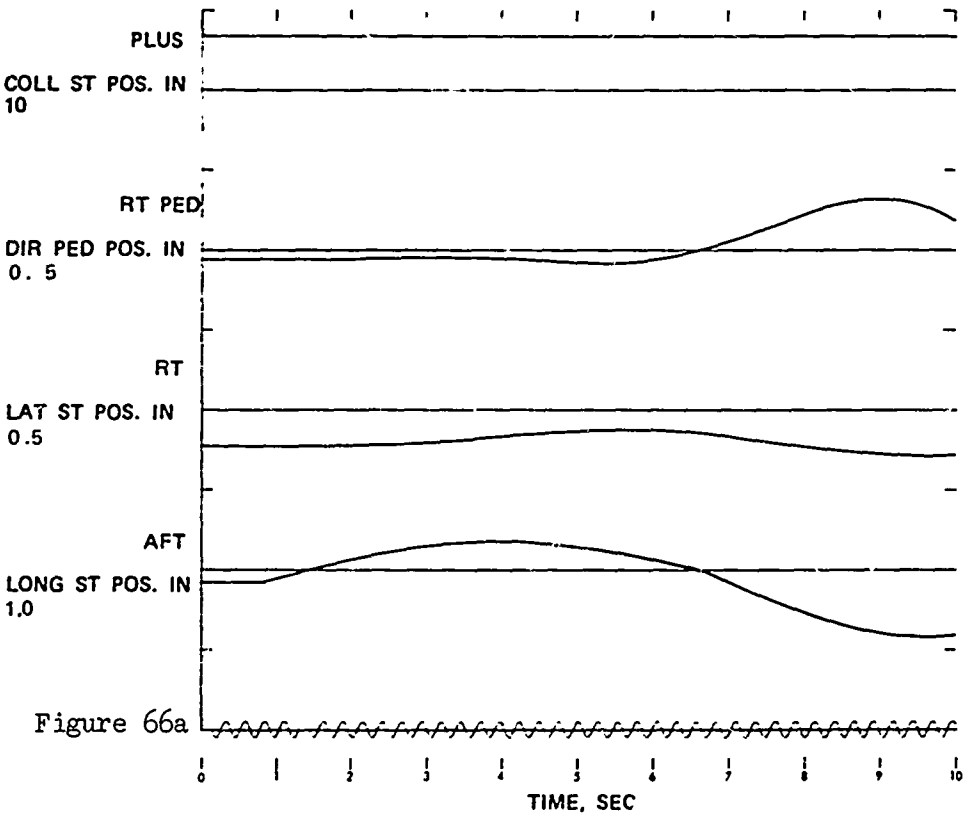

Figure 66a

Figure 66 . Time Histories Showing the Effects of Symmetrical Pull-up and Push-over: Configuration 4; Maneuver Initiated at 140 KTAS; Height Increase.

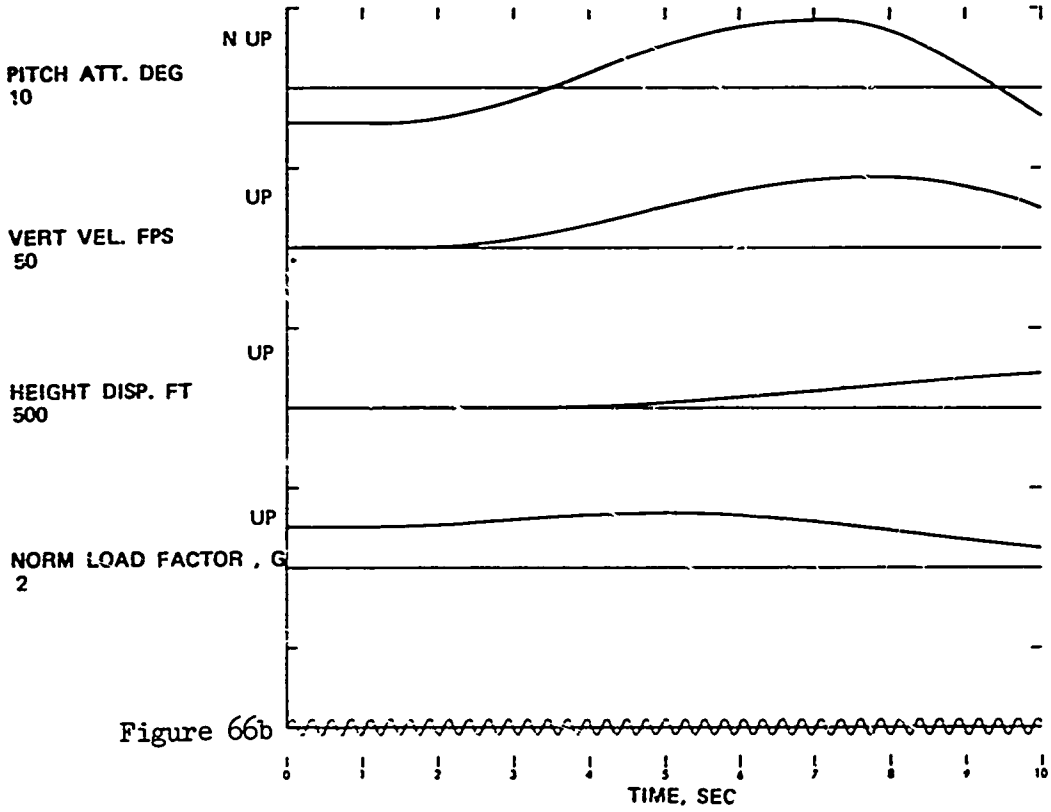

Figure 66b

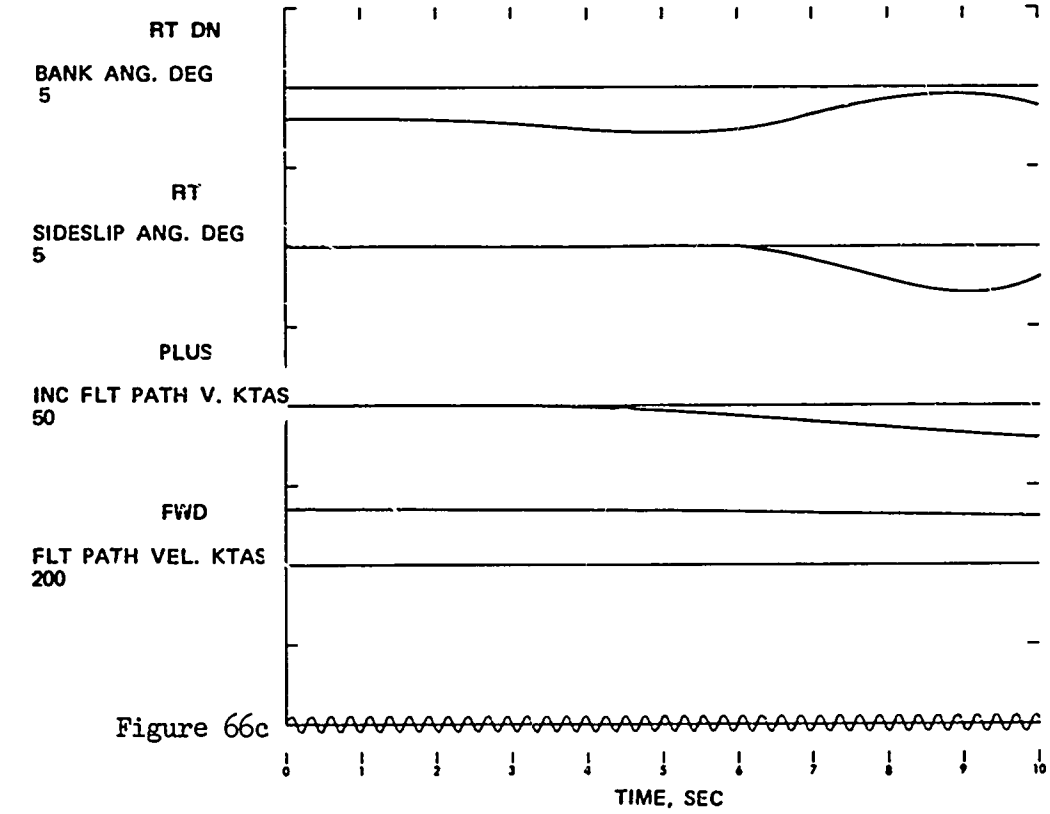

Figure 66c

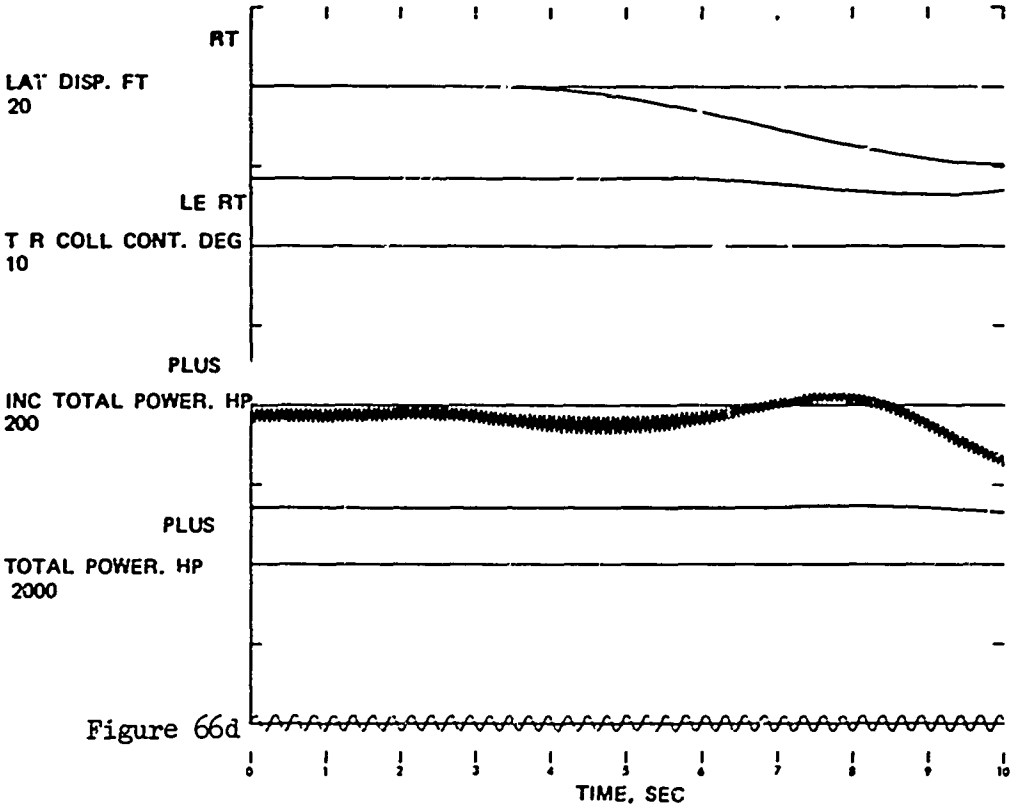

Figure 66d

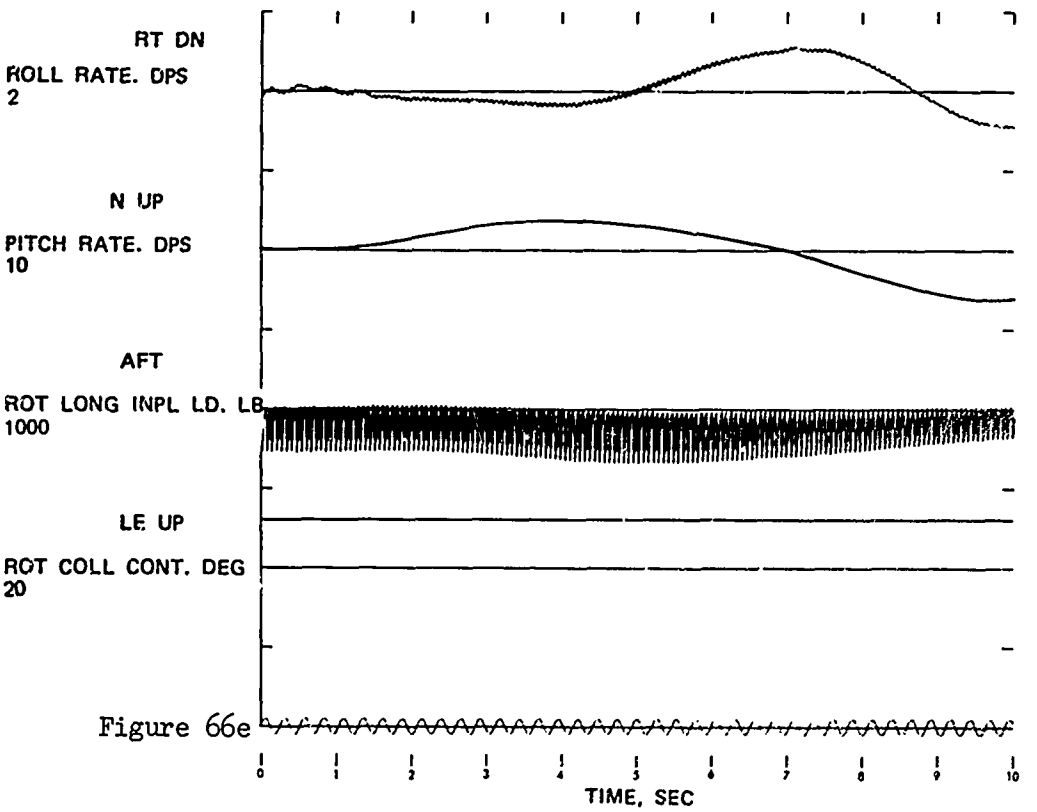

Figure 66e

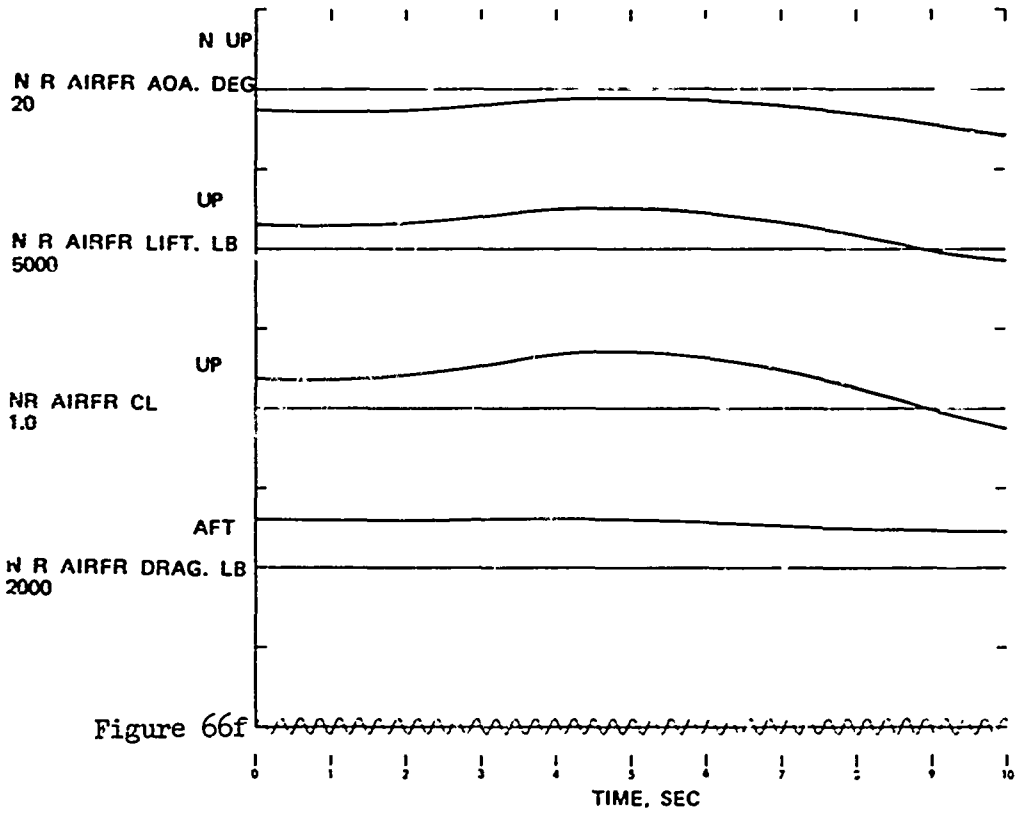

Figure 66f

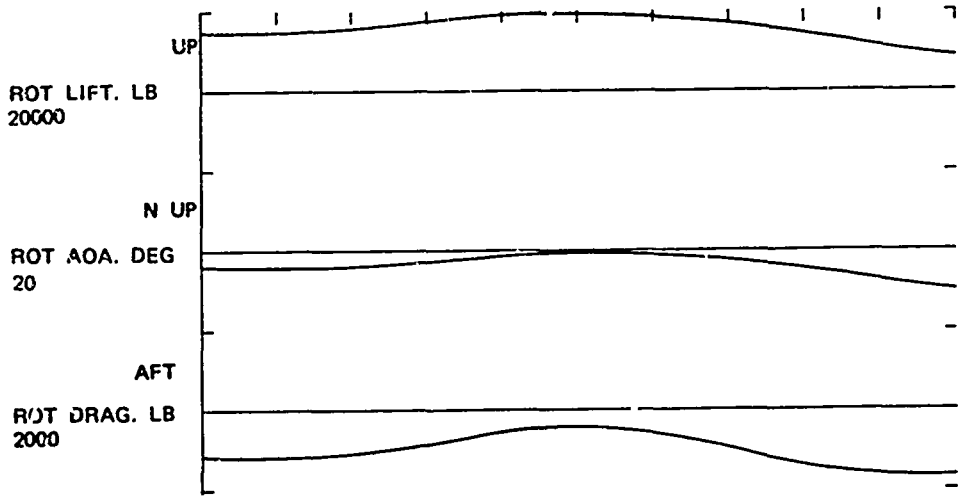

Figure 66g

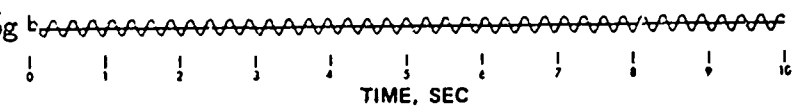

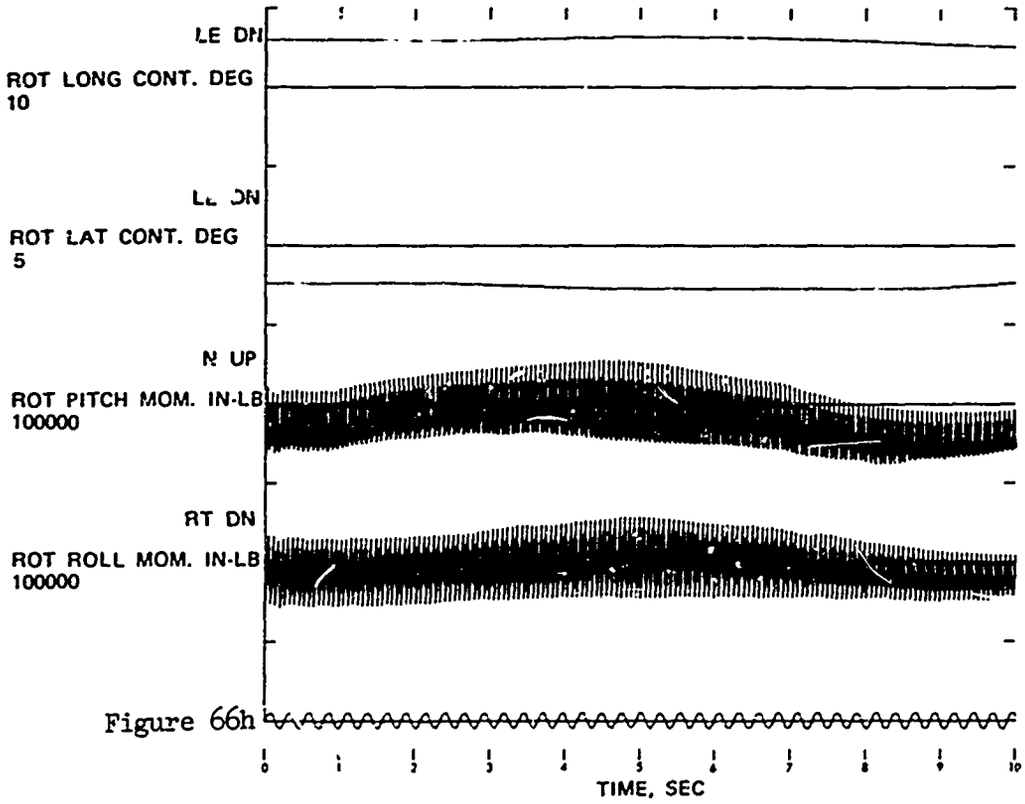

Figure 66h

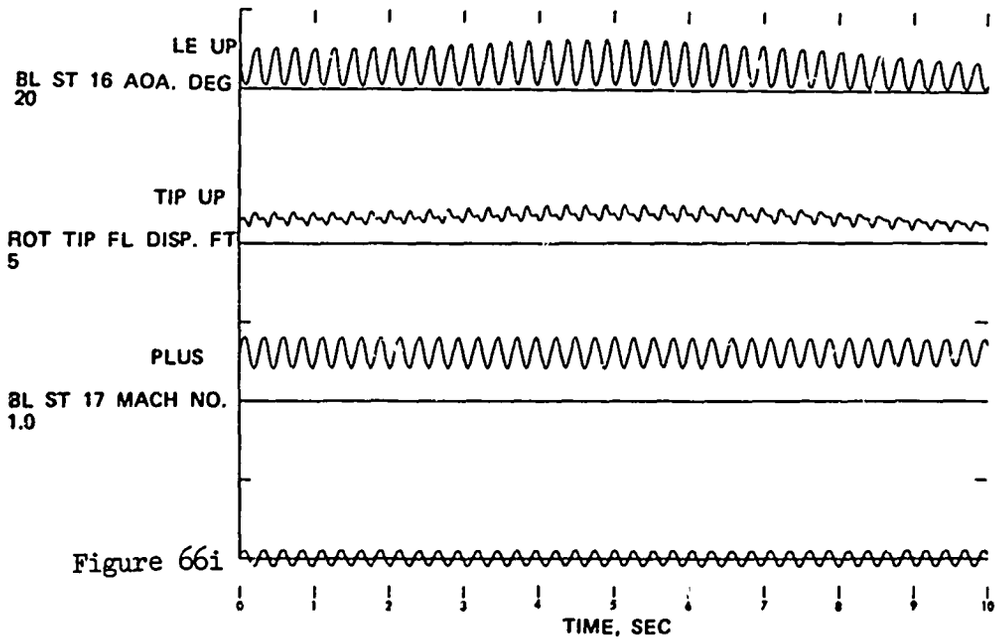

Figure 66i

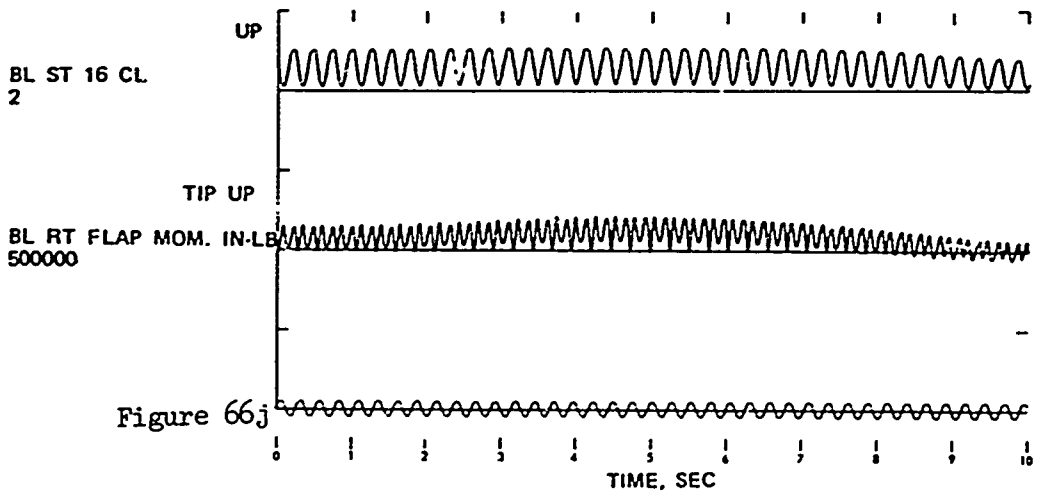

Figure 66j

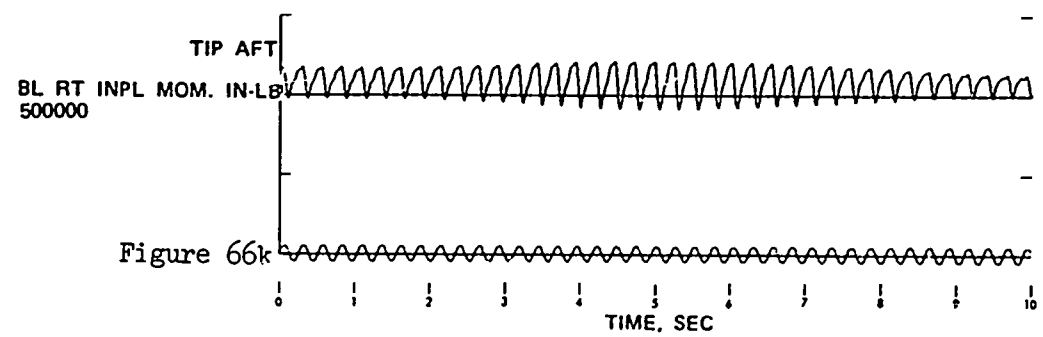

Figure 66k

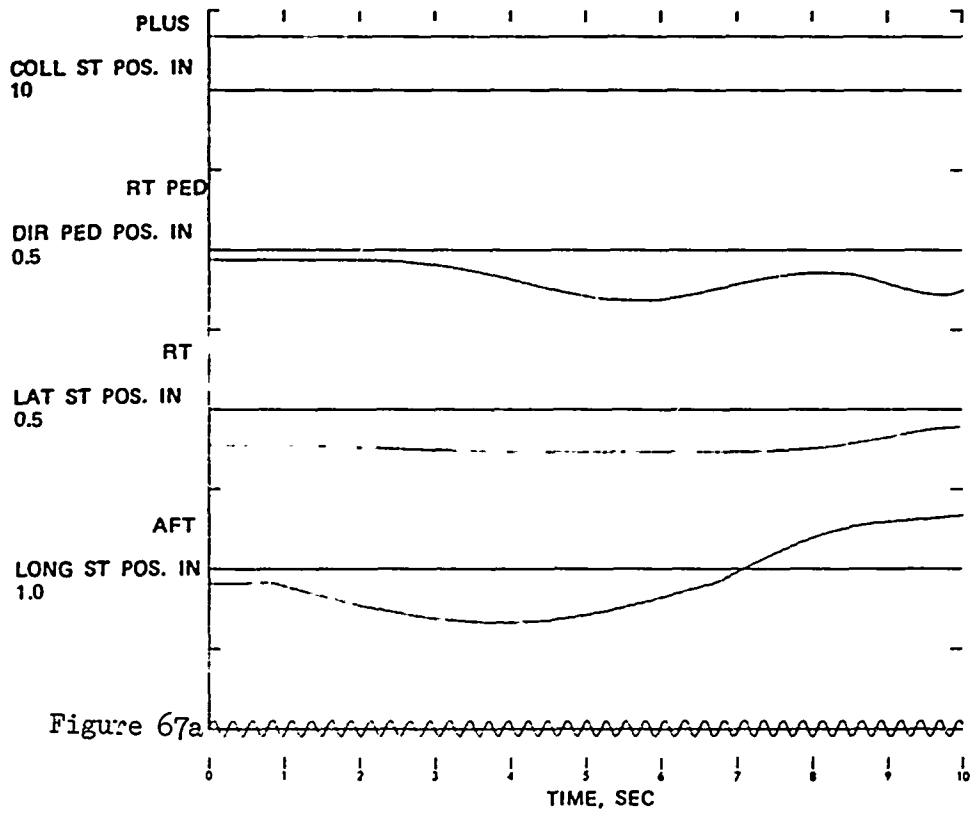

Figure 67a

Figure 67 . Time Histories Showing the Effects of Symmetrical Push-over and Pull-up: Configuration 4; Maneuver Initiated at 140 KTAS; Height Decrease .

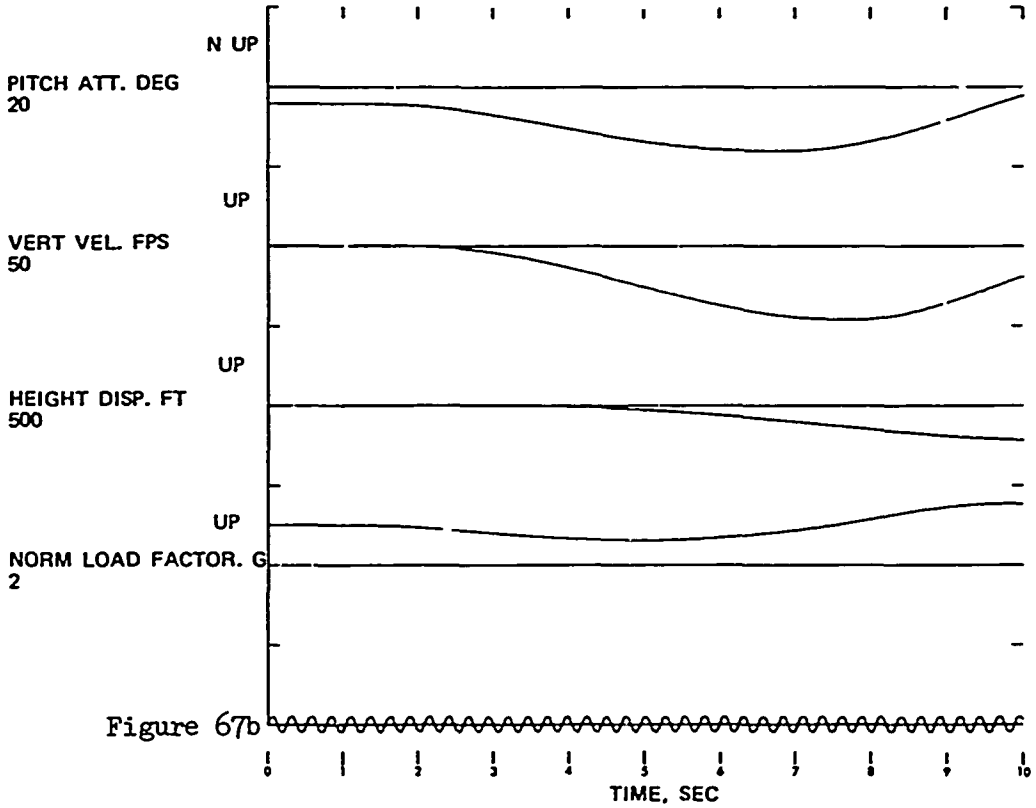

Figure 67b

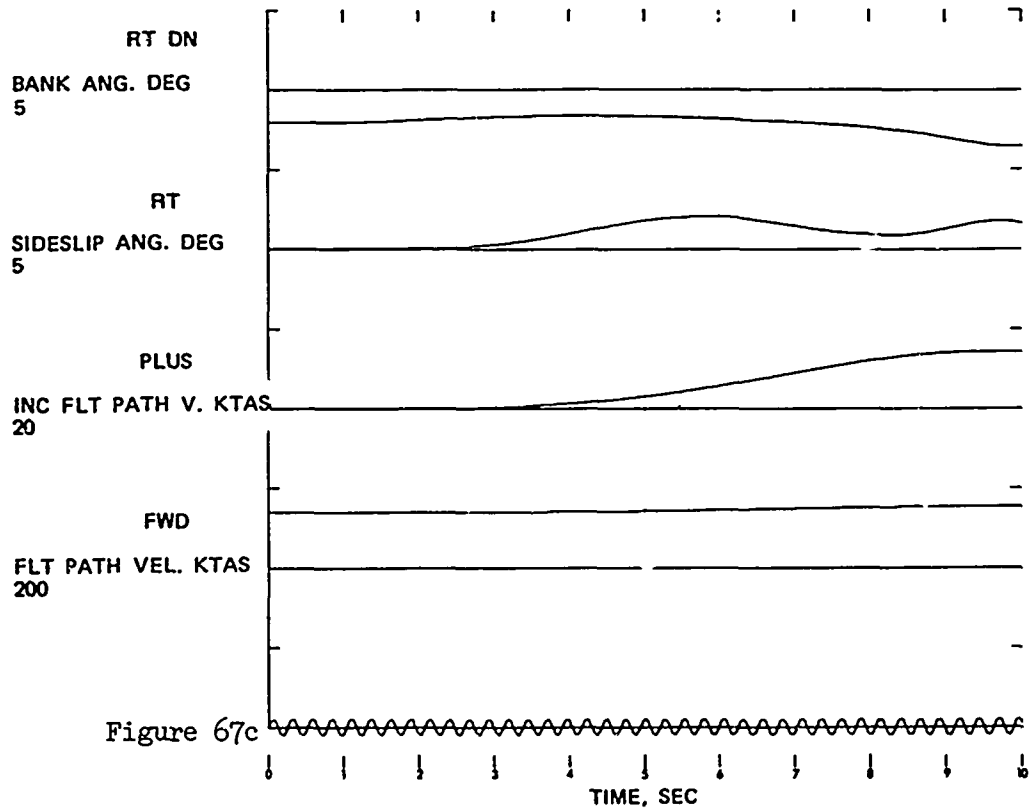

Figure 67c

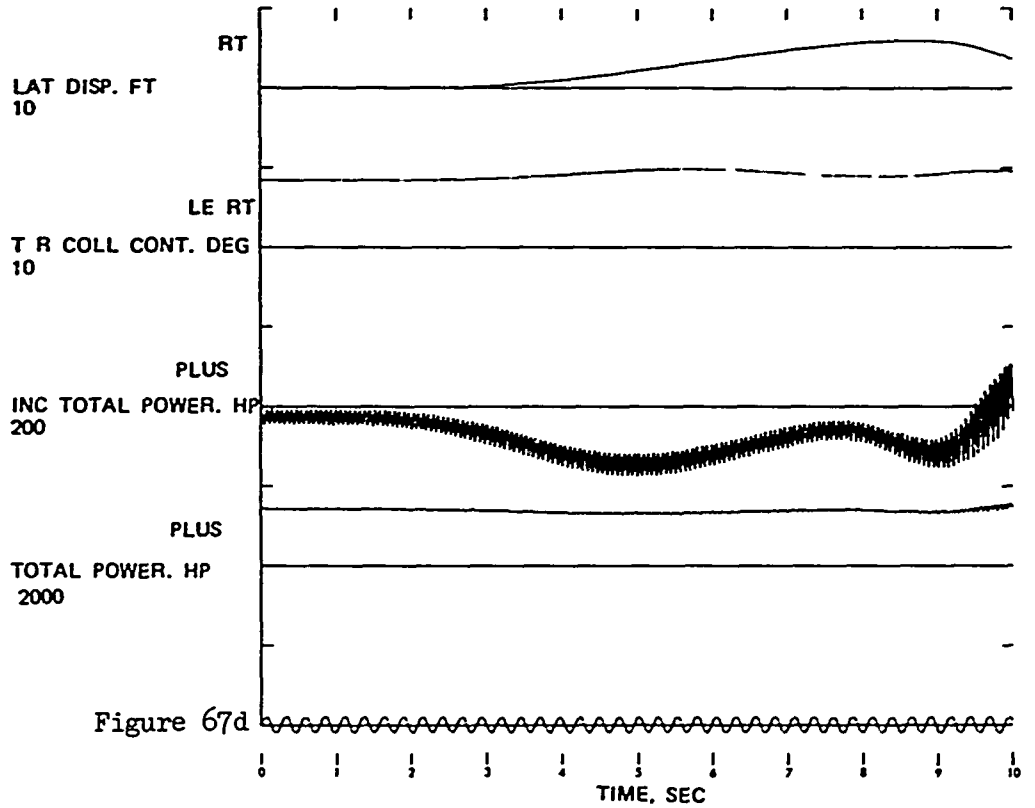

Figure 67d

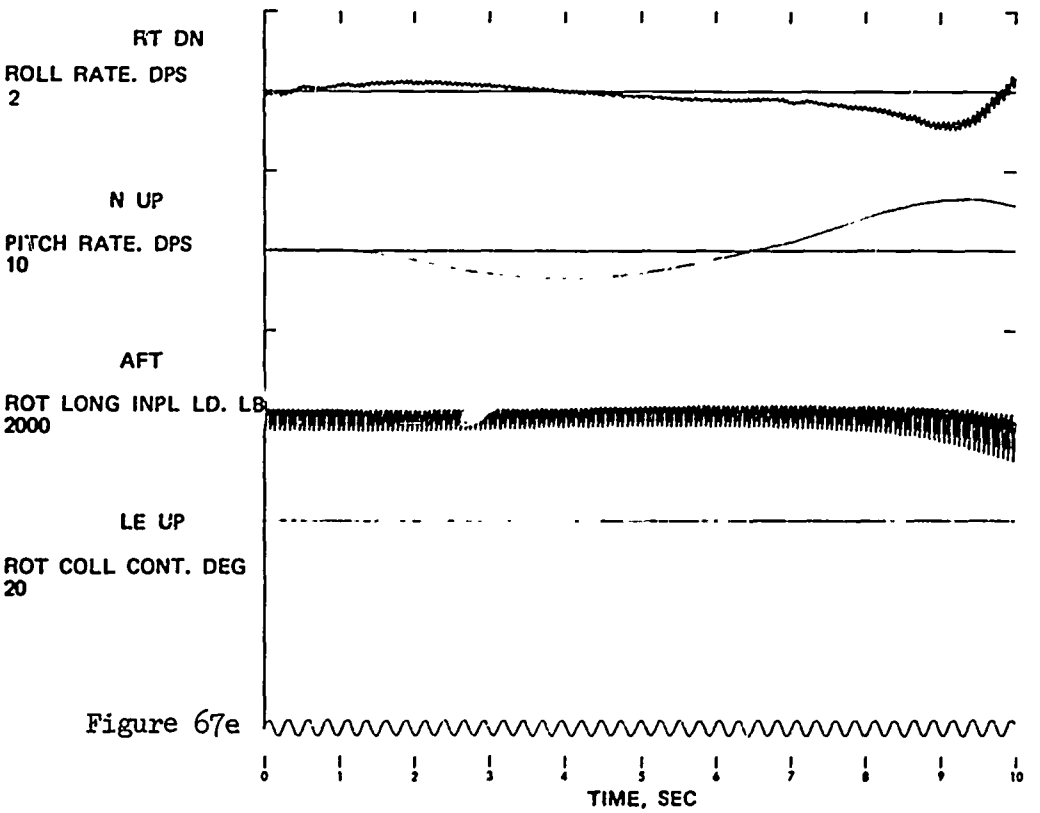

Figure 67e

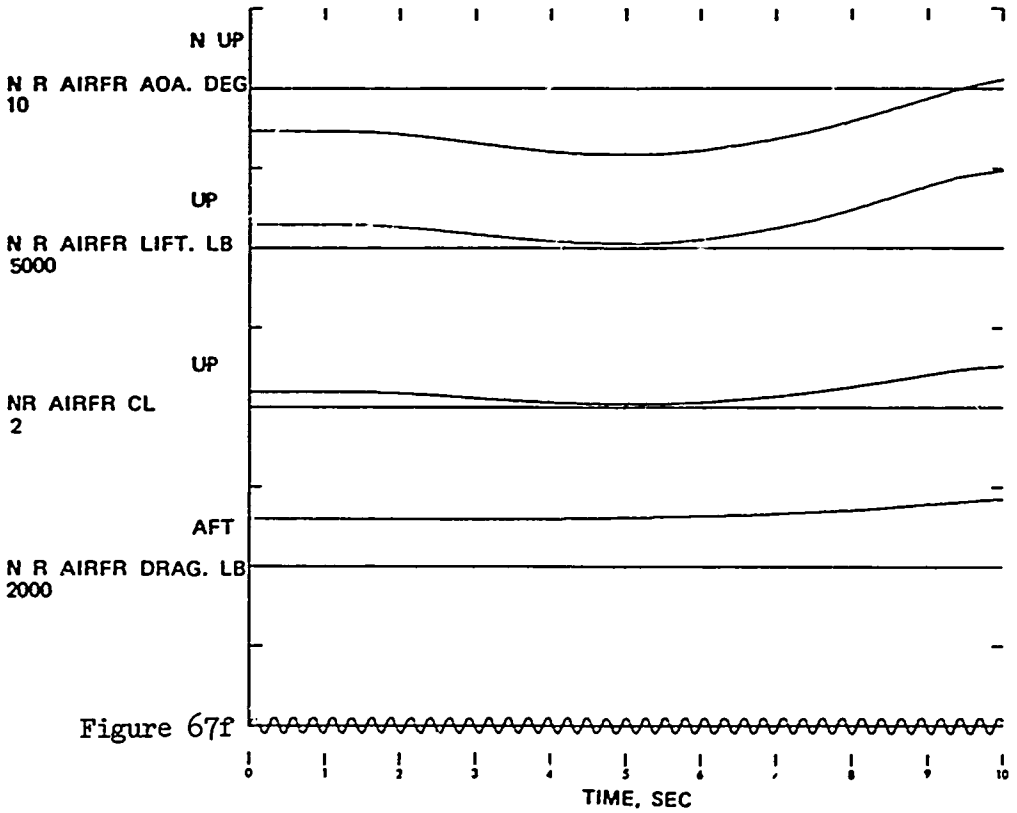

Figure 67f

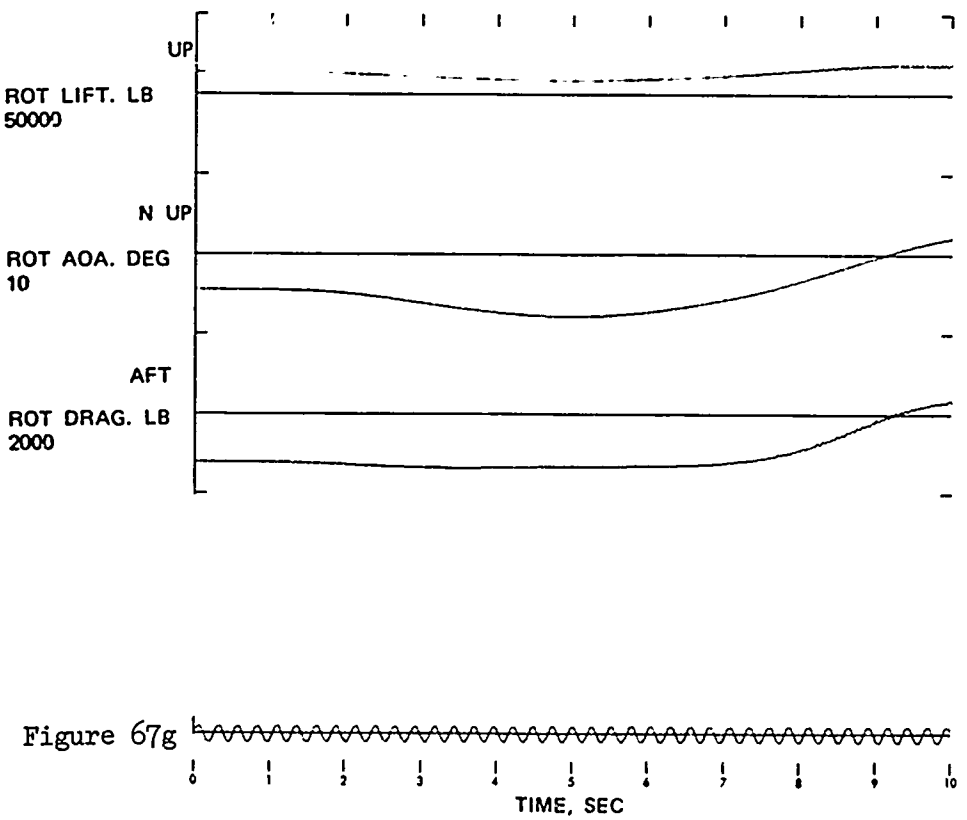

Figure 67g

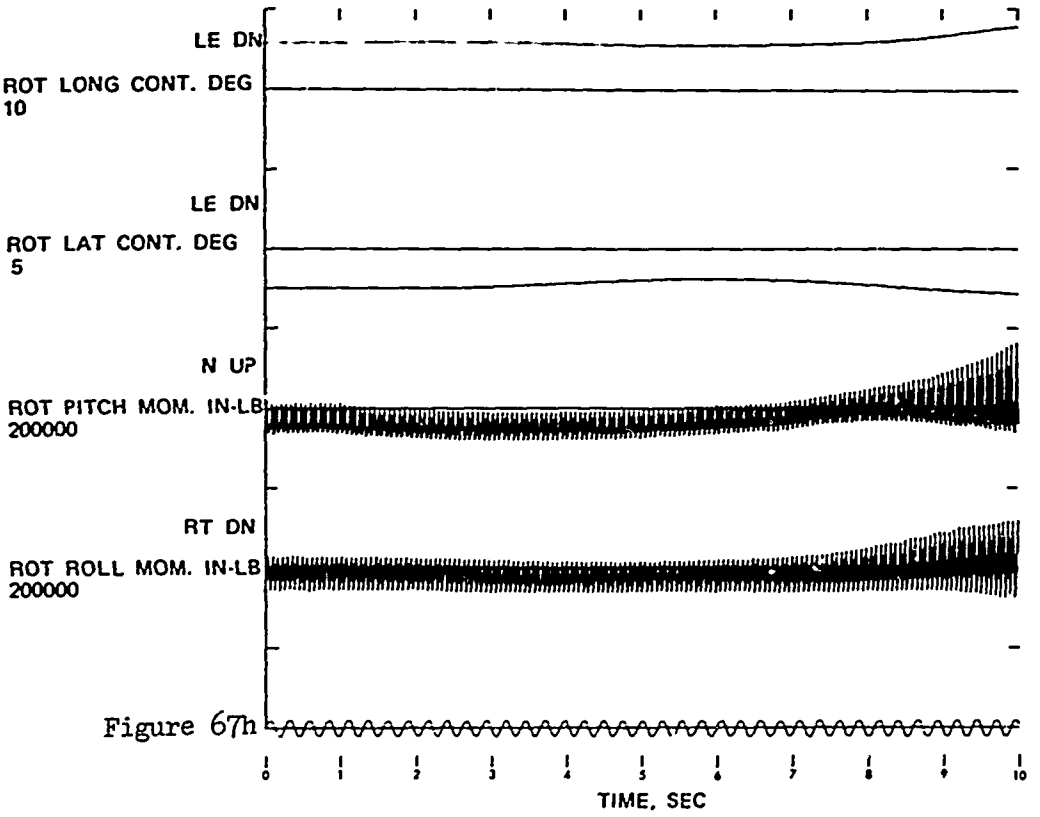

Figure 67h

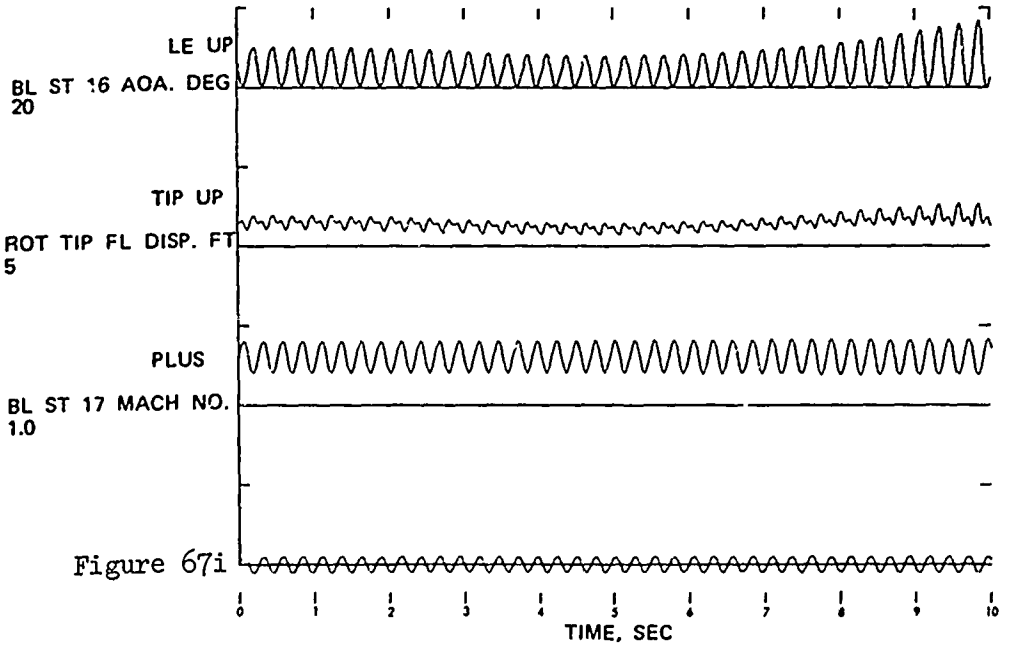

Figure 67i

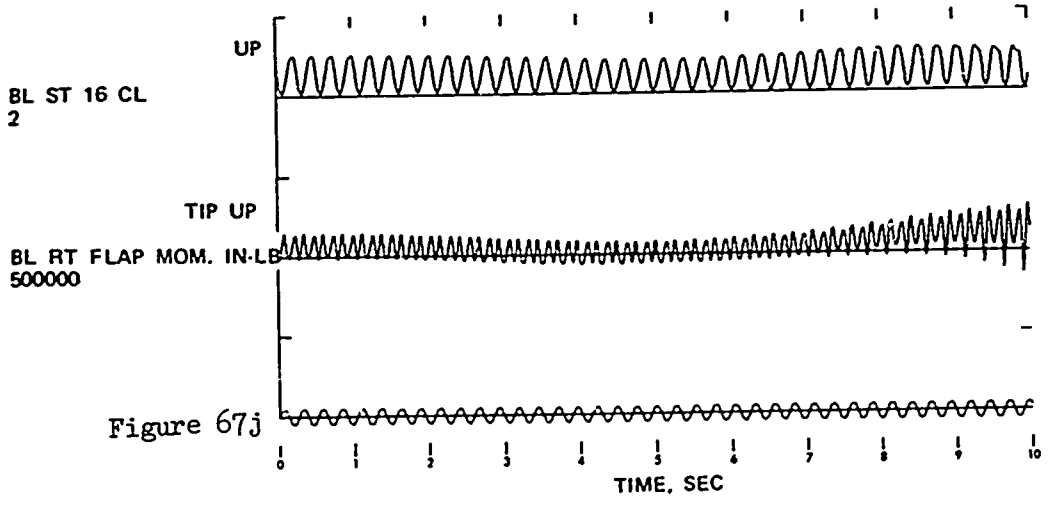

Figure 67j

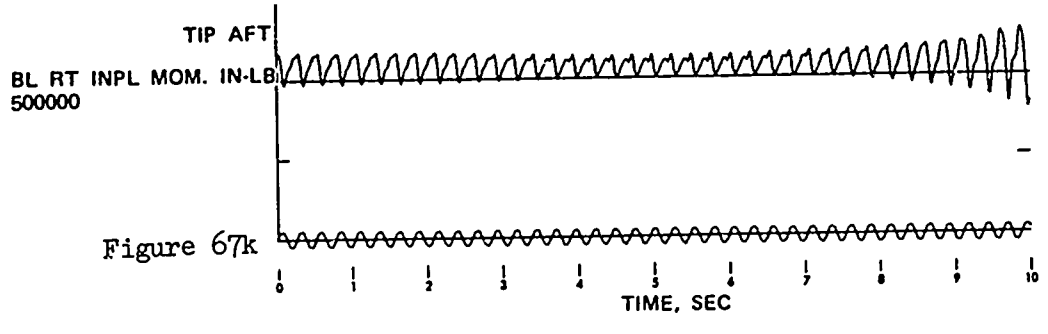

Figure 67k

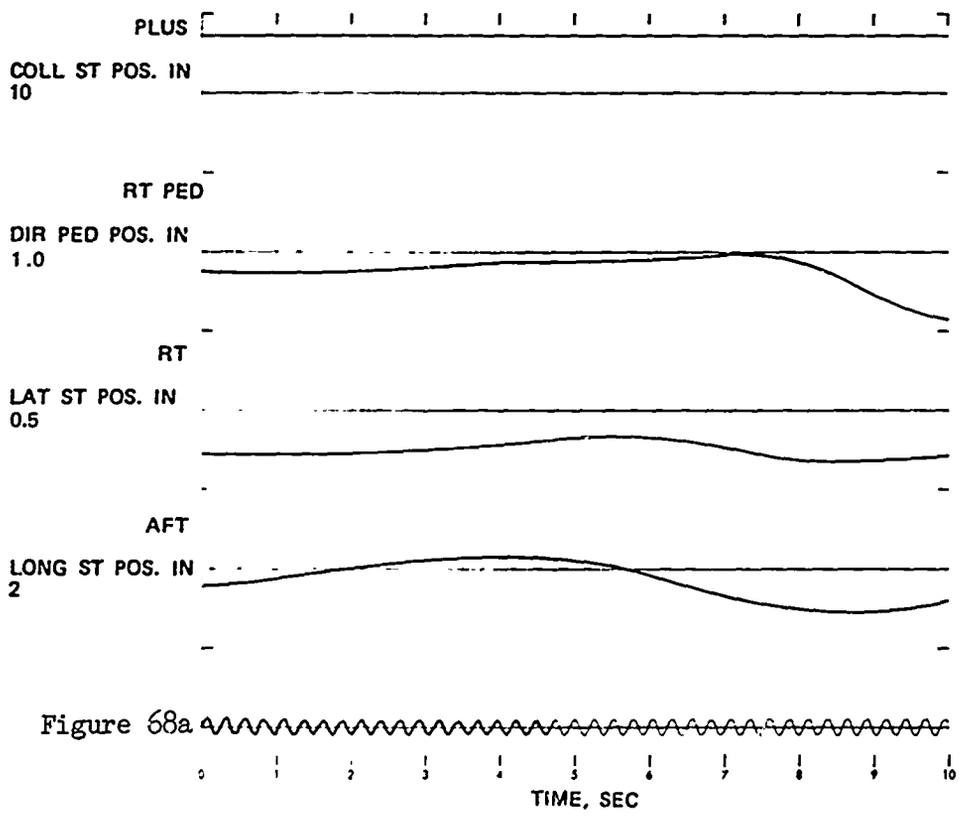

Figure 68a

Figure 68. Time Histories Showing the Effects of Symmetrical Pull-up and Push-over: Configuration 5; Maneuver Initiated at 155 KTAS; Height Increase.

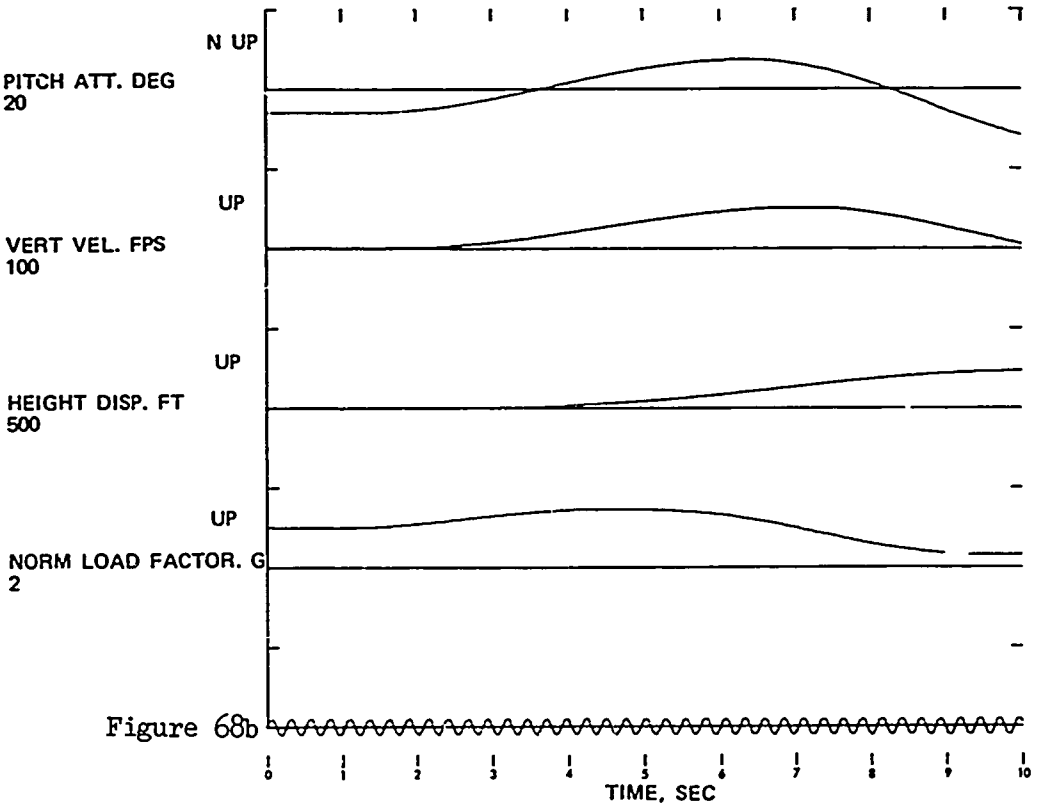

Figure 68b

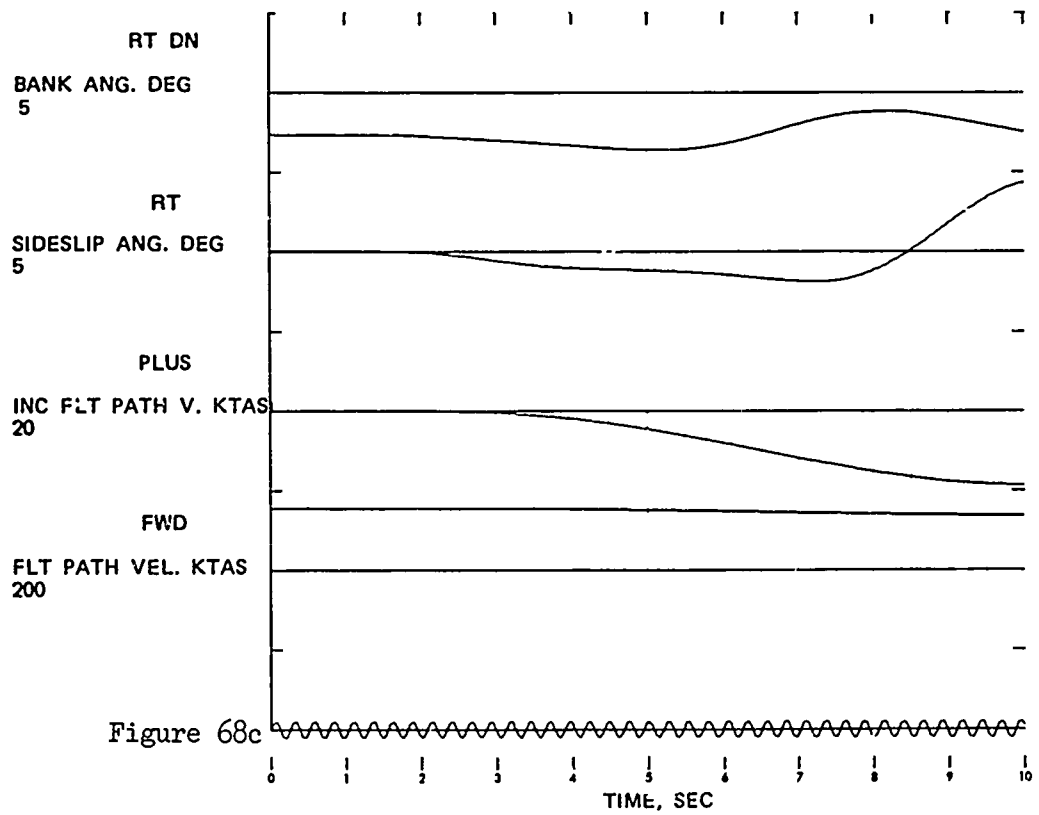

Figure 68c

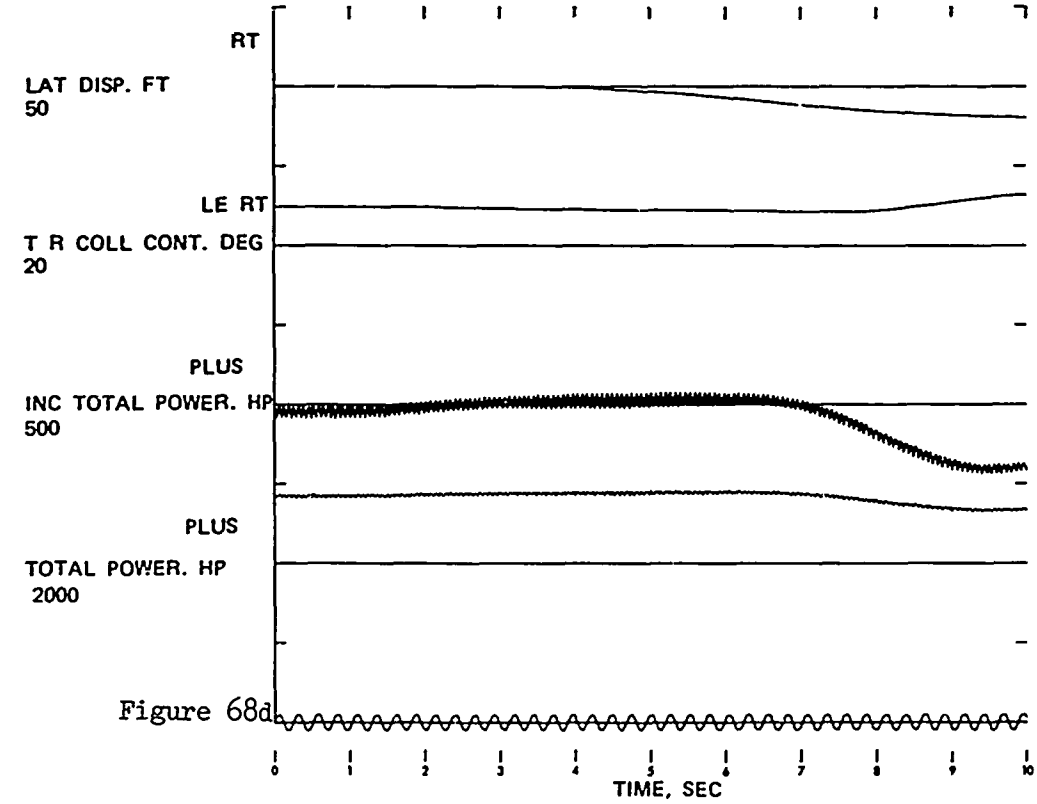

Figure 68d

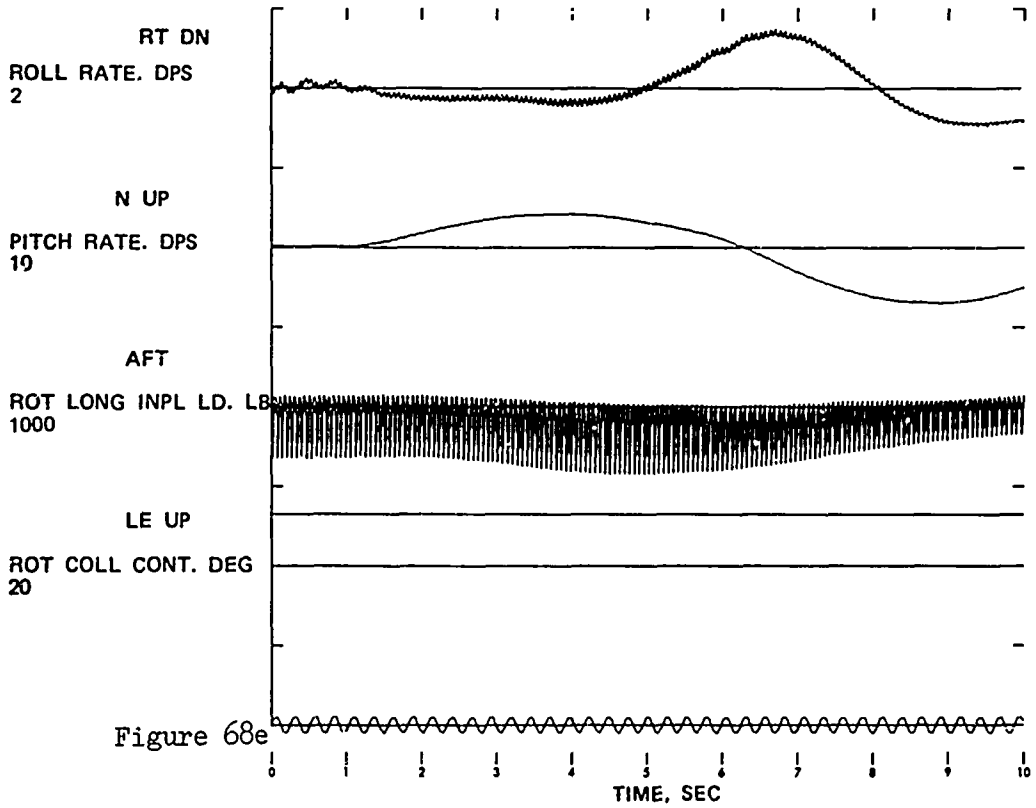

Figure 68e

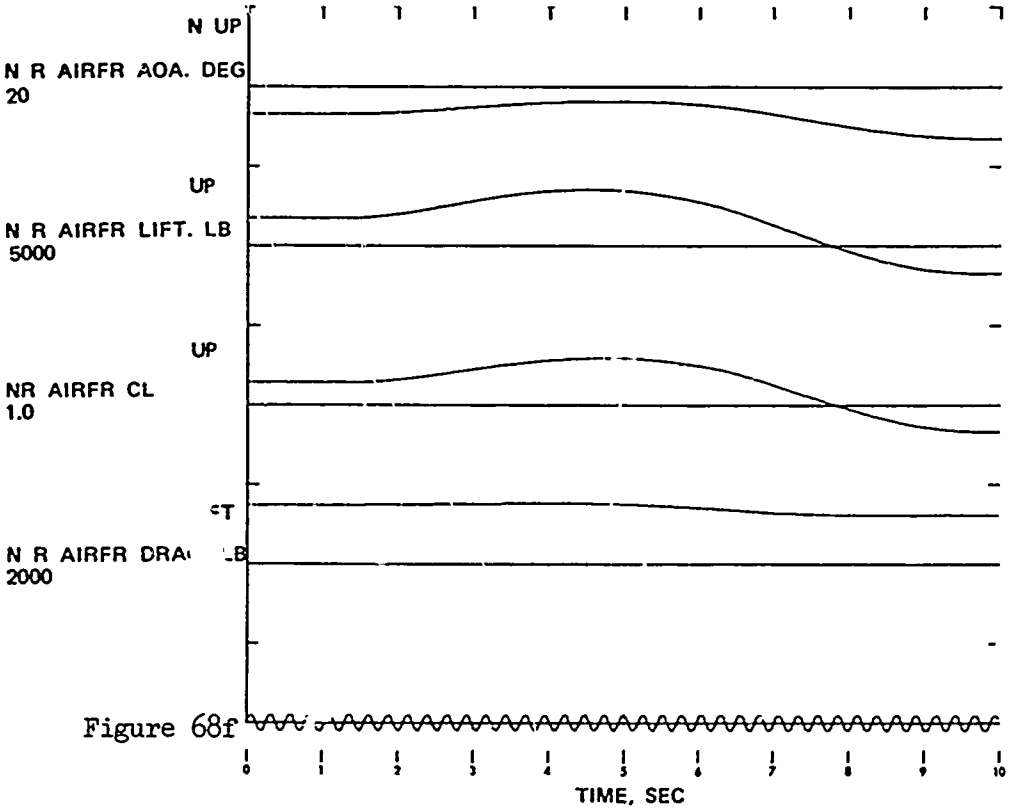

Figure 68f

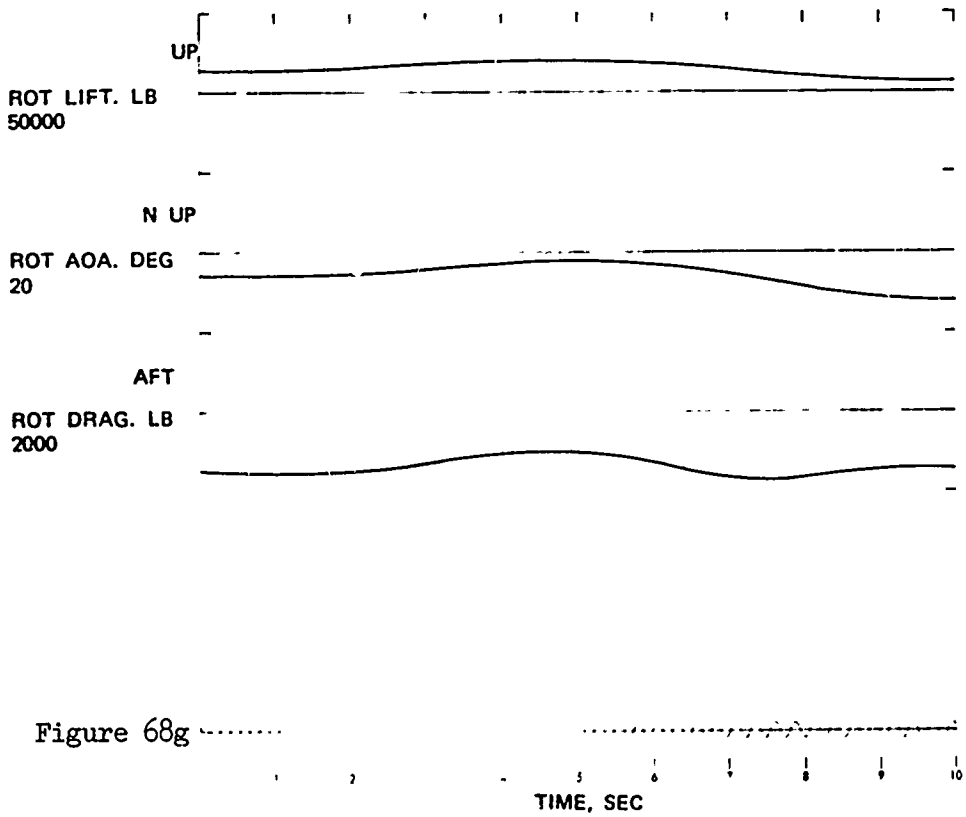

Figure 68g

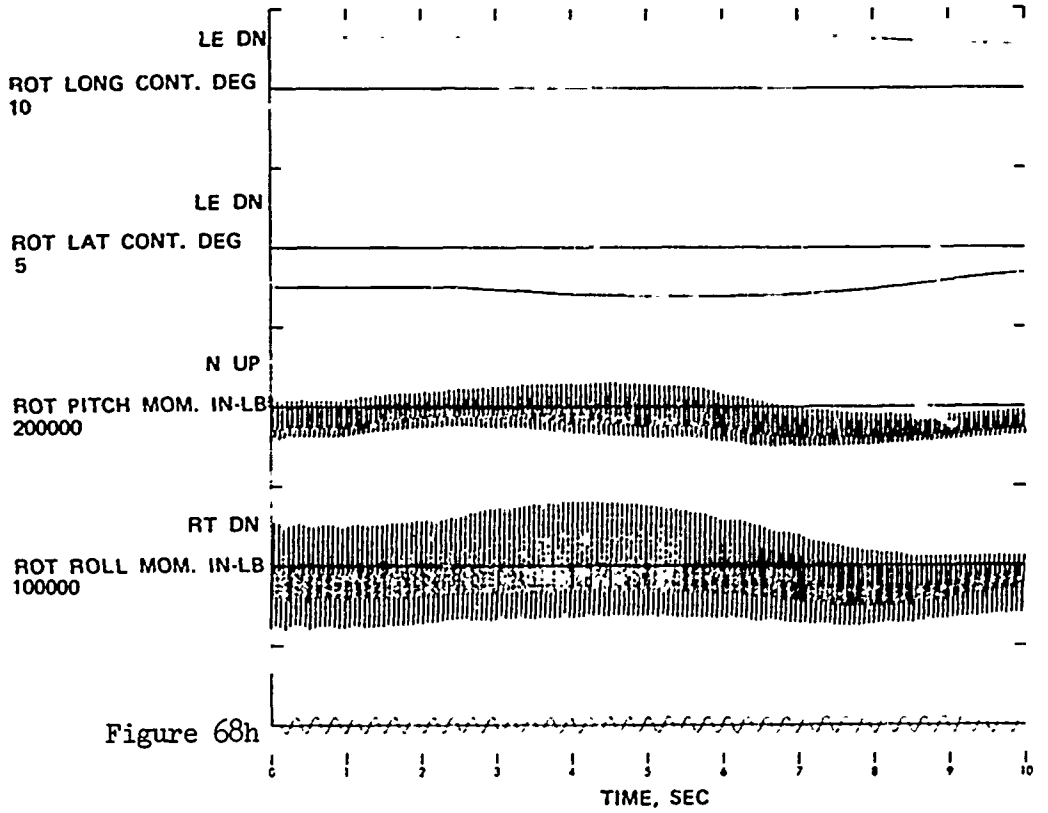

Figure 68h

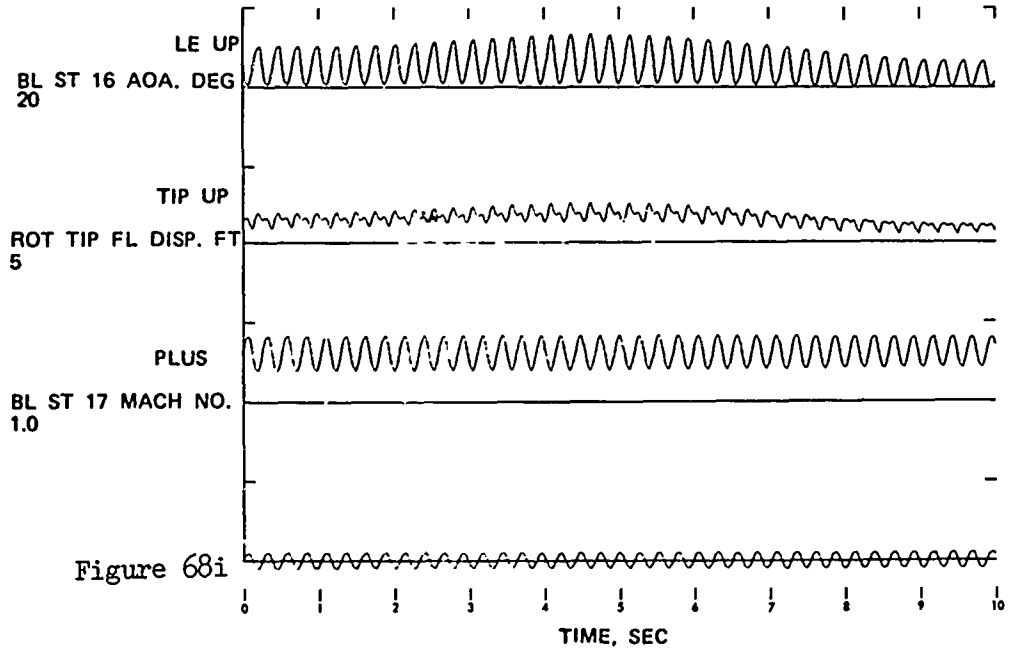

Figure 68i

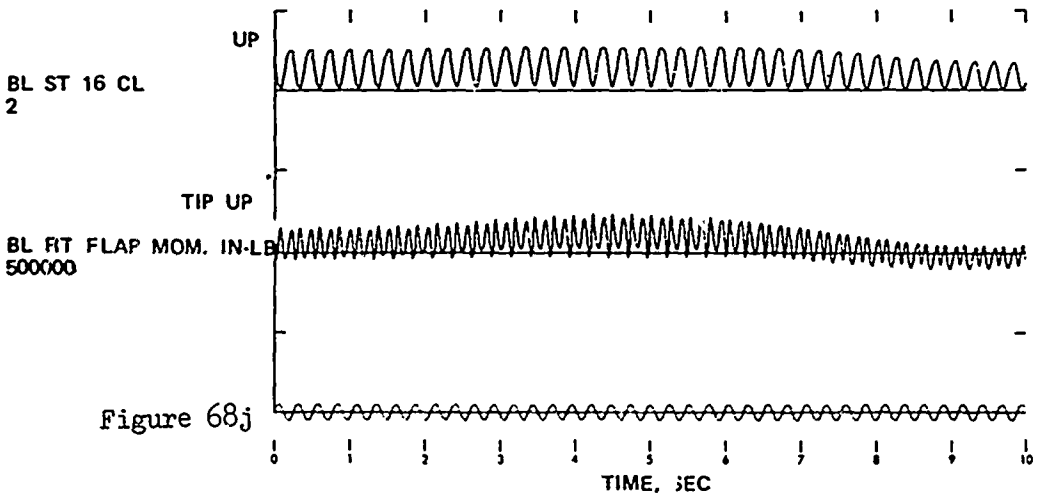

Figure 68j

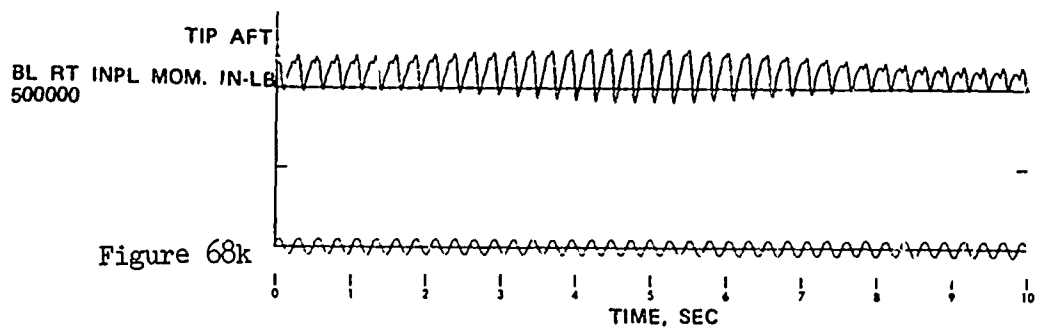

Figure 68k

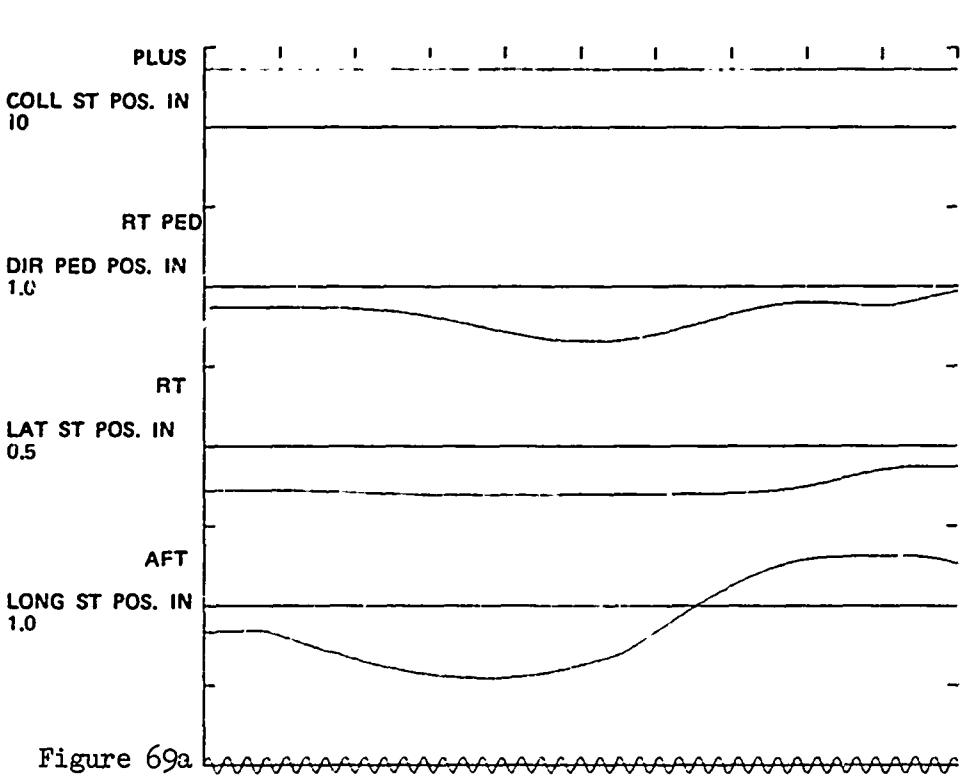

Figure 69a

Figure 69 . Time Histories Showing the Effects of Symmetrical Push-over and Pull-up: Configuration 5; Maneuver Initiated at 155 KTAS; Height Decrease.

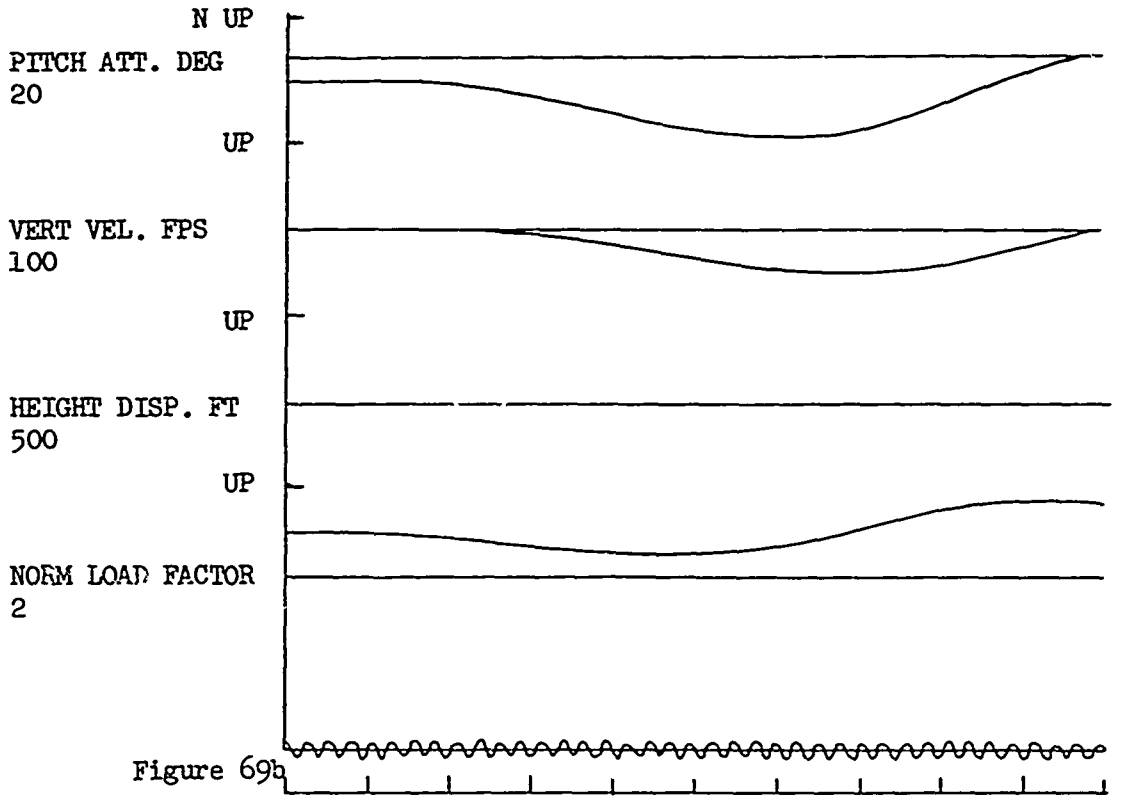

Figure 69b

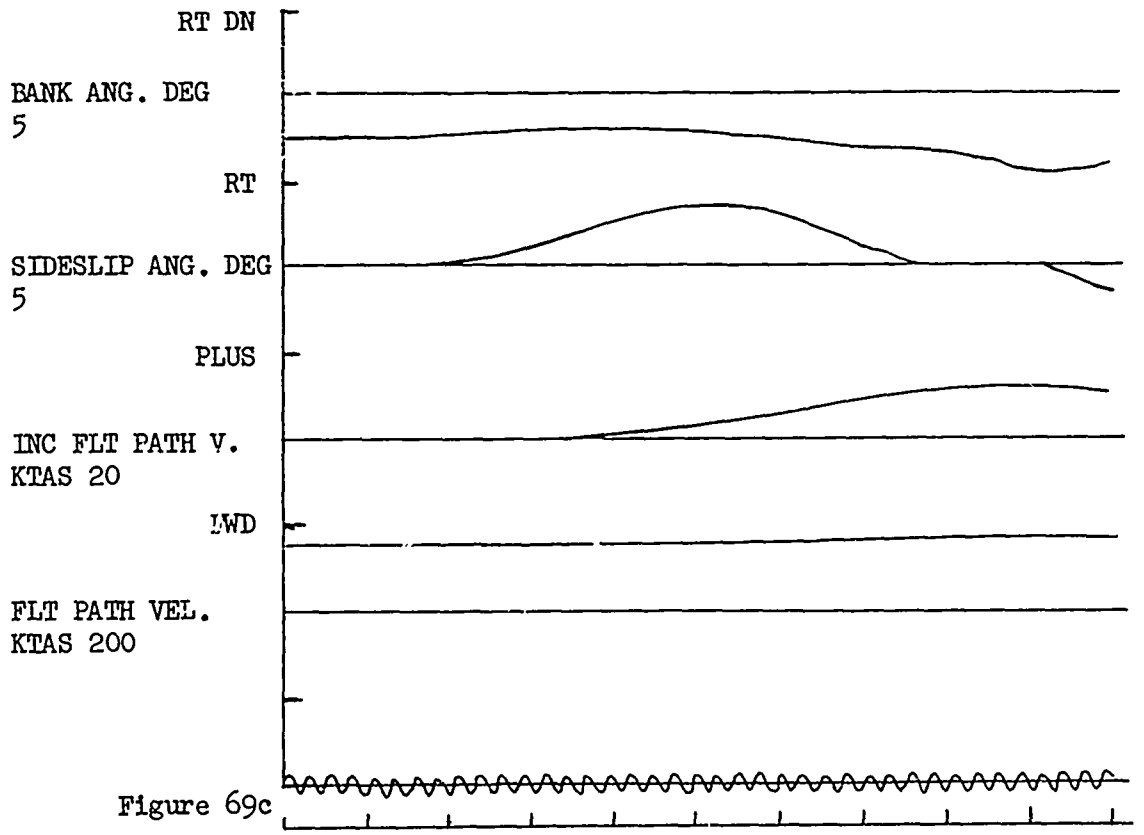

Figure 69c

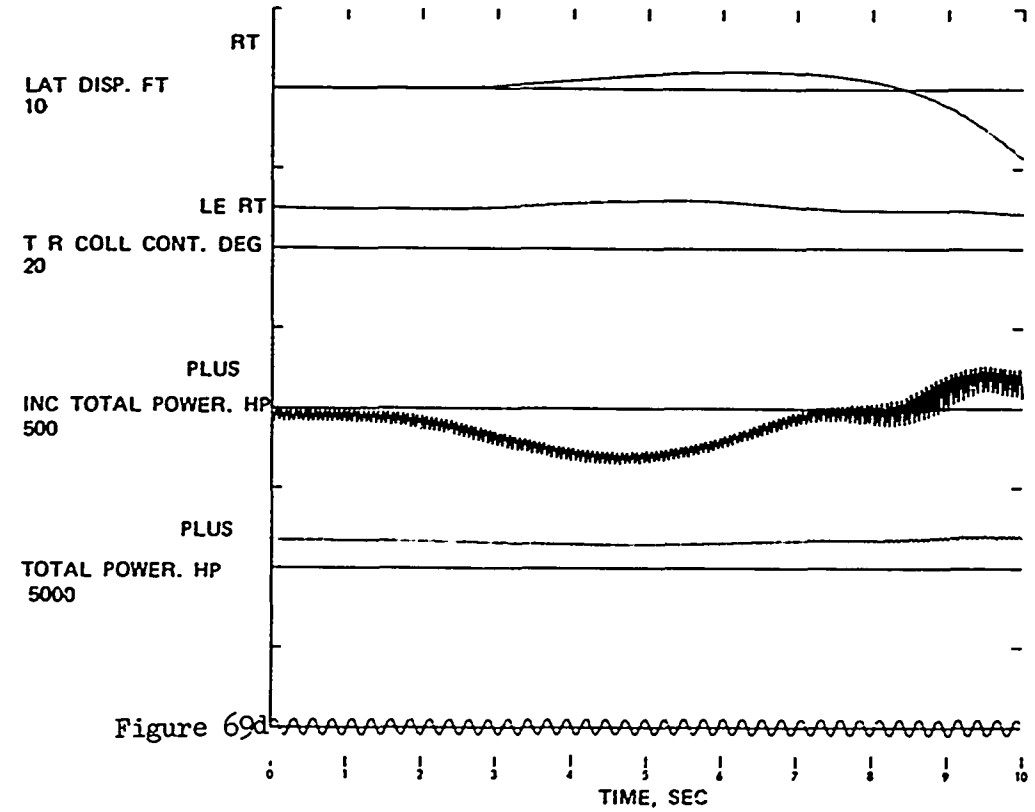

Figure 69d

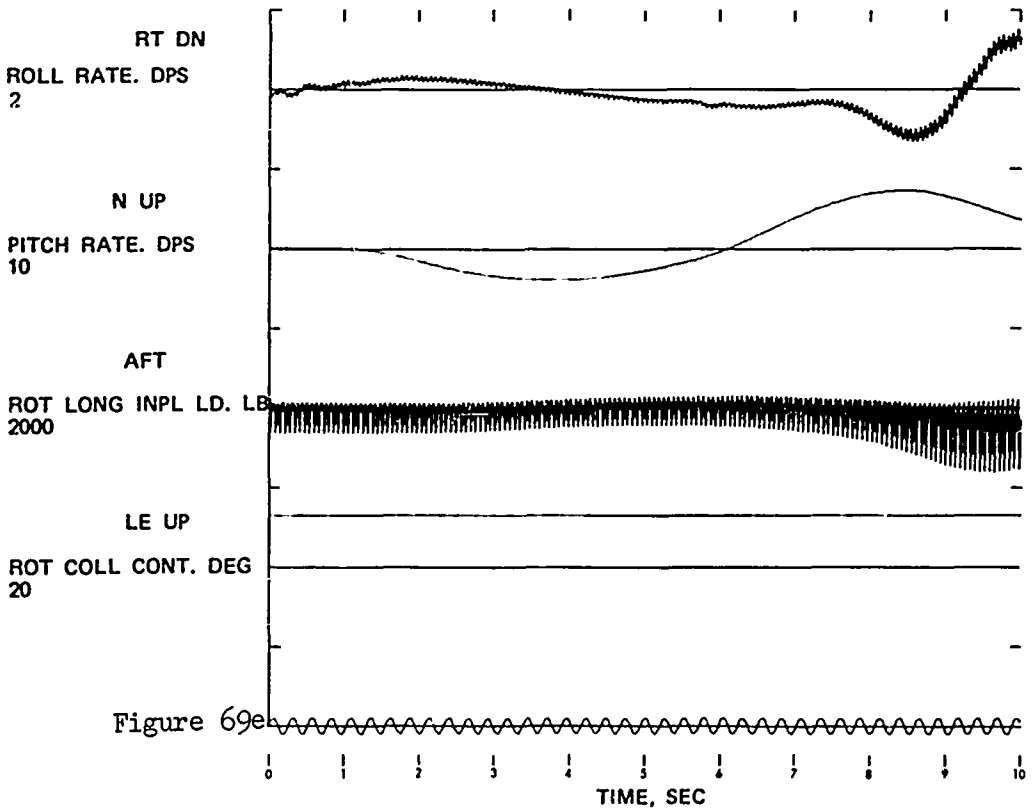

Figure 69e

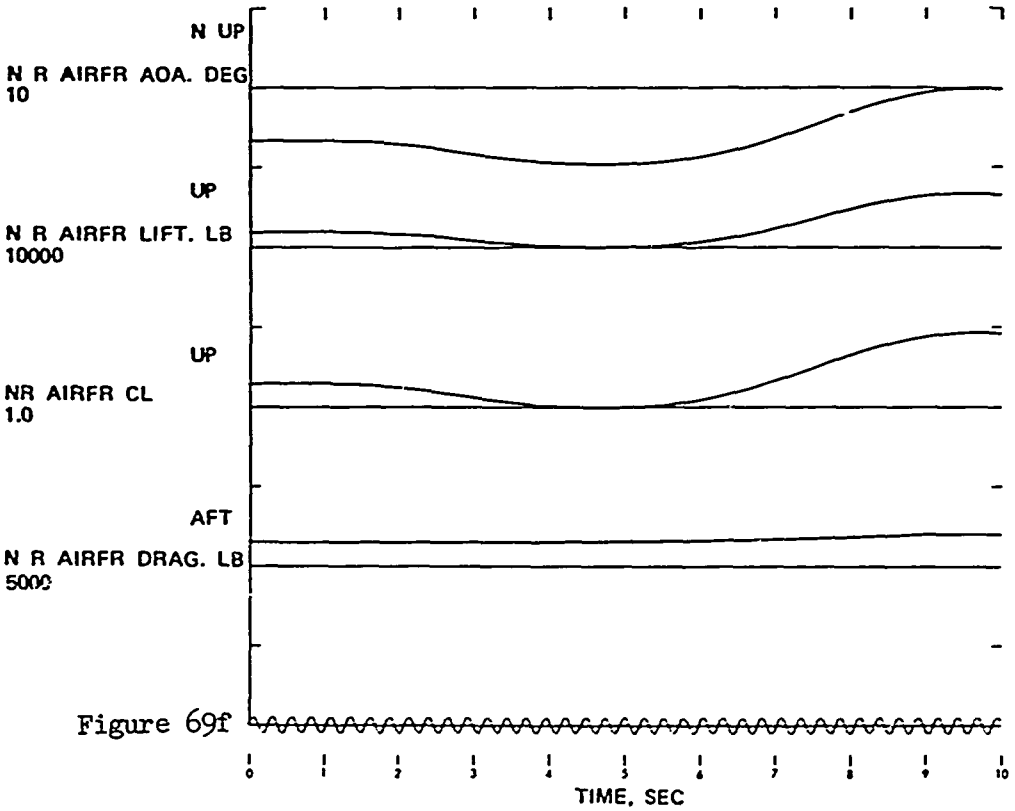

Figure 69f

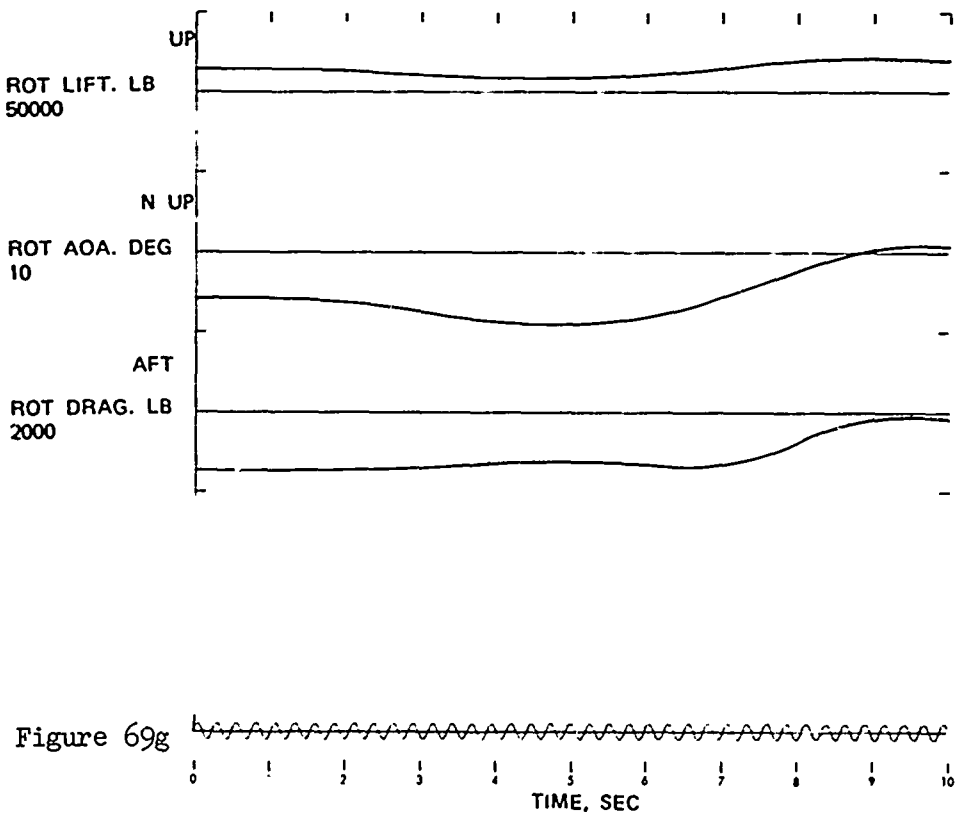

Figure 69g

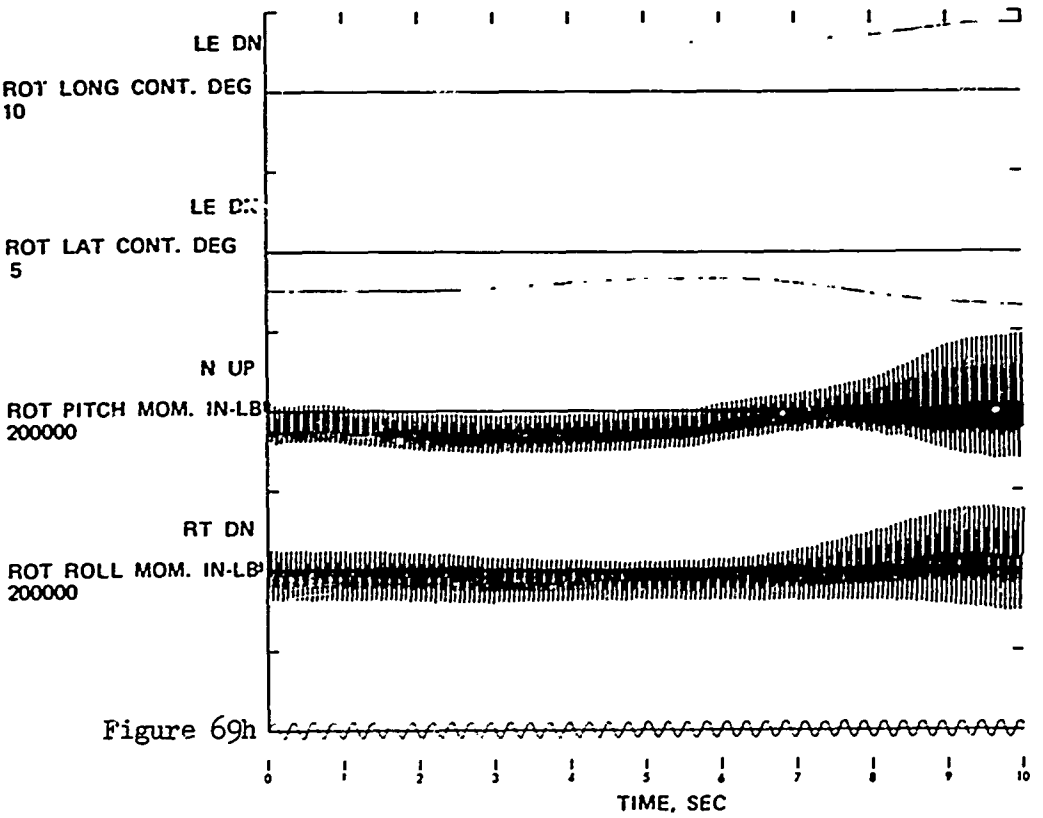

Figure 69h

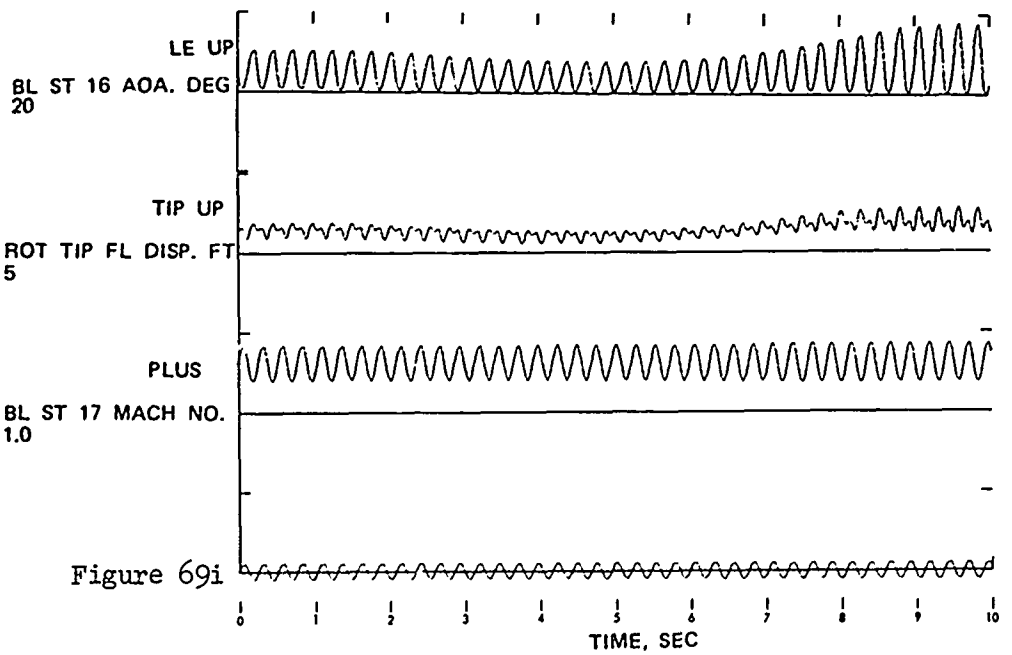

Figure 69i

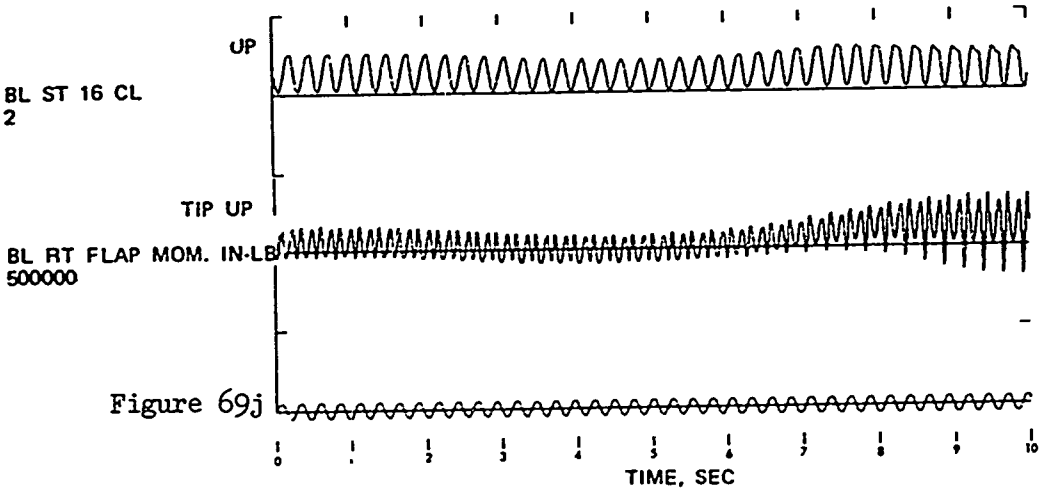

Figure 69j

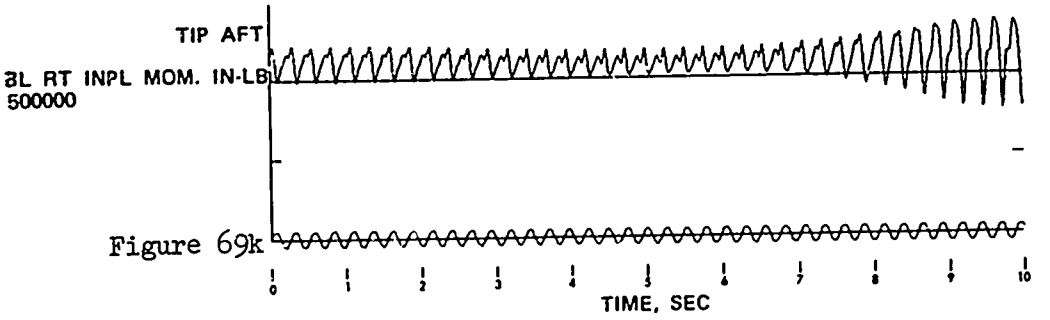

Figure 69k

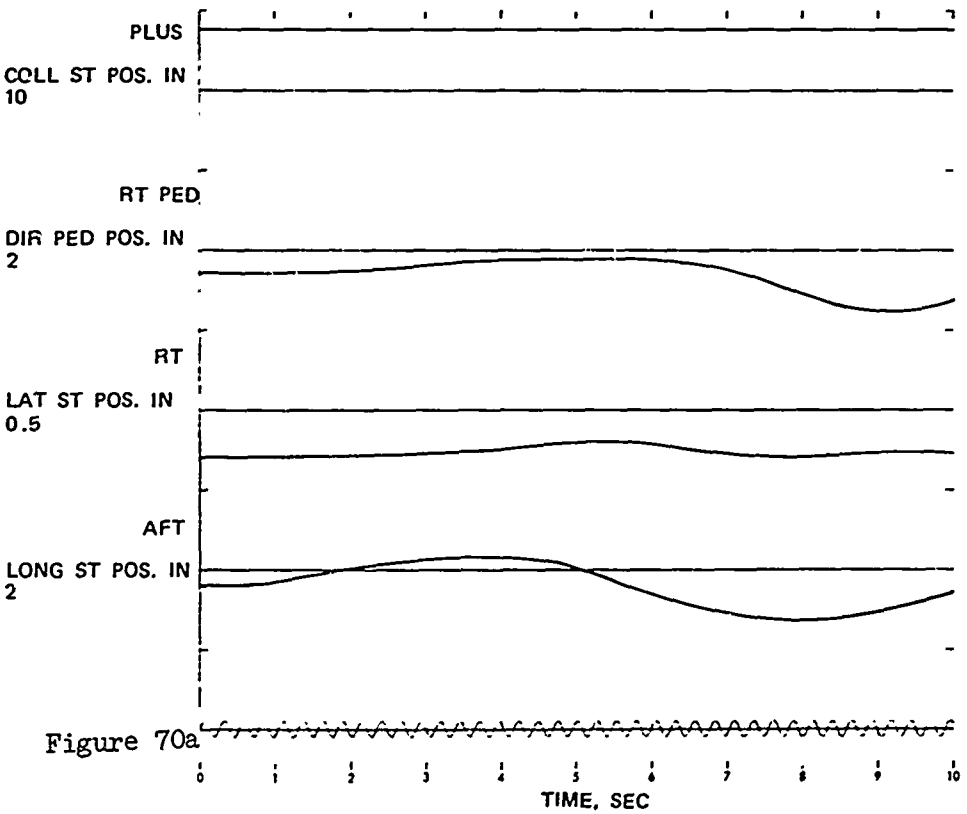

Figure 70a

Figure 70 . Time Histories Showing the Effects of Symmetrical Pull-up and Push-over: Configuration 6; Maneuver Initiated at 167 KTAS; Height Increase.

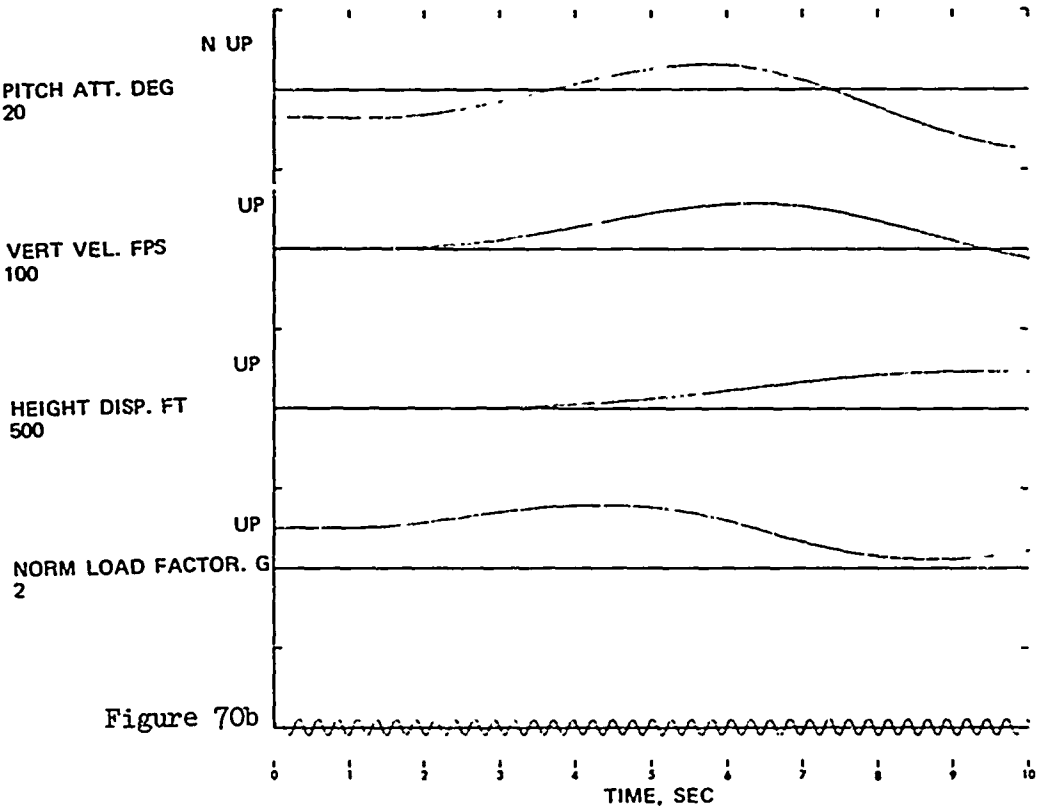

Figure 70b

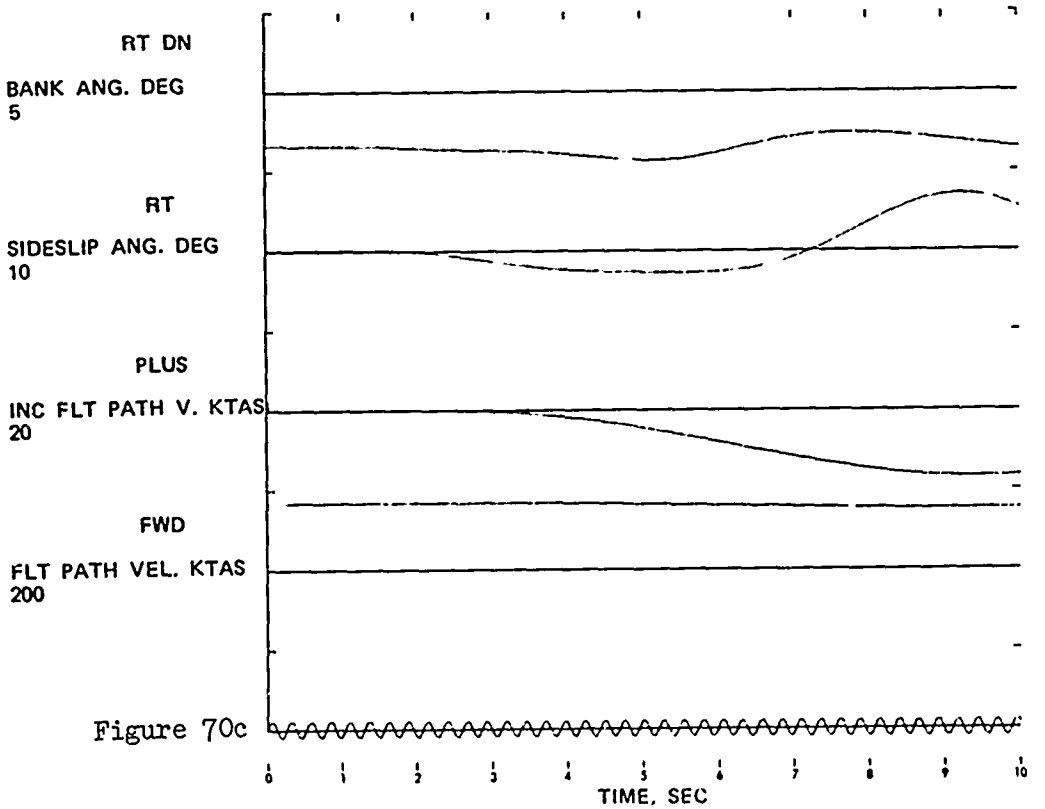

Figure 70c

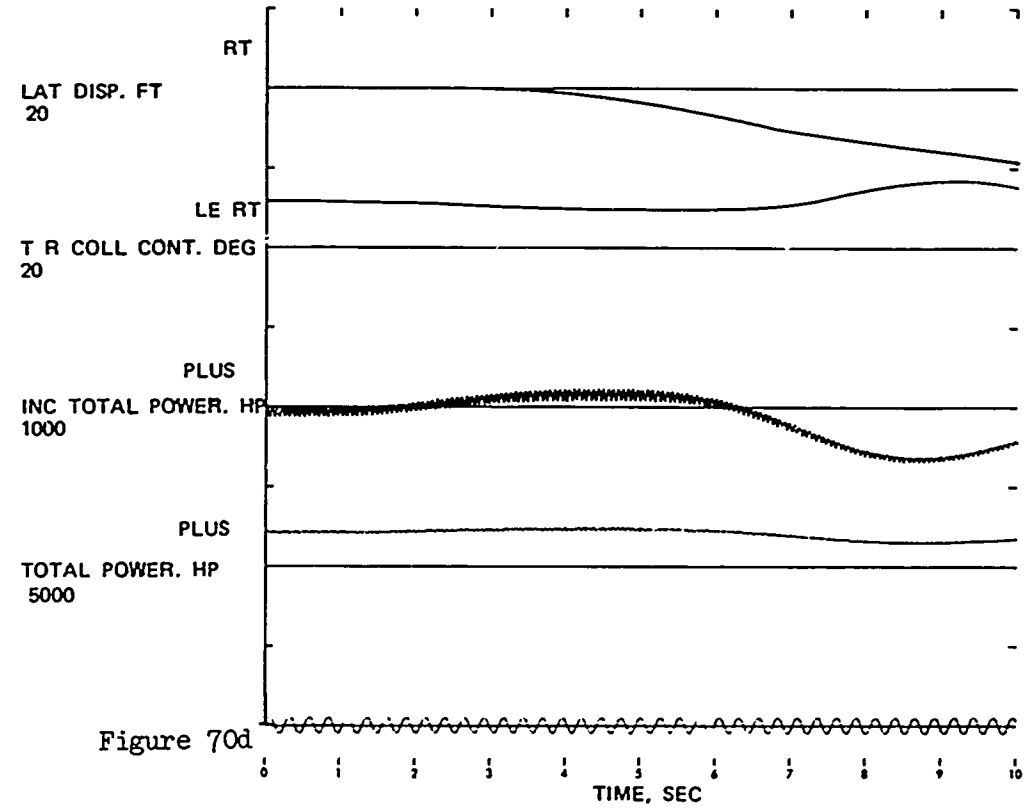

Figure 70d

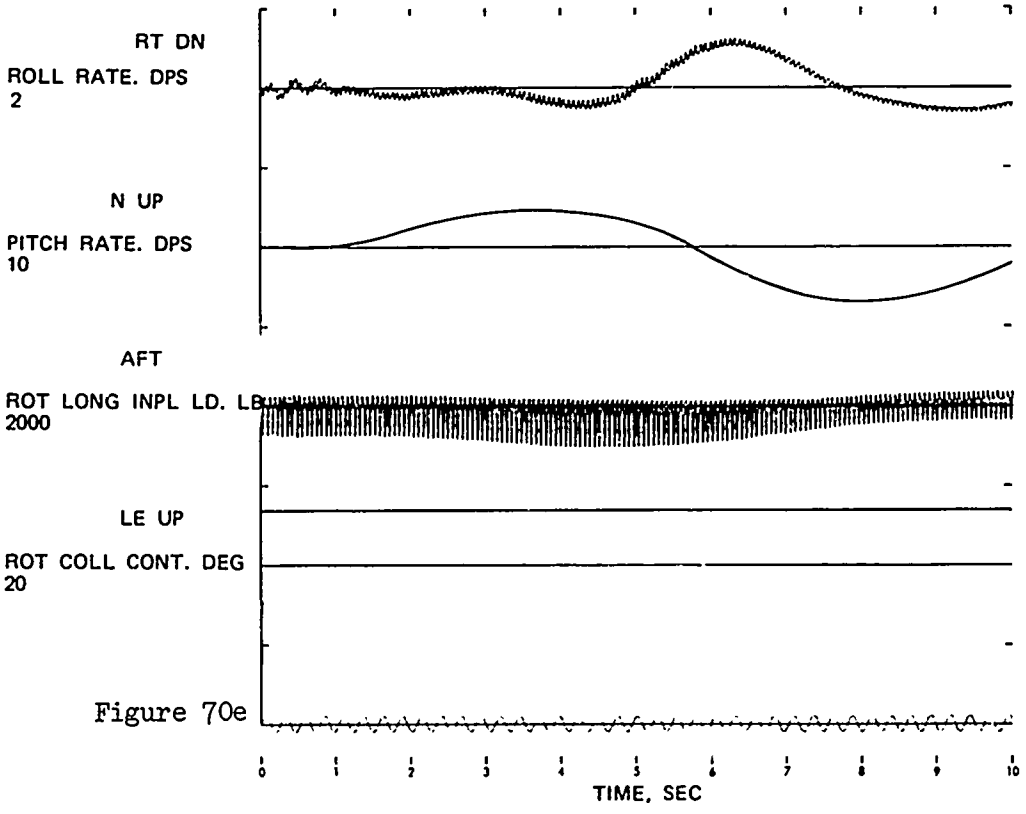

Figure 70e

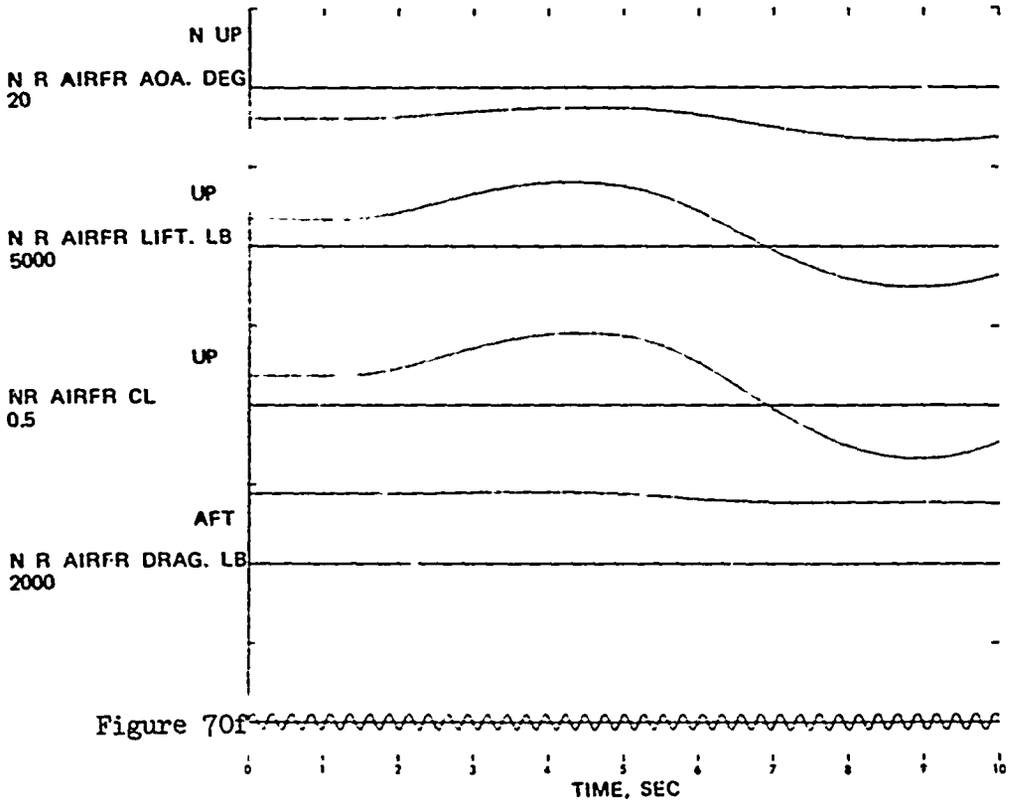

Figure 70f

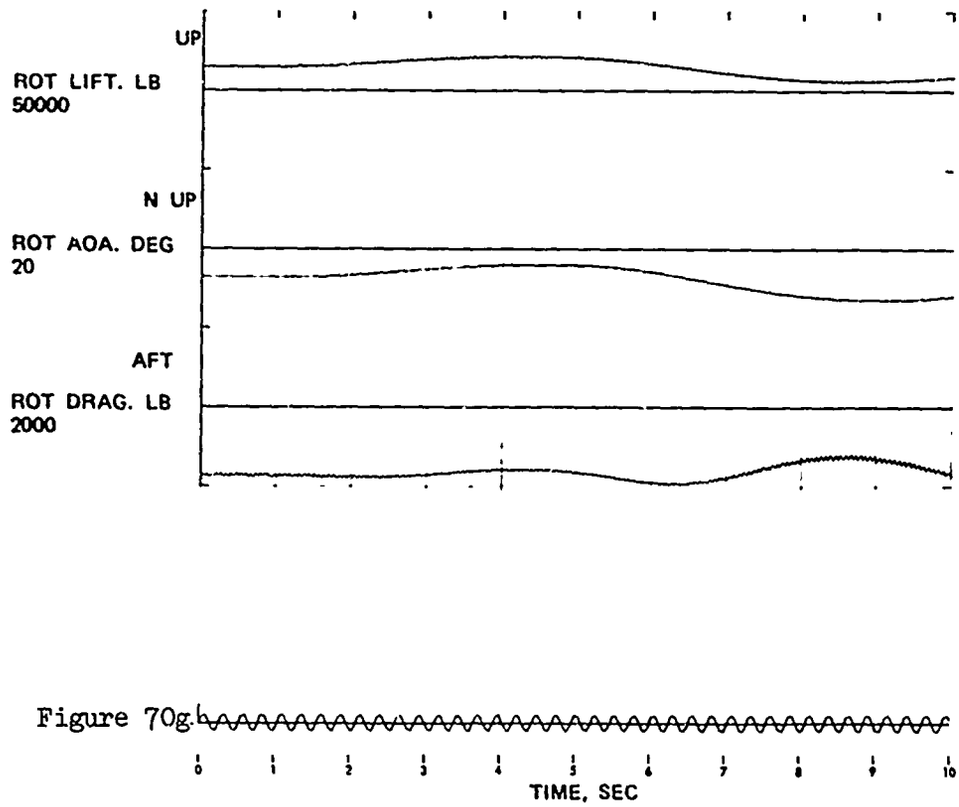

Figure 70g.

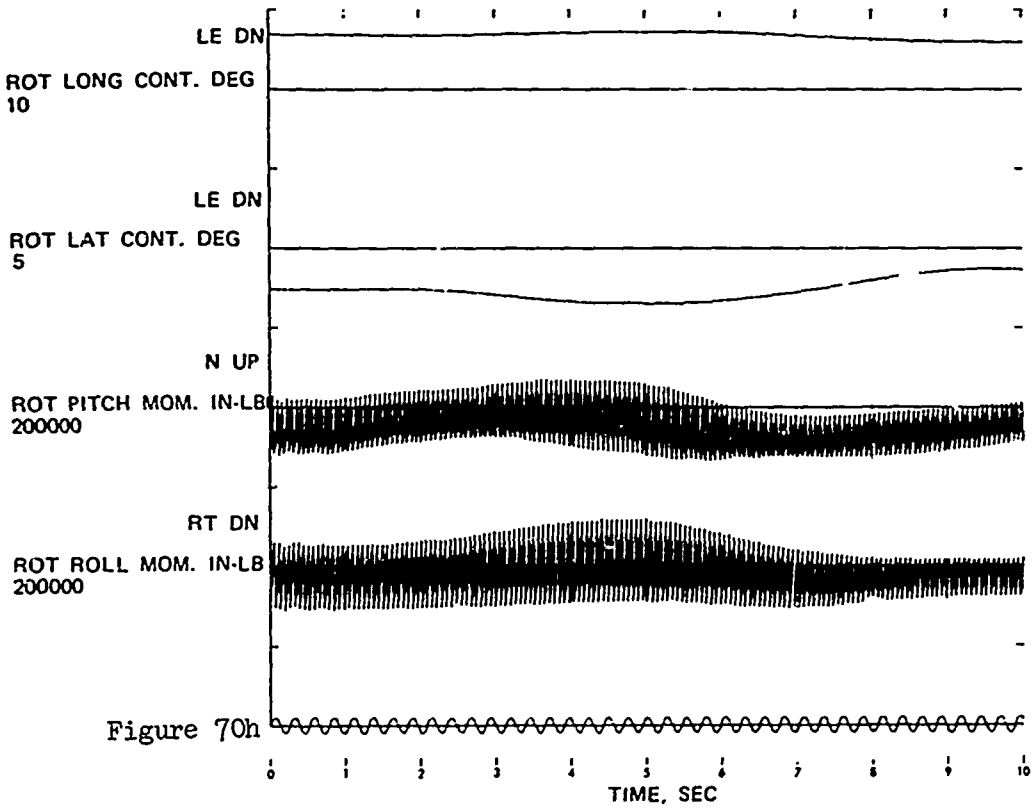

Figure 70h

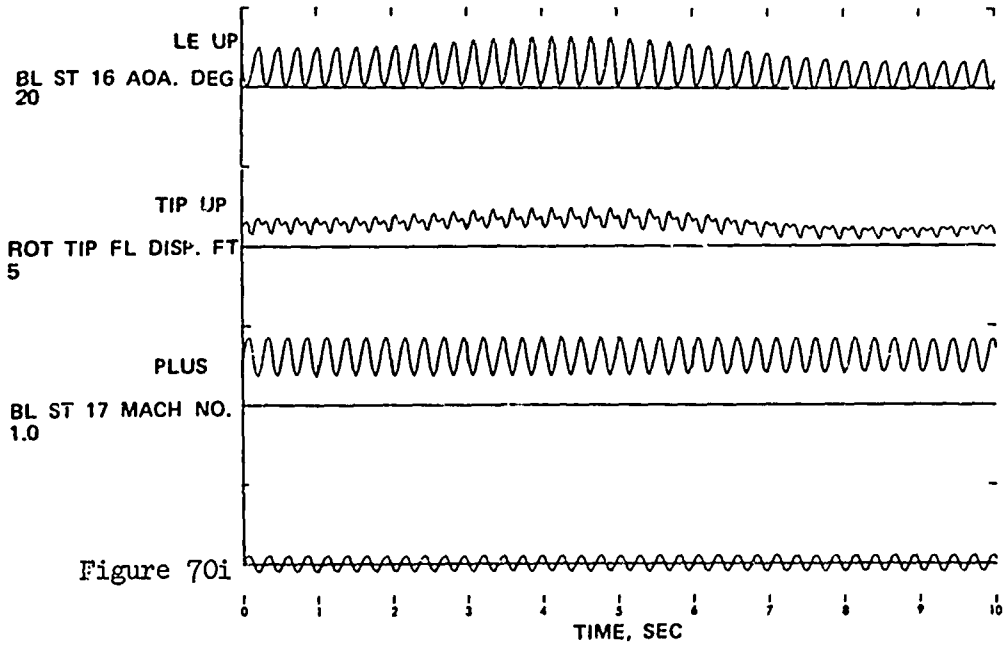

Figure 70i

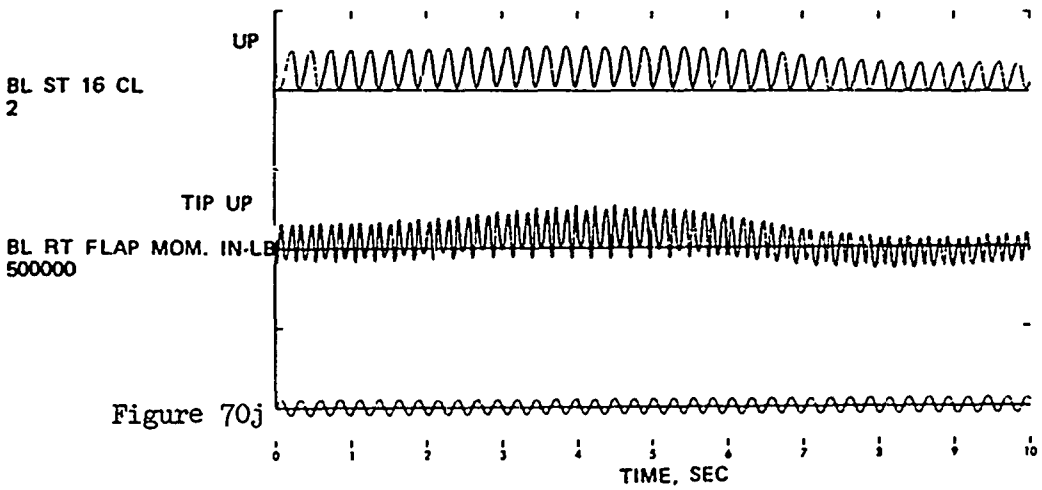

Figure 70j

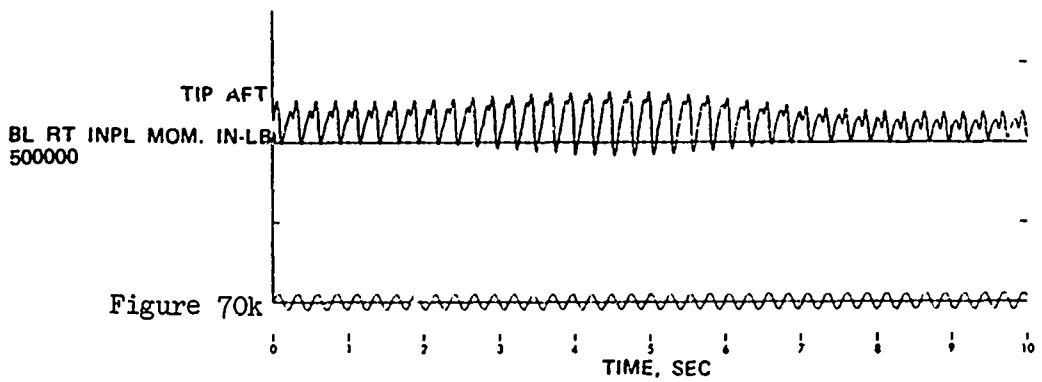

Figure 70k

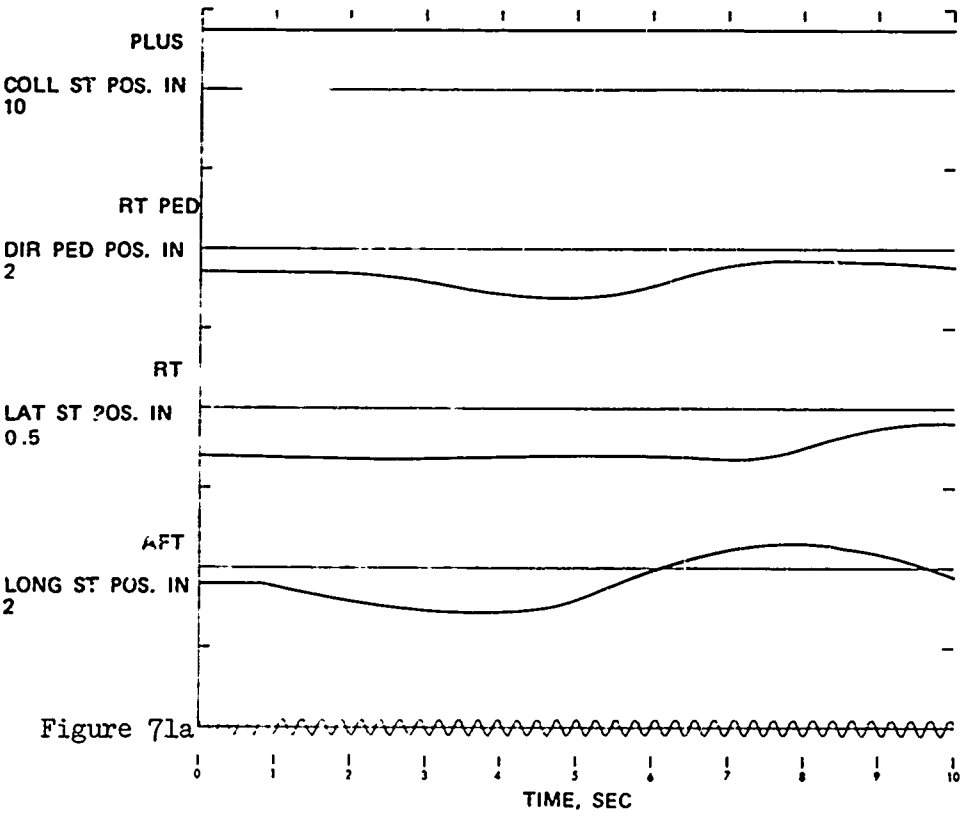

Figure 71a

Figure 71 . Time Histories Showing the Effects of Symmetrical Push-over and Pull-up: Configuration 6; Maneuver Initiated at 167 KTAS; Height Decrease.

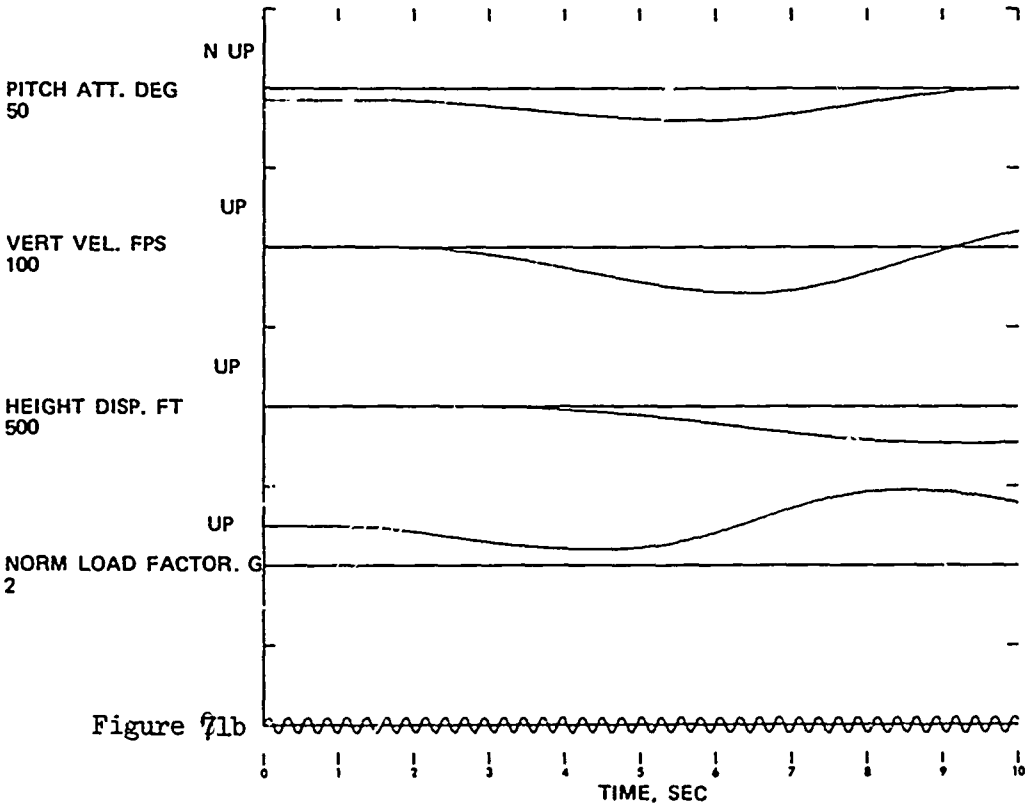

Figure 71b

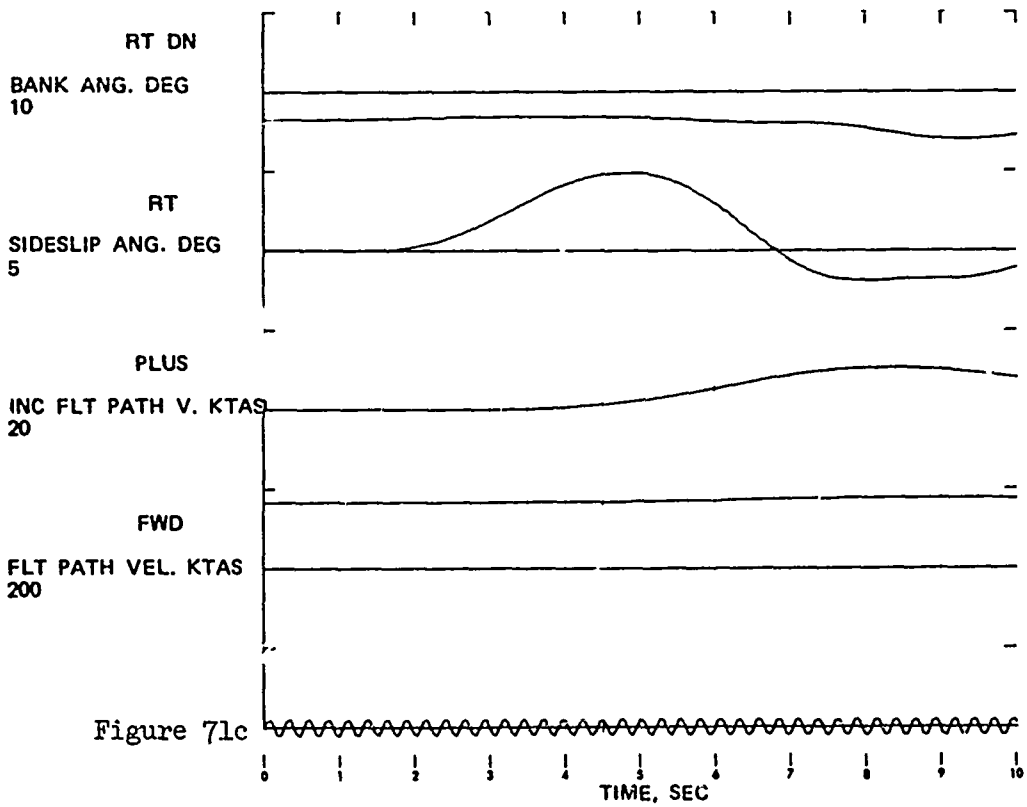

Figure 71c

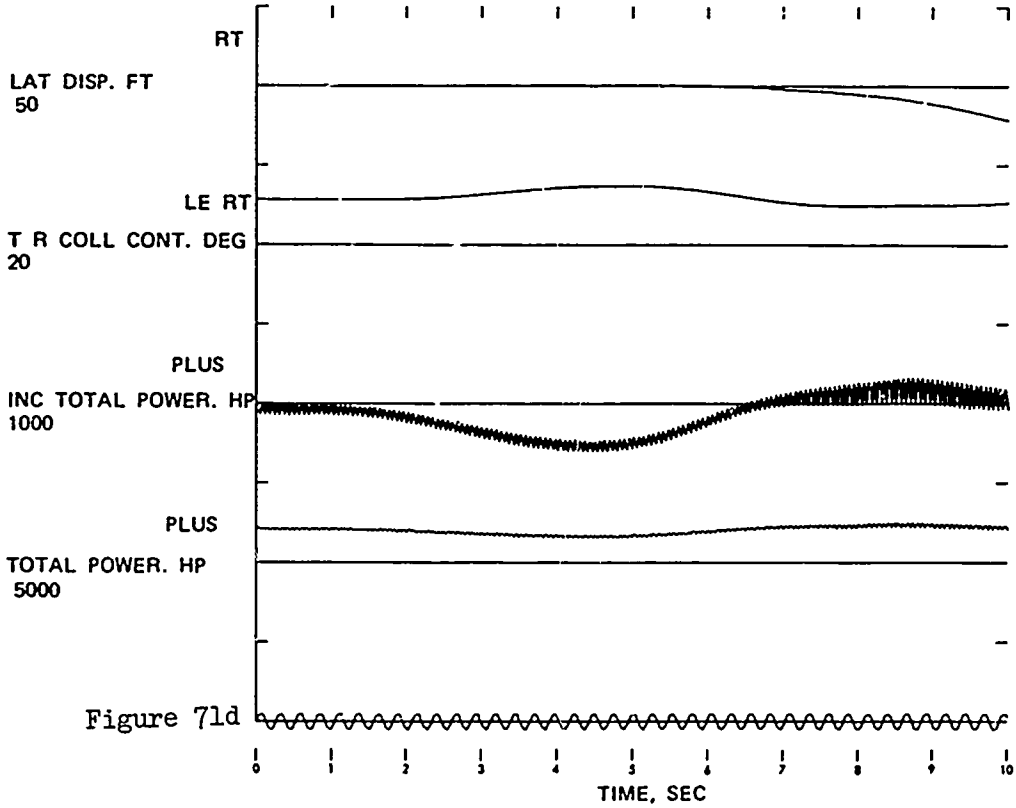

Figure 71d

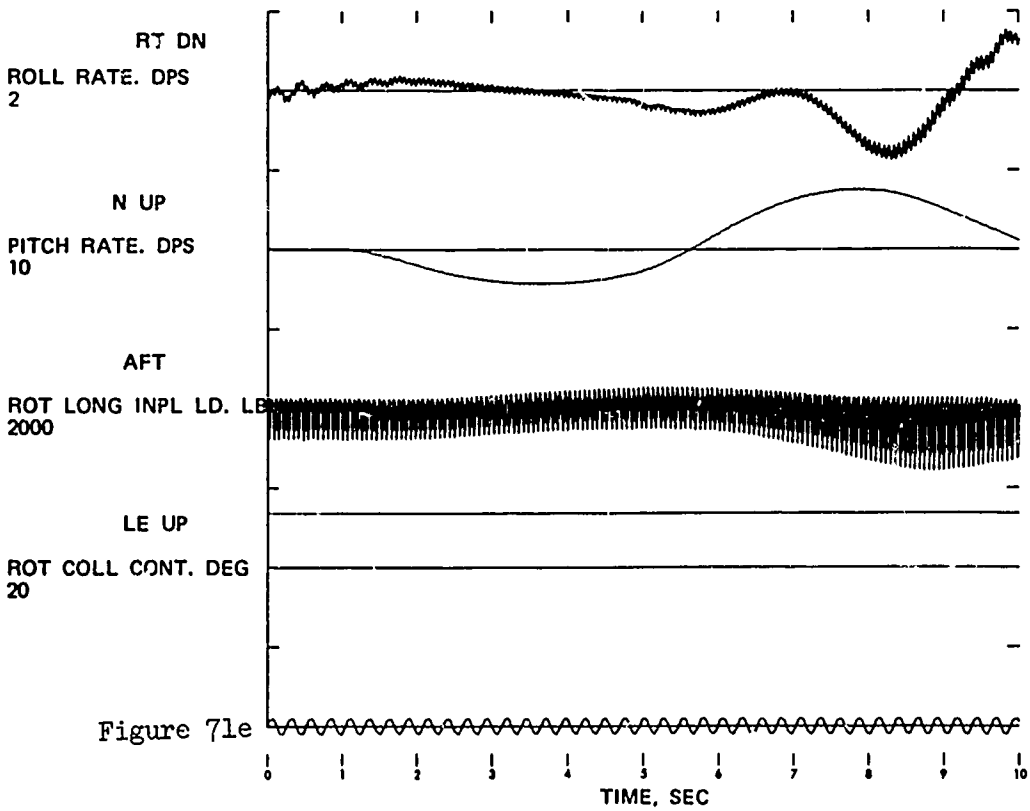

Figure 71e

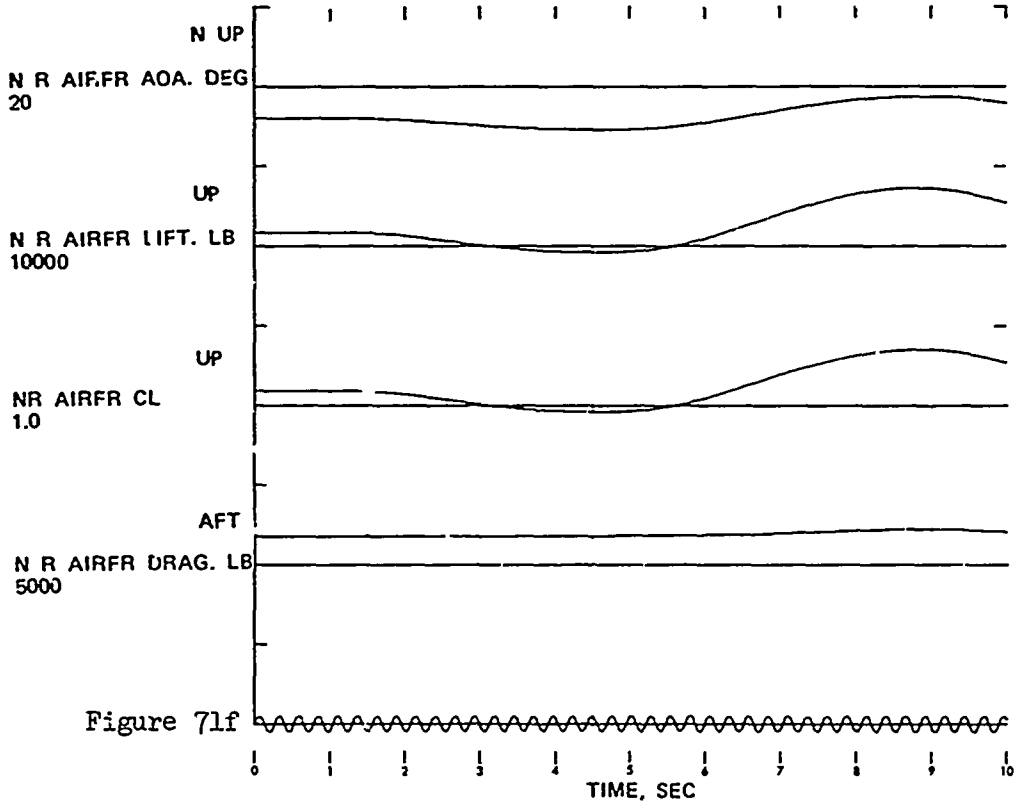

Figure 71f

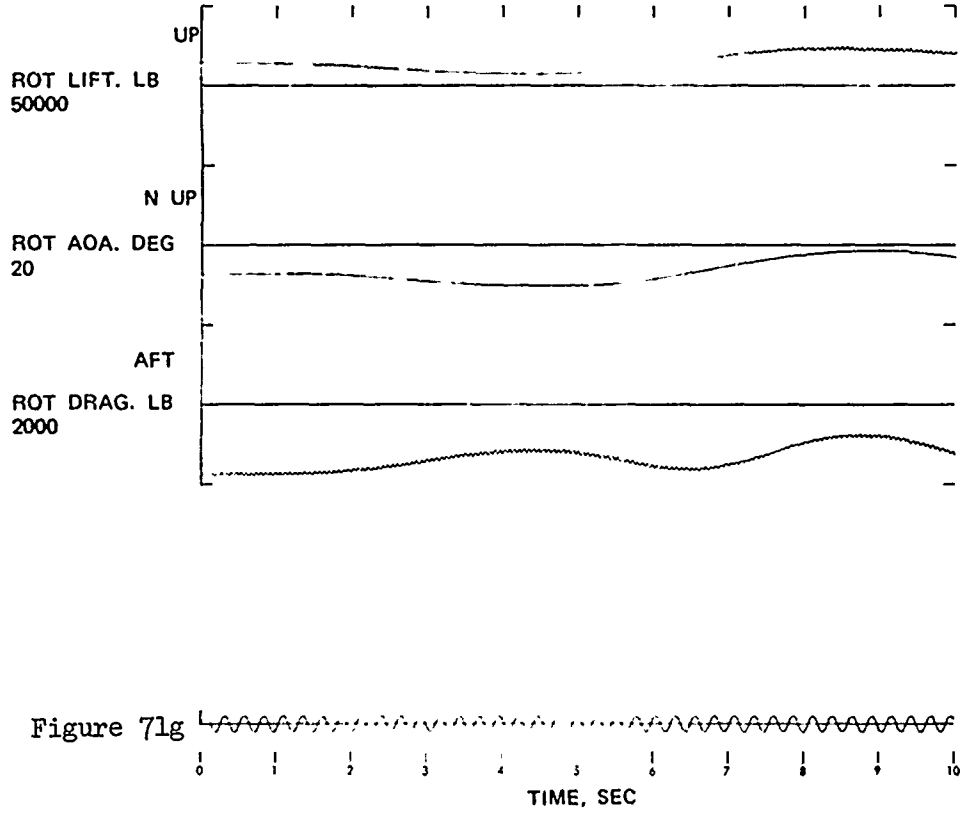

Figure 71g

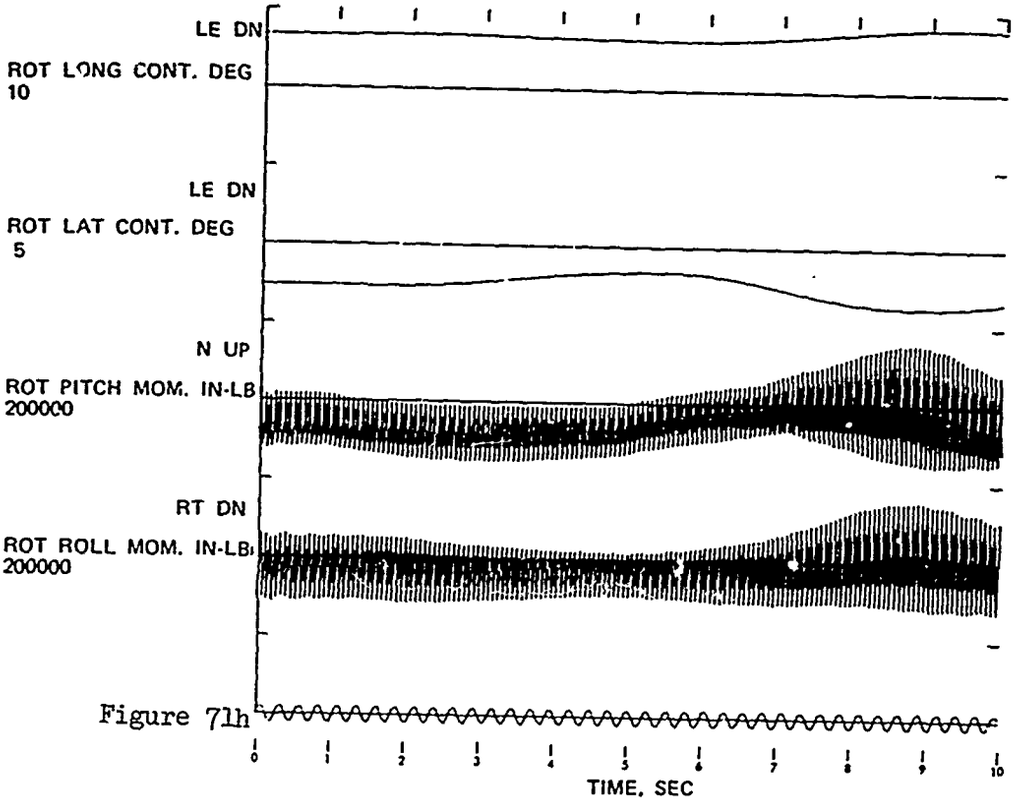

Figure 71h

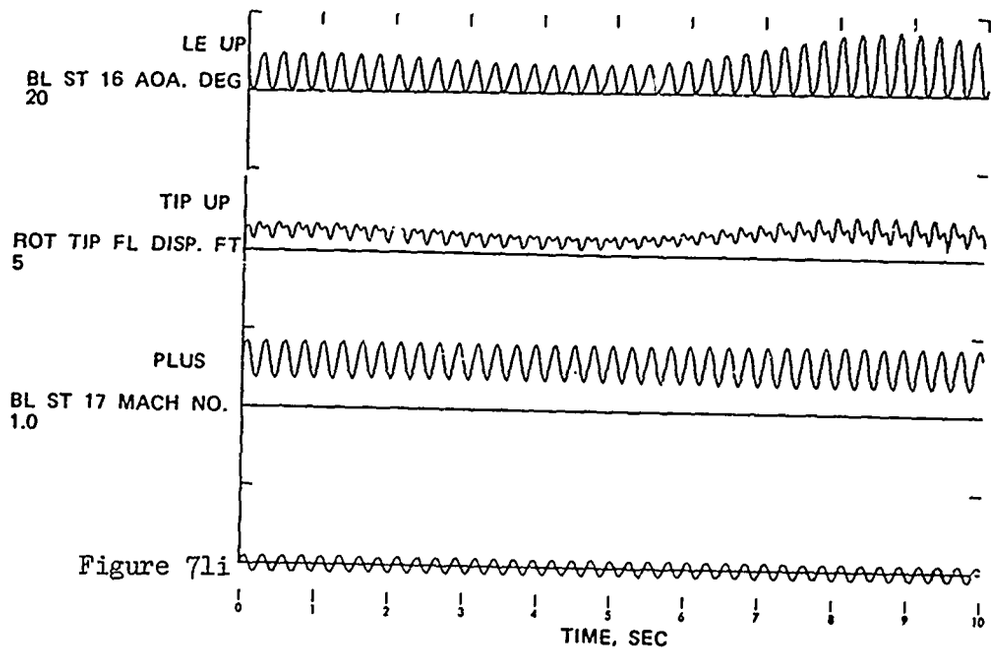

Figure 71i

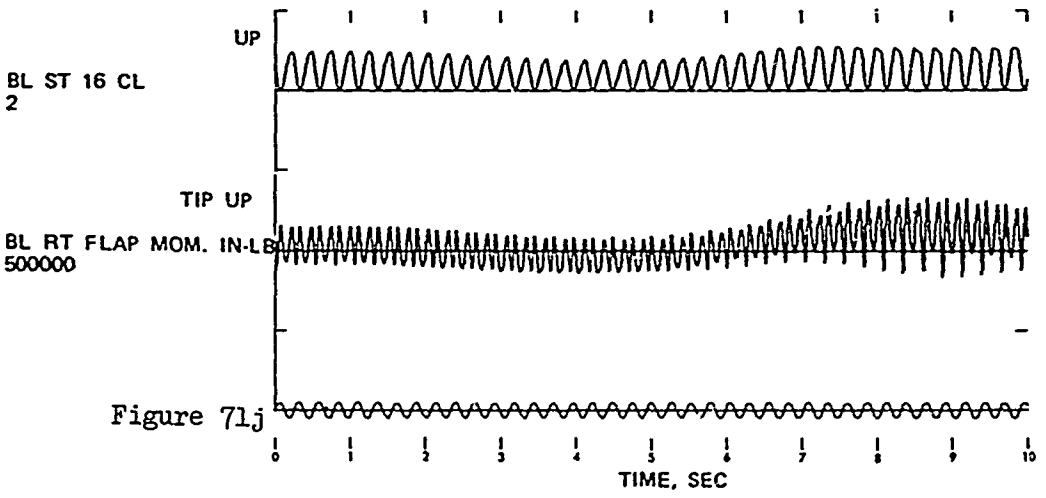

Figure 71j

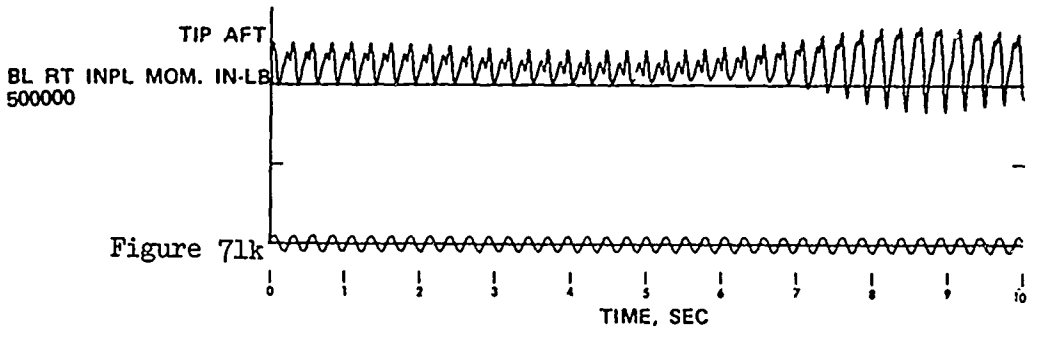

Figure 71k